Itziar Maestrojuán Biurrun

Development of Terahertz Systems for Imaging Applications
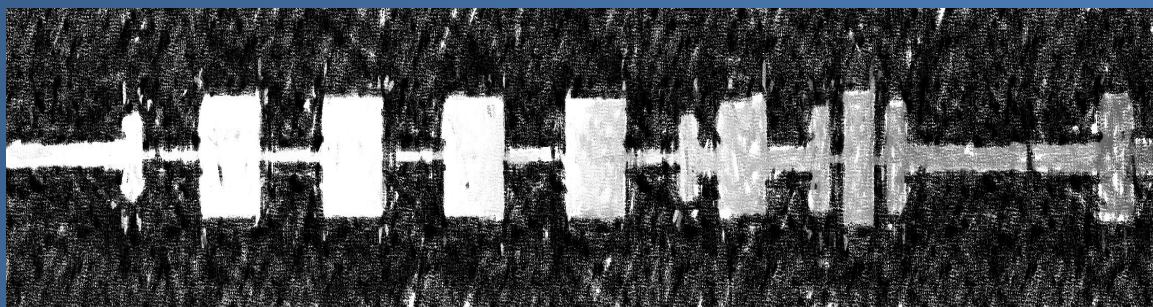
Development of Terahertz

Systems for Imaging Applications

Memoria de la tesis Doctoral realizada por
Itziar Maestrojuán Biurrun

Y dirigida por
Dr. Ramón Gonzalo García

Para optar al grado de
Doctora en Ingeniería de Telecomunicación

Development of Terahertz Systems for Imaging Applications

Memoria de la Tesis Doctoral realizada por
Itziar Maestrojuán Biurrun

Y dirigida por:
Ramón Gonzalo García

Para optar al grado de
Doctora en Ingeniería de Telecomunicación

Universidad Pública de Navarra
Departamento de Ingeniería Eléctrica y Electrónica
Pamplona, Febrero 2015

A mis padres,
A mi hermano,
A Alberto.

AGRADECIMIENTOS / ACKNOWLEDGMENTS

Después de tantas páginas escritas creo que estas son las que más me va a costar reducir, ya que me podría extender mucho solo nombrando a todas esas personas que me han ayudado a llegar a donde estoy y a realizar esta tesis.

En primer lugar querría dar las gracias al culpable de que esté escribiendo esto, Ramón, muchas gracias por tu ayuda, por estar siempre ahí, por enseñarme todo lo que aquí está escrito y mucho más, porque gracias a ti puedo decir que me gusta mi trabajo, qué digo, me encanta mi trabajo. Has confiado tanto en mí y me has abierto las puertas de tantas cosas que solo puedo decir gracias por todo, sin ti no estaría donde estoy.

Hay dos personas a las que siempre digo que la mitad de esta tesis es suya, y es verdad, Inés y Gonzalo, ¿¿qué habría hecho yo sin vosotros?? Gracias Gonzalo por todas esas horas de fabricación, gracias, gracias, gracias! Inés, ay Inés!! Deberías asegurarte esas manos de oro que tienes!!! Hemos dado a luz a un montón de "hijos" y está claro que eso no lo habría conseguido sin ti, sin ese pulso maravilloso que tienes para soldar diodos minúsculos, eso es un arte! Y tú eres una artista!

Iñigo, a ti también te debo esta tesis, por toda tu ayuda, por tus explicaciones y consejos, muchas gracias por estar siempre disponible, por ayudarme cuando me peleaba con HFSS, ADS, GRASP y hasta conmigo misma, muchas gracias Iñigo.

No creáis que me olvido del resto del grupo de Antenas, eso es imposible, porque todos y cada uno de vosotros me habéis guiado, ayudado, animado y aguantado cuando ya no sabía ni por qué estaba haciendo esto. Gracias Juan Carlos y Jorge, siempre ahí para cualquier cosa, Libe, David, y mis chicas! Ainara, Amagoia y Belén, por todos esos grandes momentos que hemos compartido, porque más que un grupo hemos sido una pequeña familia, no se puede encontrar gente mejor con la que trabajar, porque con vosotros esto no es trabajo, esto es una maravilla.

¿¿Y mis chicos de Anteral qué?? Pues gracias por aguantar esta época de transición que he tenido, sois geniales. Ahora termino una etapa de mi vida y empiezo otra con vosotros y no podría estar más feliz de hacerlo, no podría haber encontrado unos compañeros mejores, Asier, Aitor y Gonzalo, gracias chicos, es un placer trabajar con vosotros.

I would also like to thank the MMT group from RAL, thank you so much for taking me there, helping and teaching me so many things! It was a great pleasure to be there and to learn from you guys. Thank you Simon for helping me every day not only in my research but also in the many other things you let me help. Thank you Hui, Byron, Manju and Peter, for caring about me, for taking me as part of the group and helping me that much. Thank you.

Y por último y no menos importante querría dar las gracias a mis padres y mi hermano Dani, gracias por aguantarme esos días de estrés insoportable que he tenido y el resto de días también jeje, gracias por dármelo todo y hacer que haya llegado hasta aquí, por confiar en mi cada día, por animarme y apoyarme aunque ni siquiera lograrais saber de qué iba esta tesis. Gracias!!

Y gracias a ti Alberto, por estar ahí día tras día, por hacerme querer seguir los días que yo ya no quería, por ayudarme a dormir las noches que me agobiaba, por cuidarme y apoyarme cada día. Te quiero.

Muere lentamente quien no viaja. Ni lee.
Quien no sueña. Quien no confía.
Quien no lo intenta.

Pablo Neruda.

ABSTRACT

The main goal of this thesis was the study and development of technology, specifically harmonic mixers, working at millimetre and sub-millimetre frequencies in other to implement systems for imaging applications.

Before focusing on the development of this technology, it was important to go into detail about the characterisation of mixer systems. For this reason, two important studies were reported at the first parts of this dissertation. This is: the comparison between three different measurement procedures (the attenuator, gain and noise injection procedures) as well as three detection methods, and the impact of the use of different IF Chains in the measurement process. The Gain method turned to be the most reliable one in terms of more constant values and closer to the average between all procedures. According to the IF Chain study, the impact of the inclusion of an isolator between the mixer and the pre-amplifier was analysed. This Thesis has proved that the increase on the noise temperature of the mixer due to the inclusion of an isolator could be explained by the mismatch existing between devices presented in the receiver. So that, depending on the IF chain used to measure the performance of a mixer, this performance could be altered by the mismatching existing between the mixer and the IF chain, which could lead to an increase or a decrease of the mixer NT and CL. This revealed the importance of a good matching between components in order to produce comparable results.

In the last years, it has been done a relevant investigation in the development of THz systems for imaging applications based on the design of Schottky diode harmonic mixers. However, this Thesis opens the possibility of using a COC (cyclic olefin copolymer) substrate in the development of these components which leads to fewer losses and therefore, to an improved mixer performance.

Accordingly, the second part of this Thesis dealt with the design, fabrication and characterization of a Schottky diode sub-harmonic mixer working at an RF frequency of 220 GHz. This mixer exhibited best noise temperature below 1000 K and conversion loss of 7.2 dB. Moreover, in order to prove the fact that a lower losses substrate leads to a better performance, the comparison between this mixer and the same one implemented on Rogers Duroid 5880 was carried out. Results showed an improvement of 300 K and 0.5 dB in the performance of the COC mixer with respect to the Rogers one.

Once the feasibility of using this substrate in the design of mm-wave mixers was validated, the development of a 1x8 array was fulfilled. This dissertation proved the repeatability of the design/fabrication/characterisation cycle obtaining minimum noise temperature values around 1000 K and conversion loss results between 6.8 and 7.8 dB for all the elements that formed the array. Moreover, the simulated results of this array operating over a Cassegrain system for imaging applications were reported. The best performance obtained as a compromise between the S/N value, maximum value of the E field and shape of the beam cut at -3 dB was reached with an antenna of 24 dB gain. It is important to highlight that this thesis presents for the first time an imaging operational array formed by eight Schottky diode mixers.

Furthermore, new approaches in the development of heterodyne receivers were also examined. Usually, sub-millimetre-wave mixer designs are based on sub-harmonic architectures, in which the RF frequency is double the LO frequency. One of the main reasons for selecting this

configuration is the difficulties to have enough LO power at high frequencies to pump properly the diodes. With the reduction in a factor two of the LO frequency, the LO power criterion can be more easily complied with. Nevertheless, if the RF frequency keeps increasing, this problem becomes more arduous to sort out. Even at relatively low frequencies, in cases where the system (as in imaging applications) implements several pixels formed by sub-harmonic mixers, the LO power necessity is also a relevant problem. However, an advanced approach based on the use of a fourth-harmonic mixer configuration in which the RF frequency is four times the LO frequency can become in an attractive solution. This configuration can resolve the aforementioned problems by working with an LO source operating at much lower frequency where higher power is available.

A fourth harmonic configuration mixer working at an RF frequency of 440 GHz was developed and measured for the first time at the WR2.2 band. The fourth-harmonic mixer configuration consists on a harmonic mixer that by appropriate filtering selects the fourth mixing product of the LO frequency and the RF frequency. This solution is simpler than other configurations based on cancellation of the sub-harmonic mixing product by combining the response of 4 diodes with 90° phase difference. Minimum noise temperature and conversion loss values of 7914 K and 14 dB respectively were obtained for a LO power of 9.5 mW, although satisfactory results were achieved for input LO powers from 7.5 mW to 10 mW. Although they are far from being comparable with the performance of sub-harmonic mixers, they offer a good alternative when LO power at high frequencies results an issue. Moreover, a comparison with a sub-harmonic mixer operating at the same RF frequency was also presented in this manuscript. In order to carry on this comparison a frequency doubler from 110 GHz to 220 GHz was developed.

Finally, this Thesis ends with the images taken by the sub-harmonic mixer operating at 220 GHz and the complete array together with the cuasi-optical system, provided by the Alfa Imaging Company. The possibility of taken images with the designed components was proven in both cases.

Firstly, a single pixel was used, i.e. the sub-harmonic mixer, which was helped by two lenses to improve the definition over the image. Results showed a high resolution of the objects and a variation of the level of the obtained power depending on its nature. The user was able to distinguish between elements such as the human body, a metallic sheet or a ceramic material, giving the possibility to identify, via the shape, and detect them. Finally, some images of a whole person were taken using the 1x8 array and Alfa Imaging mirror´s system. The images were taken outdoors and at a distance of 4 metres from the imaging system. The person was completely distinguished and moreover, a metallic sheet placed on the chest of the person was also detected, offering an alternative to the actual airport scanners.

This dissertation was framed within four research programmes given to the Antenna Group and counted on an industrial background support which made it of high significance in the THz field. But this dissertation was not only the result of some research projects but also the starting point for the Antenna Group to set a THz lab and become a national reference in this field.

RESUMEN

El principal objetivo de esta tesis fue el estudio y desarrollo de tecnología, concretamente mezcladores armónicos, trabajando a frecuencias de milimétricas y sub-milimétricas con el fin de implementar sistemas para aplicaciones de imagen.

Antes de centrarse en el desarrollo de esta tecnología era importante conocer en detalle la caracterización de sistemas de mezcladores. Por este motivo, la primera parte de esta Tesis, presentaba dos estudios importantes. Es decir, la comparación entre diferentes procedimientos de medida (el método del atenuador, la ganancia y la inyección de ruido) así como tres métodos de detección, y el efecto de utilizar distintas cadenas de IF en la caracterización. El método de la Ganancia resultó ser el más fiable en términos de resultados más constantes y más cercanos a la media obtenida entre todos los procedimientos. En lo referido al estudio de la cadena de IF, se analizó el efecto de añadir un aislador entre el mezclador y el pre-amplificador. Esta tesis ha probado que el aumento de la temperatura de ruido del mezclador producido por la introducción del aislador podía ser explicado por la desadaptación existente entre los componentes que formaban el receptor. Por tanto, dependiendo de la cadena de IF utilizada para caracterizar el funcionamiento del mezclador, este funcionamiento podía alterarse por la desadaptación existente entre el mezclador y la cadena de IF, lo que podía llevar al aumento o disminución de la temperatura de ruido y pérdidas de conversión del mezclador. Esto reveló la importancia de tener una buena adaptación entre componentes a la hora de obtener resultados comparables.

v

En los últimos años se ha realizado una investigación de relevancia en el desarrollo de sistemas de THz para aplicaciones de imagen basados en el diseño de mezcladores armónicos de diodos Schottky. Sin embargo, esta Tesis ha abierto la posibilidad de utilizar substratos COC (cyclic olefin copolymer) en la implementación de estos componentes, lo que lleva a menores pérdidas y por tanto, a una mejoría en el funcionamiento del mezclador.

En consecuencia, la segunda parte de la Tesis trataba del diseño, fabricación y caracterización de un mezclador sub-armónico de diodos Schottky trabajando a una frecuencia de RF de 220 GHz. Este mezclador presentó mínima temperatura de ruido por debajo de 1000 K y unas pérdidas de conversión mínimas de 7.2 dB. Además, con el fin de probar el hecho de que un sustrato con menores pérdidas daba lugar a un mejor funcionamiento, se realizó la comparación entre este mezclador y uno idéntico implementado sobre substrato Rogers Duroid 5880. Los resultados mostraron una mejoría de 300 K y 0.5 dB en el comportamiento del mezclador implementado en COC con respecto al de Rogers Duroid.

Una vez comprobada la viabilidad de utilizar este substrato en el diseño de mezcladores a milimétricas, se realizó el desarrollo de un array de 1x8 elementos. Esta Tesis probó la repetitividad del ciclo de diseño/fabricación/medida obteniendo mínimas temperaturas de ruido alrededor de 1000 K y pérdidas de conversión entre 6.8 y 7.8 dB para todos los elementos que formaban el array. Además, se mostraron los resultados de simulación de este array operando en un sistema Cassegrain para aplicaciones de imagen. El mejor comportamiento, obtenido como compromiso entre el valor de S/N, máximo valor del campo E y la forma del haz a -3 dB, se obtuvo para una antena de 24 dBs de ganancia. Es importante remarcar que esta Tesis ha mostrado por primera vez un array operativo formado por ocho mezcladores de diodos Schottky para aplicaciones de imagen.

Así mismo, también se examinaron nuevas variantes en el desarrollo de receptores heterodinos. Normalmente, los diseños de mezcladores en ondas sub-milimétricas se basan en arquitecturas sub-armónicas, en las que la frecuencia de RF es doble que la de OL. Una de las principales razones a la hora de seleccionar estas conjuraciones es la dificultad de tener suficiente potencia de OL para alimentar los diodos de forma correcta. Con la reducción de la frecuencia de OL en un factor de dos, se puede alcanzar el criterio de potencia de OL. Sin embargo, si la frecuencia de RF sigue aumentando, este problema se convierte arduo de resolver. Incluso a frecuencias relativamente bajas, en casos en los que el sistema (como en aplicaciones de imagen) implementa varios píxeles formados por un mezclador sub-armónico, la necesidad de potencia de OL es un problema relevante. Sin embargo, una solución atractiva a este problema puede ser el uso de mezcladores en configuraciones de cuarto armónico en los cuales la frecuencia de RF es cuatro veces la de OL. Esta configuración puede resolver los problemas nombrados anteriormente trabajando con una fuente de OL operando a frecuencias mucho más bajas donde es posible obtener suficiente potencia.

Por primera vez se desarrollaba y medía en la banda de WR2.2, un mezclador en cuarto armónico trabajando a una frecuencia de RF de 440 GHz. Un mezclador en configuración de cuarto armónico consiste en un mezclador armónico en el que por medio del filtrado apropiado se selecciona la mezcla del producto de cuarto armónico de las frecuencias RF y OL. Esta solución es mucho más sencilla que otras configuraciones basadas en la cancelación del producto de mezclado sub-armónico combinando la respuesta de 4 diodos en cuadratura. Los mínimos valores de temperatura de ruido y pérdidas de conversión fueron obtenidos para una potencia de OL de 9.5 mW con valores de 7914 K y 14 dB respectivamente, aunque se consiguieron resultados satisfactorios para potencias entre 7.5 y 10 mW. A pesar de que estos resultados se encuentran lejos de ser comparables con el comportamiento de mezcladores sub-armónicos, ofrecen una buena alternativa cuando la potencia de OL a frecuencias altas resulta un problema. Además, este manuscrito también

presentaba la comparativa con un mezclador sub-armónico trabajando a la misma frecuencia de RF; así como un multiplicador en frecuencia de 110 a 220 GHz que fue desarrollado con el fin de poder realizar dicha comparativa.

Finalmente, esta Tesis terminaba con las imágenes tomadas por el mezclador sub-armónico operando a 220 GHz así como por el array de mezcladores y el sistema cuasi-óptico cedido por la compañía Alfa Imaging. Se probaba en ambos casos la posibilidad de tomar imágenes con los componentes diseñados. Primero de todo, se utilizó un único píxel, es decir, el mezclador sub-armónico, al que se añadieron dos lentes para mejorar la definición de la imagen. Los resultados mostraron una buena resolución de los objetos y la variación del nivel de potencia dependiendo de su naturaleza. El usuario fue capaz de distinguir entre elementos como el cuerpo humano, una placa metálica o un material cerámico, obteniendo la posibilidad de identificarlos, por medio de la forma, y detectarlos. Finalmente, se tomaron algunas imágenes de una persona completa utilizando el array de 1x8 elementos y el sistema de espejos de Alfa Imaging. Las imágenes fueron tomadas al aire libre a una distancia de 4 metros del sistema de imagen. Se distinguió a la persona completamente y lo que es más, se detectó una placa metálica colocada en el pecho de dicha persona, ofreciendo una alternativa a los escáneres de aeropuertos actuales.

Esta Tesis ha sido enmarcada dentro de cuatro programas de investigación otorgados al Grupo de Antenas y ha contado con un apoyo industrial de fondo que la ha dotado de gran significancia en el campo de los THz. Pero no solo ha sido el resultado de algunos proyectos de investigación sino el punto de partida para que el Grupo de Antenas crease un laboratorio de THz y se convirtiera en una referencia nacional en este campo.

CONTENTS

ix

CHAPTER 1

INTRODUCTION

1.1   Background

Nowadays, the millimetre, 30 to 300 GHz, and sub-millimetre frequency ranges, 0.3 to 10 THz, have become of great interest for a wide range of applications such as materials research (spectroscopy, surface analysis, solid state reactions...), non-destructive testing (imaging/inspection of foams, ceramics, plastics, paper, textile…), bio-medicine (pharmaceuticals, biopsies, imaging…), security (counterfeit, antiterrorism…) and astrophysics (radiometers, atmosphere sensing…). The main reason is the advantages that this frequency region offers compare to the infrared and the visible range. The THz region (which includes the millimetre and sub-millimetre wave range) is situated between the microwave and the infrared frequencies, Fig. 1-1, and offers the possibility of obtaining images under extreme situations, such as low visibility scenarios provoked by clouds, fog, rain or even dust storms, as well as during the day or at night; which are not possible to obtained at other frequency ranges. This capability of "seeing" under such difficult scenarios has become of great importance for a revolutionary range of applications and has set an inflexion point in the design of imaging cameras, [Sie03a; Cha07; Tes07; Bog09]. The THz frequency range compared to the microwave, infrared and X-ray offers good resolution (~mm), good penetration depth (~cm), it is non-hazardous and high sensitive. Nevertheless, both metal and water block the radiation at these frequencies.
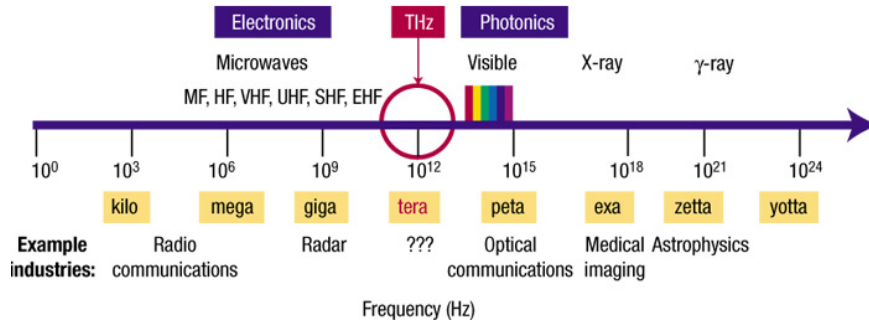
Fig. 1-1 Frequency Spectrum [Hwa05].

Furthermore, the atmospheric attenuation along the THz range is rather high; however, frequency bands in which this attenuation is relatively low can be found and for this reason, they become ideal candidates for the development of imaging formation cameras and for many other applications such as radar [Bae11; Coo11; Han11; Fut12] and communication systems [Iha95; Yu10; Hu11; Nas13]. These frequency bands are also known as "working windows" and can be found at different frequencies of the spectral range, 35 GHz, 94 GHz, 140 GHz, 220 GHz, 280 GHz, etc. [Wan09; Mar12].

The first image of Fig. 1-2 shows the atmospheric attenuation curves from 10 GHz to 1000 THz. It is possible to find out different frequency bands, "windows", in which the attenuation level decreases. The second image makes a zoom of the frequencies between 10 GHz to 1 THz. Here, the atmospheric attenuation curves under various levels of relative humidity (RH) and fog are shown. It is straightforward to identify the "working windows" aforementioned. Note also that, as the relative humidity increases the attenuation level increases and it would make more complicated to operate at these frequencies.
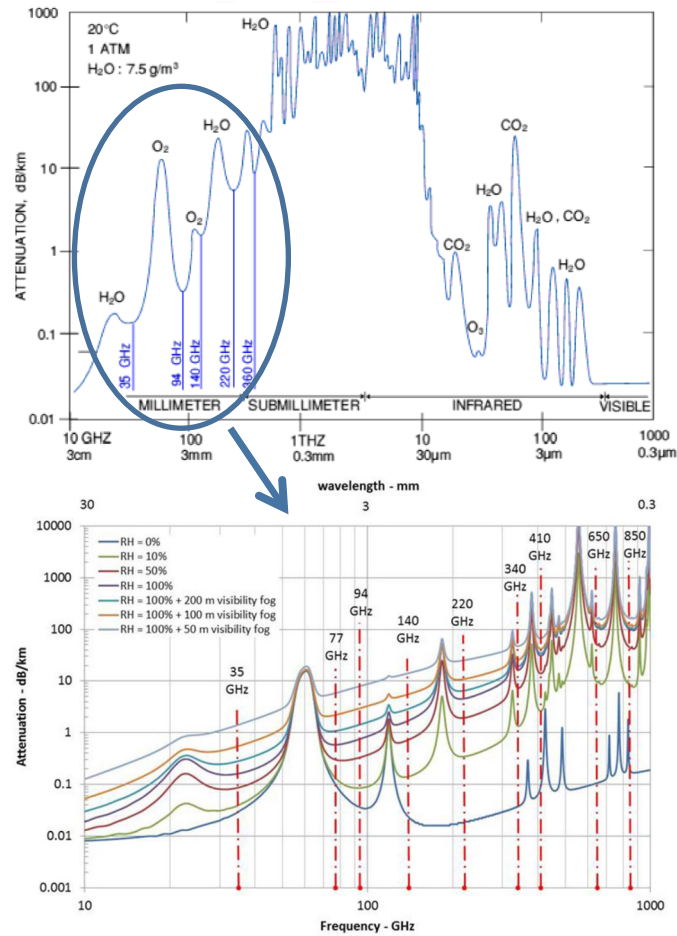
Fig. 1-2 Attenuation vs frequency, [Wan09; Mar12].

All natural objects which temperature is above absolute zero emit passive millimetre wave radiation. This radiation is related to the object temperature and important differences can be found in the radiation emitted by a cold and a hot object, see Fig. 1-3.
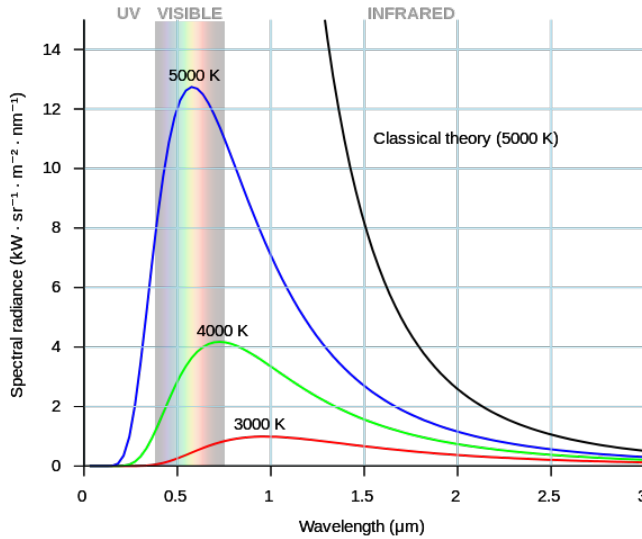
Fig. 1-3 Spectral radiation [WIKI].

Every single object has its particular absorption pattern which identifies him. Passive imaging cameras are based on this fact and, this is why, it is possible to detect and it is on the way to identify different objects that emit radiation at the THz range.

Even though the radiation emitted at the THz region is much lower compared to the emitted at the infrared, around 10^8 times less, the use of this frequency range is possible thanks to the better detector´s noise performance, 10^5 times better, and the temperature contrast, 10^3. Apart from the fact that THz detectors can reach a performance similar to the infrared ones, they also offer other important characteristics: they are non-ionizing that is, their emitted radiation is harmless to the human being; they offer a good penetration depth (~cm) compare to infrared, which can only penetrate depths of ~µm. This is of great importance in the design of imaging cameras at these frequencies since opens the possibility to detect hidden objects.

A passive imaging camera has a similar performance as a photo camera without flash, i.e., it is able to receive the energy emitted by a scene without the help of lighting unlike active cameras [Weg09; Llo10; Fri11].

Passive THz imaging cameras allow the user to see objects, materials and substances from which a different information can be obtained compare to other frequency ranges, as well as they offer the possibility to see through clothes (detecting hazardous objects, guns, explosives) [She04; App07; Liu07; Dav08; Sem08], detect chemical components [Yam04; Aji11], observe carcinogenic cells, [Cie00; Zha07], etc.; which has opened a wide variety of applications in the defence [Miy05; Hai07; Zha07] , astrophysics [Gai98; Tho04; Wan09, Tho09; Tho12], medical [Löf01; Sie04; Pic06; Sim09; Nal13] and agriculture sectors [Yon07; Eta11; Iri11; Kim12]. Some examples of the possibilities of a THz passive imaging camera are depicted in Fig. 1-4, Fig. 1-5 and Fig. 1-6.

(a)   (b)

Fig. 1-4 (a) Wooden sheet at the visible range. (b) Person and weapon detection at THz, (Image courtesy Alfa Imaging).

Fig. 1-4 (a) shows a wooden sheet. Nevertheless, it is possible to observe that a person is hidden behind it since his hands, which are holding the wooden sheet, are visible. However, it would be impossible to see that person at the visible range. This is why the same image has been taken at the THz range, Fig. 1-4 (b). Here the person who was hidden is perfectly distinguished and which is more important, a hidden gun at the chest´s person is also detected.
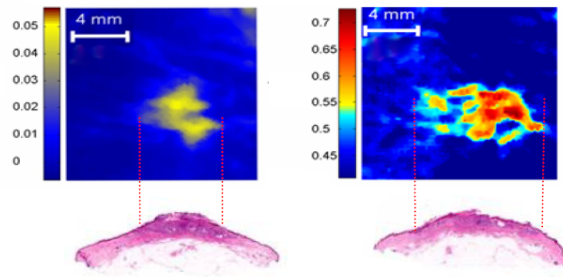
Fig. 1-5 THz skin cancer image (a) on the surface and (b) inside the tissue [TERAa].

The THz frequencies can also be really useful in the improvement of conventional biopsy processes since it is possible to identify more exactly the tissue needed to be removed and can facilitate a quicker and more precise diagnosis, Fig. 1-5.
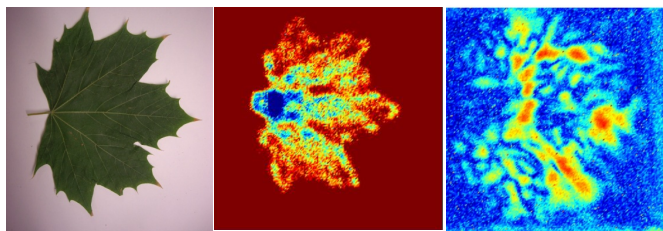
Fig. 1-6 (a) Leaf at the visible frequency range, (b) transmitted image and (c) reflected image of the leaf at the THz range, [Eta11].

Due to the absorption produced by the water at the THz frequencies, some applications to measure this value can be developed. An example could be the detection of plants´ water content, Fig. 1-6. The possibility of knowing at real time the condition of a plant and the necessity to be watered can be really useful at agriculture sectors.

At the moment, there are some companies that have developed or are on the way to develop commercial Passive millimetre-wave cameras, mostly for security and defence applications, Table 1-1.

Company	Products	Operating Frequency	Stand-off distances
Alfa Imaging [ALFA]	Alfa3Series	80-100 GHz	2-20 m

Brijot-Microsemi [MIC]	AllClear,	100-200 GHz	~cm
	Gen2,	80-100 GHz	~1 m
	MobileScan	80-100 GHz	~1 m
Digital Barriers [DIG]	ThruVision TS4	250 GHz	3-10 m
	ThruVision TS5	250 GHz	6-20 m
Millivision Technologies [MIL]	Portal System 350	Not specified	Portal area
	Walk-by System 350		~7 m
	Stand-off System 350		3-4 m
Sago Systems-Trex Enterprises [TREX]	Sago ST-150	Not specified	Not specified
Rapidscan Systems [RAP]	Rapidscan WaveScan 200	80-100 GHz	Not specified
Smiths detection [SMI]	Ego	Not specified	Not specified
QinetiQ [QIN]	SPO-7R	Not specified	14 m

Table 1-1 Commercial passive imaging THz cameras state-of-the-art.

Imaging THz cameras consist currently of a front-end and a receiver. Usually direct detection is employed in this kind of systems. However, when the operational frequency increases they become a problem since the low noise amplifiers, LNAs, used in direct detectors limit the system. This is due to the fact that they are just becoming to be developed in the last few years [Dea07; Puk08; Che10b; Kan10] and therefore, there aren´t commercial low noise amplifiers above 100 GHz, which make difficult their use at several hundreds of GHz and impossible above 1 THz. For this reason, the most commonly used receivers are based on heterodyne receivers [Llo08] instead of direct detection. Nevertheless, kinetic inductance detectors (KIDS) [Day03; Iac09; Woo11; Nar13] have become really important in the last few

years, mostly in the astronomy field, thanks to their high sensitivity values and the possibility of implementing large arrays.

Within heterodyne receivers [Sch02] superconductor insulator superconductor (SIS) [Sti94; Bar06; War08, End09; Bil12; Ker14] and hot electron bolometer (HEB) [Sch99; Bed04; Foc04; Ger05; Ger07; Rod10] can be found up to frequencies of several THz, offering good sensitivity, Fig. 1-7, with low LO power levels. However, their main disadvantage is that they need cooling in order to operate, (operational temperature 2 to 4 K) which make them expensive and unable to be used at applications in which cryogenic cooling is not possible. Then, the most typically heterodyne receivers used for the development of imaging cameras working at the millimetre and sub-millimetre wave range are based on Schottky diode (SD) mixers [Gal95; Meh98; Sil05; Guo08; Dra13] which offers a good sensitivity at this frequency range and don´t require cooling.
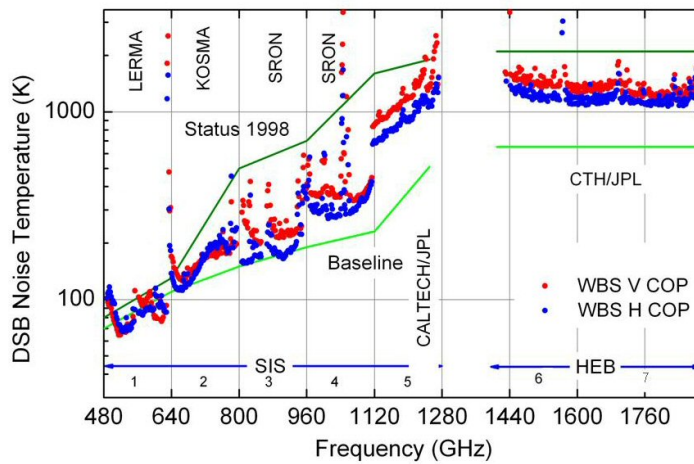
Fig. 1-7 HEB and SIS mixer state-of-the-art, [Her11].

Depending on the requirements of the receiver, i.e., sensitivity, Fig. 1-8, operating frequency, temperature and LO available power; the selection among Schottky diode mixers, HEB mixers and SIS mixers can be done.
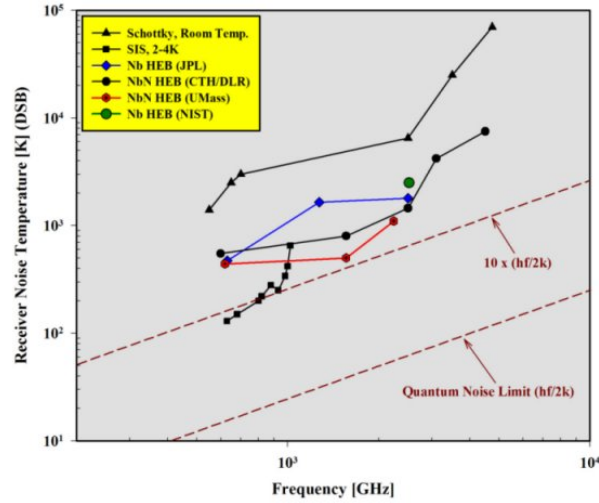
Fig. 1-8 Schottky diode, SIS and HEB mixer noise temperature comparison, [TRE].

When talking about SD mixers two kinds of configuration can be implemented. This is depending on the diodes employed: integrated diodes [Meh68; Mor05; Ald08] or discrete diodes [ACST; VDI; TERAb; UMS].

The use of discrete diodes (also known as flip-chip) is more widespread since not everybody has access to foundries in charge of the fabrication of integrated diodes and it is possible to find them commercially. Nowadays, there are several companies that commercialized flip-chip diodes. The most important ones are Virginia Diodes Inc. [VDI], ACST [ACST], United Monolithic Solutions [UMS] and Teratech Components Ltd. [TERAb]. All these companies offer varistor diodes typically used for mixer development. Moreover, VDI, ACST and Teratech also provide varactor diodes suitable for multipliers designs. Omnysis [OMN] is another company working on the development of Schottky diodes which is an important provider of THz range scientific remote sensing instrumentation for satellites.

However, if integrated diodes are employed, a better performance can be achieved compared to the use of discrete diodes especially when the operational frequency increases, [Meh94; Sta10; Ald11, Wan12]. This is due

to the fact that the diode´s physical characteristics, i.e. the series resistance and the junction capacitance, can be selected depending on the requirements of the mixer.
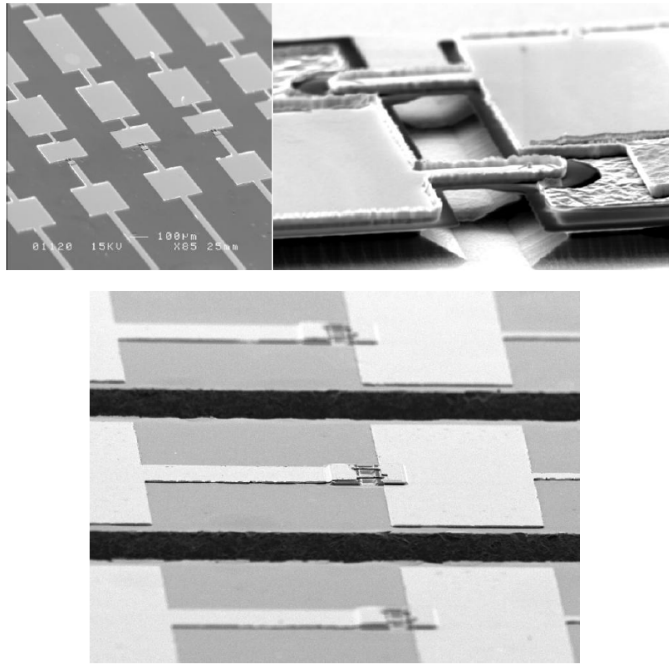
Fig. 1-9 Integrated Schottky diodes [Wan12].

Fig. 1-10 Discrete Schottky diodes [Wan12].

Moreover, when the operational frequency increases (>400 GHz) the use of discrete diodes becomes more complicated since its functionality is related to the shape and thickness of the substrate. This is why integrated diodes are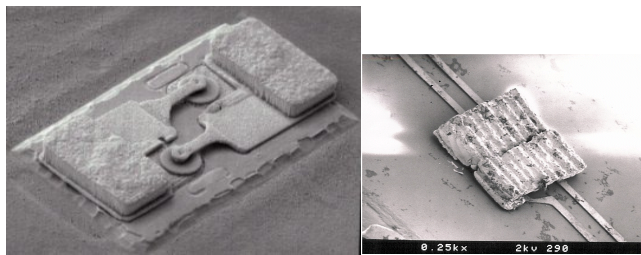 more frequently used at these frequencies since the fabrication and tolerances required need to be better. One of the reasons why discrete

diodes don´t reach mixer performances better than integrated ones is the mixer fabrication processes. These diodes need to be welded to the microstrip circuit by means of silver epoxy or beam leads which increments the diode´s series resistance and provokes a worse mixer performance. Moreover, the use of discrete diodes is usually related to universities and research laboratories which do not own the facilities to fabricate. It is also a point to take into account since diodes provided by commercial companies are never the best fabricated diodes, in terms of low series resistance, junction capacitance, etc., which influences extremely the mixer performance.

Sub-harmonic mixers are the most commonly used heterodyne receivers. This is usually thanks to the fact that this kind of mixers allow reaching higher RF frequencies without increasing the LO frequency since they use LO frequencies which are half the RF frequency.

Sub-harmonic mixers have been greatly used in the last thirty years and are well known devices. Nevertheless, there are few companies that commercialized them working at the THz range. The first one is Virginia Diodes [VDI]; the schottky diode sub-harmonic mixers commercialized by them are shown below, Table 1-2. See also Fig. 1-11 and Fig. 1-12 for more information about the mixer blocks and performance developed by VDI.

Model	*RF(GHz)*	*LO(GHz)*	*IF(GHz)*	*Tmix(K,DSB)*	*Lmix(dB,DSB)*
WR6.5SHM	110-170	55-85	<17	400-800	<7
WR5.1SHM	140-220	70-110	<22	500-1000	<7.5
WR4.3SHM	170-260	85-130	<26	600-1200	<8
WR3.4SHM	220-330	110-165	<33	700-1400	<8.5
WR2.8SHM	260-400	132-200	<40	800-1500	<9
WR2.2SHM	330-500	165-250	<40	1000-2000	<9.5
WR1.9SHM	400-600	200-300	<40	1200-2500	<10

| WR1.5SHM | 500-750 | 250-375 | <40 | 1500-3000 | <11 |
| WR1.2SHM | 600-900 | 300-450 | <40 | 7500-15000 | <15 |

Table 1-2 VDI sub-harmonic mixer characteristics.

(a)   (b)
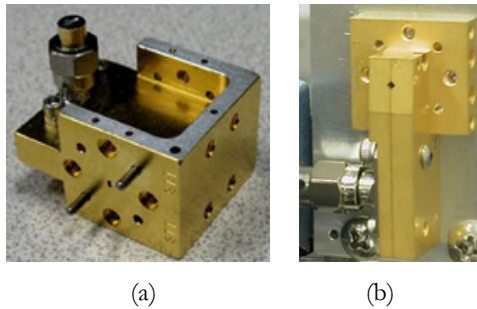
Fig. 1-11 VDI Sub-harmonic Mixers (a) WR-5.1SHM (140-220 GHz) and (b) WR-0.65SHM (1.1-1.7 THz) [VDI].
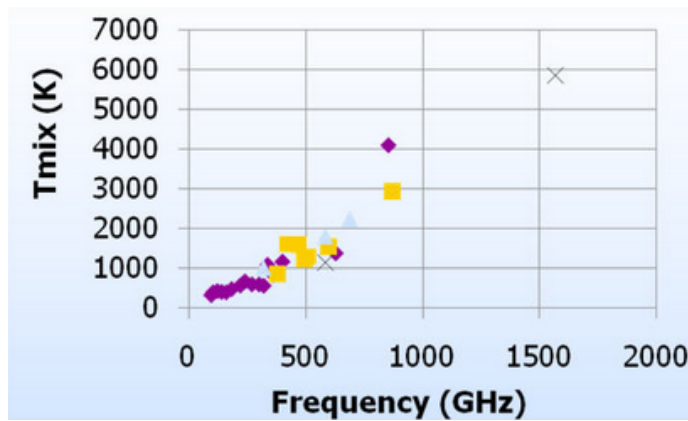
Fig. 1-12 VDI Sub-harmonic mixers performance [VDI].

Radiometer Physics GmbH, RPG, also commercialized schottky diode mixers, see Table 1-3. Their main characteristics are: extremely low noise figure, low conversion loss, high RF bandwidth, flat frequency response, and high IF bandwidth and zero bias, Fig. 1-13 and Fig. 1-14. [RPG]

Art. No.	RF [GHz]	*IF(GHz)*	*Tmix(K,DSB)*	*Lmix(dB,DSB)*
SHM-137	110-165	>20	500	6
SHM-150	130-170	>16	1000	6
SHM-183	167-200	> 16	1100	6
SHM-220	185-230	> 18	1100	6
SHM-280	265-295	> 18	700	7
SHM-300	275-300	> 18	1100	7
SHM-324	310-340	> 18	1200	8
SHM-424	380-440	>20	1650	9

Table 1-3 RPG sub-harmonic mixer characteristics.

Fig. 1-13 RPG Sub-harmonic Mixer working at 200 GHz, [RPG].
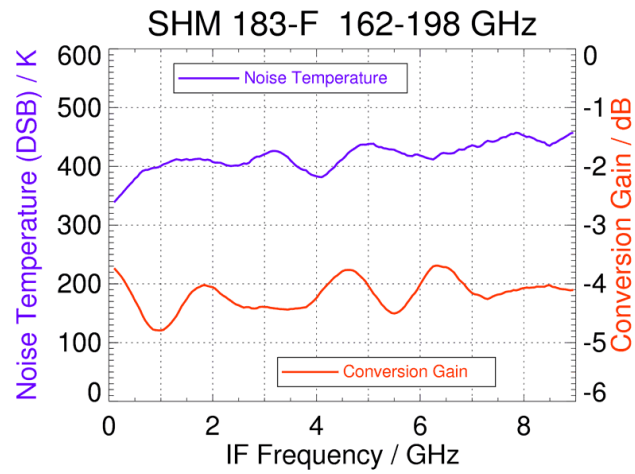
Fig. 1-14 RPG Sub-harmonic Mixer performance at 162-198 GHz, [RPG].

Another company which sells sub-harmonic mixers at the THz range is FARRAN Technology [FAR]. Their principal mixer models are shown in Table 1-4 and Fig. 1-15.

Model	*RF(GHz)*	*LO(GHz)*	*Lmix(dB,DSB)*
SPM-08	110-140	55-70	5 typ - 7 max
SPM-06	140-170	70-85	5 typ - 7 max
SPM-05	170-205	85-100	5 typ - 7 max
SPM-04	180-245	90-120	6 typ - 8 max
SPM-03	280-300	140	7 typ - 10 max
SPM-02	350-730	175	8 typ - 12 max

Table 1-4 FARRAN sub-harmonic mixer characteristics.

Fig. 1-15 Farran Sub-harmonic Mixers.

There are other companies such as Hxi, which commercializes harmonic mixers in the THz range but not sub-harmonic ones.

On the other hand, there are many research groups working on this topic. Some of the last sub-harmonic mixers results presented in bibliography are gathered in Table 1-5.

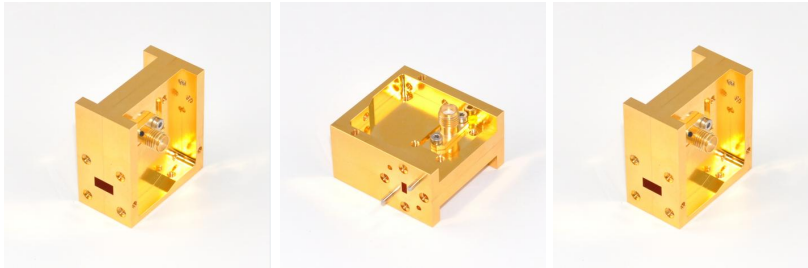| Mixer Ref	RF Freq	Substrate	Diodes	CL	NT
[Bo12]	92.1	RF/duroid 5880	Flip-chip	11.5 dB	-
[Che10a]	118	RF/duroid 5880	Flip-chip	12.6 dB	-
[Liu12]	150	Quartz (127 um)	Flip-chip	6.7 dB	-
[Wal11]	180	GaAs	Integrated	4.9 dB	608 K
[Por03]	183	Quartz	Flip-chip	5.1 dB	530 K
[Zha10a]	224	Quartz	Flip-chip	6.4 dB	-
[Wan12]	220.5	Quartz (127 um)	Flip-chip	7.1 simulated	-
[Meh98]	240	Quartz	Integrated	5.4 dB	510 K
[THo05]	330	Quartz (50 um)	Flip-chip	6.3 dB	700 K
[Wal11]	366	GaAs	Integrated	6.9 dB	1220 K
[Hes00]	380	Quartz	Flip-chip	8.5 dB	850 K
[Sch10]	520-590	GaAs (5 um)	Integrated	-	2200 K
[Hui00]	585	Quartz	Integrated	8 dB	1200 K
[Tho10]	865.8	GaAs	Integrated	8.02 dB	2660 K

Table 1-5 Research groups results on sub-harmonic mixer characteristics.

Note from Table 1-5 that, as commented previously, when the RF frequency increases integrated diodes are employed.

Apart from the research groups working in this field, there are also some European and International projects focused on the development of mmw and sub-mmw components and cameras. At the moment, the TeraScreen project (2013-2016) is working on the development of a multi-frequency THz imaging camera and the INSIDDE project (2013-2015) is making used of the THz technology in order to analyse unknown details in paintings, but during the last few years there have been other European projects focused on research at the THz range such as:

THz-bridge: Investigated the interaction of THz radiation with biological systems. (2001-2004)

OPTHER: Had the aim to develop new vacuum devices for amplification of T-rays (THz frequencies). (2008-2011)

DOTNAC: Proposed to develop a fast, high resolution, non-invasive and non-contact aeronautic composite parts during production using THz waves. (2010-2013)

MIDAS: Critical schottky varactor diodes and simulation tools for fabricating state-of-the-art sub-millimetre wave components and sources have been developed. (2010-2013)

TeraComp: Worked on THz heterodyne receiver components for future European space missions. (2010-2013)

TeraComb: Is focused on the development of quantum cascade lasers based THz frequency combs. (2012-2015)

DOTSeven: Is on the way to develop silicon germanium (SiGe) heterojunction bipolar transistor (HBT) technologies with cut-off frequencies up to 700 GHz. (2012-2016)

Moreover the European Space Agency, [ESA11], has also launched some projects related with this issue and some of the specifications they demanded for sub-millimetre wave mixers are described in Table 1-6.

RF Freq.	NT	CL	RF Bandwidth
183 GHz	<500 K	<5 dB	19.8 GHz
243 GHz	<700 K	<6.5 dB	8 GHz
325 GHz	<900 K	<5 dB	22 GHz
448 GHz	<1700 K	<7 dB	17.4 GHz
664 GHz	<2500 K	<9 dB	13.4 GHz

Table 1-6 ESA sub-harmonic mixer requirements.

Taking into account the state-of-the-art presented here, there has been a long study on millimetre and sub-millimetre wave components but

more limited in the development of systems such as imaging cameras. Therefore, it is still an important research field since there is a great commercial attention paid on it. The Spanish and European Governments are providing projects focused on this field with the intention of developing commercial devices and imaging cameras at the THz region. Due to this, this thesis has been focused on the development of millimetre and sub-millimetre wave components in order to design a THz imaging camera, framed within the following research projects:

CENIT-Seduce- Development of explosives detection systems in public institutions and infrastructures (2008024012) provided by the Spanish Industry Administration. (2009-2011)

TEC-Development of THz Imaging Cameras based on metamaterial technology provided by the Spanish Science and Innovation Administration, TEC 2009-11995. (2010-2013)

INNPACTO- Development of a sub-millimetre wave range Imaging Camera for security applications provided by the Spanish Science and Innovation Administration. (2010-2013)

FP7 TeraScreen- Multi-frequency multi-mode Terahertz screening for border checks provided by the European Commission. (2013-2016)

1.2   Framework and Scope of the research

This dissertation began when the THz frequency range was becoming of great interest due to the new applications that offered compared to other frequency ranges. Thanks to the importance this frequency range was obtaining, relevant research projects were funded with the aim of developing THz technology due to the commercial possibilities suspected. This dissertation is framed within some of these projects and counts on an industrial background support which makes it of high significance in the THz field. Applications based on guns, explosives and hazardous objects detection and identification; systems located at border checks or airports;

and luggage control; are critical for society security nowadays and become the main objective of the technology developed within this dissertation.

The funding offer by the Cenit Seduce as well as the INNPACTO and TEC projects provided the possibility to develop a complete operational receiver at 220 GHz for defence and security applications. This receiver became a 1x8 array thanks to the support offered by these projects and a complete imaging camera, whose receiver was the aforementioned array, was developed, fabricated and tested. Moreover, the 220 GHz array is also part of a multi-frequency multi-mode THz screening system which is been developed at the TeraScreen project. Taking all of this into account, a significant work has been done within this thesis with a wide range of industrial and commercial capabilities specially focused on the defence and security sectors.

Furthermore, the results of this dissertation will position the Antenna Group in the development of millimetre and sub-millimetre wave mixers as a national reference in this field, not only in the designing of mm and sub-mm wave components but also in their fabrication and testing. The main contents of this thesis have been divided into seven chapters.

First of all, Chapter 2 studies different measurement techniques commonly used in the characterization of mixers operating at this frequency range. It is of great importance since the following chapters of this dissertation will be based on the development of millimetre and sub-millimetre wave mixers and a good knowledge of the characterization techniques is crucial. The three main techniques (the attenuator, noise injection and gain procedures) are presented, analysed and compared. Moreover, three detection methods (a power meter (PM), a YIG filter together with a PM and a Spectrum Analyser) were part of the study. This research was carried out at the Rutherford Appleton Laboratory in the UK. Finally, the chapter ends with a study about the use of different IF Chains in the measurement process which reveals the importance of a good matching between the components in order to obtained comparable results.

The conclusions reached at this chapter will be employed in the characterization of the components of this thesis.

Chapter 3 presents the complete development and measurements of a sub-harmonic mixer working at an RF frequency of 220 GHz. Moreover, COC (cyclic olefin copolymer) substrate has been employed in the design of all components presented in this dissertation which adds a novelty to the THz receivers' implementation, proving that its use leads to a better performance due to its lower losses. It is also remarkable that the whole process (design, fabrication and measurement), has been done entirely by the Antenna Group of Public University of Navarra.

The fourth chapter deals with the development of a 1x8 sub-harmonic mixer array at 220 GHz which will be the receiver part of a passive millimetre wave imaging camera implemented by the aforementioned projects. In this chapter the eight mixer components are presented and measured and the quasi-optical part of the passive millimetre wave, PMMW, camera is analysed. Note that it is one of the few 1x8 heterodyne receivers design, fabricated and tested at present. Moreover, this array will also be implemented in a multi-frequency multi-mode THz screening camera. This system is been developed by the Terascreen Project and will be able to operate at 94, 220 and 360 GHz.

The main novelty of the work is presented in Chapter 5. This chapter presents new approaches in the development of heterodyne receivers and develops a 4th-harmonic mixer operating at an RF frequency of 440 GHz. Moreover, a sub-harmonic mixer working at the same RF frequency is also presented and the performances of both devices are compared. In order to collate both components, a frequency multiplier (doubler) is developed and presented in this chapter. All this work is also placed within the aforementioned research projects.

One of the last chapters, Chapter 6, is focused on the imaging results of the components presented along this dissertation. Here some images

taken at the THz range by the sub-harmonic mixer developed in Chapter 2 and the PMMW camera presented in Chapter 3 are shown.

Finally, Chapter 7 presents the conclusions and future research lines obtained from this dissertation.

To sum up, this thesis concludes with the design, fabrication and test of a set of new components for the THz field, which are totally functional and operative for this industry:

- A 1x8 sub-harmonic mixer array receiver which is part of a THz imaging camera working at 220 GHz.

- A 4th-harmonic mixer with an RF frequency of 440 GHz.

- A sub-harmonic mixer operating at an RF frequency of 440 GHz.

- A frequency doubler with an output frequency of 220 GHz.

- Results of the imaging system at 220 GHz.

CHAPTER 2

CHARACTERIZATION OF MEASUREMENT TECHNIQUES OF MILLIMETRE WAVE MIXERS

2.1 Introduction

This dissertation is focused on the development of several millimetre and sub-millimetre wave mixers as commented in Chapter 1. For this reason, it is of great importance to know the different characterization procedures available for this technology and to compare them in order to obtain a conclusion about their differences and which one is best to be used. The results obtained from this chapter will be the basis of the measurements done within this dissertation.

There are several procedures commonly employed for measuring the performance of millimetre and sub-millimetre wave mixers [Fab85; Kan11]. In general they all require the de-embedding of the mixer performance from Y-factor measurements. The performance of a mixer can vary considerably depending on the measurement technique employed. However to the best of our knowledge the different already known procedures employed to characterize mm and sub-mm wave mixers have not previously been studied in depth and compared using a reference mixer/receiver test set-up. Furthermore, as there is no standard approach adopted by the millimetre wave community for mixer characterization it is difficult to contrast the

performance of different mixers presented in the literature and in manufacturer websites.

The aim of this work is to address this issue by measuring the performance of a 183 GHz sub-harmonic mixer using the three most common procedures found in the literature, i.e. the "Attenuator procedure" [Hes99; Tho04a; Tho05; Tho08a], the "Gain procedure" [Ali93; Tre09] and the "Noise injection procedure" [Den98; Wan08]. For each of these procedures three different detection methods have been studied, i.e. a Broadband Power Meter, a Tuneable YIG Filter added to Broadband Power Meter, and a Spectrum Analyser with 50 MHz resolution bandwidth.

This comparison has never been done before and although the procedures presented in this chapter are well-known, it is important to determine the most appropriate measurement procedure and method for characterizing a mixer operating at millimetre and sub-millimetre wave frequencies. Furthermore, the deviations among the different procedures and methods need to be clarified. This chapter resolves this open interrogation by a careful analysis.

In addition to the resolution of the best approach to measure a mm/sub-mm wave mixer by cross-examination through measurement of the aforementioned procedures and methods, another important open issue has been investigated and solved – that is the effect of including or omitting an isolator between the mixer and IF pre-amplifier on the measured performance of the mixer [Pos86; Maa05]. There is still a great controversy over its possible effect since studies assuring that its use is an advantage can be found in [Maa93; Agi04], meanwhile others rejecting it [Lau01] or without considering its possible influence [Tra83; Sch06] are reported in the literature. This chapter will sort out this controversy by means of studying the influence of the mismatch when the isolator is introduced into the receiver chain. On one hand, matching between the mixer and isolator and, on the other hand, between the mixer and the first

IF amplifier, are found to be the responsible for the encountered discrepancies in the literature.

2.2   Mixer basic concepts and definitions

A receiver is a system that selects, amplifies and detects a desired signal isolating it from the rest of signals and noise. The main characteristics of a receiver are: *sensitivity*, the ability of detecting weak signals; *fidelity*, the ability of reproduce the characteristics of the desired signal; and *selectivity*, the ability of reject non-desired signals close to the desired one [Sie03].

2.2.1   Receiver classification

Different kind of receivers can be found depending on the way of isolating the signal from the interferences.

Homodyne receivers

Homodyne receivers are the simplest ones theoretically but also the least used at communication systems due to its major problems obtaining a good selectivity [Sie03b]. The topology followed by this kind of receivers is presented in Fig. 2-1.
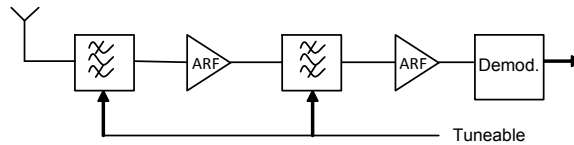

Fig. 2-1 Homodyne receiver topology.

The antenna detected signal is selected and amplified directly to the required power level for the demodulator operation. This kind of receivers requires tuneable filters which make them poor on selectivity.

Nowadays, the applications of homodyne receivers are limited to radar and radiometry working at low frequencies, below 500 MHz.

Heterodyne receivers

Heterodyne receivers perform the frequency mixing, which consists on the conversion of a low power level signal, (commonly called the RF signal) from one frequency to another (IF frequency which is different to zero) by combining it with a higher power (local oscillator) signal in a device with nonlinear impedance (such as a diode or a transistor). In these mixers its output is proportional to the product of the input voltages defined as follows, [Sie03]:

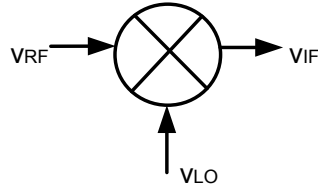$$v_{IF}(t) = K v_{RF}(t) v_{LO}(t) \qquad\qquad 2\text{-}1$$

Fig. 2-2 Mixer schematic.

Where $v_{RF}(t)$ can be defined as a modulated carrier whose frequency is f_{RF}, $v_{RF}(t) = V_{RF}x(t)\cos(w_{RF}t + \phi(t))$, and $v_{LO}(t)$ is a sinusoidal signal with frequency f_{LO}, $v_{LO}(t) = V_{LO}\cos(w_{LO}t)$. The mixing of those signals will give $v_{IF}(t)$ which will consist of two modulated carriers of frequencies $f_{RF} + f_{LO}$ and $f_{RF} - f_{LO}$ with the same modulation as $v_{RF}(t)$. The final signal $v_{IF}(t)$ will be:

$$v_{IF}(t) = \frac{K}{2}V_{LO}V_{RF}x(t)\big[cos\big((w_{RF} + w_{LO})t + \phi(t)\big) + cos\,((w_{RF} - w_{LO})t + \phi(t))\big] \quad 2\text{-}2$$

This way, the mixer output signal consists of two replicas of the input signal with a frequency shifted to $\pm f_{LO}$, Fig. 2-3.
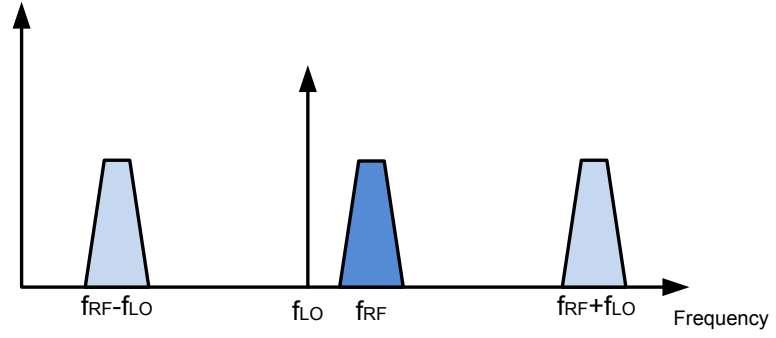
Fig. 2-3 Input and output signals of a mixer.

The mixing of the signals is usually obtained using non lineal elements such as diodes or transistors. Taking into account that the response of a non-lineal quadripole can be defined by a polynomial function:

$$v_{IF}(t) = K_1 v(t) + K_2 v(t)^2 + K_3 v(t)^3 + \cdots \qquad 2\text{-}3$$

The corresponding output signal of the mixer scheme presented in Fig. 2-2 for an input equal to the addition of v_{RF} and v_{LO} would be defined by:

$$v_{IF}(t) = K_1\big(v_{RF}(t) + v_{LO}(t)\big) + K_2\big(v_{RF}(t) + v_{LO}(t)\big)^2 + K_3\big(v_{RF}(t) + v_{LO}(t)\big)^3 + \cdots = \cdots 2K_2 v_{RF}(t)v_{LO}(t) \ldots \qquad 2\text{-}4$$

The Equation 2-4 is composed by a group of terms of the following form $K_{m,n} v_{RF}(t)^m v_{LO}(t)^n$. If a basic harmonic mixer is desired, the term that will give the product of the input voltages will depend only of the coefficient of second grade. The rest of the terms that are part of Equation 2-4 will become spurious mixing products which generate signals of frequencies $mf_{RF} \pm nf_{LO}$. These spurious mixing products are known as intermodulation products of order $m + n$ which power decreases when the order increases. It is possible to eliminate the intermodulation products by different methods: using filters or combining several mixers.

The typical topology followed by a heterodyne receiver is presented in Fig. 2-4.
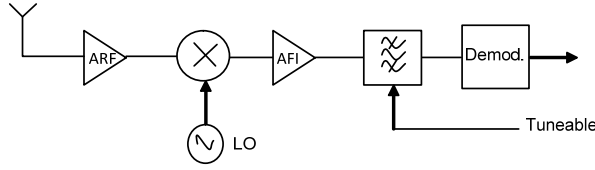
Fig. 2-4 Heterodyne receiver topology.

Sub-harmonic mixers

Sub-harmonic mixers are of great interest as a first stage in the design of receivers at the millimetre and sub-millimetre wave range. These mixers are a type of harmonic mixers in which the desired mixing product is $K_{1,2}v_{RF}(t)v_{LO}(t)^2$. This kind of mixers mixes the second harmonic of the LO with the signal giving place the following intermediate frequency $f_{IF} = |2f_{LO} \pm f_{RF}|$. They offer several advantages compared to basic harmonic mixers since they make possible to reduce the Local Oscillator, LO, frequency and so that, they increase the available power at the require frequency. This way, it is possible to feed different array configurations with the same LO. The LO frequency is half the radio frequency, RF.

When working at high RF frequencies (THz frequencies) heterodyne receivers are usually based on sub-harmonic mixers due to the important advantages that they offer compare to their colleagues. A sub-harmonic mixer, as well as a fundamental mixer, is able to detect two different RF signals (the signal and the image) separated   f: the lower side band, $f_{RF}(LSB) = 2f_{LO} - f_{IF}$, and the upper side band, $f_{RF}(USB) = 2f_{LO} + f_{IF}$.
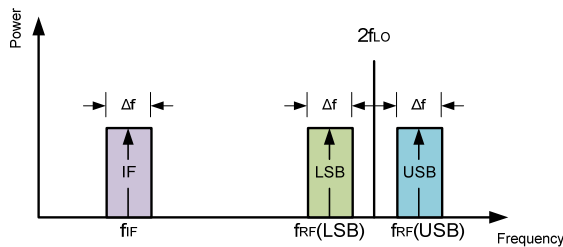

Fig. 2-5 Sub-harmonic mixer principle of operation.

The third order components, $2f_{RF} - f_{LO}$ or $2f_{LO} - f_{RF}$, are not produced by an ideally quadratic component and sub-harmonic mixers are bound to use a couple of quadratic components in order to obtain these mixing products.

Typically, mixer and frequency multipliers at the millimetre and sub-millimetre waves are implemented by means of Schottky diodes in order to mix frequencies. The principle of this kind of diodes resides in the use of metal contact deposited on a semiconductor substrate of type N, usually Gallium Arsenide (GaAs). This substrate provides high electron mobility. Then a very high-conductivity layer is grown up on the top of the substrate in order to assure low series resistance. The buffer and the substrate are heavily doped and an N epitaxial layer is grown on top of them Fig. 2.6. The contact between the metal anode and the epitaxial creates the Schottky contact [Maas03].
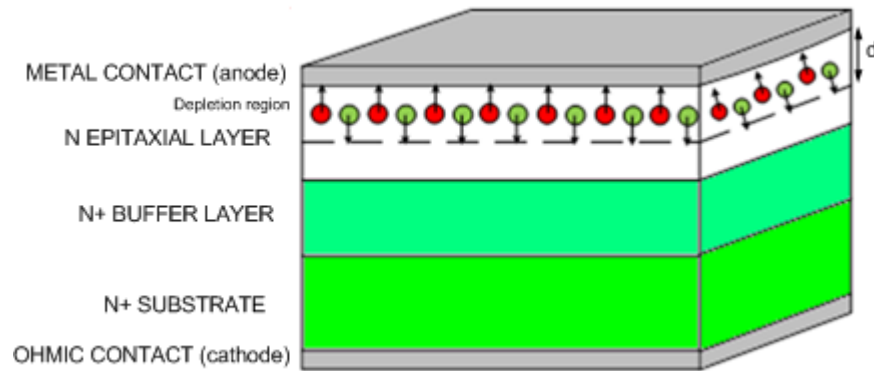

Fig. 2-6 Schottky-barrier diode cross section.

Depending on the diodes characteristics, the mixer behaviour will be different. The physical and electrical characteristics of the diode can influence heavily the mixer performance and therefore, the better the diodes are the better the mixer design can be. Playing with the anode size, the epitaxial thickness etc., better ideal factor or series resistance can be reached and a substantial difference can be seen in the mixer performance.

Three alternatives of voltage and current polarities are possible when working with diodes, [Maa03]:
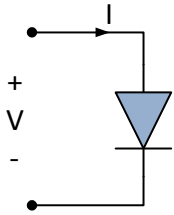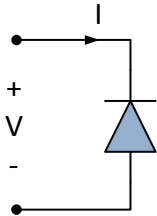
The I/V characteristic of the diode when is forward biased is given by:

$$I = f(V) = K_1V + K_2V^2 + K_3V^3 + K_4V^4 + \cdots \qquad \text{2-5}$$
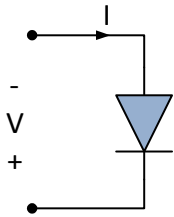
If the voltage is reversed, the odd harmonics become negative:

$$I = f(-V) = -K_1V + K_2V^2 - K_3V^3 + K_4V^4 + \cdots \qquad \text{2-6}$$

On the other side, if the diode is reversed biased, then the even harmonics are the ones that become negative:

$$I = -f(-V) = K_1V - K_2V^2 + K_3V^3 - K_4V^4 + \cdots \qquad \text{2-7}$$

The diodes employed for nonlinear devices are often connected in parallel or series in order to eliminate certain harmonics or mixing products. The possibility to eliminate spurious signals without turn to use filtering is a valuable solution. There are basically two interconnections when working with nonlinear devices, the anti-parallel and the anti-series. Sub-harmonic mixers usually make use of anti-parallel configuration.

Fig. 2-7 shows the anti-parallel interconnection of two ideal diodes. The current in diode A is found from Equation 2-5 and diode´s B current can be calculated using Equation 2-7.
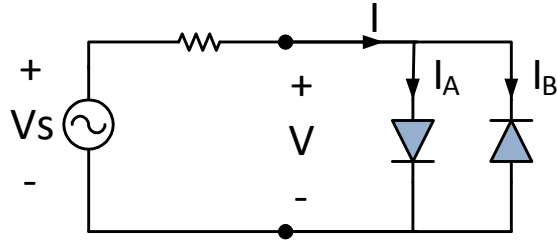

Fig. 2-7 Anti-parallel diode configuration.

$$I_A = f(V) = K_1 V + K_2 V^2 + K_3 V^3 + K_4 V^4 + K_5 V^5 + \cdots \qquad \textit{2-8}$$

$$I_B = -f(-V) = K_1 V - K_2 V^2 + K_3 V^3 - K_4 V^4 + K_5 V^5 + \cdots \qquad \textit{2-9}$$

$$I = I_A + I_B = f(V) - f(-V) = 2K_1 V + 2K_3 V^3 + 2K_5 V^5 + \cdots \qquad \textit{2-10}$$

Note that when a heterodyne mixer is analysed V can be replaced by v_{IF}, Equation 2-1. So that, the value of I for a sub-harmonic mixer with an anti-parallel diode configuration can be defined by:

$$I = 2[K_1(v_{RF} + v_{LO}) + K_3(v_{RF} + v_{LO})^3 + K_5(v_{RF} + v_{LO})^5 + \cdots]=$$
$$2[K_1(v_{RF} + v_{LO}) + K_3(v_{RF}{}^3 + 3v_{RF}{}^2 v_{LO} + 3v_{RF} v_{LO}{}^2 + v_{LO}{}^3) + K_5(v_{RF}{}^5 +$$
$$5v_{RF}{}^4 v_{LO} + 10v_{RF}{}^3 v_{LO}{}^2 + 10v_{RF}{}^2 v_{LO}{}^3 + 5v_{RF} v_{LO}{}^4 + v_{LO}{}^5) +$$
$$\cdots] \qquad \text{2-11}$$

Equation 2-11 confirms that the odd harmonics are the only ones produced by the pair of diodes while the even harmonics remain trapped inside the pair of diodes due to their anti-symmetry, if and only both diodes are the same model. This is the main reason why anti-parallel configuration is used in sub-harmonic mixers and therefore it is the configuration employed in the mixer design presented in this dissertation.

As previously commented, sub-harmonic mixers have great advantages, for instance, they offer the possibility of using an LO frequency half the RF, allowing the use of sources with enough power to pump the millimetre-wave devices. Another important advantage is the possibility of suppressing

the noise generated by the lateral bands of the LO signal, and due to the use of a pair of diodes in anti-parallel configuration, it is easier to match at the IF band. Nevertheless, they also have some disadvantages mainly owing to the use of a pair of diodes instead of a single one; they require a more important level of LO power to pump both diodes and as well, the noise generated by them will be larger.

Superheterodyne receivers

Superheterodyne receivers are heterodyne receivers which require of a tuneable local oscillator source. The topology implemented by this kind of receivers is shown in Fig. 2-8.
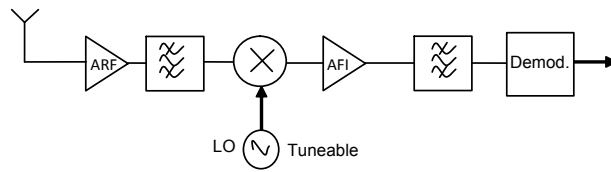

Fig. 2-8 Superheterodyne receiver topology.

This kind of receivers is one of the most remarkable and used ones [Toh14]. They are widely spread in applications such as television [Fis53] and radio [Bee29]. They are also implemented in other applications such as airbones [Chr02]. Superheterodyne receivers have been the selected ones in this kind of applications over the 20th century offering the possibility of working at IF frequencies instead of RF with good sensibilities and more stable systems compare to direct conversion receivers or tuned radio frequency receivers.

Direct conversion receivers

Direct conversion receivers have the same principle of operation as heterodyne receivers but in this case the RF frequency is equal to the LO frequency, Fig. 2-9, and the IF frequency is set to zero.
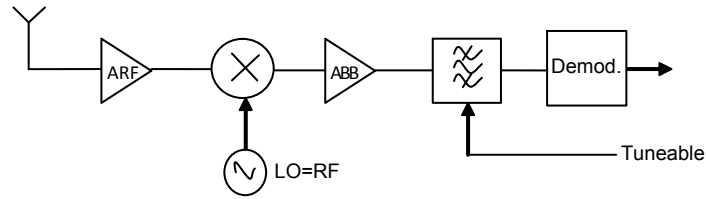
Fig. 2-9 Direct conversion receiver topology.

Their major advantages are that, in this case, they need a low pass filter and a band base amplifier, i.e. simpler IF stages, which make them easier to implement; they avoid image rejection issues and they have high selectivity. However, when talking about THz frequencies the LO source is required to be at higher frequencies, RF frequency, which complicates the system. Another important problem is the difficulty related to the synchronization between both signals, the LO and RF, when the frequency increases. Nevertheless they are really widespread at lower frequencies where the LO frequency requirements are not a problem.

Direct conversion receivers are mainly used in cell phones and communications [Gui05; Kin05], medical imaging devices [Bass12] and astrophysics [Hoe14].

Double conversion receivers

Sometimes it is necessary to make receivers with more than one conversion since the selectivity required is too high or they work at a really wide frequency band. In those cases double conversion receivers are employed. The topology followed by these receivers is presented in Fig. 2-10.
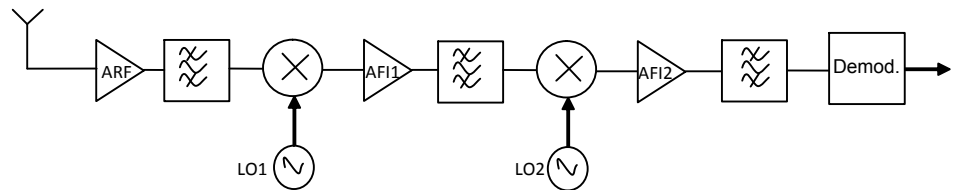

Fig. 2-10 Double conversion receiver topology.

2.2.2   Receiver parameters

In order to characterize the sensitivity of a receiver, in general, and a mixer, in particular, two important parameters are used: the conversion loss and the equivalent noise temperature.

The mixer conversion loss, L_{mix}, is defined by the ratio between the input power of the RF signal to the IF output power signal. It is usually express in dB and can be calculated as follows, [Sie03]:

$$L_{mix}(dB) = -10log\left(\frac{P_{IF}}{P_{RF}}\right) \qquad\qquad 2\text{-}12$$

Mixers, as any other electronic components, are noise sources. So that, it is important to have a general idea of the principal kinds of noise that can be found: Thermal noise, Shot noise and Flicker noise.

Thermal noise: Also called Nyquist noise or Johnson noise. It is caused by the random movement of the free electron in a conductor due to thermal agitation. It is generally the most common and can be found in any lossy element of a passive circuit, such as, resistances, transmission lines or any other lossy component. In a mixer, a critical point is the diode series resistance; minimizing it, the noise temperature can be decreased.

Shot noise: Results from the crossing of the free electrons through the potential barrier. This type of noise only exists when currents are going over the device. It can be found on Schottky junctions.

Flicker noise: It is thought to be associated to the crystalized structure of the component. It is considered negligible against thermal noise when frequency increases.

The different noises which are presented in a mixer can be grouped and considered as a white noise source. Moreover, the white noise source can be modelled on a thermal noise equivalent source, and it is characterized by an equivalent noise temperature, Te, which is proportional to noise power and expressed in Kelvin degrees (K), Fig. 2-11 .

$$T_e = \frac{N_0}{kB} \qquad\qquad 2\text{-}13$$

Where N_0 represents the noise power, k is the Boltzmann´s constant ($k=1.38 \cdot 10^{-23}$ W/Hz/K) and B is a fixed bandwidth determined by the most restrictive bandwidth of the receiver chain in Hz.
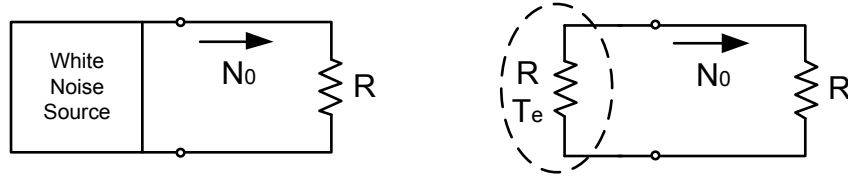

Fig. 2-11 Schematic of equivalent Noise Temperature of a white noise source.

The equivalent noise temperature can also be express as a function of the Noise Factor of a device, F:

$$T_e = (F - 1)T_0 \qquad\qquad 2\text{-}14$$

Where T_0 is the room temperature in Kelvin degrees, and F measures the deterioration of Signal to Noise Ratio (SNR) between the input and output of a device, Equation 0-15.

$$F = \frac{S_i/N_i}{S_0/N_0} \qquad\qquad 2\text{-}15$$

Where S_i and N_i are the input power of the signal and the noise respectively and S_0 and N_0 represents the output power values respectively.

The mixer noise temperature of a device can be measured by means of the Y factor which will be explained further on this chapter. It is important to take under consideration that when measuring the mixer noise temperature two cases can be contemplated. This is the case of considering the noise coming from the imaging band or not. In the case of considering that both, the noise coming from the desired frequency as well as the imaging band frequency affects the mixer noise temperature; the mixer will be characterized by the double side band temperature model, T_{DSB}. If only the noise coming from the desired signal band is considered the mixer will be characterized by the single side band noise temperature, T_{SSB}. This

dissertation will consider the DSB noise temperature model which is generally half the SSB mixer noise temperature, Fig. 2-12.
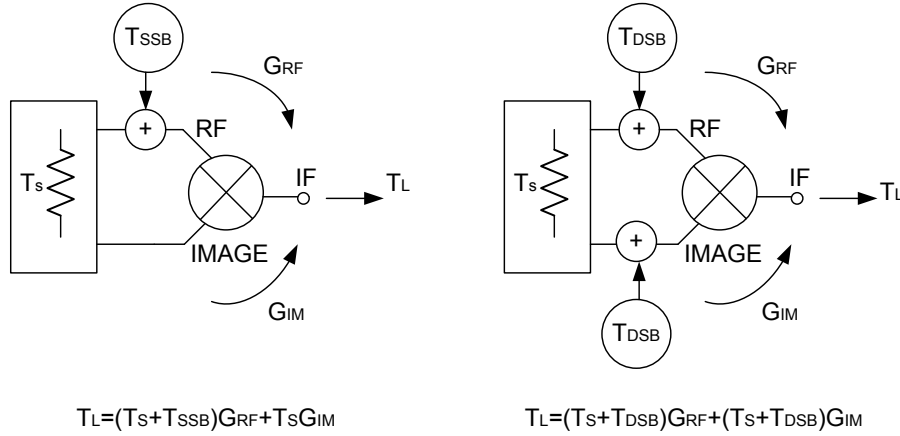

$$T_L=(T_S+T_{SSB})G_{RF}+T_S G_{IM} \qquad\qquad T_L=(T_S+T_{DSB})G_{RF}+(T_S+T_{DSB})G_{IM}$$

Fig. 2-12 T$_{SSB}$ and T$_{DSB}$ mixer noise temperature models of a mixer device.

Independently of the mixer noise characterization model, TSSB and TDSB, the noise presented in a mixer is the same, TL. This is why; a relation between both mixer noise characterization models can be reached:

$$T_{SSB} = T_{DSB}\left(1 + \frac{G_{IM}}{G_{RF}}\right) \qquad\qquad 2\text{-}16$$

If a receiver is composed by multiple cascade noisy components with its own noise temperature, noise figure and gain, the overall noise temperature can be expressed using the Friss Formula, [Maa93].

$$T_e = T_{e1} + \frac{T_{e2}}{G_1} + \frac{T_{e3}}{G_1 G_2} + \frac{T_{e4}}{G_1 G_2 G_3} \ldots \qquad\qquad 2\text{-}17$$
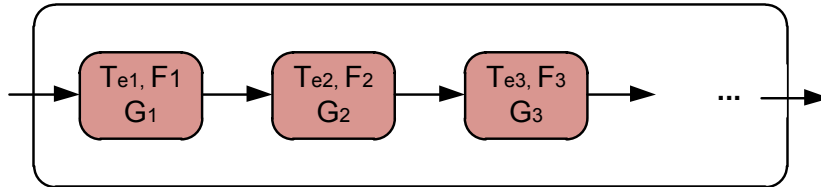

Fig. 2-13 Cascade system.

The overall noise can also be expressed in terms of noise figure as follows:

$$F = F_1 + \frac{F_2 - 1}{G_1} + \frac{F_3 - 1}{G_1 G_2} + \frac{F_4 - 1}{G_1 G_2 G_3} \dots \qquad \textit{2-18}$$

Equations 2-17 and 2-18 are obtained assuming that:

- The noise contribution outside the system´s final bandwidth will be rejected by the corresponding filters.
- The most important filtering is done at the final stages of the system.
- There is no frequency conversion or the spurious noise bands have been rejected.
- Every component has a lineal behaviour.

The cascade noise system characteristics are dominated by the first stages since the effect of every stage is softened by the product of the gain of previous stages. The best option when trying to minimize the noise of a receiver is locating a low noise amplifier as first stage which allows ignoring the noise of subsequent stages. Note that in order to design a low noise temperature system it is important to obtain high gain, G_n, and low T_{en} values in the first stage. Nevertheless typical LNAs do not usually counts with really high gains. Moreover, at the sub-millimetre wave range there are no LNA´s available and the mixer is the only component at the first stage of the system which results in noisier systems.

Another important issue of a receiver is the sensitivity, which is directly related to the noise temperature of the complete system, and can be defined as the smallest change of temperature of the signal that can be detected. In order to improve the sensitivity of the system it is important to maintain the noise temperature as low as possible. It can be express by:

$$\Delta T = \frac{T_{sys}}{\sqrt{B\tau}} \qquad \textit{2-19}$$

Where Tsys is the noise temperature of the receiver, B is the operational bandwidth and   the integration time.

2.3   Measurement Procedure

Here the three most commonly employed procedures are described. But first, in order to understand every measurement procedure a significant concept has to be explained. This is the Y-factor method, [Räi80; Agi10; Roh12; Agi14]. This method is widely employed in the characterization of amplifiers and mixers in order to calculate its gain and noise temperature. When a noise source is employed, the Y-factor method allows the user to calculate the internal noise of the device under tests (DUT) and therefore its noise figure or effective input noise temperature.

In order to carry on with the Y-factor measurements, the DUT is connected to a source and its power is measured with the source ON and OFF (N_{ON} and N_{OFF}), Fig. 2-14. The ratio of these two values determines the Y-factor:

$$Y = \frac{N_{ON}}{N_{OFF}} \qquad\qquad 2\text{-}20$$
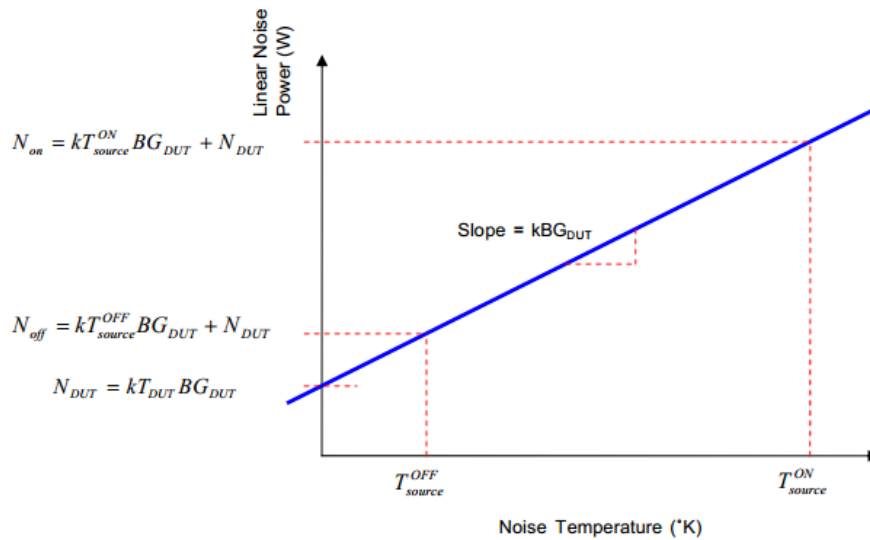

Fig. 2-14 Y-factor variables [Roh12].

2.3.1   Attenuator Procedure

This measurement procedure requires receiver and IF Y-factor measurements to be performed with and without a coaxial attenuator connected to the input of the IF chain (between mixer and pre-amplifier). The measurements result in two simultaneous equations from which mixer noise temperature and conversion loss can be de-embedded. Fig. 2-15 presents the two receiver measurement scenarios. The receiver Y-factor measurements are performed by presenting hot (295 K) and cold (80K) blackbody loads to the feedhorn input. The IF Y-factor measurements are performed by terminating the input of the IF chain with a 50 Ω coaxial load via a short length of semi-rigid cable. The coaxial load acts as a hot load at room temperature and a cold load when immersed in liquid nitrogen.
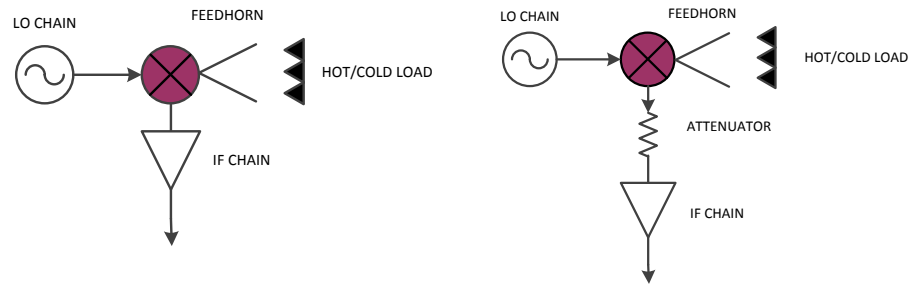

Fig. 2-15 Attenuator Method set-up.

With the attenuator omitted the receiver Y-factor is:

$$Y_{rx} = \frac{P_{HOT}}{P_{COLD}} = \frac{T_{HOT} + T_{rx}}{T_{COLD} + T_{rx}} \qquad\qquad 2\text{-}21$$

Rearranging, the noise temperature of the receiver is:

$$T_{rx} = \frac{T_{HOT} - Y_{rx} T_{COLD}}{Y_{rx} - 1} \qquad\qquad 2\text{-}22$$

With the attenuator in position the receiver Y-factor is:

$$Y_{rx,att} = \frac{P_{HOT}}{P_{COLD}} = \frac{T_{HOT} + T_{rx,att}}{T_{COLD} + T_{rx,att}} \qquad\qquad 2\text{-}23$$

Rearranging, the noise temperature of the receiver is:

$$T_{rx,att} = \frac{T_{HOT} - Y_{rx,att} T_{COLD}}{Y_{rx,att} - 1} \qquad\qquad 2\text{-}24$$

Two simultaneous equations result:

$$T_{rx} = T_{mix} + L_{mix}T_{IF} \qquad \qquad 2\text{-}25$$

$$T_{rx,att} = T_{mix} + L_{mix}T_{IF,att} \qquad \qquad 2\text{-}26$$

T_{IF} and $T_{IF,att}$ are calculated following the same process described above.

Rearranging Equations 2-25 and 2-26 the conversion loss and the noise temperature of the mixer are calculated from

$$L_{mix} = \frac{T_{rx} - T_{rx,att}}{T_{IF} - T_{IF,att}} \qquad \qquad 2\text{-}27$$

and

$$T_{mix} = T_{rx} - L_{mix}T_{IF} \qquad \qquad 2\text{-}28$$

2.3.2   Noise-Injection Procedure

This procedure for measuring mixer performance is similar to the previous method. The only difference is the equipment used to generate the two different IF noise temperatures. Here, noise is injected into the input of the IF chain using a noise source and directional coupler. Fig. 2-16 presents the two receiver measurement scenarios with the noise source switched ON or OFF. The receiver and IF Y-factor measurements are performed as described previously.
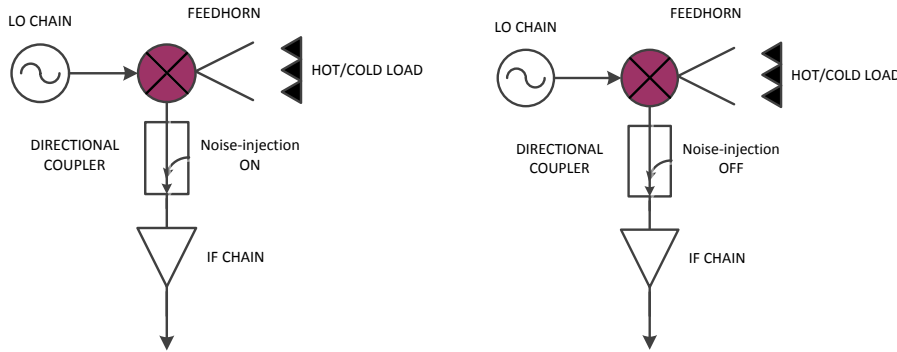

Fig. 2-16 Noise-injection method set-up.

With the noise source OFF, the receiver Y-Factor is:

$$Y_{OFF} = \frac{P_{HOT}}{P_{COLD}} = \frac{T_{HOT} + T_{rx,OFF}}{T_{COLD} + T_{rx,OFF}}$$

2-29

Rearranging, the noise temperature of the receiver is:

$$T_{rx,OFF} = \frac{T_{HOT} - Y_{OFF} T_{COLD}}{Y_{OFF} - 1}$$

2-30

With the noise source ON, the receiver Y-Factor is:

$$Y_{ON} = \frac{P_{HOT}}{P_{COLD}} = \frac{T_{HOT} + T_{rx,ON}}{T_{COLD} + T_{rx,ON}}$$

2-31

Rearranging, the noise temperature of the receiver is:

$$T_{rx,ON} = \frac{T_{HOT} - Y_{ON} T_{COLD}}{Y_{ON} - 1}$$

2-32

As before, two simultaneous equations result:

$$T_{rx,OFF} = T_{mix} + L_{mix} T_{IF,OFF}$$

2-33

$$T_{rx,ON} = T_{mix} + L_{mix} T_{IF,ON}$$

2-34

With knowledge of $T_{IF,OFF}$ and $T_{IF,ON}$ the mixer performance can be calculated.

Rearranging Equations 2-33 and 2-34 the conversion loss and the noise temperature of the mixer are calculated from:

$$L_{mix} = \frac{T_{rx,OFF} - T_{rx,ON}}{T_{IF,OFF} - T_{IF,ON}}$$

2-35

And

$$T_{mix} = T_{rx,OFF} - L_{mix} T_{IF,OFF}$$

2-36

2.3.3 Gain Procedure

This measurement procedure is different from those previously described requiring Y-factor measurements of a single receiver and IF chain. These measurements are used to directly calculate the gain of the mixer. The Y-factor measurements are performed in an identical manner as described previously.

From the Y-factor measurement of the receiver the following equations result:

$$P_{HOT,rx} = (T_{rx} + T_{HOT})kG_{rx}B \qquad\qquad \textit{2-37}$$

$$P_{COLD,rx} = (T_{rx} + T_{COLD})kG_{rx}B \qquad\qquad \textit{2-38}$$

Rearranging, the receiver gain is obtained:

$$G_{rx} = \frac{P_{HOT,rx} - P_{COLD,rx}}{KB(T_{HOT} - T_{COLD})} \qquad\qquad \textit{2-39}$$

From the Y-factor measurement of the IF chain the following equations result:

$$P_{HOT,IF} = (T_{IF} + T_{HOT})kG_{IF}B \qquad\qquad \textit{2-40}$$

$$P_{COLD,IF} = (T_{IF} + T_{COLD})kG_{IF}B \qquad\qquad \textit{2-41}$$

Rearranging, the gain of the IF chain is obtained:

$$G_{IF} = \frac{P_{HOT,IF} - P_{COLD,IF}}{KB(T_{HOT} - T_{COLD})} \qquad\qquad \textit{2-42}$$

The mixer gain is then calculated as:

$$G_{mix} = \frac{G_{rx}}{G_{IF}} = \frac{P_{HOT,rx} - P_{COLD,rx}}{P_{HOT,IF} - P_{COLD,IF}} \qquad\qquad \textit{2-43}$$

and

$$L_{mix} = \frac{1}{G_{mix}} \qquad\qquad \textit{2-44}$$

Once the conversion loss is known, the noise temperature of the mixer can be calculated using Equation 2-28.

2.4   Description of the test receiver

2.4.1   Nominal Receiver Configuration

The configuration of the test receiver is shown in Fig. 2-17. A frequency synthesiser attached to a sextupler is used to generate the desired LO frequency. Following an isolator can be found in order to avoid the reflected signal to go back to the synthesiser. After that, a variable

attenuator is employed to control the power of the LO signal that will get the mixer. The mixer under test is a sub-harmonic mixer; model number FDP-044 MTT C developed at the Rutherford Appleton Laboratory, with an RF bandwidth 160-200 GHz. This device comprises an integrated anti-parallel diode circuit fabricated using the UMS foundry process. The mixer, with feedhorn attached, is shown in Fig. 2-18. The feedhorn is from TRG Alpha industries (SN861G/387).
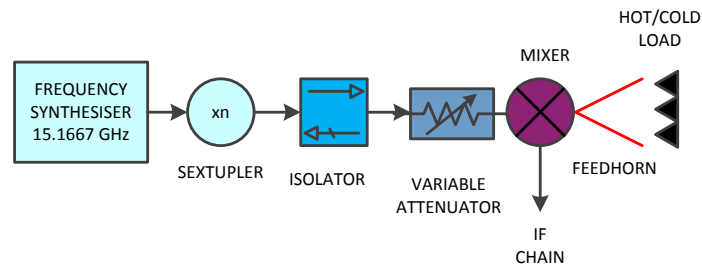

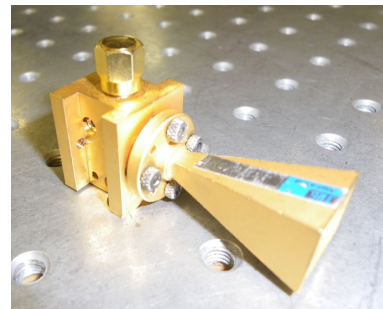Fig. 2-17 Schematic of the Test Receiver.

Fig. 2-18 Mixer Block and Feedhorn.

The IF Chain, operating over the bandwidth 2.5-3.5 GHz, consists of the following components:

- Pre-amplifier: Miteq JS2-02300370-045-0P (SN838791)

Gain: 35 dB

Noise Figure: 0.5 dB

Bandwidth: 2.3-3.7 GHz

Bias: +4V @ 102 mA

- Bandpass filter: Lorch Microwave 71Z5-3000/R1000-S

Center frequency: 3 GHz

Bandwidth: 1 GHz

- Amplifier: Herotek A801-251 (SN167864), +12V

Gain: 35 dB

Noise Figure: 3.5 dB

Bandwidth: 1-10 GHz

Bias: +12V @ 149 mA

- Isolator: MfN AT-11A-G0136-AF (SN90373726)

Bandwidth: 2-4 GHz

The IF chain is thermally stabilised using an active controller. This hardware is described in Section 2.3.2.
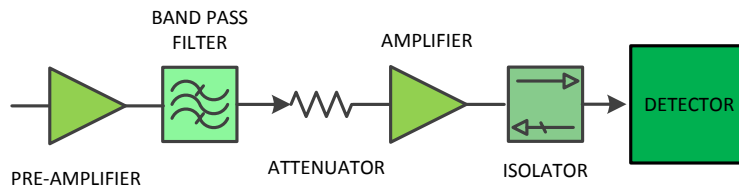

Fig. 2-19 Schematic of the IF Chain.

An identical isolator as listed above shall be connected to the input of the IF chain to determine its effect on the measured mixer performance.

The Local Oscillator chain, shown in Fig. 2-20, consists of the following components:

- Frequency synthesiser: HP83752A

- W-band sextupler: RPG AFM-X6-110

- W-band isolator: RPG WFI-110

- W-band 90° waveguide twist
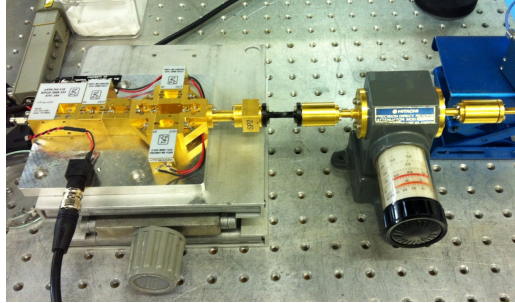
- W-band variable attenuator: Hitachi W1518

Fig. 2-20 LO Chain.

2.4.2 Thermal Stabilisation of IF Chain

The temperature of the IF chain is actively stabilised to achieve the best gain stability of the amplifiers. A Minco heater and PT100 temperature sensor were mounted to the baseplate of the IF chain, and are controlled via a Eurotherm 2416 PID controller. The IF chain is enclosed in a polystyrene box for good thermal insulation. The Eurotherm controller was tuned and a set-point of 43 °C was selected. The thermal stabilisation hardware is shown in Fig. 2-21 and Fig. 2-22.
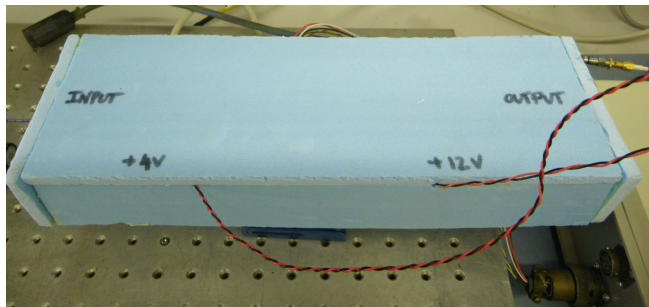

Fig. 2-21 IF Chain in Box.

Fig. 2-22 Eurotherm Active Temperature Controller.

The effect of temperature stabilisation is shown in Fig. 2-23 and Fig. 2-24. The graphs show the output power level versus time and noise temperature of the IF chain for three cases:

- With active temperature control as described above

- With passive temperature control (i.e. with the IF chain enclosed in the insulated box and allowed to warm up for 45 minutes)
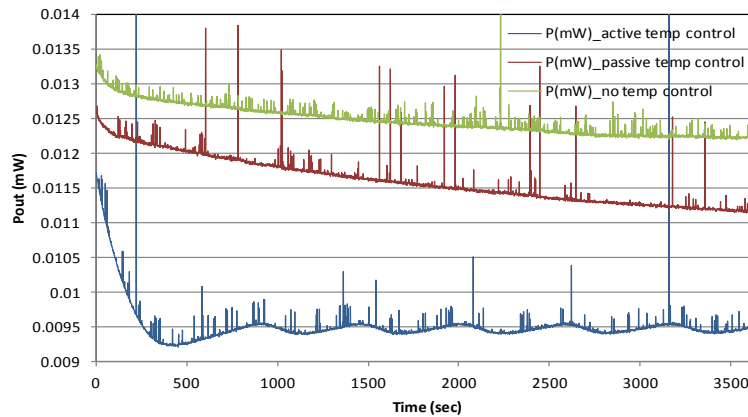
- With no insulated box

Fig. 2-23 IF Output Power with/without Thermal Stabilisation.

In Fig. 2-23 the output power level of the IF chain is plotted over a 60 minute interval. It can be seen that the output power gradually decreases (as component temperature increases) for the cases of no temperature

control and passive temperature control. A constant output power level is achieved, after an initial settling time, when active temperature control is employed. The ripple in the constant output power level can be reduced with fine tuning of the Eurotherm controller.

The IF noise temperatures presented in Fig. 2-24 (calculated using the gain method and extracting the T_{DSB}) show similar performance when passive and active control is employed. More variation in the noise temperature is observed when no temperature control is used. The benefit of temperature control is not highly evident in this example. This is due to the fact that the IF bandwidth is narrow (2.5-3.5 GHz). As the bandwidth increases and component input/output VSWR degrades and varies more over the bandwidth, it is expected that the benefit of active temperature control will become more evident.
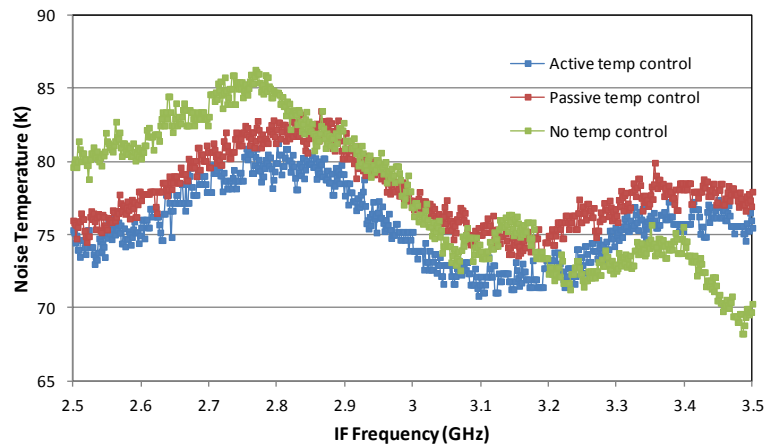

Fig. 2-24 IF Noise temperature with/without Thermal Stabilisation.

2.4.3   Preliminary Receiver Set-Up

An LO test frequency of 91 GHz was selected for the mixer tests. A preliminary receiver Y-factor measurement was undertaken to determine a suitable LO pump power for all the measurements. The performance of the receiver is shown in Table 2-1. An LO pump power of 2.5 mW was selected.

Pout (mW)	Attenuation (dB)	PHOT (µW)	PCOLD (µW)	Y-Factor	Trec (K)
1	17.4	2.45	2.37	1.0337	6299.82
2	14.5	2.60	2.22	1.17117	1176.06
2.5	13.6	2.57	2.18	1.17889	1121.86
3	12.9	2.69	2.29	1.17467	1150.89
4	11.7	2.85	2.45	1.16326	1236.92
5	10.9	2.98	2.60	1.14615	1391.09

Table 2-1 Mixer performance at 91 GHz LO frequency.

2.5   Detection Methods

Three detection techniques have been employed for each measurement procedure. The first uses a microwave power meter (Gigatronics 8542B Universal Power Meter) with associated broadband power sensor (Gigatronics Power sensor model 80303A 0.01-26.5 GHz), Fig. 2-25. This broadband measurement technique provides an average value of mixer noise temperature and conversion loss over the IF bandwidth. The limitation of this technique is that no resolution is provided across the IF bandwidth.

Fig. 2-25 Gigatronics Power Meter & Sensor.

The second detection technique incorporates a tuneable YIG filter (PM 7440) between the output of the IF chain and the input of the Gigatronics power sensor. The filter has a bandpass response with a

bandwidth of 34 MHz. The filter tuning is computer controlled via GPIB interface. The filter requires a bias voltage of 22V.
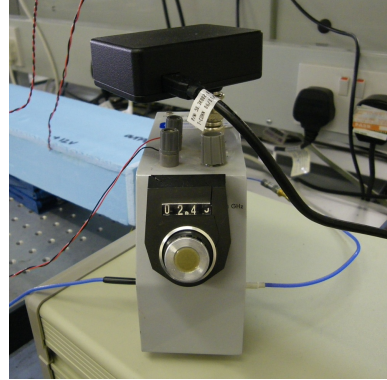

Fig. 2-26 YIG Filter.

The third detection method makes use of a Rohde and Schwarz FSU series spectrum analyser, Fig. 2-27. The Analyser is connected to the output of the IF chain. The settings used for the measurements were RBW=50 MHz, VBW=30 Hz, ST= 1.7s, Detector=RMS.
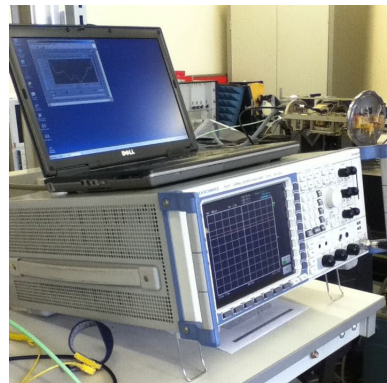

Fig. 2-27 Rohde & Schwarz FSU Spectrum Analyser.

2.6 Mixer Results for Attenuator Procedure

2.6.1 Broadband Measurements using Power Meter

Table 2-2 presents the measured mixer performance employing the attenuator method and broadband power meter. Performance is presented with and without an isolator connected between the mixer and IF pre-amplifier. A considerable change in mixer performance is observed with the inclusion of the isolator.

Use of Isolator	Mixer Noise Temperature (K)	Mixer Conversion Loss (dB)
Without isolator	691	7.8
With isolator	824	6.9

Table 2-2 Measured Mixer Performance: Attenuator Method, Broadband Power Meter

2.6.2 Narrowband Measurements using YIG Filter and Power Meter

The measured mixer performance employing the attenuator method and YIG filter / power meter is shown in Fig. 2-28. Again a considerable change in performance is observed with the inclusion of the isolator. A comparison with the broadband results shows that in both cases the mixer noise temperature is higher and conversion loss is lower with the isolator included.
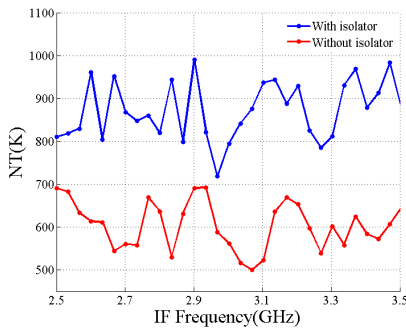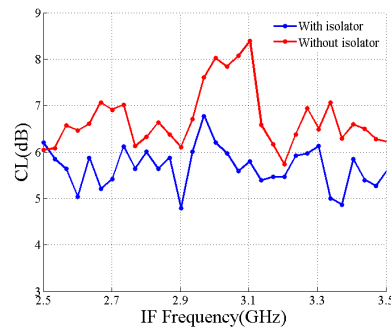
(a)   (b)

Fig. 2-28 (a) Noise temperature and (b) conversion loss: Attenuator procedure, YIG Filter/Power meter.

2.6.3 Narrowband Measurements using Spectrum Analyser

Fig. 2-29 depicts the measured mixer performance employing the attenuator method and the spectrum analyser. As with the previous results, the mixer noise temperature is higher and conversion loss is lower with the isolator included.
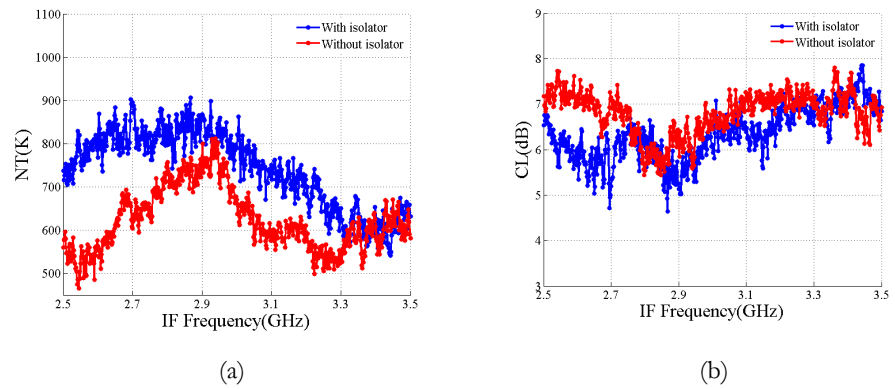

(a)   (b)

Fig. 2-29 (a) Noise temperature and (b) conversion loss: Attenuator procedure, Spectrum Analyser.

2.7 Mixer Results for Noise-injection Procedure

2.7.1 Broadband Measurements using Power Meter

The measured mixer performance employing the noise-injection test procedure and the broadband power meter are presented in Table 2-3. For this set of measurements the isolator is positioned between the mixer and coupler. As with the previous test method, the mixer noise temperature is higher and conversion loss lower when as isolator is employed.

Use of Isolator	Mixer Noise Temperature (K)	Mixer Conversion Loss (dB)
Without isolator	750	7.3
With isolator	971	6.5

Table 2-3 Measured Mixer Performance: Noise-Injection Method, Broadband Power Meter.

2.7.2 Narrowband Measurements using YIG Filter and Power Meter

Fig. 2-30 exhibits the mixer performance employing the noise-injection method with YIG filter and the power meter.
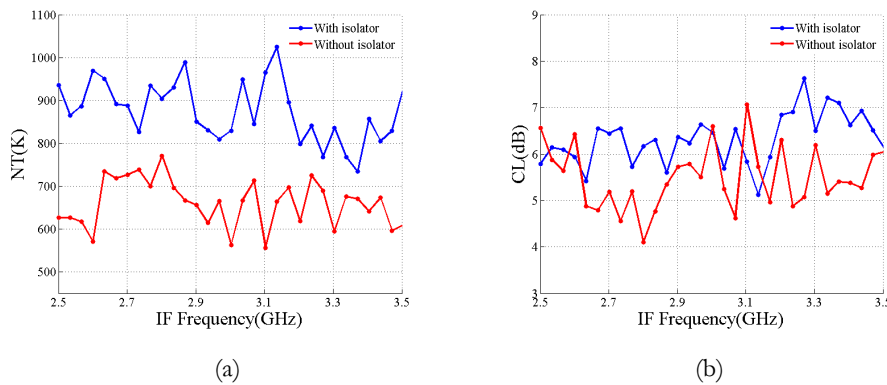

Fig. 2-30 (a) Noise temperature and (b) conversion loss: Noise-injection procedure, YIG Filter / Power meter.

2.7.3 Narrowband Measurements using Spectrum Analyser

The mixer performance using the noise-injection method with spectrum analyser is shown in Fig. 2-31.
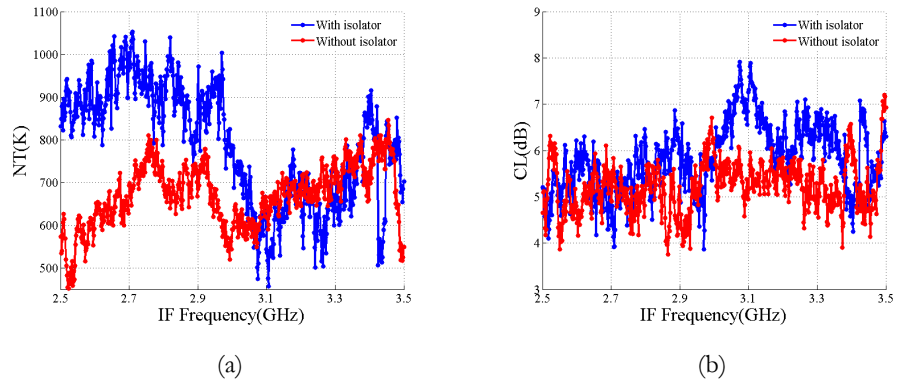
Fig. 2-31 (a) Noise temperature and (b) conversion loss: Noise-injection procedure, Spectrum Analyser.

2.8 Mixer Results for Gain Procedure

2.8.1 Broadband Measurements using Power Meter

Table 2-4 presents mixer performance employing the gain test method with broadband power meter. Again noise temperature is higher and conversion loss is lower when an isolator is included.

Use of Isolator	Mixer Noise Temperature (K)	Mixer Conversion Loss (dB)
Without isolator	803	6.2
With isolator	896	6.0

Table 2-4 Measured Mixer Performance: Gain Method, Broadband Power Meter.

2.8.2 Narrowband Measurements using YIG Filter and Power Meter

The mixer performance employing the gain method with YIG filter and power meter is depicted in Fig. 2-32.
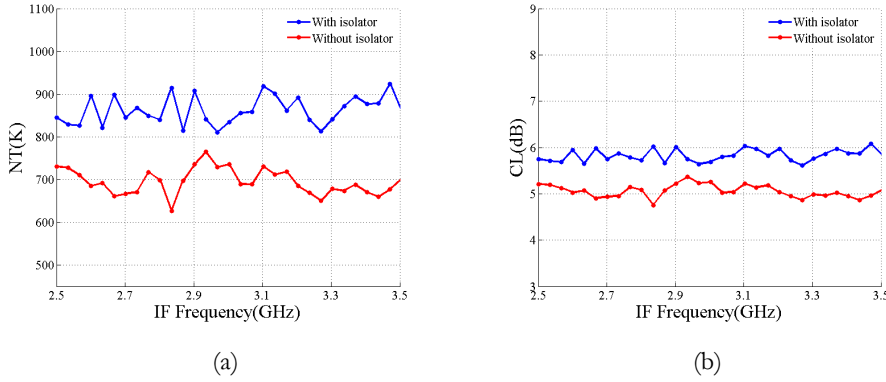
Fig. 2-32 (a) Noise temperature and (b) conversion loss results gain procedure, YIG Filter.

2.8.3 Narrowband Measurements using Spectrum Analyser

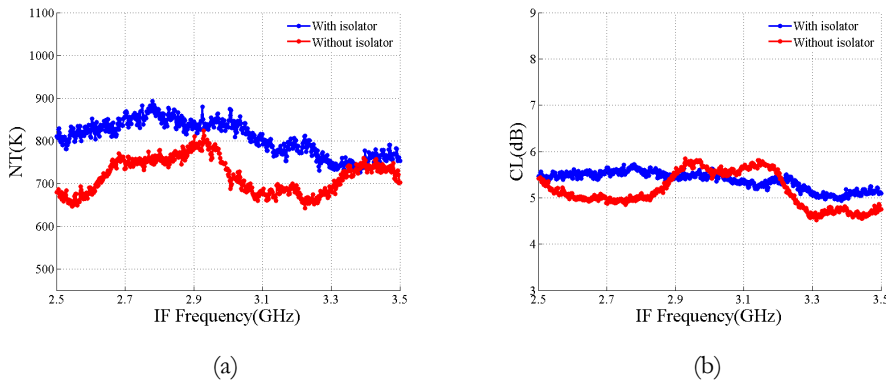Fig. 2-33 presents mixer performance employing the gain method with spectrum analyser.

Fig. 2-33 (a) Noise temperature and (b) conversion loss results gain procedure, Spectrum Analyser.

2.9 Comparison of results

A comparison of the results previously shown is done in this section. The results of every measurement procedure are presented for the different detection methods employed.

2.9.1 Broadband Power Meter Results

The three different procedures of calculating the mixer NT and CL show that in the case of not having the isolator between the mixer and the pre-amp, the noise temperature is lower. This difference can be appreciated in Table 2-5 which sums up all the results measured with the Power meter.

Method	Set-up	Noise Temperature (K)	Conversion Loss (dB)
Attenuator method	Set-up +isolator	824	6.9
Attenuator method	Set-up	691	7.8
Noise-inject method	Set-up +isolator	971	6.5
Noise-inject method	Set-up	750	7.3
Gain method	Set-up +isolator	896	6.0
Gain method	Set-up	803	6.2

Table 2-5 Summary of the Power meter results.

The isolator adds noise to the system but it also makes the results measured with the different procedures were more similar to each other than without having it.

Analysing the conversion loss results it is straightforward to see that they are lower when having the isolator into account independently of the method employed. Note that some discrepancies can be caused by the measurement process. The process that has been followed to carry on with this study is: for every detection method, the setup was ready and the necessary measurements were done in order to apply the three calculation procedures. The fact that the setup was reassembled every time the detection device changed can be the reason why these discrepancies appear.

2.9.2 Narrowband Results using YIG Filter and Power Meter

Fig. 2-34 shows the summary of all procedures results for the mixer Noise temperature with, (a), and without using an isolator, (b), at the IF input measuring it with the YIG filter and the Power meter.

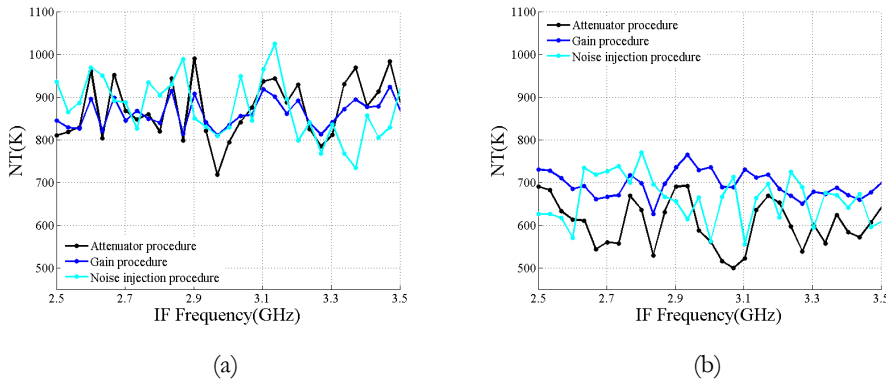(a)   (b)

Fig. 2-34 Mixer noise temperature (a) with and (b) without isolator, YIG filter.

The Noise temperature average when having the isolator is around 870 GHz. The Gain procedure is the one that less variation has between different values, so this would make this procedure the most stable one.

In the case of not having the isolator at the IF chain input the mixer noise temperature is lower and the results calculated by the three procedures are further away. When the Attenuator procedure is used the average is around 600 K. For the Gain procedure the NT average is around 700 K. In the case of the noise-injection procedure the NT average is also around 700 K but its values are less stable than using the gain procedure.

Fig. 2-35 depicts the summary of all procedures results for the mixer conversion loss with and without the isolator at the IF input using the YIG Filter and the power meter to measure them.

As happening with the noise temperature results, in this case the most stable conversion loss is obtained when the gain procedure is used. The average value of the mixer conversion loss, when using the isolator is around 6 dB, Fig. 2-35 (a).

In the case of not using the isolator the results are similar, Fig. 2-35 (b). Using the attenuator procedure the CL average is around 6.5 dB. When using the gain procedure the CL average approx. 5 dB. For the noise-

injection procedure the average value is around 5.5 dB. The most stable procedure in this case is also the gain one.
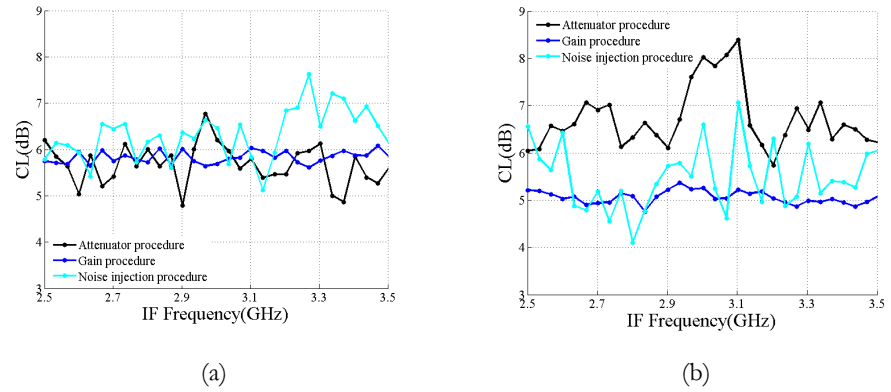

(a)   (b)

Fig. 2-35 Mixer conversion loss (a) with and (b) without isolator, YIG filter.

2.9.3   Narrowband Results using Spectrum Analyser

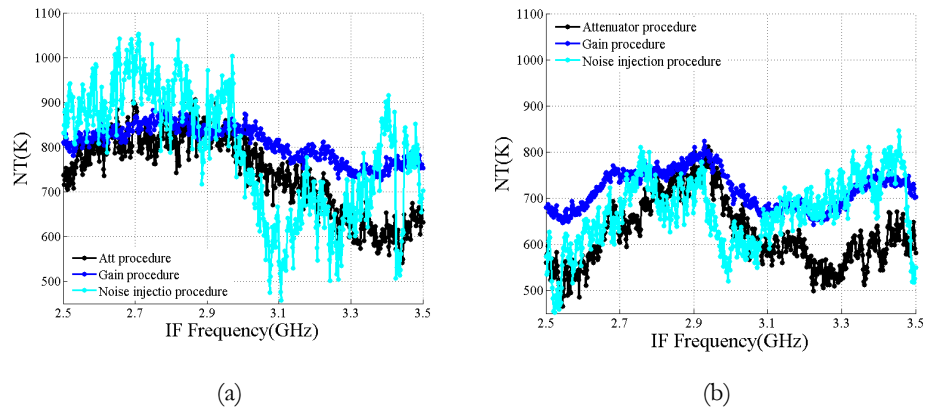The summary of all procedure results for the mixer Noise temperature with and without the isolator using the Spectrum Analyser is presented in Fig. 2-36.

(a)   (b)

Fig. 2-36 Mixer noise temperature (a) with and (b) without isolator, Spectrum Analyser.

In the case of having the isolator the noise temperature results are approximately between 900 K and 600 K and the average value is around 800 K. It is clear that the most stable results are obtained employing the

gain procedure although results obtained by the attenuator procedure are not really far away from them.

For the case in what the isolator is not used, as expected, the noise temperature decreases. The average value is around 650 K.

Fig. 2-37 exhibits the summary of all procedures results for the mixer Conversion loss with and without the isolator at the IF input using the Spectrum Analyser.
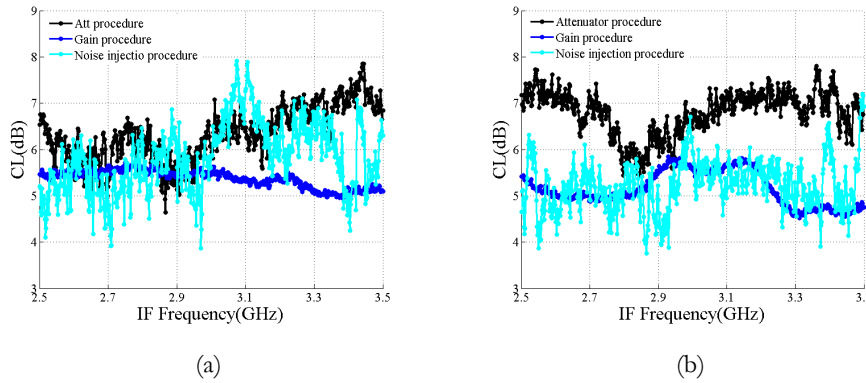

(a)   (b)

Fig. 2-37 Mixer conversion loss (a) with and (b) without isolator, Spectrum Analyser.

The average value for the conversion loss in both cases, having the isolator and not, is around 5.5 dB, and again the most stable method is the Gain procedure. Anyway, when the isolator is used all the procedures present similar trends and less variation among them.

2.10   Comparison of Detection Methods

The results obtained for every measurement procedure are now compared depending on the detection method used.

2.10.1   Attenuator Method

The complete results of the mixer Noise temperature with and without the isolator for the different detection methods calculated using the attenuator procedure are presented in Fig. 2-38.
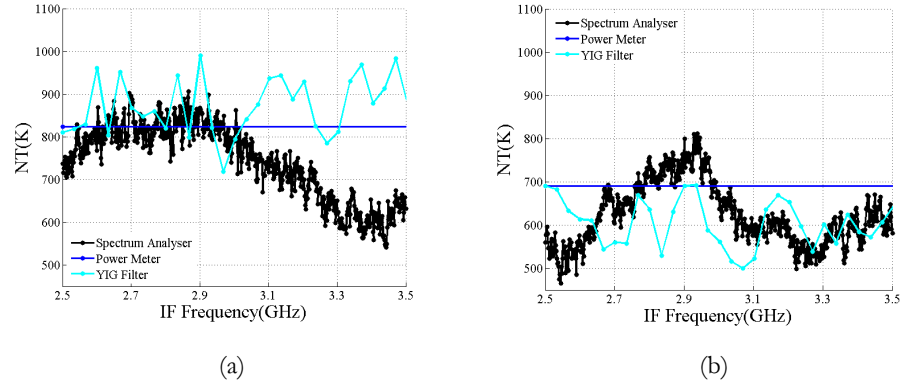
Fig. 2-38 Mixer noise temperature (a) with and (b) without isolator, Attenuator method.

Fig. 2-39 shows the summary of the mixer Conversion Loss with and without the isolator for the same case.
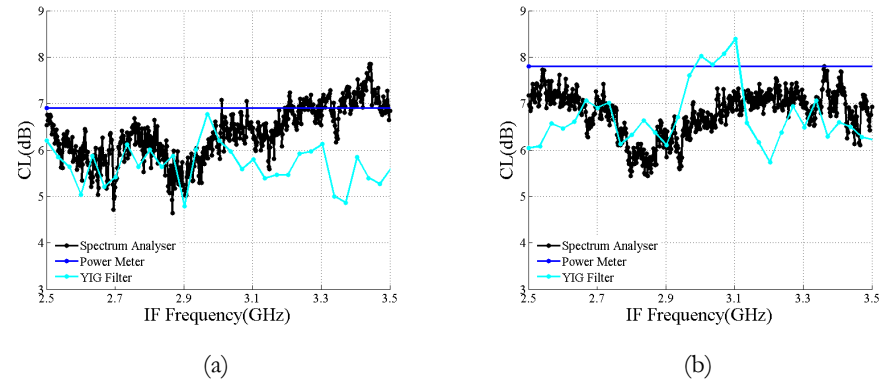

Fig. 2-39 Mixer conversion loss (a) with and (b) without isolator, Attenuator method.

For the attenuator method both, the noise temperature results, with and without the isolator; and the conversion loss results, also with and without the isolator; have similar values when using different detection methods. The small discrepancies that might appear are due to the process followed when measuring, since the set up was reassembled every time the detection method changed.

2.10.2   Noise-Injection Method

Fig. 2-40 shows the summary of the mixer Noise temperature with and without the isolator for the different detection methods using in this case the noise injection procedure.

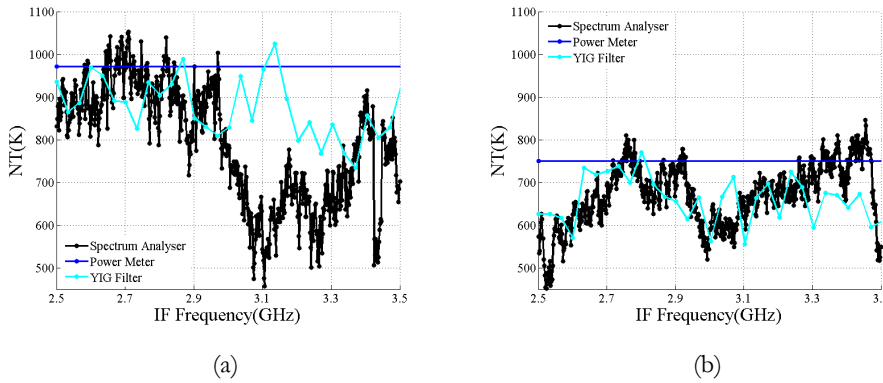(a)   (b)

Fig. 2-40 Mixer noise temperature (a) with and (b) without isolator, Noise injection method.

Again, a collection of the mixer Conversion Loss measurements with and without the isolator for the different detection methods using the noise injection procedure is depicted in Fig. 2-41.

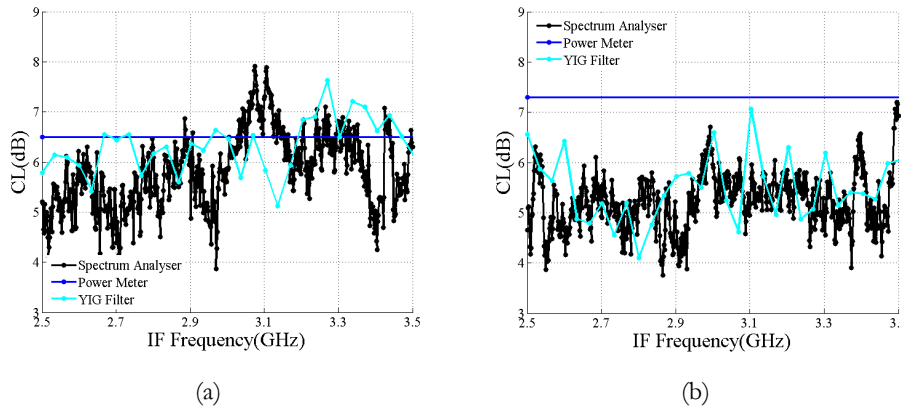(a)   (b)

Fig. 2-41 Mixer conversion loss (a) with and (b) without isolator, Noise injection method.

In the case of the noise injection procedure, more variation between consecutive values is appreciated. This can be caused by the noise source

that is used. Using a better noise source could improve the results. Even though, results obtained using the different detection method are not really far away, and its behaviour is the expected one.

2.10.3   Gain Method

The compilation of the mixer Noise temperature with and without the isolator for the different detection methods using the gain procedure is presented in Fig. 2-42.
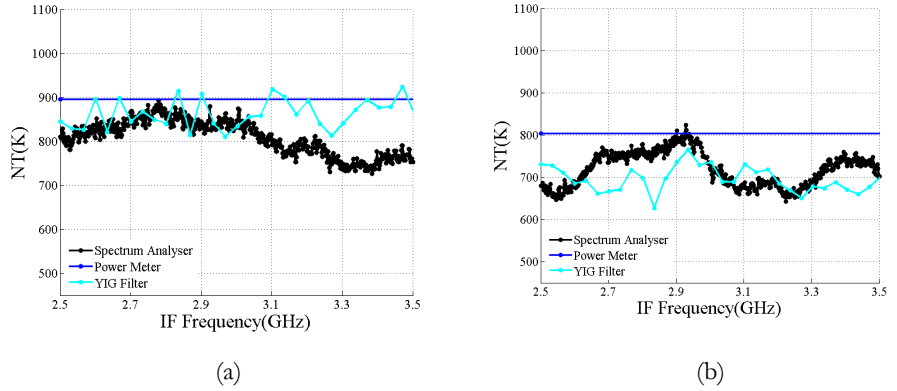

Fig. 2-42 Mixer noise temperature (a) with and (b) without isolator, Gain method.

Fig. 2-43 shows the summary of the mixer Conversion Loss for every detection method when employing the isolator and not.
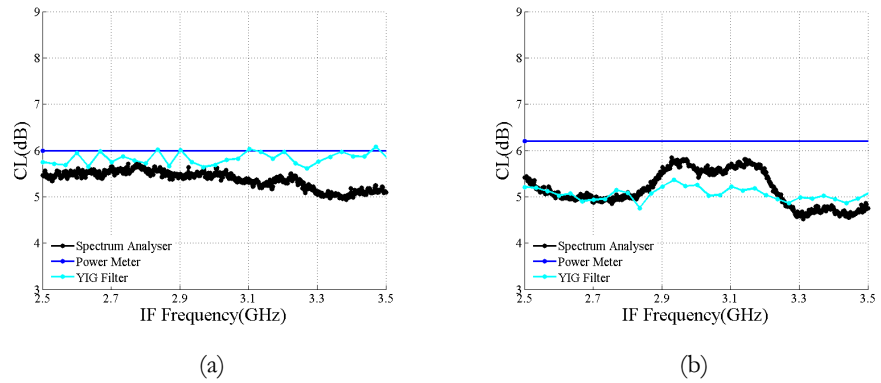

Fig. 2-43 Mixer conversion loss (a) with and (b) without isolator, Gain method.

The gain procedure is the most stable method in terms of less variation between consecutive values and flatter results along all the frequency range. When using different detection techniques, results are similar and close to each other. It is also appreciable that they are closer when using the isolator between the mixer and the pre-amplifier. So that, it is clear that the use of this isolator can provide more reliable results.

2.11   Conclusions

After analysing all the results some conclusions can be extracted.

The use of an active temperature controller makes results being more stable and reliable. The fact of having the IF Chain under a constant temperature, avoid variations cause by the scene where the mixer is measured, the term of the year, or how many people might be at the room when measuring it. Although the results obtained when not using any temperature controller are not quite different, it can't be assured they be as good when the room conditions change.

Talking about the calculation method, the Gain method seems to be the more reliable one. Independently of the detection method used, the gain procedure always have more constant values and comparing them to other procedures, they are closer to the average between all of them. This might be because this procedure, unlike the attenuator or the noise-injection procedures doesn't use any component that generates noise to calculate the NT or the CL, such as an attenuator pad or a noise source. For this reason, it can be concluded that the Gain procedure should be the one to be used along this dissertation since it is the most stable one in terms of less variation between consecutive values.

The detection method that provides the highest resolution at the IF frequency range and indeed, gives a better idea of the performance of the mixer along different frequencies is the Spectrum Analyser. However, it does not necessary means that gives the best performance.

With regards to the used of the isolator, the next section describes a deeper study about its influence when characterizing millimetre and sub-millimetre wave mixers.

2.12 Isolator inclusion analysis

Within this section an explanation about the isolator behaviour is driven. The change produced in the noise temperature of the mixer due to the inclusion of the isolator is caused by the existing mismatch between components. Not only the isolator might affect the noise temperature but also the different components used in the measurements. This is the reason why a new set of formulas have been obtained taking into account the matching between the different elements presented in the set-up. For the sake of simplicity and to facilitate the comprehension of this section only the new formulas for the Gain procedure are presented. Two scenarios have been analysed, having the isolator between the mixer and the IF chain and without it.

It is known that interface mismatches affect the gain of the system, and thus indirectly its noise temperature. The gain of a unilateral two-port device with mismatched termination is defined as, [Maa05]:

$$G_t = \frac{1-|\Gamma_s|^2}{|1-\Gamma_i\Gamma_s|^2} G_{t0} \frac{1-|\Gamma_L|^2}{|1-\Gamma_0\Gamma_L|^2} \qquad 2\text{-}45$$

Where Γ_i, Γ_s, Γ_0 and Γ_L are respectively the input, source, output and load reflection coefficients, and G_{t0} is the transducer gain with a source and load of impedance Z_0. From Equation 2-45 it can be deduced that an interface mismatch can increase or decrease the gain, (G_t), depending on the reflection coefficients´ phase.

2.12.1 Gain method without isolator

The receiver scenario is presented in Fig. 2-44. This figure shows the different mismatching coefficients between components.
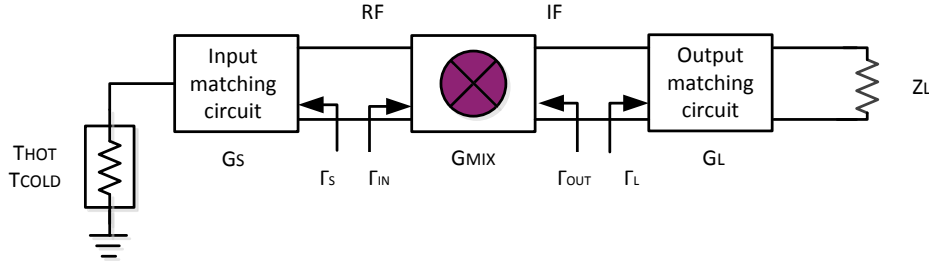
Fig. 2-44. Receiver scenario.

Taking into account these coefficients the gain of every component can be rewritten using Equation 2-45 as follows:

$$G_S = \frac{1-|\Gamma_s|^2}{|1-\Gamma_{in}\Gamma_s|^2} \qquad\qquad 2\text{-}46$$

$$G_{MIX} = |S_{21}|^2 \qquad\qquad 2\text{-}47$$

$$G_L = \frac{1-|\Gamma_L|^2}{|1-\Gamma_{out}\Gamma_L|^2} \qquad\qquad 2\text{-}48$$

where every component is considered as a unilateral two-port with mismatched termination.

For this analysis, the Mixer is considered to be matched with the load, so that, $\Gamma_{in} = \Gamma_S{}^*$, where $*$ represents the conjugate. Therefore,

$$G_S = \frac{1}{1-|\Gamma_s|^2} \qquad\qquad 2\text{-}49$$

Note that the matching between the RF port of the mixer and the load cannot be measured, so it won´t be taken into account from now on.

The mixer total gain taking into account the mismatching can be expressed by the following equations in which G_{MIX} includes the input mismatching:

$$G_{TMIX} = G_{MIX} \cdot G_L \qquad\qquad 2\text{-}50$$

Expressing the previous equation is terms of conversion loss:

$$\frac{1}{L_{MIXT}} = \frac{1}{L_{MIX}}G_L \qquad\qquad 2\text{-}51$$

The mixer conversion loss can be rewritten as:

$$L_{MIX} = L_{MIXT}G_L \qquad\qquad 2\text{-}52$$

Calculating the power of the system with the hot and cold loads, Equations 2-53 and 2-54 are obtained:

$$P_{HOTrx} = kBT_{HOT}G_{rx}(1 - |\Gamma_L|^2) + kBT_{MIX}G_{rx}(1 - |\Gamma_L|^2)$$
$$+ kBG_{IFrx}T_{IF} \qquad\qquad 2\text{-}53$$

$$P_{COLDrx} = kBT_{COLD}G_{rx}(1 - |\Gamma_L|^2) + kBT_{MIX}G_{rx}(1 - |\Gamma_L|^2)$$
$$+ kBG_{IFrx}T_{IF} \qquad\qquad 2\text{-}54$$

The Y-factor can be calculated from Equations 2-53 and 2-54 in order to calculate the receiver noise temperature taking into account the existing mismatching.

$$Y_{rx} = \frac{P_{HOTrx}}{P_{COLDrx}} = \frac{kBG_{rx}\left(T_{HOT}(1-|\Gamma_L|^2)+T_{MIX}(1-|\Gamma_L|^2)+T_{IF}\frac{G_{IF}}{G_{rx}}\right)}{kBG_{rx}\left(T_{COLD}(1-|\Gamma_L|^2)+T_{MIX}(1-|\Gamma_L|^2)+T_{IF}\frac{G_{IF}}{G_{rx}}\right)} \qquad 2\text{-}55$$

$$Y_{rx} = \frac{\left(T_{HOT}+T_{MIX}+T_{IF}\frac{1}{G_{MIX}\left(1-|\Gamma_L|^2\right)}\right)}{\left(T_{COLD}+T_{MIX}+T_{IF}\frac{1}{G_{MIX}\left(1-|\Gamma_L|^2\right)}\right)} = \frac{T_{HOT}+T_{rxT}}{T_{COLD}+T_{rxT}} \qquad 2\text{-}56$$

$$T_{rxT} = T_{MIX} + \frac{T_{IF}}{G_{MIX}(1-|\Gamma_L|^2)} \qquad\qquad 2\text{-}57$$

Rearranging Equation 2-57 the mixer noise temperature can be calculated:

$$T_{MIX} = T_{rxT} - L_{MIX}\frac{T_{IF}}{(1-|\Gamma_L|^2)} \qquad\qquad 2\text{-}58$$

If the mixer conversion loss calculated in 2-52 is written in terms of measured conversion loss, L$_{MIXT}$, and mismatching parameters:

$$L_{MIX} = L_{MIXT}G_L = L_{MIXT}\frac{(1-|\Gamma_L|^2)}{|1-S_{22MIX}\Gamma_L|^2} \qquad\qquad 2\text{-}59$$

Then, the mixer noise temperature de-embedding the output mismatching circuit can be written as:

$$T_{MIX} = T_{rxT} - L_{MIXT}\frac{T_{IF}}{|1-S_{22MIX}\Gamma_L|^2} \qquad\qquad 2\text{-}60$$

Where L_{MIXT} and T_{rxT} corresponds to the measured conversion loss and receiver noise temperature and L_{MIX} and T_{MIX} are the mixer conversion loss and noise temperature excluding the output mismatching.

2.12.2   Experimental Analysis

In order to check the conclusions derived into previous section, an experimental analysis with the components that will be used in Chapter 4 is included. The S parameters of the IF mixer port, and the IF chain with and without the isolator have been measured and are shown in Fig. 2-45 (a) and Fig. 2-45 (b) for one of the mixers of the array. Appendix A gathers the results for the complete array that will be presented in Chapter 4.
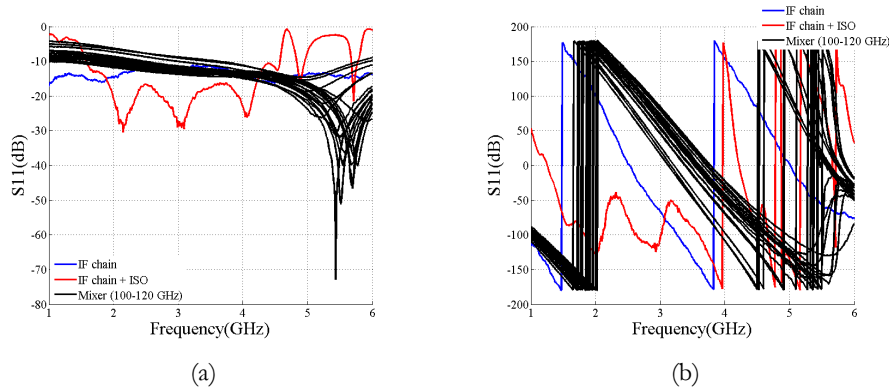
Fig. 2-45. S parameters of the Mixer and the IF chain with and without isolator.

Once the S_{11} parameters are known, the value of G_L, Equation 2-48, can be obtained, Fig. 2-46 (a), and the de-embedding of the conversion loss can be calculated, Fig. 2-46 (b).
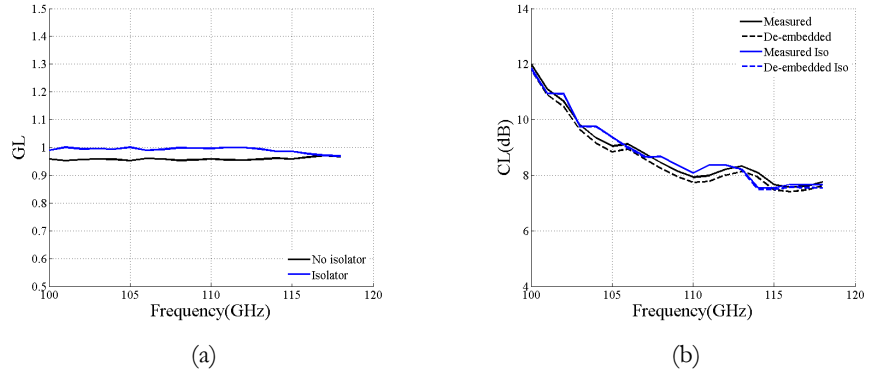
Fig. 2-46. (a) GL and (b) mixer conversion loss with and without isolator.

The mixer NT has been recalculated for every LO frequency point at two different scenarios, taking into account the measured values of the IF chain with and without isolator. The comparison between the measured values and the calculated applying the de-embedding presented in Equation 2-60 is depicted in Fig. 2-47.
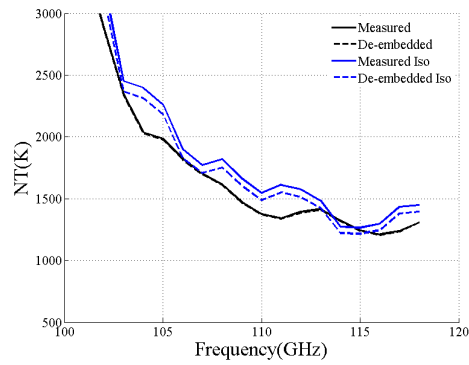

Fig. 2-47. Mixer noise temperature before and after de-embedding.

Fig. 2-47 shows the measured NT and the de-embedded NT, which is the recalculated NT taking into account the mismatching coefficient; when the isolator is part of the IF chain and without it. There is an approach between both cases, with and without isolator, when the de-embedding is applied. That confirms the theory that the mixer parameters are affected by the mismatching presented between the components of the receiver. The

better the matching is the more realistic the NT measured value will be. Note that the results in both cases (with and without isolator) have still some discrepancies, this is due to the fact that the components have been considered a unilateral two-port devices, which in the real case they are bilateral components since the input and the output are affected by each other.

Therefore, the increased on the noise temperature of the mixer due to the inclusion of an isolator can be explained by the mismatch existing between components presented in the receiver. Otherwise, although the inclusion of an isolator has been proved that increments the NT of the mixer, it has been also proved that results obtained using it had similar values independently the calculation procedure used, the gain, attenuator or noise injection method. The pre-amplifier possess a better matching with the mixer but less stable with frequency, which produces a larger variation of the NT along the frequency, Fig. 2-45.

Another important issue is the fact that depending on the IF chain used to measure the performance of a mixer, this performance can be altered by the mismatching existed between the mixer and the IF chain, which can lead to an increase or a decrease of the mixer NT and CL. It is of real importance to characterize this mismatching since the performance of several mixers are not comparable if they haven´t been measured under the same conditions since, as it has been proven in this chapter, the performance of the mixer is related to the matching between components.

CHAPTER 3

Design of a Sub-Harmonic Mixer Working at MM-Wave Frequencies

THz imaging cameras are taking importance nowadays especially for defence and security applications. This thesis is therefore focused on the development of an imaging camera for this kind of applications and, this chapter is concentrated in a 220 GHz Schottky diode heterodyne receiver. The research presented here is framed within three different and important programmes funded by several Spanish Ministries: Cenit-Seduce, TEC and INNPACTO. When designing a millimetre-wave receiver numerous parameters need to be taken into account, one of the most important is the operational frequency. Another one is the selected frequency which comes from a compromise between the resolution, the penetration depth and the atmospheric absorbance level.

This chapter presents the design, fabrication and measurement of a 220 GHz room temperature heterodyne sub-harmonic mixer implemented on a polymer substrate. This material, cyclic olefin copolymer (COC) is a promising dielectric material with interesting properties, such as high chemical resistance, low water absorption, good metal adhesion, flexibility, low permittivity, and low losses in the THz region (0.1–10 THz) [Fis13; Sen06]. This material, commercialized as TOPAS® [TOP], has been already employed in several applications, like THz fibers, low-loss interconnects, waveguides [Nie09] and mesh filters [Pav13]. In addition, transmission lines

built on this material have been studied up to 220 GHz, showing low losses [Pey11]. However, despite these encouraging results it has not been previously used in receiver applications at the millimetre wave frequency range. Until now, the most commonly used substrate for developing mm-wave mixers based on the use of discrete flip-chip diodes soldered on a transmission line at this frequency range was quartz [Che10a; Hes99; Tho04; Tho05; Tho08a; Tre09], although substrates as Rogers duroid can also be found [Ali93; Zho12]. Therefore, the implementation in general of mm-wave devices, and in particular, a mm-wave mixer on this novel substrate is a new and innovative approach. As it is proven within this chapter, COC substrates provide several advantages regarding quartz or Rogers substrates: lower losses and, as it is proven for the first time in this thesis, the capability of direct gold sputtering avoiding the use of any intermediate material, such as chromium or nickel which is needed when quartz or Roger substrates are used [Tan09; Ves97]. On the other hand, their lower melting temperature, when compared with quartz, can be compensated with longer curing processes if conductive epoxy materials are used when dye soldering the diodes. Furthermore, the reduced losses versus conventional substrates lead to better noise temperature values when designing a millimetre-wave mixer as demonstrated in this chapter.

3.1   COC Substrate

Millimetre-wave mixers are mainly developed in Gallium arsenide (GaAs) [Wal11; Wan08] when using integrated Schottky diodes. Although mixer designs that make use of integration diodes have better results [Tho11; Wan13] the inability to fabricate diodes at the Antena Group facilities has forced the use of commercial flip-chip diodes. When working with discrete diodes the most common substrates are quartz or rogers duroid [Tho05; Che10]. Within this dissertation the possibility of using COC substrate is presented offering an innovative option when implementing this kind of devices. TOPAS© is the trade name for Topas Advanced Polymers´cyclic olefin copolymers (COC), [TOP]. The TOPAS

COC substrate family consist of amorphous, transparent copolymers based on cyclic olefins and linear olefins.
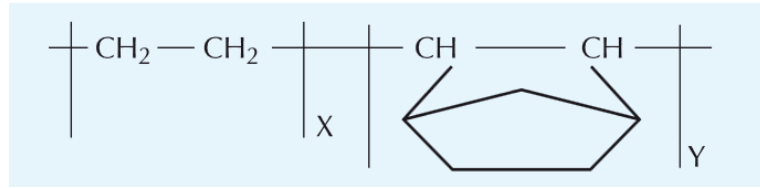

Fig. 3-1 TOPAS© COC structure, [TOP].

Cyclic olefin materials are a new class of polymeric materials with property profiles that can be customized varying the chemical structure of the copolymer. Some of the most important benefits that this material offers are:

- Low density
- High transparency
- Low birefringence
- Extremely low water absorption
- Excellent water vapour barrier properties
- Variable heat deflection temperature up to 170 °C
- High rigidity, strength and hardness
- Very good resistance to acids and alkalis
- Very good electrical insulating properties

TOPAS© COC has very good electrical insulating properties and a low dissipation factor. The dielectric constant of TOPAS© COC is 2.34, which is typical of the values obtained with olefinic materials, Fig. 3-2 (a). It stays constant in the high frequency area up to 20 GHz. The very low temperature dependence of the dielectric constant and dissipation factor is shown by measurements on biaxially oriented film, Fig. 3-2 (b). At 10 kHz and 100 °C, a value of $0.2 \cdot 10^{-4}$ was determined.
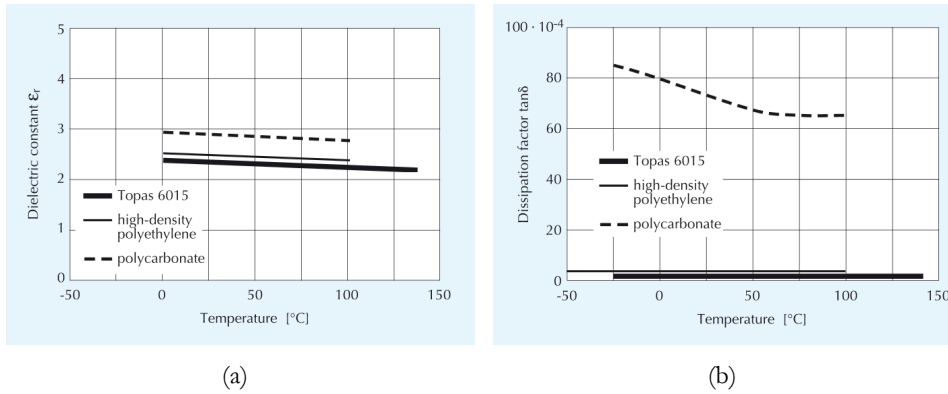
(a)   (b)

Fig. 3-2 Effect of temperature (a) on the dielectric constant and (b) on the dissipation factor tan δ of various polymers, [TOP].

These properties are expected to be different in the sub-millimetre wave range. Therefore, the dielectric constant and the losses of this material in the 100 to 1000 GHz band have been measured using the Teraview Spectra 3000 TDS system. For the sake of comparison, these performances have also been obtained for rogers duroid 5880 and quartz (fused silica) substrates [Vil02]. The results are shown in Fig. 3-3.

(a)   (b)
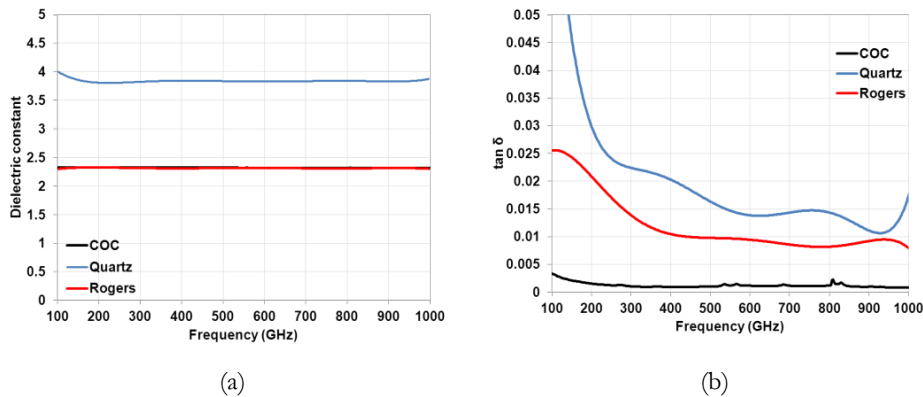
Fig. 3-3 COC, quartz and Rogers duroid 5880 measurements (a) dielectric constant, (b) loss tangent.

Fig. 3-3 (a) shows the measured dielectric constant for the three substrates meanwhile the losses are presented in Fig. 3-3 (b). Losses are higher than the manufacturer´s previsions since the measured frequency

range is much higher. Despite that, the measured COC tan   much lower than typically used substrates, quartz (fused silica) and Rogers. Note also that the values measured around 100 GHz are quite high, it is due to the loss of dynamic range at low frequencies that the Teraview Spectra 3000 has.

Considering a microstrip (100 μm width) line built on a 120 μm thick COC substrate, the attenuation due to dielectric losses can be determined as:

$$\alpha_d = \frac{k_0 \varepsilon_r (\varepsilon_{eff} - 1) tan\delta}{2\sqrt{\varepsilon_{eff}(\varepsilon_r - 1)}} \qquad \text{3-1}$$

Where tan δ is the loss tangent of the dielectric, ε_r the dielectric constant, ε_{eff} the effective dielectric constant and k_0 the propagation constant in vacuum [Poz05]. Table 3-1 shows the corresponding values of the dielectric loss for each of the measured substrates at 220 GHz which will correspond with the mixer operational frequency.

Material	*tan δ*	*α_d(dB/mm)*
COC	0.0019	0.0412
Quartz	0.025	0.7890
Rogers	0.018	0.3758

Table 3-1 Calculated Dielectric Loss for the Different Substrate Materials.

Analysing the results calculated in Table 3-1 it is straightforward to check that the COC substrate has the lowest dielectric loss, 0.04 dB/mm, which is one order of magnitude smaller than Rogers and 19 times less than quartz (fused silica).

On the other hand, the dielectric constant of COC is similar to Rogers 5880 substrate which will be used later on to compare the performances of two millimetre wave mixers implemented with these substrates. Note that the properties of this kind of polymers make them suitable to be used as substrate of microwave designs at high frequency.

One of the most interesting properties of COC substrate is the ability to support a direct sputtering of gold avoiding the use of any intermediate material such as chromium or nickel. On the other hand, note that COC requires low cure temperatures which has to be compensated with longer time processes. All these characteristics make it ideal for developing components/devices in applications at the mm and sub-millimetre frequency range.

3.2   Design process

In this section the sub-harmonic mixer design process is presented. Note that the design of this mixer is placed within three research projects focused on the development of receivers on the millimetre and sub-millimetre wave range for security applications such as explosives detection. For this reason the operational frequency has been settled to 110 GHz for the LO frequency and 220 GHz for the RF frequency. It has been chosen an RF frequency of 220 GHz due to the fact that an atmospheric attenuation window can be found there, [Ula73; Wan09; Mar12]. Moreover, the resolution and penetration depth are good enough to detect hidden objects and explosives (~cm), which are the goals of this dissertation. As it will be presented later on this thesis, the mixer explained in this chapter will be part of a 1x8 mixer element array shown in Chapter 3 which will be the receiver part of a totally functional imaging camera, see Chapter 3 and Chapter 6.

The design and optimization of the sub-harmonic mixer has been done combining two software tools: Ansys High Frequency Simulation Software (HFSS), [ANS], and Agilent Advanced Design System (ADS), [AGI].

HFSS is a software package that analyses the electrodynamics behaviour of passive structures based on finite element, integral equation or advanced hybrid methods to solve a wide range of applications. It computes scattering parameters (S-parameter) response and electromagnetic field

distributions for passive and three dimensional structures at high frequency. In the case of study, the linear behaviour of the sub-harmonic mixer will be analysed using this software tool.

On the other hand, ADS is a powerful electronic design automation software for RF, microwave, and high speed digital applications. In this case, it has been the selected software tool to analyse the non-linear behaviour of the sub-harmonic mixer. The Harmonic Balance simulation method has been used in this dissertation, which is a frequency-domain analysis technique for simulating distortion in non-linear circuits and systems. This method allows one to determine the noise temperature and conversion loss of the correspondent mixer.

The use of these two software packages has been done alternatively in order to optimize the performance of the sub-harmonic mixer. Note that generally, a mixer design is composed by two input waveguides (LO and RF) and a channel in which the microstrip circuit will be placed, several filters employed to select the IF frequency and reject the rest of the signals (called LO and RF filters) and two diodes placed in anti-parallel configuration (in order to avoid half the generated harmonics, see Section 2.1.1). With this in mind, a mixer design can be developed. First of all, an ideal mixer design was done with the goal of calculating the optimal impedance of the diodes and finding out the best noise temperature and conversion loss reachable. In order to perform this ideal design some steps were followed, Fig. 3-4. This ideal mixer design was completely implemented using ADS.
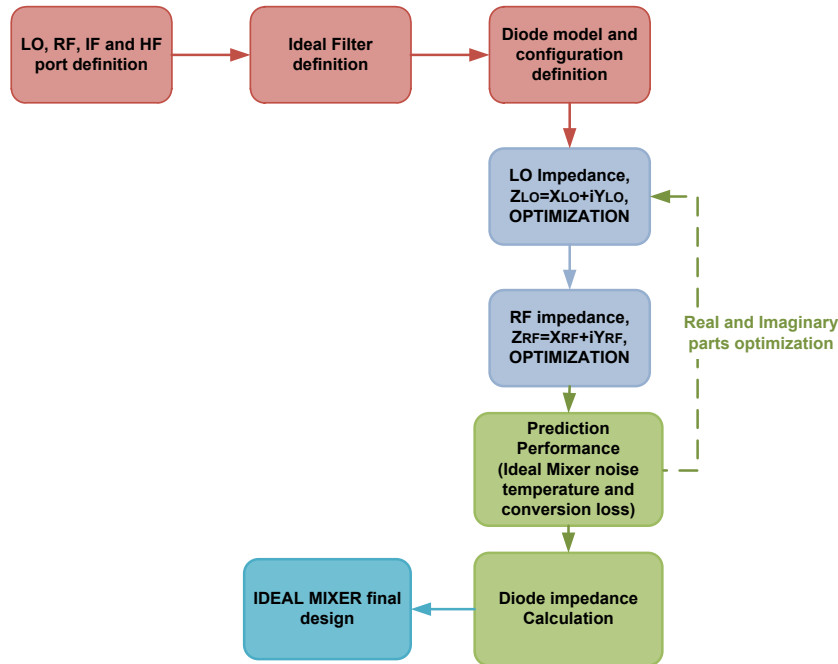
Fig. 3-4 Simulation flow of the ideal mixer design and optimization.

Different steps are followed when the ideal mixer parameters are calculated. First of all, the local oscillator, LO; radiofrequency, RF; intermediate frequency, IF and high harmonics, HF; ports are defined in ADS. After that, LO, RF, IF and HF filters are created. These filters are defined as band pass filters by the ideal S-parameters at the corresponding frequencies. Moreover, the diode model with its main characteristics is defined, Fig. 3-5 . The selected parameters correspond to a commercial model brought to VDI which will be presented later on.
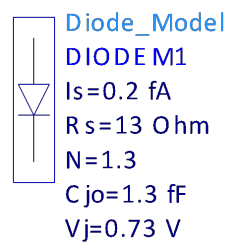
Fig. 3-5 VDI diode model for ADS software.

Once, all the parameters have been settled, the LO and RF impedance ports are optimized with the aim of obtaining the minimum noise temperature and conversion loss possible. Whenever these parameters are minimized, the diode impedance is calculated and therefore, the final ideal mixer design is obtained.

The harmonic balance definition used for the simulation is presented in Fig. 3-6. Its principal parameters are:

- Max Order: represents the maximum order of the mixing products.
- Freq[1]: is the LO frequency which is swept from 100 GHz to 120 GHz.
- Freq[2]: is the RF frequency which is settled to 2*LOfreq-1.5 GHz.
- Order[1] and Order[2]: are respectively the number of LO and RF harmonics taken into account.
- Noisecon[1]: represents noise that will be presented at the frequency of interest.
- BandwidthForNoise: is the bandwidth for spectral noise simulation which is recommended to be 1 Hz for measurements of spectral noise power.
- NoiseConMode: it is "yes" in order to enable noise simulation with NoiseCons.

```
HARMONIC BALANCE

HarmonicBalance
HB2
MaxOrder=11
Freq[1]=LOfreq
Freq[2]=RFfreq
Order[1]=10
Order[2]=10
BandwidthForNoise=1.0 Hz
Noisecon[1]="NC_USB"
NoiseConMode=yes
```
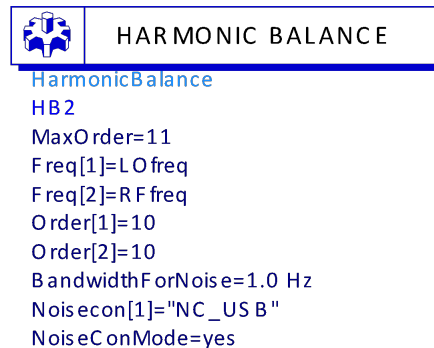
Fig. 3-6 Harmonic balance parameters.

Note that the noise contribution (Noisecon[1]) is modelled on an harmonic noise controller presented in Fig. 3-7.

HB NOISE CONTROLLER

NoiseCon
NC_USB
InputFreq=RFfreq
FreqForNoise=2*LOfreq-RFfreq
NoiseInputPort=4
NoiseOutputPort=2
NoiseNode[1]=V_IF
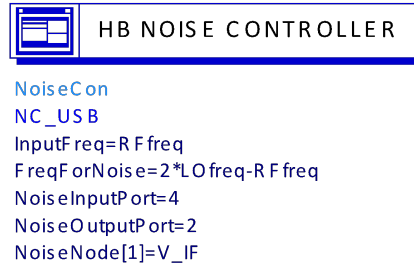
Fig. 3-7 Noise source parameters definition.

- InputFreq: represents the noise input frequency which corresponds to the RF frequency.
- FreqForNoise: is the frequency at which the noise is calculated.
- NoiseInputPort: is the number of the input port, RF port, in the circuit.
- NoiseOutputPort: is the number of the output port, IF port, in the circuit.
- NoiseNode[1]: represents the noise voltage value at the IF port.

The ideal schematic of the sub-harmonic mixer is presented in Fig. 3-8. This model counts with ideal filters to select the corresponding frequency in each band. The ideal conversion loss and noise temperature are calculated taking into account the RF and LO frequency impedances. The best value obtained varying these impedances is shown in Fig. 3-9. Best conversion loss values obtained are in the order of 5.7 dB using the diodes aforementioned and noise temperature values are around 600 K.
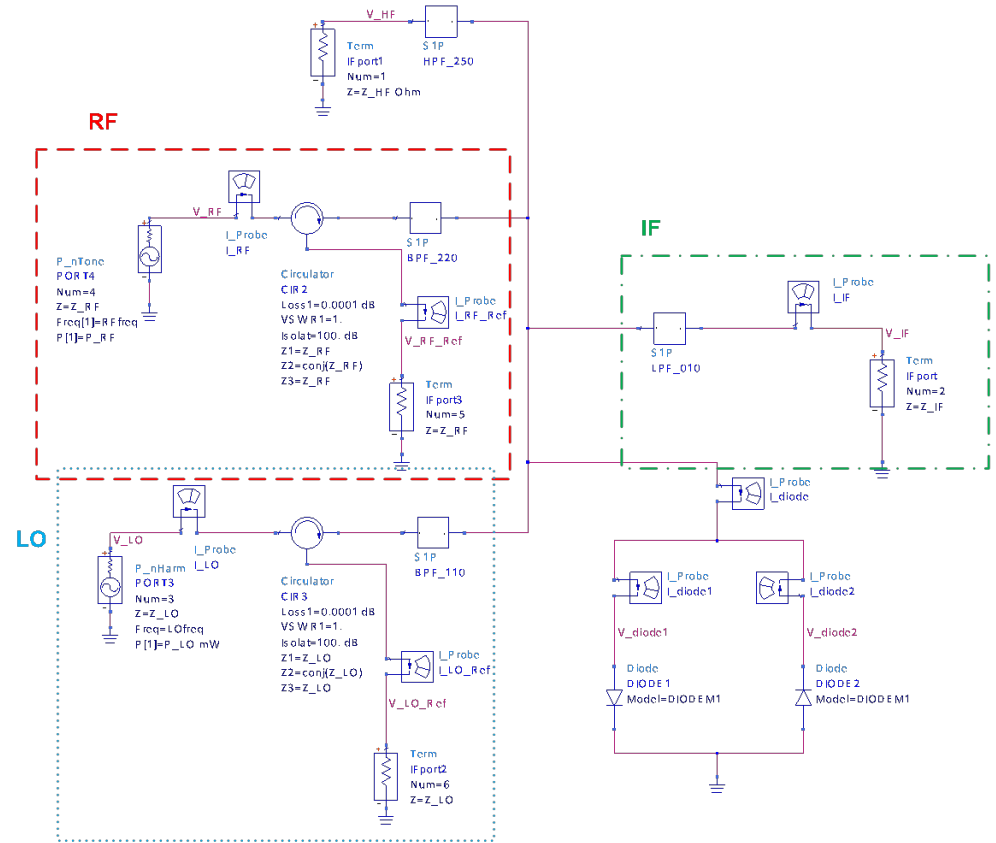
Fig. 3-8 Ideal sub-harmonic mixer model.

(a)   (b)
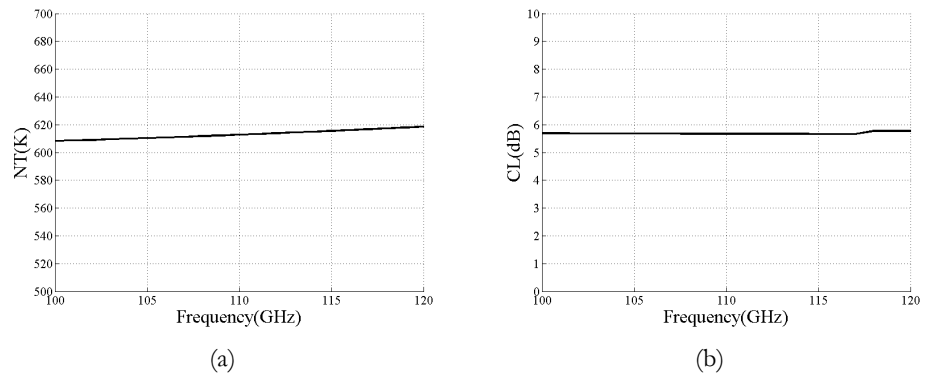
Fig. 3-9 (a) Noise temperature and (b) conversion loss of the ideal sub-harmonic mixer

The diode impedances have been calculated from the currents and voltages at the LO and RF frequencies for the ideal mixer design presented in Fig. 3-8. The obtained impedances correspond to a minimal noise temperature of the mixer, which can be obtained when there is an optimal impedance matching of the diodes, so that $Z_{RF}=(Z_{diode1RF}//Z_{diode2RF})^*$ and $Z_{LO}=(Z_{diode1LO}//Z_{diode2LO})^*$, where * means conjugate. The results have been obtained for DIODE1 but DIODE2´s impedances are supposed to be the same since both diodes are identical ($Z_{diode1LO}=Z_{diode2LO}$ and $Z_{diode1RF}=Z_{diode2RF}$). Taking this into account, the impedance at the RF and LO ports can be expressed as $Z_{RF}=(Z_{diode1RF}/2)^*$ and $Z_{LO}=(Z_{diode1LO}/2)^*$. The obtained values related to the analysed LO frequency band are presented in Table 3-2. These values have been calculated by means of the currents and voltages presented in each port, LO, RF and diodes, taking into account an LO frequency band of 20 GHz, an IF frequency of 1.5 GHz and a bandwidth of noise of 1 Hz, see Fig. 3-6.

Freq. (GHz)	ZdiodeLO (Ω)	ZdiodeRF (Ω)	ZLO (Ω)	ZRF (Ω)
100	485.64 - 325.52i	184.99 - 72.339i	242.82 + 162.76i	92.50 + 36.17i
101	482.58 - 326.58i	184.46 - 72.83i	241.29 + 163.29i	92.23 + 36.42i
102	479.53 - 327.62i	183.92 - 73.318i	239.77 + 163.81i	91.96 + 36.66i
103	476.5 - 328.63i	183.39 - 73.801i	238.25 + 164.32i	91.69 + 36.90i
104	473.48 - 329.62i	182.85 - 74.28i	236.74 + 164.81i	91.43 + 37.14i
105	470.47 - 330.58i	182.31 - 74.755i	235.24 + 165.29i	91.16 + 37.38i
106	467.48 - 331.52i	181.78 - 75.226i	233.74 + 165.76i	90.89 + 37.61i
107	464.5 - 332.43i	181.24 - 75.693i	232.25 + 166.21i	90.62 + 37.85i
108	461.54 - 333.31i	180.7 – 76.156i	230.77 + 166.66i	90.35 + 38.08i
109	458.59 - 334.18i	180.17 - 76.615i	229.30 + 167.09i	90.08 + 38.31i
110	455.66 - 335.01i	179.63 - 77.069i	227.83 + 167.51i	89.81 + 38.53i
111	452.74 - 335.83i	179.09 - 77.52i	226.37 + 167.91i	89.55 + 38.76i
112	449.83 - 336.62i	178.55 - 77.967i	224.92 + 168.31i	89.28 + 38.98i
113	446.94 - 337.39i	178.02 - 78.409i	223.47 + 168.69i	89.01 + 39.20i

114	444.07 - 338.13i	177.48 - 78.848i	222.03 + 169.07i	88.74 + 39.42i
115	441.21 - 338.86i	176.94 - 79.283i	220.60 + 169.43i	88.47 + 39.64i
116	438.36 - 339.56i	176.4 - 79.714i	219.18 + 169.78i	88.20 + 39.86i
117	435.53 - 340.24i	175.86 - 80.141i	217.77 + 170.12i	87.93 + 40.07i
118	432.71 - 340.9i	175.32 - 80.564i	216.36 + 170.45i	87.66 + 40.28i
119	429.91 - 341.54i	174.78 - 80.984i	214.96 + 170.77i	87.39 + 40.49i
120	427.12 - 342.16i	174.25 - 81.4i	213.56 + 171.08i	87.12 + 40.70i

Table 3-2 Ideal diode impedance.

The optimum diode impedance calculated at the LO frequency has values around 460 Ω for the real part and -330 Ω for the imaginary part. On the other hand, the optimum diode impedance calculated at the RF frequency presents values around 180 Ω for the real part and -80 Ω for the imaginary part.

Fig. 3-10 shows their corresponding LO and RF reflection coefficients. A good sub-harmonic mixer design should have diode impedances as close as possible to the calculated ideally, in order to have the lowest conversion loss, related to Z_{RF}, with a low input power, related to Z_{LO}.

(a)   (b)
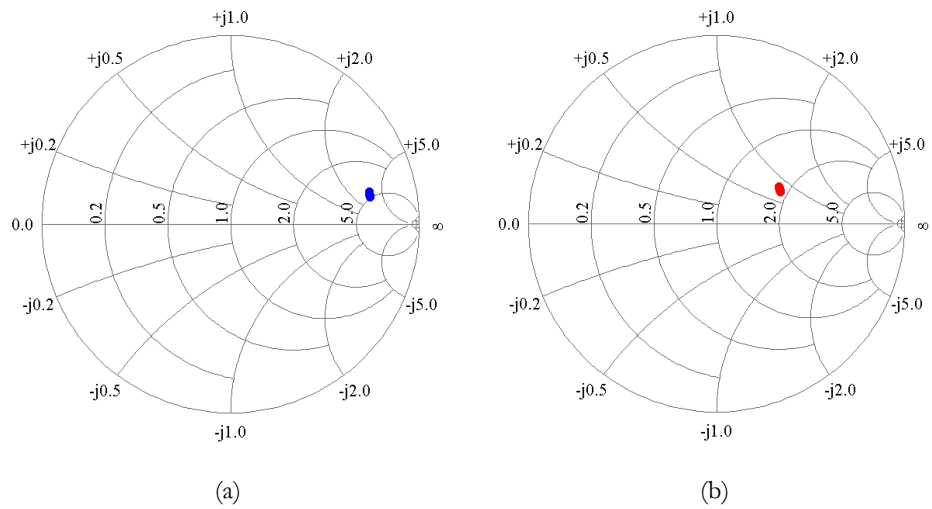
Fig. 3-10 Optimum (a) LO, (b) RF reflection coefficient for an LO frequency of 100 to 120 GHz.

Once the ideal mixer design has been completely done and a general idea of the values of the matching diode impedance and the minimum noise temperature and conversion loss reachable has been obtained, the mixer design is worked out. It is important to recall the main existing differences between the ideal design and the "real" mixer design. The first one comes from the definition of the LO and RF ports which are simple ports in the ideal case but waveguide ports when the "real" mixer design is implemented. Moreover, the waveguide to microstrip transitions are also defined in the "real" mixer design, which are not used in the ideal one. In addition, the LO and RF filters will change from ideal filters to "real" filters designed in microstrip technology and taking into account the kind of substrate and the waveguide channel on which they will be placed. With all of these considerations in mind the mixer design is performed.

As commented, the aim of the mixer design was obtaining the minimum noise temperature and conversion loss in the widest frequency range. Taking this into account, several steps have been carried out as presented in Fig. 3-11.
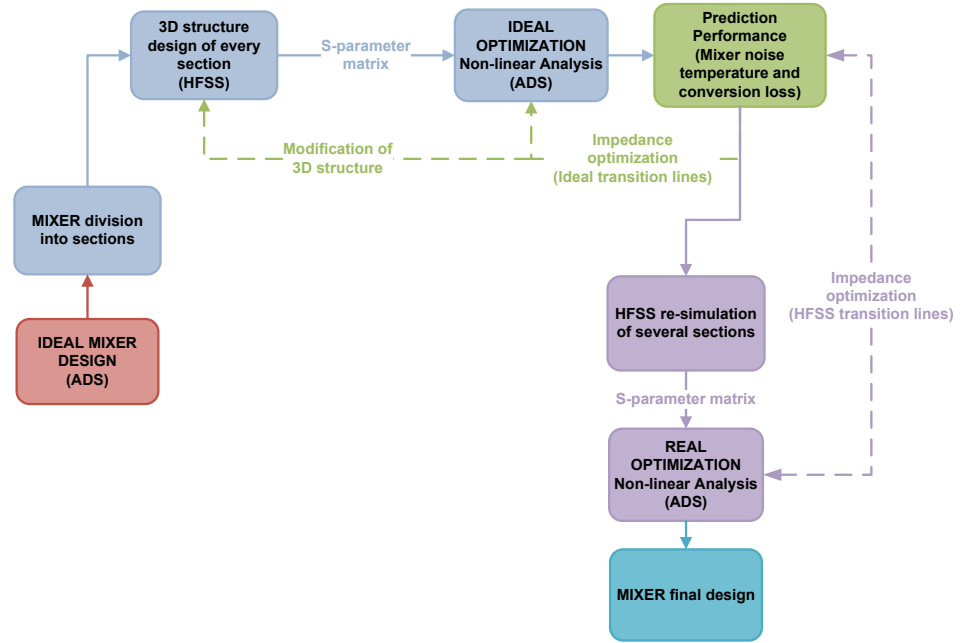
Fig. 3-11 Simulation flow of the mixer design and optimization

First of all, the mixer was divided into different parts for the purpose of minimize the simulation time and simplify the design. So that, the mixer design was split into five different parts: the 3D diodes model, the RF and LO filters and the RF and LO transitions. All of them were designed using HFFS and after that, the S-parameters of every section were obtained. Once the S-parameters were calculated, they were imported in an ADS mixer analysis model. ADS software was used to analyse the non-lineal behaviour of the mixer and calculate its noise temperature and conversion loss. The best performance of the mixer, in terms of less noise temperature and conversion loss, will be obtained when the impedance at the diodes, is closed to the calculated in the ideal design. A typical manner of varying this impedance is using different ideal transition lines in order to gather the mixer sections (i.e. the LO and RF filters, the diodes and LO and RF transitions) and do a de-embedded of the diode impedance. The ideal optimization is done using ideal transitions lines from ADS library. Straightaway, their corresponding optimized transition line is simulated in

HFSS and once more, it is imported in the ADS model and optimized again. Those steps are repeated until an optimised design is obtained.

3.3   Sub-harmonic Mixer Results

The mixer device employs Schottky diodes in anti-parallel configuration, Fig. 3-12, in order to mix the RF and LO signals. The diode 3D model has been created by the Antenna Group taking into account the physical dimensions of the commercial diodes as well as the different layers that form a diode. Note that this is an approximate model of the VDI diodes that will be employed in the fabricated mixer, which can lead to slight differences between the simulation performance and the measured one.
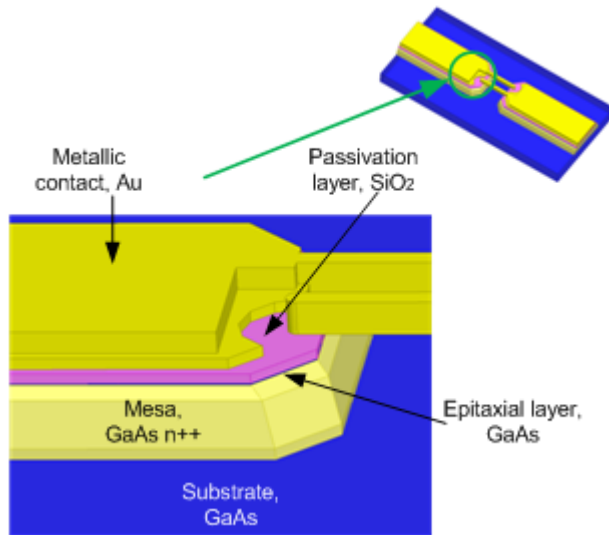
Fig. 3-12 HFSS scheme of the Schottky diode.
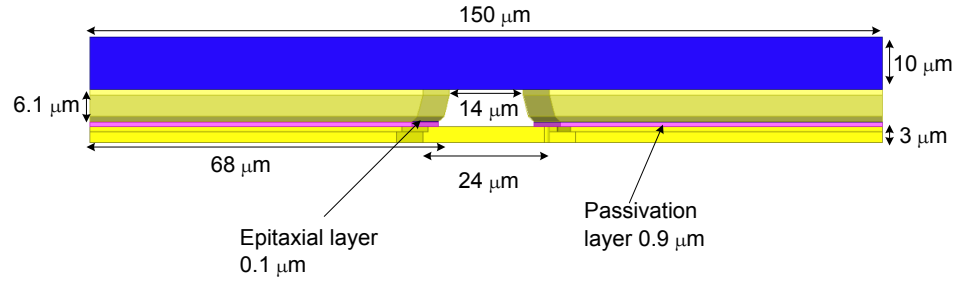
Fig. 3-13 HFSS Schottky diode dimensions.

As commented previously, the use of an anti-parallel configuration has been decided in order to avoid the mixed even harmonics, as they will be trapped inside the pair of diodes. However, the Antenna Group doesn´t have either the resources nor the capability to fabricate diodes so that, commercial diodes have been used for this mixer, namely the VDI SC1T2-D20 [VDI], with the following characteristics: saturation current Is= 0.2 fA, series resistance Rs= 13 Ohm, ideality factor η= 1.3, the zero voltage junction capacitance Cjo= 1.3 fF and the diode forward voltage Vj= 0.73 V. These parameters determine the diode characteristics and are defined as:

- Saturation current: It is also known as reverse saturation current and represents the part of the reverse current in a semiconductor diode caused by diffusion of minority carriers from the neutral regions to the depletion region.

- Series resistance: It can be calculated as the voltage deviation from the extrapolated line at its high-current end, see Fig. 3-14.

- Ideality factor: is a measure of how closely the diode follows the ideal diode equation. It represents the unavoidable imperfections in the junction, typically between 1 and 2.

- Zero voltage junction capacitance: It is related to the depletion layer charge in a p-n diode at zero bias.

- Diode forward voltage: Refers to the voltage drop that occurs when an electrical current passes through a diode in an electrical circuit. For silicon diodes the diode forward voltage drop is about 0.7 volts (V).
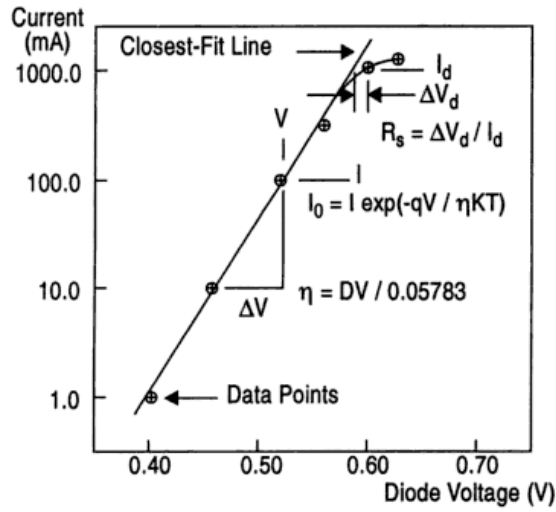
Fig. 3-14 Diode I/V characteristic [Maa03].

The sub-harmonic mixer is implemented in microstrip technology over the COC substrate, and the different parts shown in Fig. 3-15 composed it.
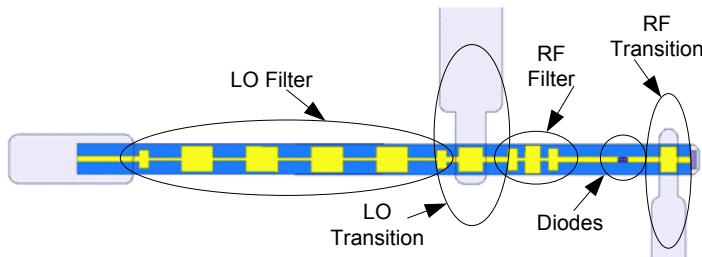

Fig. 3-15 Longitudinal section of the sub-harmonic mixer showing its different parts and components.

The RF and LO signals are coupled to the mixer through standard rectangular waveguides. The RF frequency has been set to 220 GHz so the rectangular waveguide chosen has the following dimensions: 1092x546 μm,

WR-4. For the LO waveguide the dimensions chosen are: 2032x1016 μm, WR-8.

The LO Filter is a stepped-impedance Low Pass Filter, LPF, with a cut-off frequency below 110 GHz. This filter will not let the LO signal pass through the IF port and will completely direct it towards the diodes. The RF Filter is also a stepped-impedance LPF but in this case the cut-off frequency is between 110 GHz and 220 GHz letting the LO frequency pass towards the diodes but avoiding the RF frequency to go through the LO and IF ports (see Fig. 3-16 and Fig. 3-17) [Maa98]. Stepped-impedance filters have been selected due to their simplicity and easiness to be fabricated.

(a)

(b)

(c)
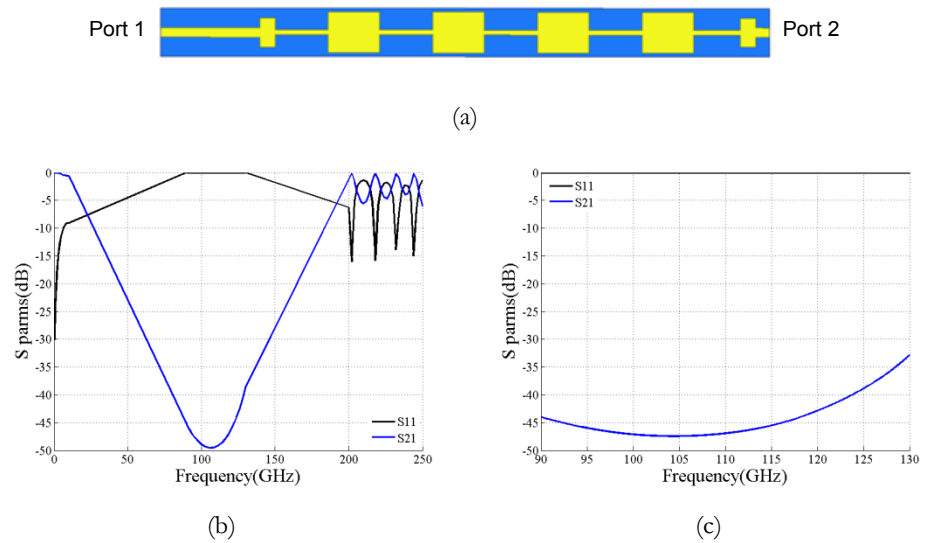
Fig. 3-16 (a) LO filter model and (b), (c) S_{11} and S_{21}.

(a)   (b)
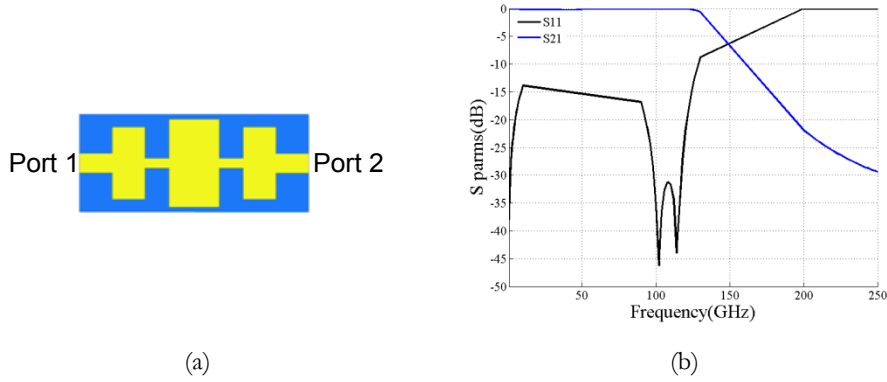
Fig. 3-17 (a) RF filter model and (b) S_{11} and S_{21}.

The LO and RF transitions are designed to gather the maximum power for the mixer. The input LO and RF waveguides have been reduced in height to improve the operational bandwidth when adapting the TE_{01} mode to the quasi-TEM mode of the microstrip line, (0.5 x 2.030 mm and 0.3 x 1.092 mm respectively) [Hes97; Shi97], see Fig. 3-18.


(a)   (b)

(c)   (d)
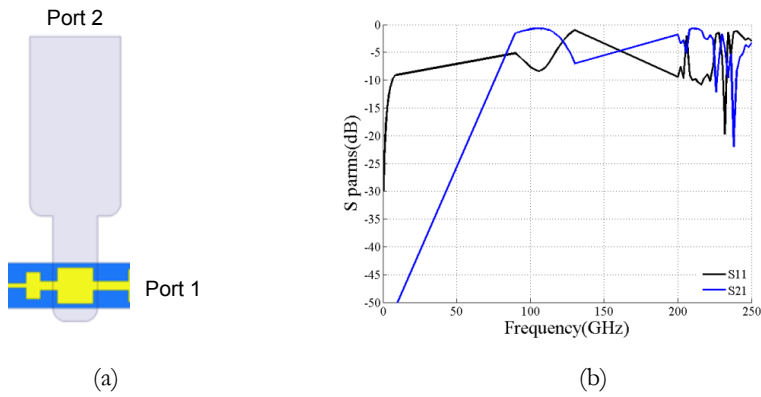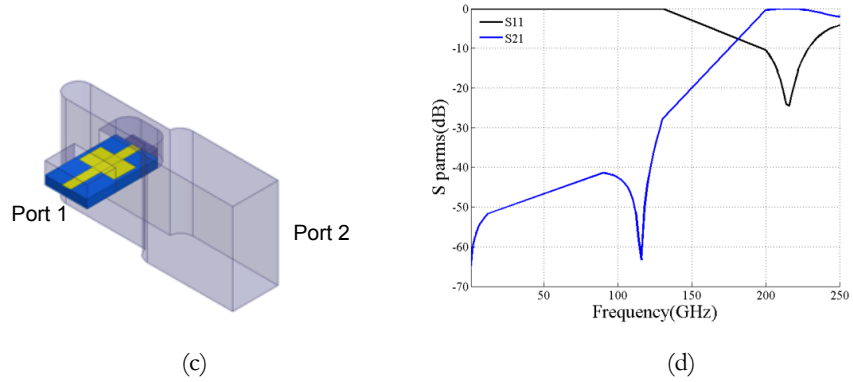
Fig. 3-18 (a) LO Transition, LOT, model and (b) LOT S_{11} and S_{21}, (c) RF Transition , RFT, model, (d) RFT S_{11} and S_{21}.

The microstrip channel dimensions are 0.5 x 0.254 mm. The channel width has been chosen taking into account that the waveguide is working as monomode and the height has been chosen double the substrate thickness which initially was 127 μm.

The dimensions of the complete mixer design are presented in Appendix B as well as the ADS simulation schematic components.

In order to analyze how the substrate thickness influences the mixer performance a parametric study has been carried out. Note that this study has been done before optimizing the mixer design; this is why some differences with the final mixer results can be appreciated.

(a)   (b)

(c)   (d)
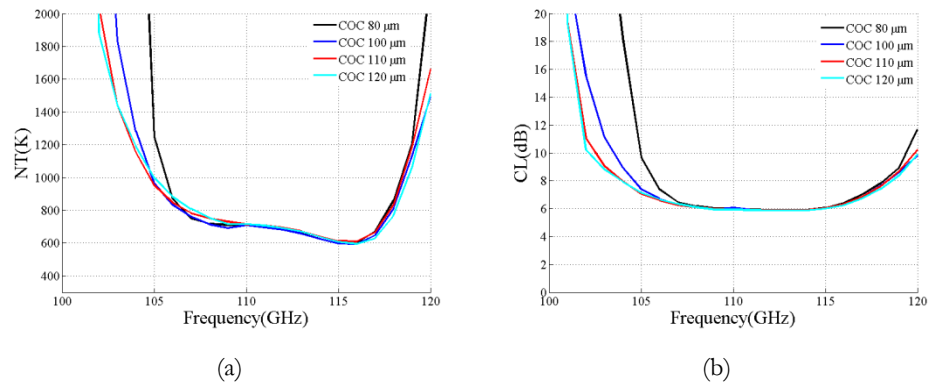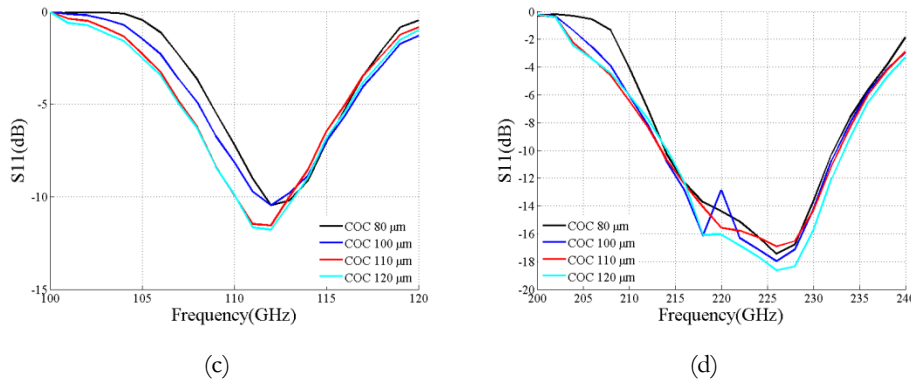
Fig. 3-19 (a) Noise temperature, (b) conversion loss, (c) LO matching, (d) RF matching
variation as function of the thickness substrate.

It can be seen in Fig. 3-19 that if the operational bandwidth (107 to 118 GHz) is taken into account the mixer performance is almost the same independently the thickness substrate. According to the noise temperature another variation can be found, the performance becomes less flat when the substrate´s thickness increases, see frequencies around 107 GHz in Fig. 3-19 (a). Small differences can be appreciated for the case at LO and RF matching. Finally a substrate thickness of 4 mils (101.6 μm) has been selected because it is possible to find it commercially (TOPAS 6015).

The mixer performance can also be influenced by the diode series resistance, for this reason, a parametric study of this variable has also been performed. Although it is a parameter that the designer can´t change physically it is important to know how it can influence the mixer performance.

(a)   (b)
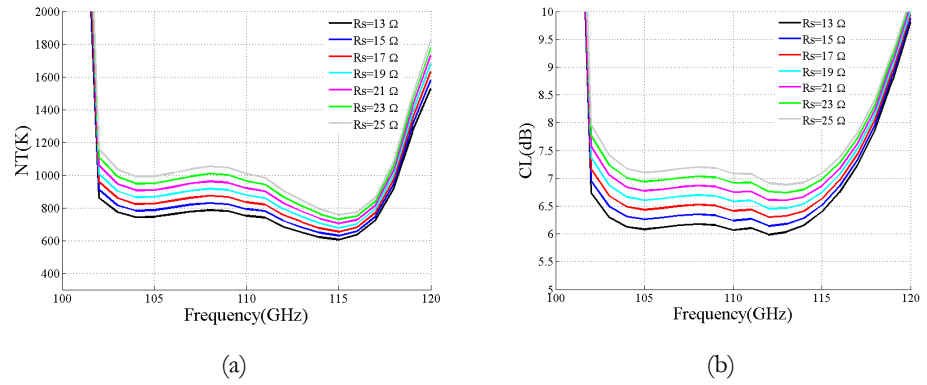
Fig. 3-20 (a) Noise temperature and (b) conversion loss dependences with the Diode series resistance.

Fig. 3-20 shows that the higher the diode´s series resistance is the higher the mixer noise temperature and the conversion loss will be. It is important to keep the diode Rs as low as possible in order to achieve good performances. The diode Rs is defined by the anode length, the epilayer thickness and some other characteristics of the diode structure. Nevertheless, although commercial diodes are used and the manufactures provide its series resistance value, this value increases when the diodes are welded to the microstrip circuit of the mixer due to the use of silver epoxy. Another element that increases the resistance of the complete mixer is the connector, since it is also welded by means of silver epoxy. Therefore a careful fabrication process will become in an important issue for the final results.

In order to optimize the design, analyse the diode´s non-lineal behaviour and reach a good performance of the mixer in terms of low noise temperature and conversion loss, ADS is used. The ADS simulation process is presented next. This simulation process is divided into 3 steps. The first simulation step was done importing all the HFSS parameters of each mixer section. Every single block is connected by means of an ideal transition line provided by the ADS library.

TLIN
TL1
Z=Ohm
E=Degree
F=GHz

This transition line allows the user to select the impedance and the operational frequency. So that, once these values are fixed, the mixer design can be optimized changing the length of the ideal TL.

As well as with the ideal mixer design, Harmonic Balance analysis has been used to study the performance of the mixer, see Section 2.3.

The impedance of every port has to be defined in ADS. Z_RF and Z_LO are the port impedances of the corresponding waveguides for the TE_{10} mode and can be calculated using HFSS. Z_LO is determined by the simulation of the LO transition, its value corresponds to the impedance of the LO port of the waveguide, Fig. 3-21 (a). Z_RF can be found the same way, i.e. it is the impedance value of the RF port of the simulated RF transition, Fig. 3-21 (b).

(a)   (b)
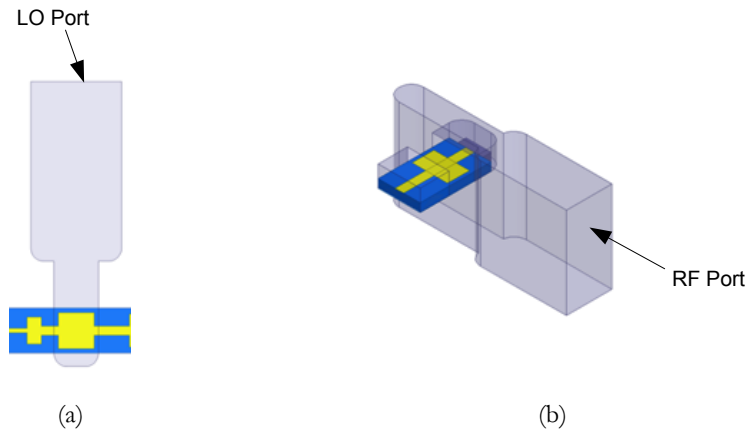
Fig. 3-21 HFSS 3D model (a) LO transition and (b) RF transition.

The obtained HFSS values 482 Ω and 512 Ω (port impedances of the waveguide in HFSS at the corresponding frequencies 110 and 220 GHz) respectively have been settled in ADS. Z_IF defines the impedance of the IF port and it has been set to 100 Ω which is a compromise between the expected IF impedance of the pair of diodes 150 Ω and the input impedance of the IF low noise amplifier (LNA) 50 Ω, [Tho05]. The

harmonics of higher order than 2*f_{LO} are modelled with embedding impedance of Z_HF=10+j0 [Hes96].
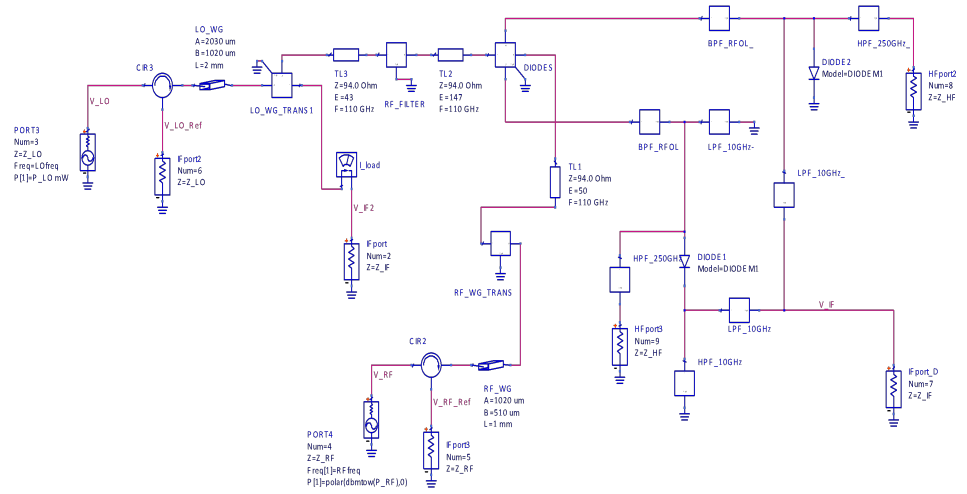

Fig. 3-22 Schematic of the first step of the Mixer ADS simulation process.

Once the mixer model is determined, Fig. 3-22, the first optimization run can be performed. For this optimization the TL employed to connect the different mixer blocks are swept in order to reach a valuable result in terms of low noise temperature and conversion loss (which will be equivalent to a good diode matching). Whenever a good solution is obtained, the next step can be done. In the second step of the simulation process, the ADS ideal transition lines are replaced by S-parameter blocks with the corresponding transition line simulated in HFSS, i.e. the ideal TL becomes real TL, Fig. 3-23. This transition line is calculated by means of a proportional rule between the wavelength and the degrees of the ADS TL. For example, if an ideal transition line of the following characteristics in ADS, see Fig. 3-23 (a), has to be simulated in HFSS, Fig. 3-23 (b), the ideal to real transition line transformation is done as follows:
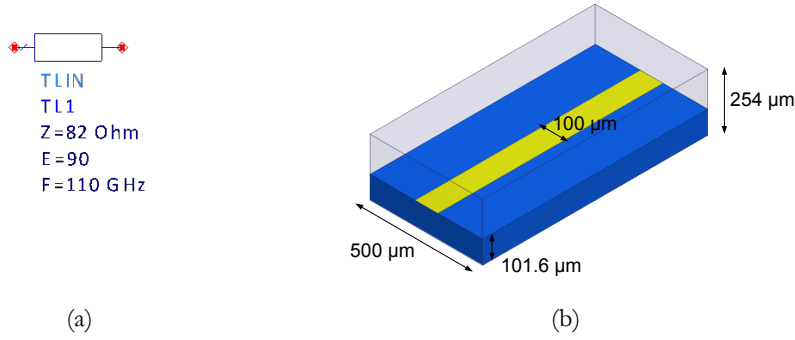
<div align="center">(a)   (b)</div>

Fig. 3-23 (a) ADS ideal transition line and (b) equivalent transition line in HFSS (real TL).

Z= 82 Ω corresponds to a microstrip transition line of 100 μm width over a COC substrate of 101.6 μm located inside a metallic block of 500 μm width x 254 μm height.

The parameter E corresponds to the electrical length of the ideal transition line in degrees. In this example E= 90. This value is the one that determines the TL length. If a transition line of the characteristics shown in Fig. 3-23 is simulated in HFSS its wavelength at 100 GHz is   2049.9 μm. So that, the following rule can be applied in order to know the equivalent length of an ideal TL line of E=90.

$$\lambda_{TL} = \frac{E_{TL}\lambda}{E} \qquad\qquad 3\text{-}2$$

In this case, λ_{TL}=512.5 μm.

Fig. 3-24 shows the ADS schematic of the second step done during the sub-harmonic mixer simulation process.
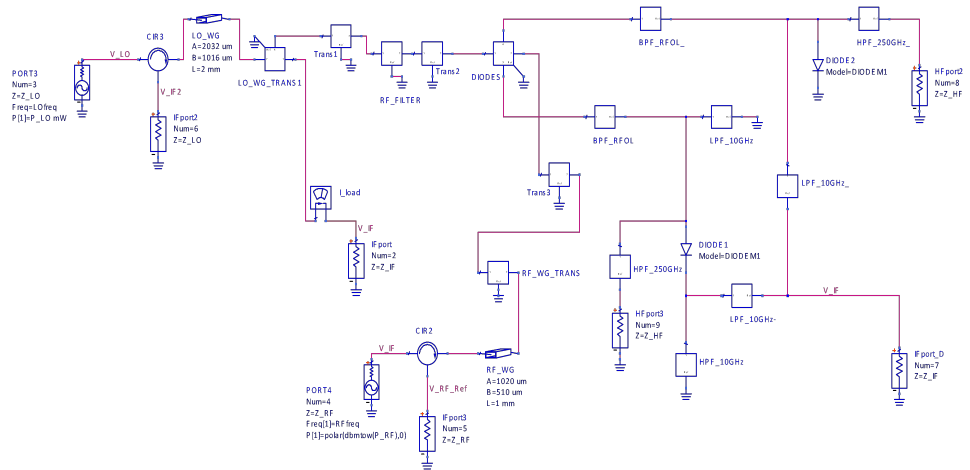
Fig. 3-24 Schematic of the second step of the Mixer ADS simulation process.

The S parameters of the equivalent TL simulated in HFSS are inserted in ADS. In the second step of the ADS simulation process a fine optimization can be done changing the length in HFSS of these real TLs in order to get the best NT and CL possible. Whenever a competitive solution is obtained (understood as low noise temperature and conversion loss), the simulation process can continue with the final step.
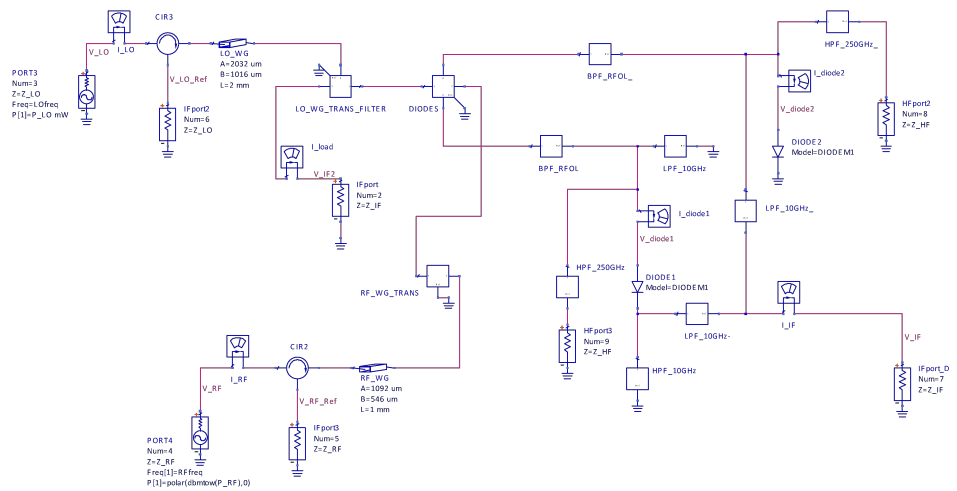

Fig. 3-25 Schematic of the third step of the Mixer ADS simulation process.

The final simulation step corresponds to the simulation of the complete circuit, i.e. all the blocks are connected. The circuit (see Fig. 3-26) is simulated completely in HFSS and its S-parameters are imported to ADS aiming to confirm that the mixer performances; noise and conversion loss, are close to their ideal values calculated in Section 3.3. Note that the dimensions of the complete mixer device depicted in Fig. 3-25 are gathered in Appendix B.
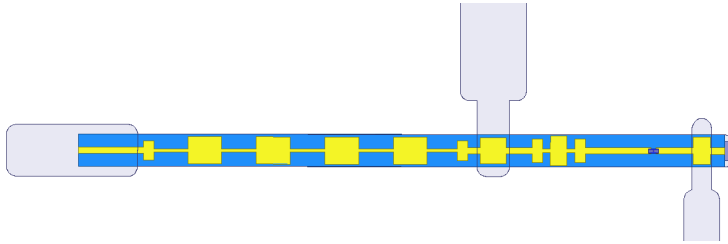

Fig. 3-26 Schematic of the HFSS complete mixer design.

Fig. 3-27 shows the differences along the optimization process. The red line refers to the last simulation which corresponds to the most realistic one since a full HFSS simulation has been performed with the complete mixer. Obviously some differences can be appreciated. Nevertheless, these discrepancies are quite small and can confirm that the simulation process followed is consistent.

(a)   (b)

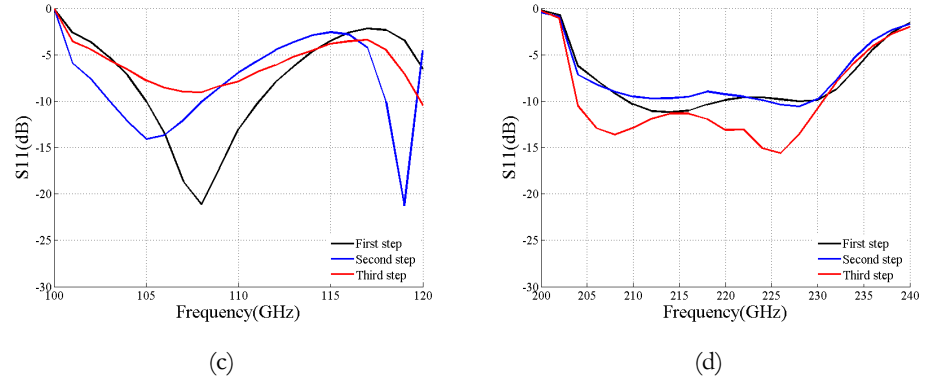(c)   (d)
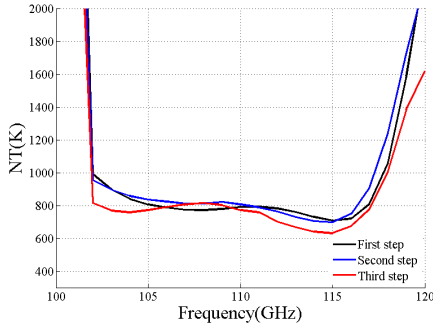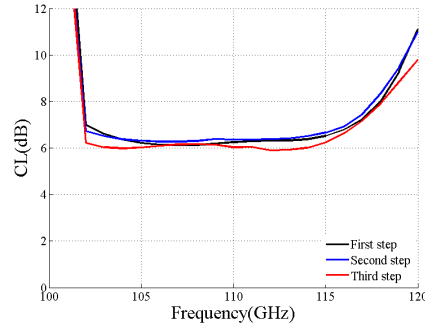
Fig. 3-27 (a) Noise temperature, (b) conversion loss, (c) LO matching, (d) RF matching, for the optimization process.

Simulated noise temperature, Fig. 3-27 (a), presents values below 1000º K over a 14 GHz bandwidth (centred on 107 GHz) in all cases, with a minimum value of 631 K at 115 GHz. On the other hand, conversion loss, Fig. 3-27 (b), has minimum values of 6 dB and they are below 7 dB in a bandwidth wider than 12 GHz (centred on 107 GHz). The final simulation, third step of the process, shows an LO matching below -5dB in a bandwidth of 10 GHz. Analysing also the RF matching it can be seen that the S_{11} presents values below -10dB in a bandwidth of 26 dB (centred on 213 GHz).

The diode impedance as well as the impedance at the LO and RF port have been calculated for the final mixer design.

Freq.(GHz)	ZdiodeLO (Ω)	ZdiodeRF (Ω)	ZLO (Ω)	ZRF (Ω)
100	NaN-NaNi	NaN-NaNi	NaN-NaNi	NaN-NaNi
101	481.78 - 322.57i	NaN-NaNi	240.89 + 161.29i	NaN-NaNi
102	460.37 - 280.46i	173.6 - 74.325i	230.19 + 140.23i	86.80 + 37.1625i
103	437.06 - 241.86i	166.65 - 68.804i	218.53 + 120.93i	83.33 + 34.40i
104	421.63 - 220.41i	162.46 - 65.747i	210.81 + 110.21i	81.23 + 32.87i
105	409.13 - 204.73i	159.24 - 63.515i	204.57 + 102.36i	79.62 + 31.76i
106	401.21 - 196.05i	157.25 - 62.347i	200.61 + 98.02i	78.62 + 31.17i

107	398.25 - 194.25i	156.51 - 62.272i	199.12 + 97.13i	78.25 + 31.14i
108	395.85 - 193.19i	155.89 - 62.359i	197.92 + 96.60i	77.95 + 31.18i
109	399.08 - 200.19i	156.75 - 63.724i	199.54 + 100.09i	78.38 + 31.86i
110	401.21 - 205.68i	157.31 - 64.866i	200.60 + 102.84i	78.65 + 32.43i
111	409.52 - 221.82i	159.63 - 67.709i	204.76 + 110.91i	79.81 + 33.85i
112	414.92 - 234.48i	161.29 - 70.007i	207.46 + 117.24i	80.64 + 35.00i
113	426.15 - 260.68i	164.98 - 74.373i	213.08 + 130.34i	82.49 + 37.19i
114	433.63 - 282.85i	167.92 - 78.175i	216.81 + 141.42i	83.96 + 39.09i
115	443.76 - 318.48i	172.73 - 84.148i	221.88 + 159.24i	86.36 + 42.07i
116	446.33 - 334.84i	174.86 - 87.228i	223.17 + 167.42i	87.43 + 43.61i
117	447.93 - 348.94i	176.79 - 90.021i	223.97 + 174.47i	88.40 + 45.01i
118	432.14 - 292.3i	168.99 - 81.622i	216.07 + 146.15i	84.50 + 40.81i
119	407.47 - 231.95i	160.39 - 72.872i	203.73 + 115.97i	80.20 + 36.44i
120	385.32 - 190.28i	153.99 - 67.601i	192.66 + 095.14i	76.99 + 33.81i

*NaN=Not available. It is employed for really high values.

Table 3-3 "Real" approx. diode impedances.

Table 3-3 shows that the diode impedance at the LO frequency has values between 385 to 480 Ω for the real part and between -200 to -350 Ω for the imaginary part. Remember that the ideal design had values around 460 and -330 Ω respectively. On the other hand, the diode impedance at the RF frequency has values between 153 to 173 Ω for the real part and -60 to -90 Ω for the imaginary part. Note that these values are close to the obtained for the ideal mixer design (around 180 and -80 Ω respectively), see Section 2.3.

Fig. 3-28 shows the corresponding reflection coefficients in the Smith Chart as function of frequency for the LO and RF ports. Note the good agreement with the calculated for the ideal sub-harmonic mixer analysis, Fig. 3-10. Note also, that the minimum noise temperature, 631 K, and conversion loss, 5.9 dB, values obtained, Fig. 3-27, are close enough to the ideal ones, 600 K and 5.7 dB respectively, Fig. 3-9.
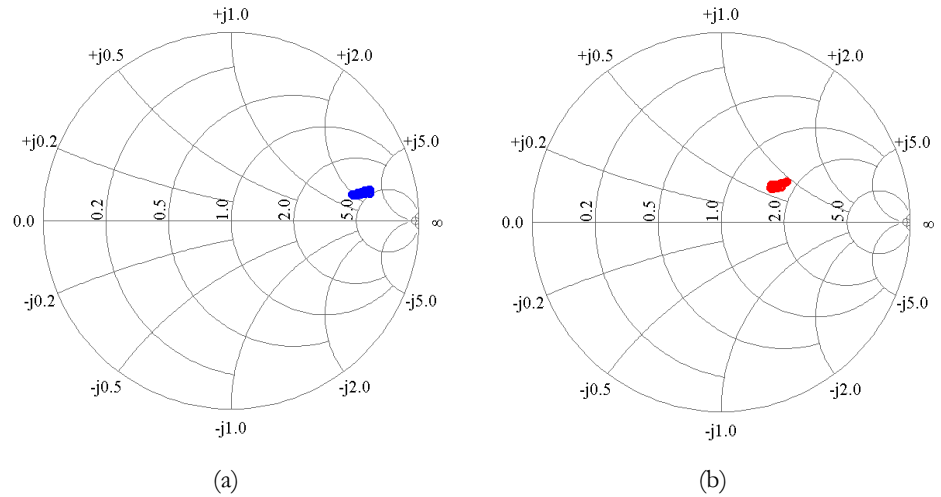
Fig. 3-28 Real (a) LO, (b) RF ports reflection coefficients.

A comparison of the port impedances for the ideal mixer and the final design is depicted in Fig. 3-29. The real and imaginary part of the LO and RF port impedance are compared. Note that a good agreement is achieved for the RF impedance port which is related to a low conversion loss. On the other hand, the LO matching port is also quite good (related to a low input power) and the best matching point is located between 114 GHz to 118 GHz in which, as it will be presented later on this chapter, the best mixer performance has been measured.
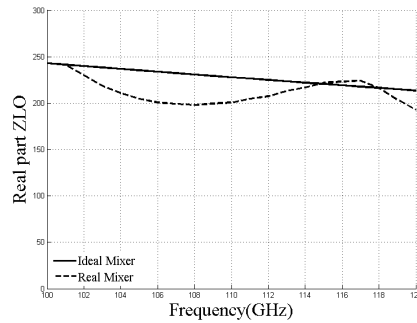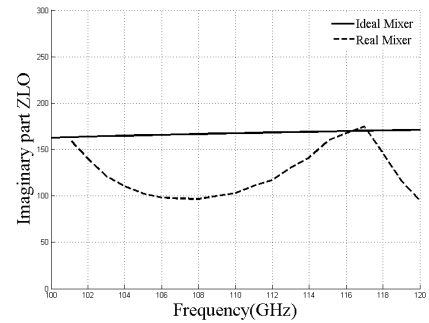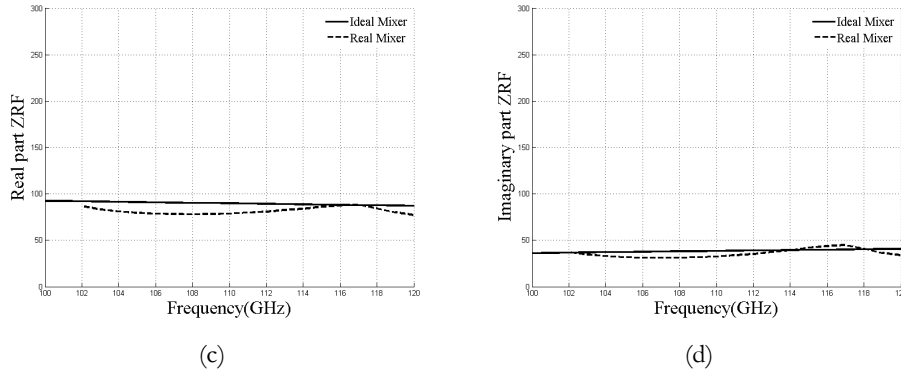

(a)   (b)

Fig. 3-29 LO and RF port impedances comparison between ideal and final mixer design (a) Z_{LO} real part, (b) Z_{LO} imaginary part, (c) Z_{RF} real part and (d) Z_{RF} imaginary part.

The mixer behaviour has been optimized for an LO input power of 2.5 mW but in order to analyse its behaviour a simulation of the noise temperature and conversion loss have been done for different power input values, see Fig. 3-30.
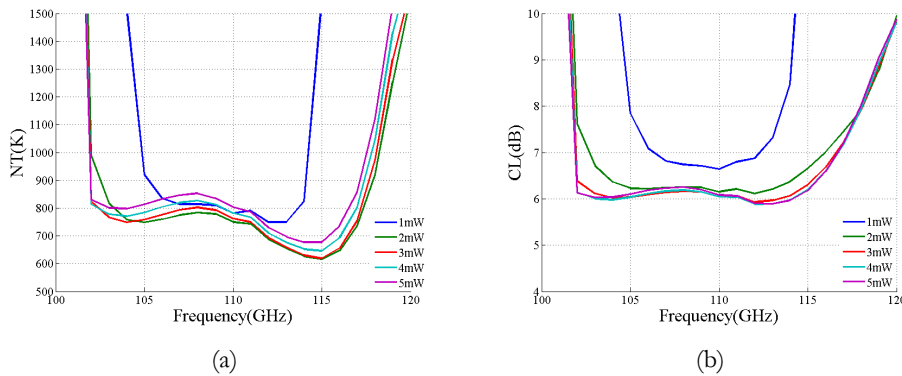

Fig. 3-30 (a) Noise temperature and (b) conversion loss dependences with the Lo input power.

The best performance is obtained for input values between 2 and 3 mW, as expected since it was optimized for similar input values. Nevertheless, neither the noise temperature nor the conversion loss varies considerably when the input power changes except for the case in which the LO power is 1 mW. For this case the operational bandwidth, understood as

bandwidth in which the NT is below 900 K, is reduced and the CL increases heavily.

3.4 Mixer fabrication process

This section describes the complete fabrication process of the mixer presented in this chapter. The COC material will be the substrate to fabricate the microstrip mixer circuit.

A thin layer of gold (between 1-2   ) is for the first time directly deposited on the COC substrate as conductor material using a QUORUM Q 150 TS Sputtering system. As a difference with other sub-mm wave materials, it has been proven that COC can be directly gold sputtered, without using any intermediate material, such as chromium or nickel, as needed when quartz is used. This clearly simplifies the manufacturing process.

Afterwards, the microstrip circuit is printed into the golden substrate using a laser milling machine, LPKF ProtoLaser 200. This equipment allows the user to print circuits at high frequencies over substrates specially design to work at these high frequencies. The equipment parameters are adjusted to obtain a precise finished and to avoid coarse edges. ProtoLaser 200 has a power of 12 W and it is able to print structures with a resolution of 25 μm although best results are obtained for details above 50 μm. Taking into account the mixer design, the critical distance comes from the gap left for the diode´s welding. This gap has a size of 80 μm, therefore it is not considered a problem.

<div align="center">(a)   (b)</div>
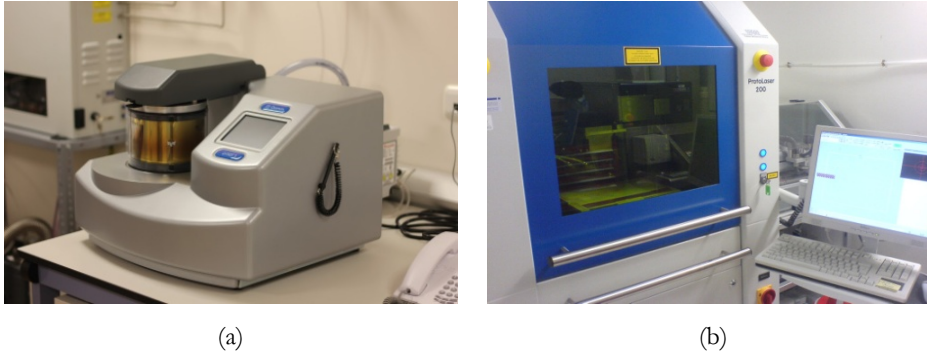
<div align="center">Fig. 3-31 (a) QUORUM Q 150 TS Sputtering System, (b) LPKF ProtoLaser 200.</div>

A set of circuits has been fabricated. They are removed by means of using a Disk Dicing Saw 321. In this case the COC thickness doesn´t have to be lowered down since a commercial substrate thickness is employed; nevertheless, if necessary, it could be done using the same tool.

<div align="center">Fig. 3-32 Disco Automatic Dicing SAW DAD 321.</div>

Some photos of the resulting microstrip mixer circuit are shown in Fig. 3-33; i.e., (a) the RF transition and the gap where the diodes will be welded (this gap is 80   long), (b) the RF filter together with a section of the LO Filter, (c) the LO filter and (d) the microstrip section where the IF connector is placed.
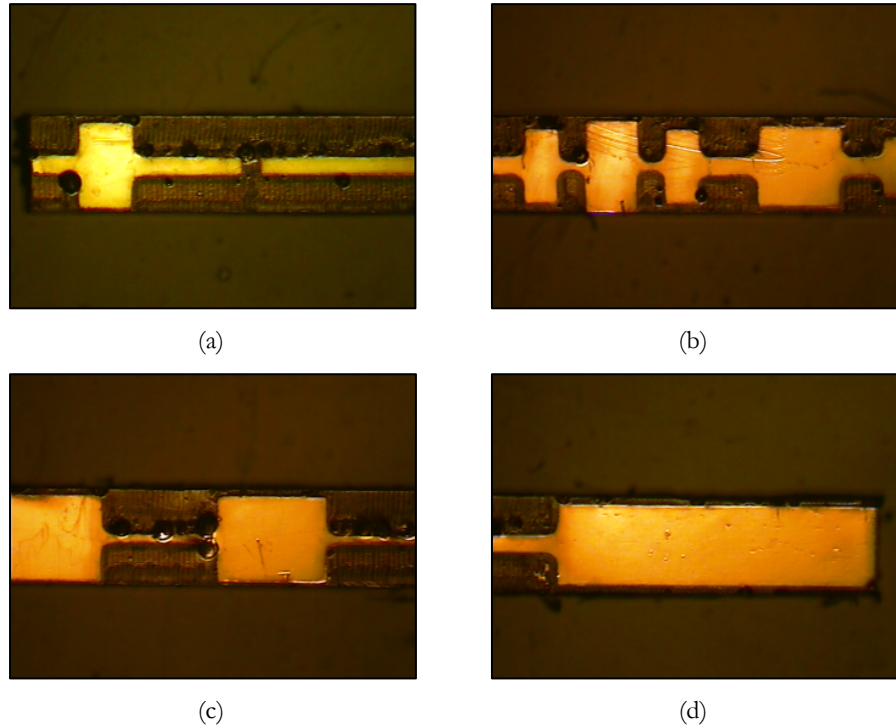
(a)

(b)

(c)

(d)

Fig. 3-33 Several photos of the microstrip mixer circuit on Topas substrate.

The diode used for the sub-harmonic mixer implementation is a VDI model in antiparallel configuration. This diode is welded to the microstrip line, within the microstrip gap, using EPO-TEK-H20E silver loaded epoxy adhesive. This epoxy is specifically designed for microelectronics and optoelectronics applications. The microstrip circuit is positioned and aligned into the metallic block where the metallic waveguides are implemented (see next section) and then it is also welded to it. The temperature used for the welding procedure is kept low in order to ensure the COC' characteristics are not affected since its melting temperature is 180° C; in particular, a curing process of 4 hours at 100° is followed. Some photos of the welding results are depicted in Fig. 3-34.
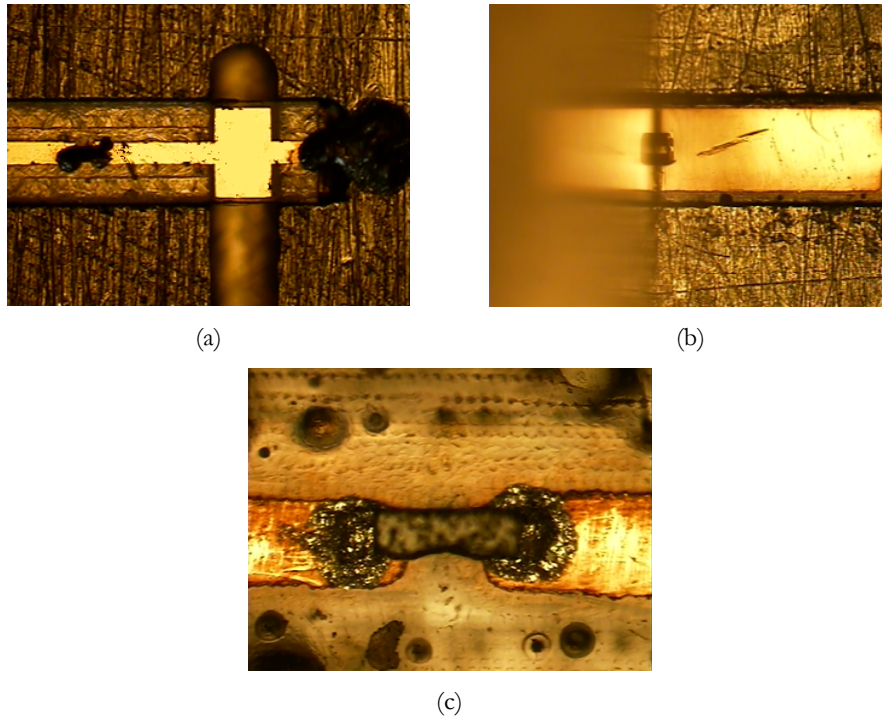
(a)

(b)

(c)

Fig. 3-34 Photos of the (a) microstrip welded to the metallic block, (b) the IF connector area and (c) the diodes welded to the microstrip.

Once the mixer is assembled, the diode series resistance was measured. First the current through the diodes is measured using Keithley 2611 System Source Meter and the series resistance is calculated thanks to the I-V curve. The obtained values are 18.8 Ω for the positive side and 16.3 Ω for the negative side for a voltage value of 0.8 V.

Note that according to the diode specifications, its series resistance is 13 Ω, therefore, an increase between 3 and 5 ohms has been obtained due to the losses produced by the silver epoxy and the microstrip line.

3.5   Mixer Block design

The mixer block designed for the sub-harmonic mixer is presented in this section. The block was fabricated on aluminium and the IF connector

used was a K-connector. Moreover, the LO and RF ports have the standard flange at WR8 and WR4 with 4-40 UNC screws. The block is divided into two parts and each one has half the waveguide circuit. Both mixer block parts will be assembled together using metric screws 2 as well as the IF connector.
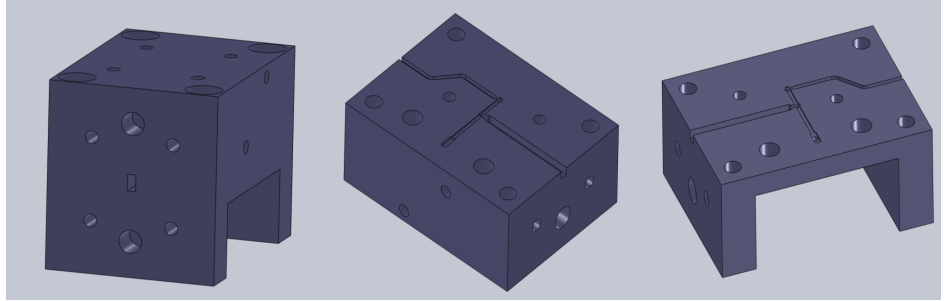

Fig. 3-35 Images of the designed mixer block.

More information about the block dimensions and some images of the final fabricated block are gathered in Appendix B.

3.6   Mixer Measurement

The setup used to characterize the sub-harmonic mixer is shown in Fig. 3-36.

The LO signal is generated by a high power mm-wave source Elva Backward Wave Oscillator in the range of 100 to 125 GHz. The signal gets to an isolator, Elva Mod: IF-08 S-0405/05, which avoids reflections towards the LO generator. After that, the LO signal power is selected to achieve the appropriate power level at the LO port of the mixer. The IF chain employed to measure the sub-harmonic mixer consists of two IF amplifiers (GAMP0100.0600SM10) with 35dB gain, a Hewlett Packard power sensor and the EPM Series Power Meter from Agilent. Both amplifiers are biased +5 V using a Power Supply FAC-363B from Promax. An RF feedhorn, 32240-25 S/N203160 Flann Microwave, is attached to the RF port of the mixer.
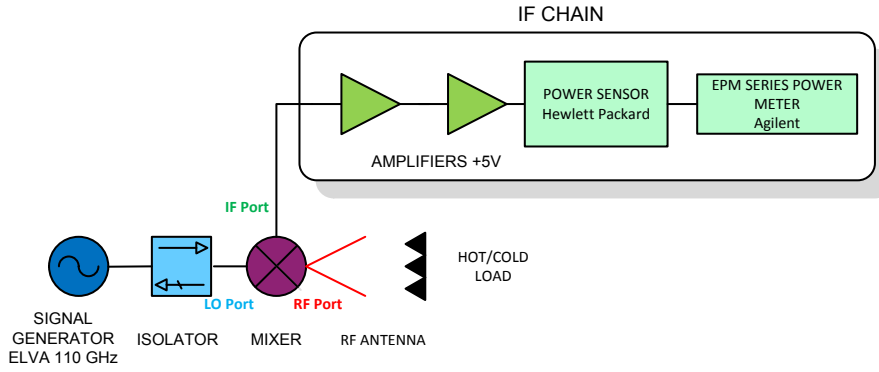
Fig. 3-36 Mixer setup for characterization.

The mixer noise temperature and conversion loss are calculated using the Y-Factor method [Agi04] using liquid nitrogen and room temperature as cold and hot sources respectively [Maa93]. The hot load is obtained placing an absorbance material, Tesselating TeraHertz RAM, in front of the RF feed horn. In order to get the cold load, the absorbance is submerged into liquid nitrogen and place in front of the RF antenna. Thanks to the difference in power between the hot load and the cold load the Y-factor is calculated. The IF chain noise temperature is also calculated following the same procedure. In this case, a cable with a 50 Ohm load is attached to the IF pre-amplifier in order to simulate the hot load. The cold load is obtained submerging this cable into liquid nitrogen.

The IF Y-factor measurements and the calculated noise temperature are presented below:

- Power with hot load (290 K): 1.267 mW.
- Power with cold load (77 K): 0.623 mW.

$$Y = \frac{1.267}{0.623} = \frac{290 + T_{IF}}{77 + T_{IF}} \qquad\qquad 3\text{-}3$$

$$T_{IF} = 129.2 \ K \qquad\qquad 3\text{-}4$$

The performance of the mixer is extracted from these measurements. Note that this process is carried out for different LO frequencies and

powers. The measured mixer noise temperature is shown in Fig. 3-37 (a) for an LO power of 2 mW, 2.5 mW and 3 mW. The best result is obtained for 118 GHz for a supplied LO power of 2.5 mW.

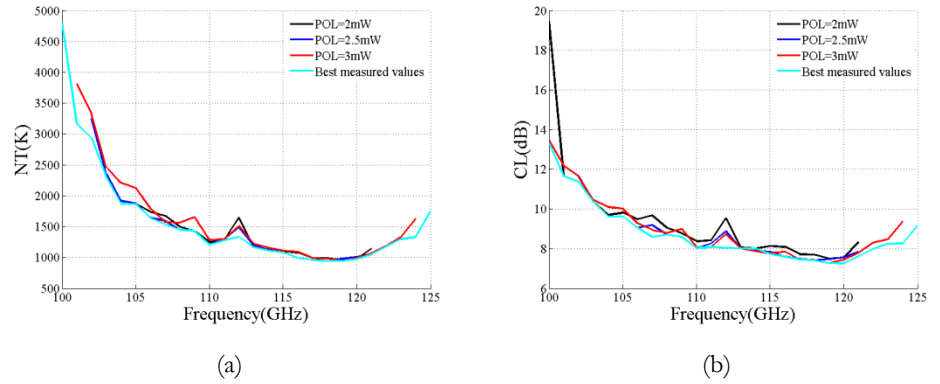(a)   (b)

Fig. 3-37 Measured (a) noise temperature and (b) conversion loss of the mixer vs. frequency for different LO Powers.

Fig. 3-37 (b) includes the conversion loss values obtained for different LO power levels. Note that the best results are obtained for a LO power level of 2.5 mW.

It is important to note the low levels of LO power needed to feed the sub-harmonic mixer. Good performances of the mixer have been obtained from power levels of 2 mW, this means that a good matching of the diodes has been obtained.

The dependence of the DSB noise temperature with the frequency for the best LO power levels (between 2 and 3 mW) is plotted in Fig. 3-38 (a). The best result is obtained for an LO frequency of 118 GHz having the minimum noise temperature value of 946 K. Conversion loss results have a minimum value of 7.2 dB measured for an LO frequency of 120 GHz, Fig. 3-38(b).
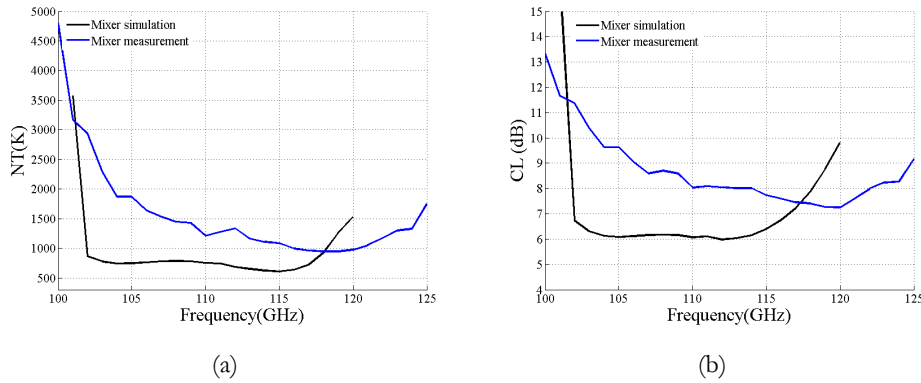
Fig. 3-38 (a) Noise temperature, (b) conversion loss comparison between mixer simulation and measurement.

Fig. 3-38 also presents the comparison between the simulated and measured results. The differences are noticeable and can be produced by several factors. First of all, the fabrication process can influence the results, moreover, the variations in the diode characteristics (anode area, epitaxial doping...) compared to the simulated model and in the chip mounting (position of the microstrip to the waveguide transition, position of the diode, waveguide short…) can also cause discrepancies. Higher noise temperature and conversion loss can also be due to the unbalance of the diodes. If the diode characteristics change then also the embedding impedances change. All that, will affect the mixer performance and so that, the discrepancies observed could be understood.

One of the most important claims of this chapter is the use of the COC substrate due to its lower losses when compared with conventional substrates used in the development of sub-mm wave components. In order to demonstrate this issue, the same mixer design has been fabricated and measured using Rogers duroid 5880 substrate. The choice of this substrate versus quartz comes from the fact that both materials, i.e., COC and Rogers duroid 5880 exhibit a similar dielectric constant value and the same mixer design can be used for both.

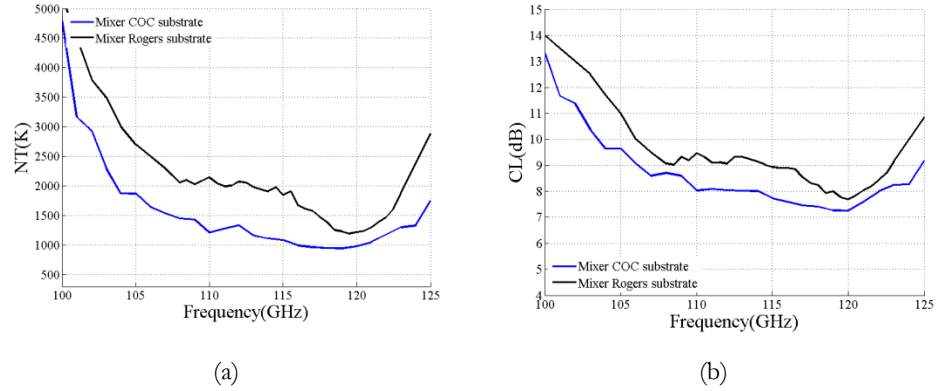(a)   (b)

Fig. 3-39 (a) Noise temperature and (b) conversion loss comparison between mixers fabricated using Topas and Rogers 5880 substrate.

Fig. 3-39 shows the measured noise temperature and the conversion losses for the two identical mixers fabricated in COC and Rogers 5880 substrates for an LO power between 2 and 3 mW. Once manufactured, the measured series resistance of the mixer implemented in Rogers is 21.10 Ω for the positive side and 22.3 Ω for the negative side. Note that when measuring the series resistance once the mixer block is assembled, the substrate is taken into account.

The results clearly indicate better performance offered by the mixer fabricated with COC substrate versus the one built in Rogers 5880. In particular, an improvement of 300 K in noise temperature values and 0.5dB for the conversion losses has been obtained.

3.7   New sources of noise

Due to the differences appreciated between the simulated and measured performance of the mixer, see Fig. 3-38, a deeper study in bibliography has been done with the intention of finding a reason for this fact. Searching around, a new source of noise presented in mixer has been found [Tho04]. This is called the hot electron noise and was demonstrated by [Heg85] and [Cro87]. They said that when the current density that crosses the junction is quite important, the electrons distribution is warmed

up and an excess noise appears. For this reason, the equivalent noise temperature of the series resistance varies during an LO cycle and can be expressed as:

$$T_{R_S} = T_0 + K I_d^2 \qquad\qquad 3\text{-}5$$

Where K is the noise constant and I_d the current that crosses the diodes. In order to determine the contribution of this source of equivalent noise at IF, it is necessary to take into account the correlation between the different current harmonics generated by the LO signal. ADS software is not considering this noise and indeed it is not possible to model it in a rigorous way. Nevertheless, it is possible to do an approximation of the hot electron noise contribution considering the LO current as non-correlated. These harmonic currents generate noise in an independent way at the IF output. In order to estimate the excess noise, the equivalent noise source for the hot electron noise is considered as proportional to the sum of squares of the LO harmonic currents.

[Tho04] says that in the case of a sub-harmonic mixer with LO currents in the order of mW, 4 current harmonics are taken into account. Therefore, the spectral power density of the noise source is determined by:

$$\langle v^2 \rangle = 4 k_B R_S K \sum_{n=1}^{4} |i_d(n)|^2 \qquad\qquad 3\text{-}6$$

Where K is the noise constant determined by the anode diameter, the relaxation time, the electronic mobility and the doping of the epitaxial zone [Cro87]. [Tho04] selects a K=2.44*10^7 K/A^2 and we will take the same value since it is not possible for us to know or measure the diode parameters required to calculate it.

Taking into account the current values of the different LO harmonics calculated in ADS, the spectral power density can be calculated. The series resistance, R$_S$ in our case is considered 13 Ω and the K value is 2.44*10^7 K/A^2. Therefore the spectral power density is:

$$\langle v^2 \rangle = 4 * 1.38 * 10^{-23} 13 * 2.447 * 10^7 * 1.9 * 10^{-5} = 3.33 * 10^{-19} \frac{V^2}{Hz} =$$
$$5.77 * 10^{-10} \ \frac{V}{\sqrt{Hz}} \qquad\qquad 3\text{-}7$$

Once the spectral power density has been calculated it can be added to the mixer performance including two Noise voltage sources in series with the diodes, see Fig. 3-42 and Fig. 3-41.
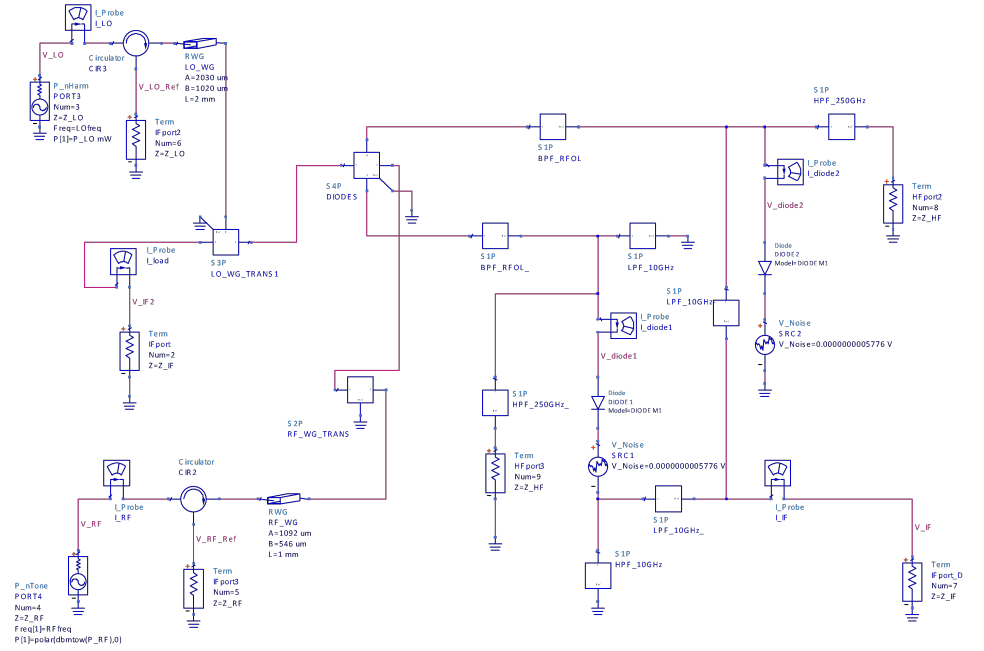

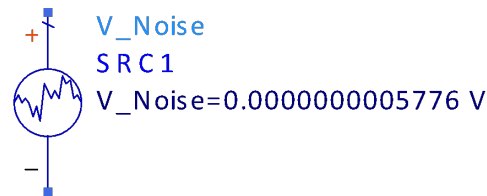Fig. 3-40 Schematic of the ADS mixer design including the calculated Hot Electron Noise Source (HENS).

Fig. 3-41 Schematic of the Noise Voltage Source implemented in ADS.

V_Noise represents the Spectral Density Power in $\frac{V}{\sqrt{Hz}}$ calculated in Equation 3-25. Finally, including the hot electron noise the simulation of the sub-harmonic mixer at 220 GHz has been carried out obtaining an increase of noise temperature value. A frequency shift in the simulation is again obtained compared to the measured results (5 GHz shift) probably due to fabrication tolerances, for this reason this shift has been applied to the simulation results in order to compare them to the measured results, see Fig. 3-42.
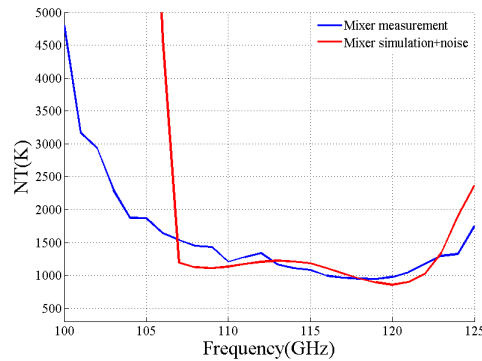
Fig. 3-42 Noise Temperature comparison between measurements and simulation with HENS.

Fig. 3-42 shows a better agreement between simulation and measurements. For this reason a conclusion can be reached: the increment noise appreciated in measurements compared to previous simulations can be explained thanks to the hot electron noise and the fabrication process and tolerances.

The hot electron noise source does not influence the conversion loss simulation. For this reason, a study about the parameters that can affect it has been done. It is well know that the diode series resistance contributes to the increment of its value, see Section 2.3, but it is not the only one. A mismatching between the mixer IF port and the connector also increases the conversion loss. Varying the IF port impedance of the ADS schematic mixer the conversion loss changes, obtaining higher values, more similar to

the measured ones. Fig. 3-43 shows the increase in the conversion loss related to the IF port impedance.
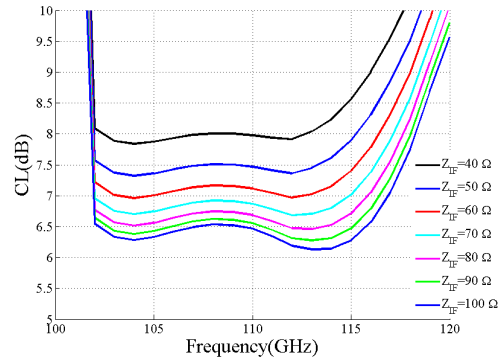

Fig. 3-43 Conversion loss dependence with the IF port impedance.

Taking these results into account a comparison between the measured conversion loss and the simulated results including a mismatching in IF port has been done, see Fig. 3-44.
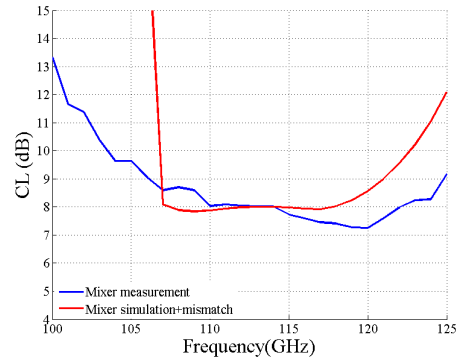

Fig. 3-44 Noise Temperature comparison between measurements and simulation including the IF mismatching.

Fig. 3-44 shows a good agreement between simulation and results, therefore, the previous discrepancies can partially be explained.

3.8   Conclusions

Within this chapter a heterodyne receiver which will be part of an imaging array explained in Chapter 4 has been introduced. Moreover, this chapter has shown the improvement in the performance achieved by using COC substrates in millimetre wave devices. In particular the design, fabrication and measurement of a sub-harmonic mixer working at mm-wave frequencies implemented on a COC substrate have been presented. Its performance (noise Temperature values below 1000 K together with conversion losses values of 7.2 dB have been obtained with very low supplied levels of LO power, 2.5 mW) represent 300 K noise temperature and 0.5 dB conversion loss reduction with respect to those obtained by the same mixer built on a Rogers substrate. Therefore, the use for the first time of COC substrate at sub-mm wave frequencies has led to obtain better performances when designing sub-mm wave devices due to its lower losses. Furthermore, direct sputtering of gold over COC substrate has been proven to be reliable which introduces a strong advantage versus other conventional substrates. The use of COC material opens the possibility of improving the state-of-the-art performances of mm-wave mixers by integrating the flip-chip diodes on this substrate.

<div align="right">

CHAPTER 4

</div>

DESIGN OF AN IMAGING ARRAY AT 220 GHz

This chapter presents the development of an imaging camera operating at 220 GHz for defence and security applications. The development of this camera is implemented within two research projects, INNPACTO and Terascreen. Here the array receiver design, the measured performance of each mixer element that forms the array and the cuasi-optical system are presented.

4.1 Array Design

The array presented in this chapter is based on the sub-harmonic mixer developed in Chapter 3. Here a configuration of eight mixer elements is implemented. The only difference compared to the mixer design of Chapter 3 is the fabrication process since instead of using a proto laser a lift off procedure will be employed, see Section 3.3.

The main goal of this section is the metallic block design in which the microstrip circuit will be inserted. Several issues (array configuration, assembled, IF connection…) have to be taken into account when designing the blocks since it is important to develop a compact and functional array to be integrated with the imaging camera.

The same model block is used in the eight mixer elements in order to reduce the total cost owing to it is easier and cheaper to fabricate a single model. It is also important to consider the optimal array configuration.

<div align="center">

113

</div>

Note that this array will be part of an imaging camera (at the Terascreen project the array will be integrated with a receiver at 94 GHz and another one at 360 GHz), for this reason the resolution (understood as distance between beams) and swept area (understood as area possible to capture) has to be the better and the larger as possible. First of all a symmetrical (both array lines perfectly aligned) 2x4 array configuration was considered. The main problem this set up presents is based on the resolution obtained since the pixels captured by every mixer element are separated a distance around 100 mm and what it´s more, due to the configuration of the imaging camera, see Section 3.4, the system is able to do a mechanical movement to sweep a vertical area which this configuration is not taking advantage of (detectors situated on the same vertical will capture almost the same information). This is why an offset configuration was taking into account. In this case, the array is composed by two lines of 4 elements in which the line on top is misfit to align the joint of two of the elements of the line below, see Fig. 4-1.
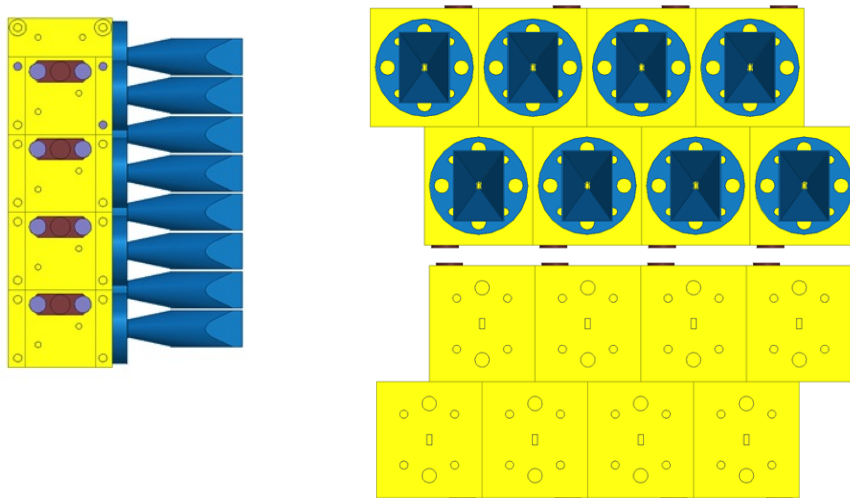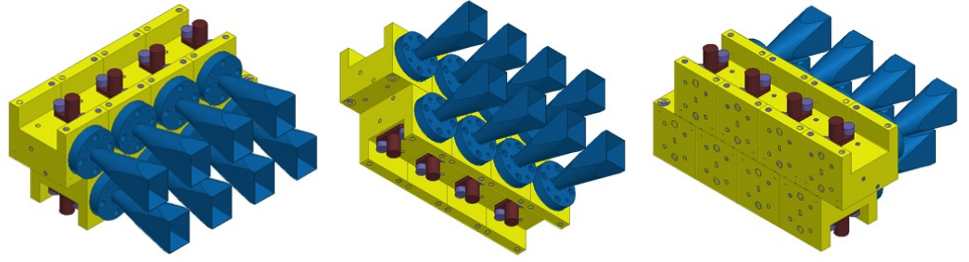
Fig. 4-1 Different views of the proposal mixer array configuration.

The principal advantage of this configuration is the increase in the resolution without losing any information since the pixels are now separated a distance approximately of 50 mm, half the distance of the previous set-up.

Nevertheless, although the offset configuration was the ideal one and the selected to be implemented, finally an array set-up of 1x8 elements was fabricated, see Fig. 4-2. The reason of this change was due to fabrication issues. In order to feed the LO mixer ports, a power splitter is used. This power splitter was designed by members of the Antenna Group and the initial idea was fabricating two 1x4 power divisors. Finally due to fabrication costs this was replaced by a single power 1x8 splitter and indeed the mixer array configuration was changed to 1x8 elements. Although the resolution is lower, the possible horizontal sweeping area has been increased giving the possibility to obtain larger images. Moreover, in order to avoid extra losses in the splitter fabrication the waveguide channels need to be cut in the E plane and therefore, the input LO and RF waveguides of the mixer will have horizontal polarization, see Fig. 4-2.
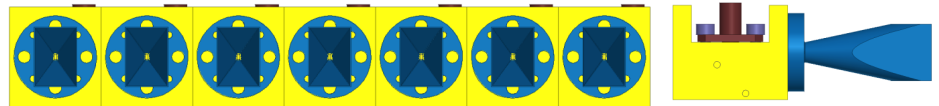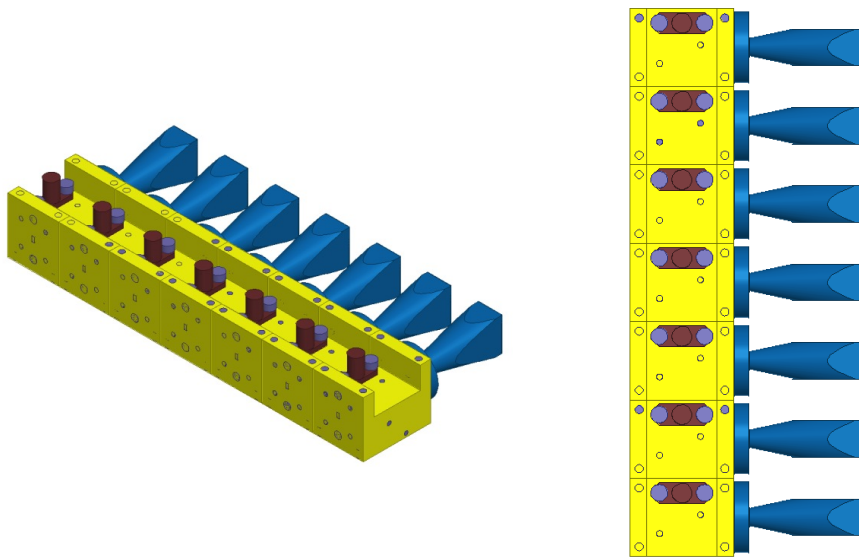
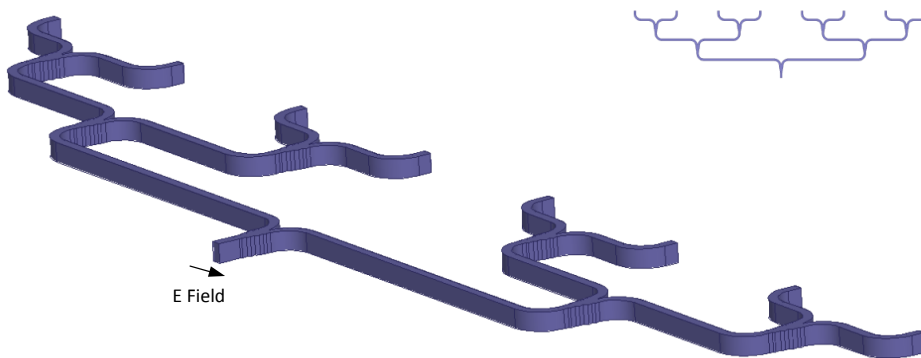Fig. 4-2 Schematic of the final mixer array configuration.

E Field

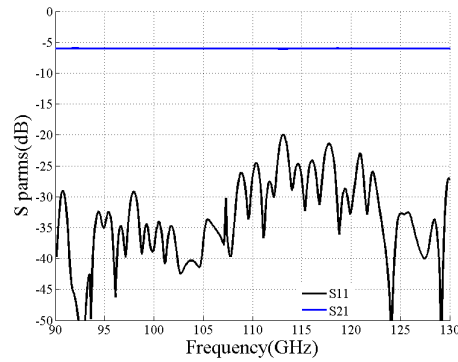Fig. 4-3 Schematic of the 1x8 splitter.

Fig. 4-4 Simulated S-params of the 1x8 splitter.

Fig. 4-4 represents the HFSS simulated S-parameters of 1x8 splitter. Note that the S11 is below -20 dB for the complete operational frequency band and S21 (which represents the transmission of each of the output waveguides of the splitter) is -6 dB also in the whole frequency band.

The array elements are aligned to each other by means of pins allocated at the lateral sides of the blocks, see Fig. 4-5. The blocks also have alignment pins placed on the back face in order to align two lines which are not used in this configuration.
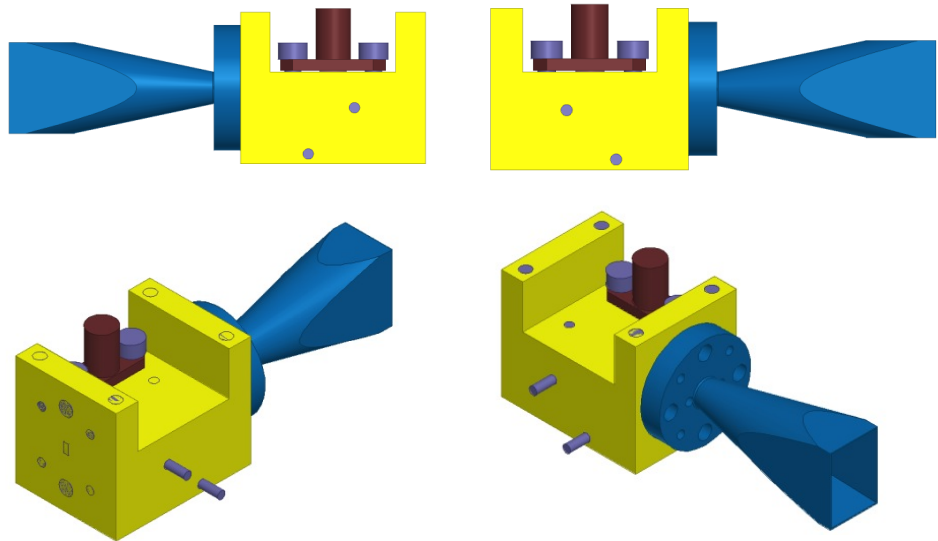
Fig. 4-5 Pins alignment of the blocks.

Once the array configuration was fixed the IF connector position had to be considered; a K-connector K103F from Anritsu. Due to the fact that each mixer block will be assembled laterally with another one, the only possibility for the IF connector position was having it vertically to the microstrip circuit, i.e. on the top side of the mixer blocks. Some options were considered in order to weld it to the circuit, i.e. a wire bonding (between the connector pin and the microstrip circuit), welding it using silver epoxy (directly depositing silver epoxy touching both the connector and the microstrip circuit). Finally, because of its simplicity, (make a bonding on the connector pin was quite tricky since it is not a planar surface), the option of welding it to the microstrip circuit by means of silver epoxy was chosen. The IF connector configuration is presented in Fig. 4-6.
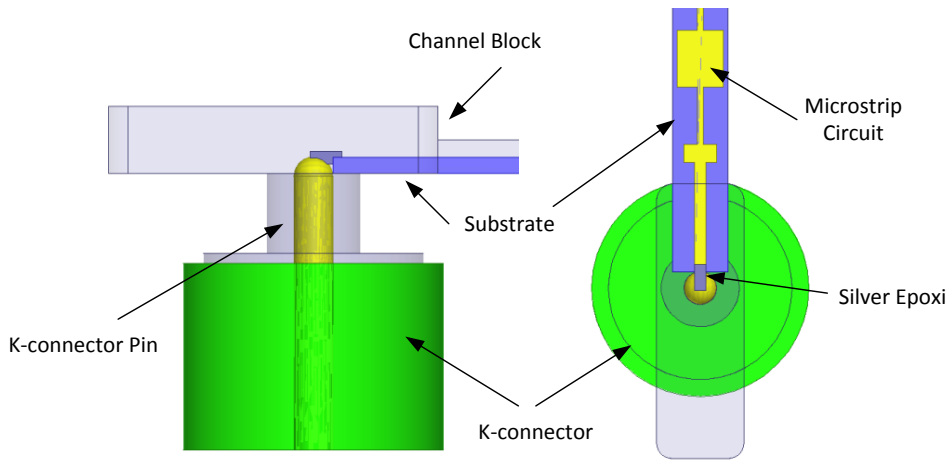
Fig. 4-6 IF connector configuration.

Note that the connector pin and the substrate are perpendicular and touching each other.

4.2   Array fabrication

In this section the microstrip circuit fabrication process is presented. Note that the mixer presented in Chapter 3 was fabricated using a Proto-

laser machine, here the circuits are elaborated using photolithography. This process is more complicated and requires a good parameters set-up in order to get a high quality result. If the process is followed correctly the results obtained are better than with other techniques.

This process requires the following elements:

- The substrate to fabricate the microstrip circuit is TOPAS with 4 mils (101.6 μm) thickness.
- A gold target used for the deposition process.
- Photoresist AZ9260.
- Developer 400K.
- Az100K in order to use it as stripper.

To carry out the complete fabrication process some equipment is employed. All this equipment is located inside the Antenna Group Clean room ISO 7.
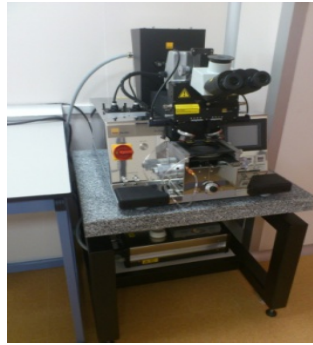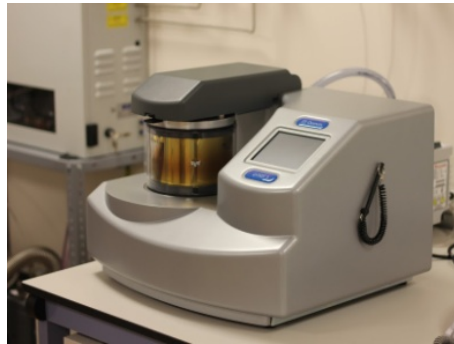

Fig. 4-7 Clean Room ISO 7.

- LabSpin 6 Spin from SUSS for the coating process.
- MaskAligner MBJ4 from SUSS used to expose the circuits to UV light.
- A mask with the circuits printed on it.
- Sputtering system Q150T from QuarumTech employed to deposit gold on the TOPAS substrate.

(a)

(b)

(c)

Fig. 4-8 (a) SUSS LabSpin 6, (b) Mask Aligner and (c) Sputtering system.

The process followed to fabricate the mixer circuits using photolithography is presented below.

- Clean & Dry: First of all it is necessary to clean the wafer, 4´´ diameter, using isopropyl. After that it is warmed up during 2 minutes at a temperature of 100 º C in order to dehydrate it and favor the adhesion of the photoresist to the substrate.

- Coating: This step consists on covering the wafer using photoresist, PR. In order to get a uniformly coating, the wafer is placed in the Spincoater (rotatory platform) and, by means of a syringe, the PR is poured. The parameters used for the coating process are: 2400 rpm during 45 seconds which

provides a thickness of 5-6 μm of PR. The thinner the deposited PR layer the better if it is thicker than the gold layer that will be deposited after that. After several tests it can be concluded that these values are the optimal ones. See Fig. 4-9 (a).

- Softbake: The photoresist needs to be cured; this is achieved leaving it on a hot-plate at 100 ° C during 6 minutes (1 minute for every μm of deposited PR).

- Rehydrate: It is recommendable to rehydrate the photoresist before exposing it to the UV light in order to get a better absorption and therefore achieve a correctly developing.

- UV exposure: With the purpose of "transferring" the circuits to the wafer, it is necessary to expose the PR to UV light, to that end; the wafer with the PR coating is placed in the mask aligner. The exposure parameters are: exposure type: Hard Contact (10 sec), exposure time: 30 sec (1093 mJ/cm^2).

- Developing: In order to complete the circuits transferring process it is required to do a developing. To get that, the wafer is submerged into a solution 1:4 of AZ400K with deionised water, DI water, during 90 seconds and after that, it is cleaned with DI water in order not to develop it too much. Next, it is dried using the spincoater working at 4000 rpm. This process can be compared to a photography developing.

- Metallization via sputtering: Finally the wafer needs to be metallized, so that, it is completely put inside the sputtering system and it is covered with gold, see Fig. 4-9 (b). Between 1 and 2 μm of gold is deposited.

<table>
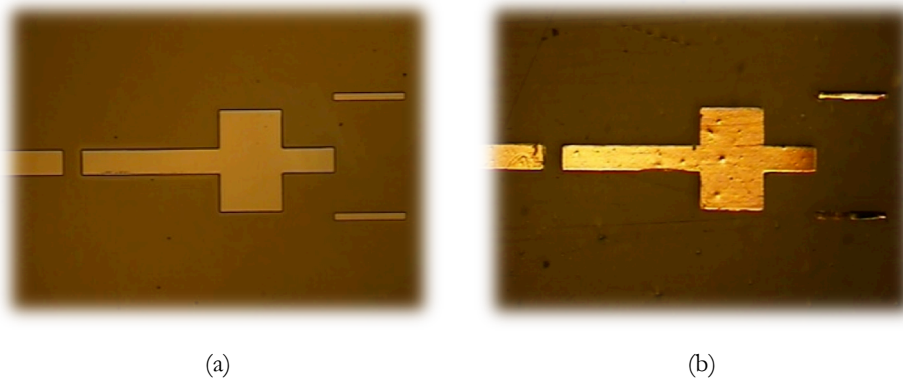<tr><td>(a)</td><td>(b)</td></tr>
</table>

Fig. 4-9 Microstrip mixer circuit (a) at the coating process (photoresist) and (b) at the metallization process (gold).

- Stripping: The excess PR and gold that covers the PR needs to be removed. With this intention, the wafer is submerged into a solution 1:1 of AZ100K and DI water. It is left there during 5 minutes and after that, the PR is easily moved away. If any excess is left, Fig. 4-10, acetone can be used to completely remove it.
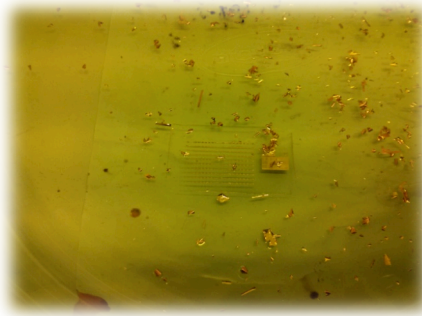

Fig. 4-10 Some excess after cleaning with the stripper.

A photo of one of the final mixer circuits is presented in Fig. 4-11. It is possible to appreciate all the sections of the mixer microstrip circuit: the LO filter, the LO transition, the RF filter, the space left for the diodes and the RF transition. The circuit is perfectly defined and no imperfections are appreciated.

Fig. 4-11 Photo of the complete microstrip mixer circuit.

4.3   Array Measurement

The eight mixer blocks that form the receiver array have been fabricated and the microstrip circuits have been assembled on them.
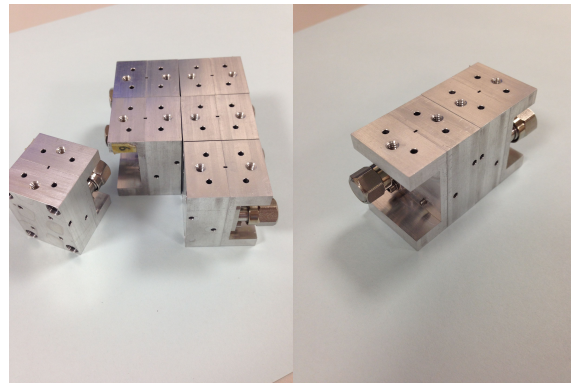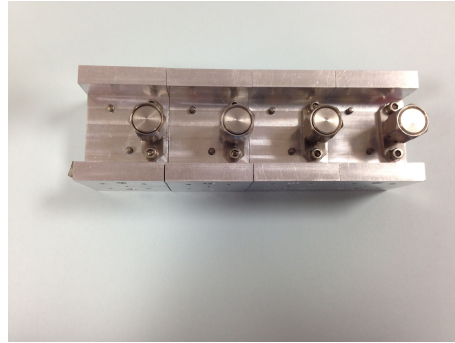

Fig. 4-12 The eight mixer fabricated blocks that form the array.

This section presents the characterization of each of the mixer elements of the array. In order to reduce the length of the results presented here only the comparison of the performance of the eight detectors are presented. The complete set of results is gathered in Appendix C.

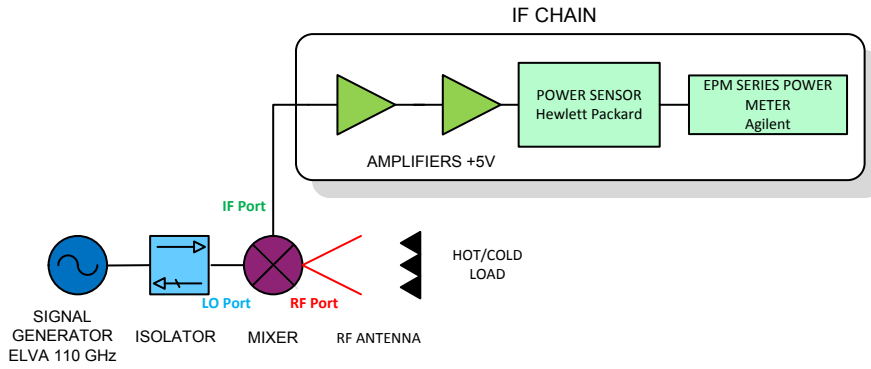The setup used to characterize the mixer array is shown in Fig. 4-13.

Fig. 4-13 Mixer setup for characterization.

This is the same set-up that was used for the characterization of the sub-harmonic mixer presented in Chapter 3. Note that the IF chain employed to measure the performance of the mixer array elements is the same that the one in Chapter 3, same IF noise temperature. The same process is followed to measure the performance of every element of the array. In this case 8 mixers based on the same designed model have been measured. For every single mixer a VDI diode in antiparallel configuration has been used and its series resistance, before and once the complete block has been assembled, has been calculated. The performance of every mixer is presented in Fig. 4-14.
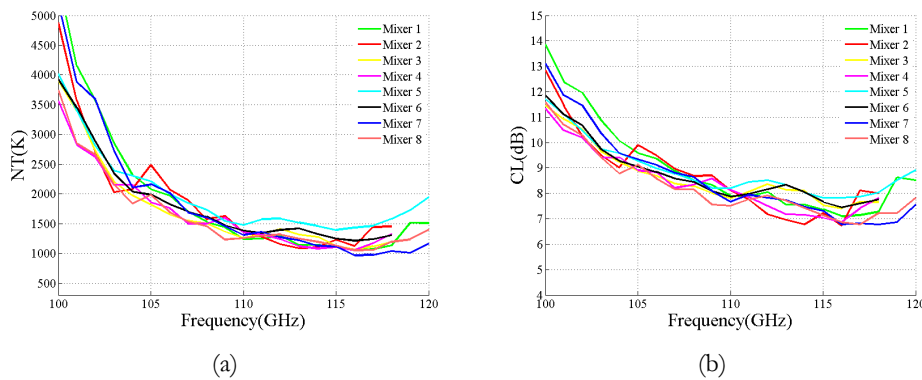

Fig. 4-14 Measured (a) noise temperature and (b) conversion loss of the elements of the array.

Fig. 4-14 shows the comparison results of the measured noise temperature and conversion loss of the different mixers of the complete array.

It is possible to apreciate a similar behavious of all the receivers. After analysing individually every element a conlusion can be reached: the best frequency point of performances can be found at 116 GHz. Almost every mixer has its minumun NT and CL located at this frequency. This is a good result since it can be determined that the mixer fabrication is repeateble and every element provides a comparable performance.

	Diode Series Resistance (Ω)		Block Series Resistance (Ω)		Block Rs Unbalance (Ω)	Best Mixer Noise Temperature (K //GHz)	Best Mixer Conversion Loss (dB //GHz)
Mixer 1	13.5	12.4	20.7	21.5	-0.8	1044 @116	7.1 @116
Mixer 2	14.5	14.7	17.27	17.32	-0.05	1082 @113	6.8 @114
Mixer 3	12.5	12.4	17.57	17.24	0.33	1066 @116	7.4 @116
Mixer 4	11.7	12	23.62	24.09	-0.47	1052 @116	6.8 @116
Mixer 5	12.7	14.1	23.41	24.54	-1.13	1394 @115	7.8 @115
Mixer 6	13.7	15.3	18.97	20.31	-1.34	1211 @116	7.5 @116
Mixer 7	14.3	14.6	20.97	21.53	-0.56	962 @116	6.7 @116
Mixer 8	13.2	12.6	15.58	14.5	1.08	1052 @116	6.8 @116

Table 4-1 Summary of the performance of the eight mixer elements.

Table 4-1 summarizes the series resistance of the diode and the complete block as well as the best performance of each mixer component. In general, a low block series resistance provides lower mixer noise temperature values, see Mixer 1, Mixer 2, Mixer 3, Mixer 7 and Mixer 8 results. However, an increase in the mixer conversion loss is appreciatede if the diodes are unbalanced, see Mixer 1, Mixer 3. Mixer 5 and Mixer 6 have high series resistance and their diodes are quite unbalanced which gives a worse mixer performance. Although this is not happening in Mixer 7 and Mixer 8. The reason for Mixer 8 disagreement can be that the unbalance of the diodes is compensated with really low values of series resistance,

however, Mixer 7 presents the best NT anc CL values despite the Rs is not the lowest one and either the unbalance value. Althogh it is well known that the diode series resistance influences the mixer performance it is not the only paramenter. The junction capacitance (which is not measured within this dissertation) as well as the fabrication tolerances (microstrip dimensions, block dimesions, diode position) are also essential and difficult to compare since we are dealing with differences of μm. Nevertheless, a general conclusion can be done, if the diodes series resistance and the diode unbalance is high this will lead to higher mixer noise temperature and conversion loss.

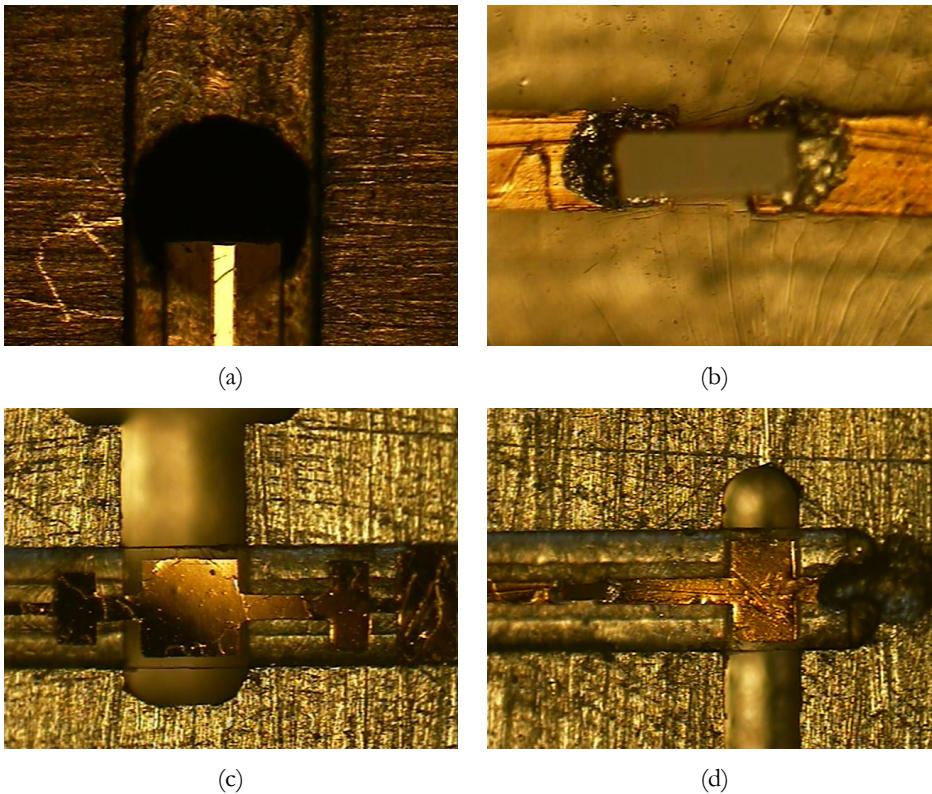Some photos of sections of different mixers of the array are presented below.

| (a) | (b) |

| (c) | (d) |

Fig. 4-15 (a) IF connector gap and microstrip port, (b) diode, (c) LO and (d) RF transition.

(a)   (b)
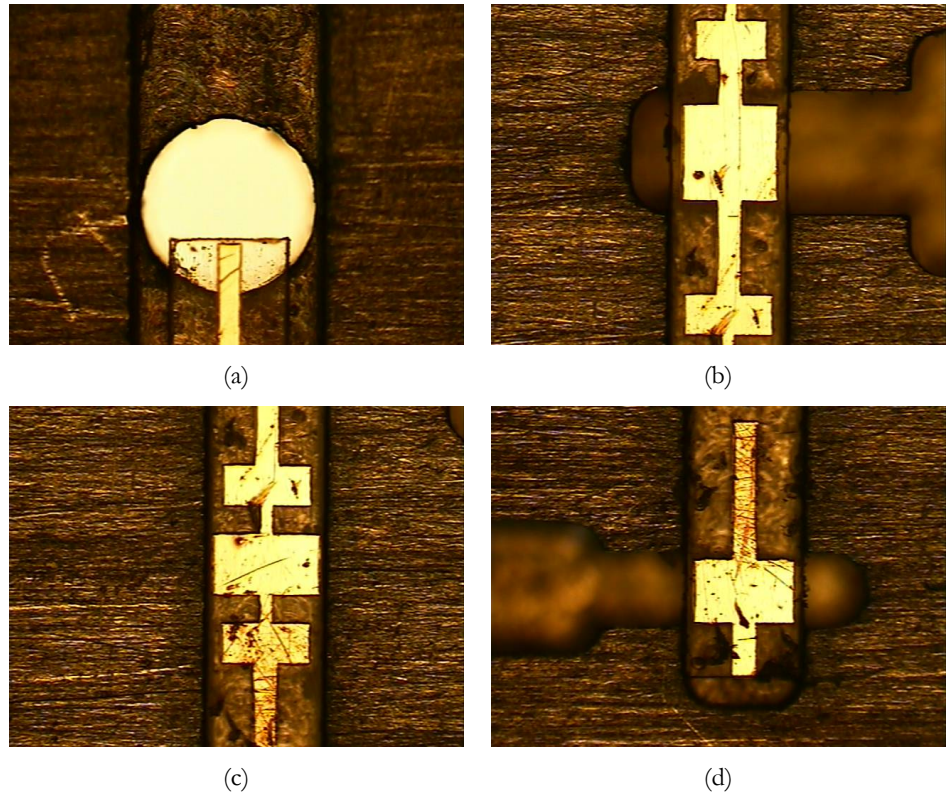
(c)   (d)

Fig. 4-16 (a) IF microstrip port and gap for connector, (b) LO transition, (c) RF filter and (d) RF transition.

In these pictures some of the LO transitions, the diode welding and the filters are depicted.

4.4   Imaging System Description

The imaging array developed within this thesis is the receiver part of a millimetre-wave passive imaging camera developed in the INNPACTO project leaded by Alfa Imaging [ALFA] as well as in the TeraScreen project. Within TeraScreen project a multi-frequency (94, 220 and 360 GHz) scanning imaging camera is expected to be developed. First off all a receiver operating at 94 GHz was developed by Alfa Imaging and as a consequence

the imaging system was adjusted to work at this frequency, since it is the lowest operational frequency. The quasi-optical system employed for the imaging system consists of two mirrors placed in a Cassegrain configuration. Note that the 220 GHz receiver array will be attached to the imaging system which is already fabricated and working.

That imaging system consists of a main reflector, a hyperbolical with a curvature radius of 1508.4 mm, a taper constant of -1.83 and a diameter of 840 mm. A sub-reflector which is an oval spheroid with a curvature radius of 3703.7 mm, tapper constant of 81.05 and a diameter of 280 mm. The distance between both reflectors is 635 mm. The receiver is situated at 370 mm. The main reflector is at an angle of 3.3187º while the sub-reflector is at 10.0856º, see Fig. 4-17.
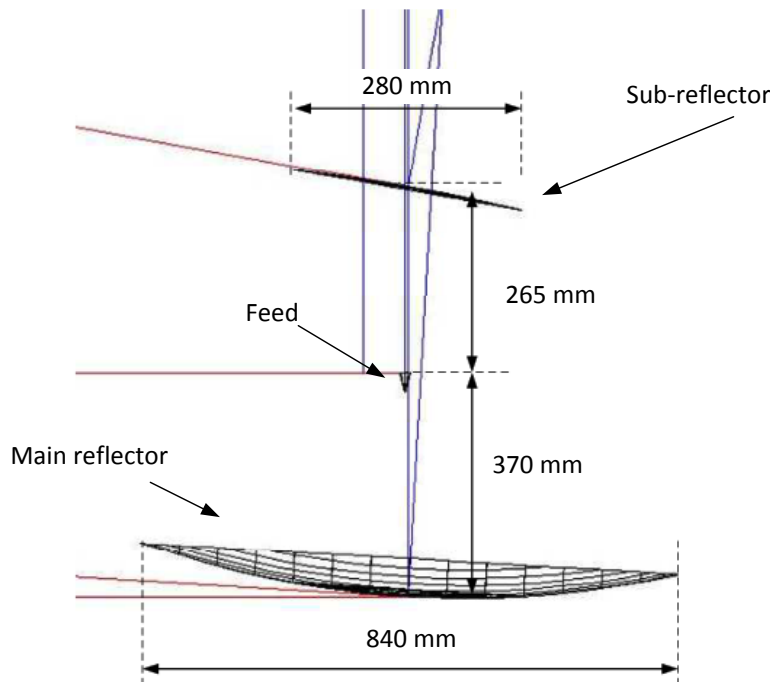

Fig. 4-17 Dimensions of the analysed cassegrain system.

This configuration provides a vertical sweep generated by the rotation of both the main reflector and the sub-reflector thanks to two motors. This rotation will draw an ellipse depending on the angle of rotation of the reflectors, (main reflector, sub-reflector), see Fig. 4-18.
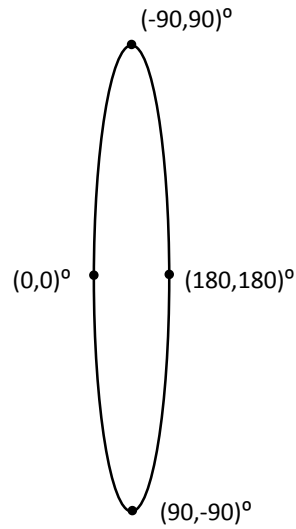

Fig. 4-18 Ellipse draw of the equivalent movement of the beam generated by an array element situated at the positive side when rotating the reflectors, for elements on the negative side the ellipse draw will be the symmetrical to this one.
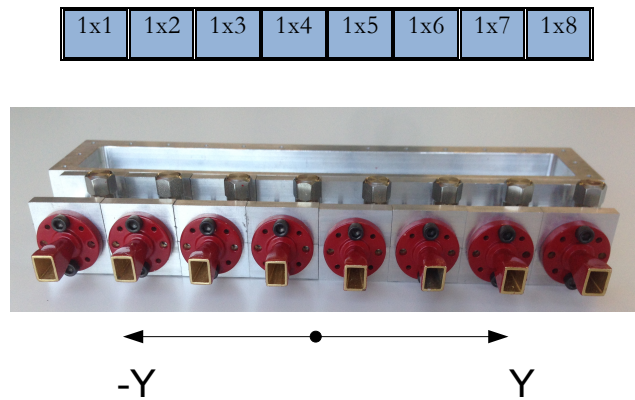

Fig. 4-19 Schematic and real image of the positioning of the array receiver.

When studying the central position, the complete array has been analysed for the (0,0)° rotation of the reflectors, since the elements situated at the positive side (elements 5,6,7 and 8 Fig. 4-19) with no rotation will generate the symmetrical points of the elements at the negative side (elements 1,2,3 and 4 Fig. 4-19) with a rotation of (180,180)°. For this reason, only this position (0,0)°, is simulated for all the imaging system.

Element Array	X-Position	Y-Position
1x1	-73.5	0
1x2	-52.5	0
1x3	-31.5	0
1x4	-10.5	0
1x5	10.5	0
1x6	31.5	0
1x7	52.5	0
1x8	73.5	0

Table 4-2 Summary of the position of each mixer element inside the imaging system.

The mixer element X-position of Table 4-2 is determined by the width of the mixer block, 21 cm. The Y-position is the height of the receiver regarding the imaging system which in this case is set to zero.

The imaging system configuration together with the positioning of a single feed and a simulation of the beam path is shown in a 3D simulation in Fig. 4-13.
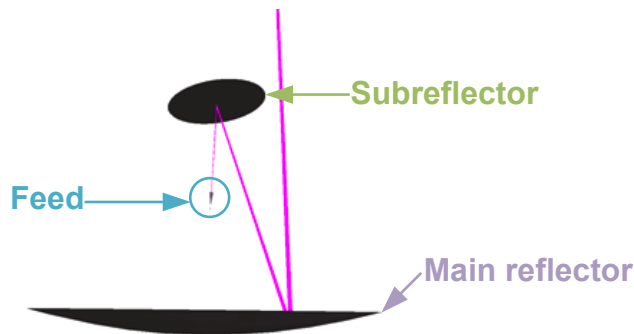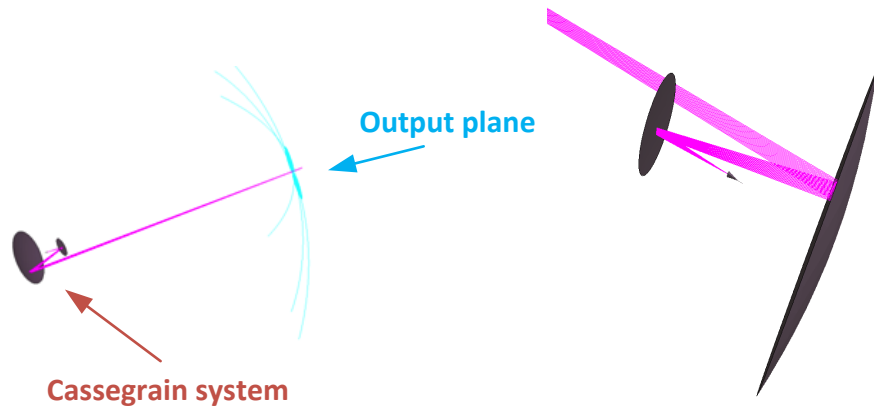
Fig. 4-20 Cassegrain mirror configuration used for the imaging set-up.

4.5   Imaging System Analysis

The mirror set-up was optimized by the Antenna Group for the imaging system operating at 94 GHz and with a 21 dB feedhorn feed. This configuration is already fabricated and available for measurements. Nevertheless, this set up has also been used with no change for the current imaging system operating at 220 GHz.

Taking into account that the imaging system was optimized for a lower operational frequency the performance of the quasi-optical system will get worse when working at 220 GHz. Anyway, the receiver was optimized to match with the best performance with the imaging system. Initially the configuration was analysed taking into account a receiver with a 26 dB feedhorn since a couple of antennas of this characteristics (standard gain horns) were already available at the Antenna Group. Nevertheless, some simulations have been carried out using different antenna directivities in order to select the appropriate directivity for the system to work the best way. To carry out these simulations the software GRASP 9.8 has been used.

The GRASP analysis is defined by different steps done during the simulation in order to calculate the performance of the system. These steps

are called TASKS. Note that GRASP does not allow the user to work with a passive system, i.e. the receiver will become an emitter in order to analyse the behaviour of the system. The different steps followed in the simulation of the imaging camera presented in this thesis are:

TASK 1: Get currents from Feed to Subreflector.

TASK 2: Get currents from Subreflector to Main reflector.

TASK 3: Get field from Main reflector to the field cut plane at 4 m.

TASK 4: Get currents from Main reflector to Subreflector, equivalent to calculate the reflector block.

TASK 5: Add field from the Subreflector to the field cut plane.

The goal of this simulation is to analyse the behaviour of the different elements of the array at the reflectors that form the system as well as in the imaging plane which is set at a distance of 4 metres. In order to compare these behaviour a relation of the improvement between the desired signal/noise and the non-desired one is calculated at the imaging plane, called SNR. Moreover, GRASP is able to calculate the relative power hitting the scatter (Power) normalized to 1 W, also known as the spill-over efficiency (η_{spill}), and the maximum value of the electrical field (MaxE) at the imaging plane which is another parameter to take into account when analysing the behaviour of the array elements. These parameters are shown in the following tables for different antenna directivities (26 dB, 24 dB, 22 dB and 20 dB).

Taking into account the power hitting the Main reflector, TASK 2, and the reflector block, TASK4, the power at the Imaging plane, called here $P_{Imaging}$, can be calculated as the subtraction of both values. Moreover, the S/N parameter has been defined as:

$$SNR = 20 \, log(maxE) - Spillover \qquad\qquad 4\text{-}1$$

In which the Spillover is obtained from the η_{spill} calculated by GRASP.

$$Spillover = 10log\,(1 - \eta_{spill}) \qquad\qquad 4\text{-}2$$

The final array configuration has been analysed taking into account different antenna directivities for the eight elements. In this chapter the simulation results of elements 1x5 (central element), 1x8 (far right of the array) and 1x1 (far left) are presented. The performance of the complete array is gathered in Appendix D. The choice of these elements is due to the location in the array since it is important to know how the central elements will work as well as the lateral ones as they are further from the optical axis and indeed their performance will get worse. Note also; as it will be presented later on this chapter, the performance of element 1 and 8 won´t be the same considering that they represent different sides of the swept ellipse and their distance to the reflectors are different due to the taper of the mirrors, see Fig. 4-17 and Fig. 4-18.

- Mixer 1x5

Antenna Directivity	TASK 1		TASK 2		TASK 4	
	Power	η_{spill} (dB)	Power	η_{spill} (dB)	Power	η_{spill} (dB)
26 dB	0.971	0.128	0.951	0.220	0.121	9.171
24 dB	0.963	0.162	0.930	0.314	0.134	8.734
22 dB	0.965	0.154	0.929	0.321	0.165	7.819
20 dB	0.933	0.300	0.903	0.445	0.183	7.382

Antenna Directivity	Imaging Plane				SNR
	Power	η_{spill} (dB)	Spill-over	Max E	
26 dB	0.829	0.812	-7.683	0.033	-21.921
24 dB	0.796	0.988	-6.914	0.035	-22.180
22 dB	0.764	1.171	-6.264	0.031	-23.994
20 dB	0.720	1.427	-5.528	0.023	-27.238

Table 4-3 GRASP results for element 1x5 of the mixer array.

The performance of the mixer located in the position 1x5 of the array has been evaluated in GRASP. The results obtained for this mixer are presented in Table 4-3. Different antenna directivities have been taking into account, from 26 dB to 20 dB. Evaluating the results, the best antenna directivity for this element would be 26 dB in terms of best S/N value.
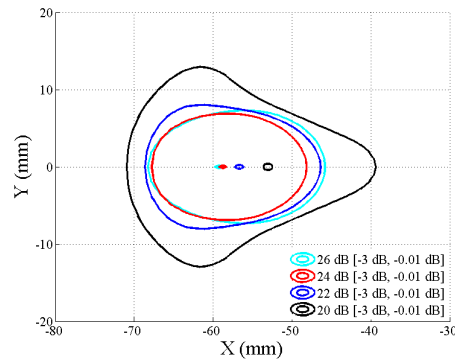

Fig. 4-21 Beam cut at -3 dB of element 1x5 for different antenna directivities at the imaging plane.

The beam cut at -3 dB at the imaging plane (4 metres distance) for the antenna directivities analysed are shown in Fig. 4-21. See that the 20 dB antenna would be automatically dismissed since the 3 dB beam cut provides deformed shape which will generate a distorted view. The most circular beam cut is generated by the 24 dB antenna; moreover, the maximum MaxE value is also provided by this antenna. For this reason, taking into account only element 1x5 the choice of the antenna directivity will be between 26 and 24 dB. Note also that depending on the directivity of the antenna the illuminated region of the mirror will change. The higher the directivity of the antenna is the more concentrated the beam will be and as a consequence the better the spill-over efficiency will be however, these will lead to a higher blockage.

- Mixer 1x8

Antenna Directivity	TASK 1		TASK 2		TASK 4	
	Power	η_{spill} (dB)	Power	η_{spill} (dB)	Power	η_{spill} (dB)
26 dB	0.957	0.192	0.938	0.277	0.068	11.687
24 dB	0.938	0.277	0.915	0.385	0.062	12.074
22 dB	0.934	0.299	0.898	0.467	0.081	10.924
20 dB	0.923	0.346	0.890	0.506	0.119	9.260

Antenna Directivity	Imaging Plane				SNR
	Power	η_{spill} (dB)	Spill-over	Max E	
26 dB	0.870	0.603	-8.873	0.034	-20.601
24 dB	0.853	0.690	-8.332	0.033	-21.325
22 dB	0.817	0.877	-7.378	0.029	-23.344
20 dB	0.771	1.127	-6.411	0.023	-26.279

Table 4-4 GRASP results for element 1x8 of the mixer array.

In the case of the 1x8 element, the best performance, in terms of best S/N, is obtained with an antenna directivity of 26 dB.
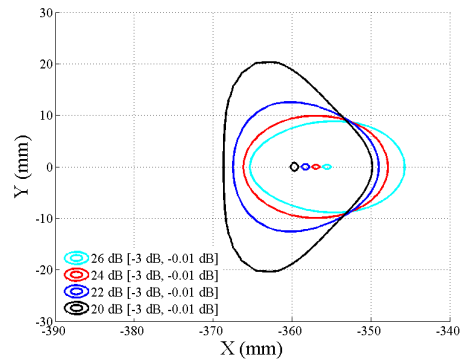

Fig. 4-22 Beam cut at -3 dB of element 1x8 for different antenna directivities.

Fig. 4-22 shows the beam cuts at-3 dB of element 1x8 for different directivities. A less circular pixel shape can be observed since the ray is now hitting the external part of the mirror. This will cause a higher aberration of the image captured by these elements. Nevertheless, the most circular beam cut shape is obtained when the 24 dB antenna is employed.

- Mixer 1x1

Antenna Directivity	TASK 1		TASK 2		TASK 4	
	Power	η_{spill} (dB)	Power	η_{spill} (dB)	Power	η_{spill} (dB)
26 dB	0.944	0.252	0.931	0.310	0.192	7.161
24 dB	0.925	0.337	0.920	0.363	0.208	6.827
22 dB	0.931	0.313	0.923	0.347	0.236	6.279
20 dB	0.902	0.446	0.879	0.560	0.238	6.230

Antenna Directivity	Imaging Plane				SNR
	Power	η_{spill} (dB)	Spill-over	Max E	
26 dB	0.739	1.315	-5.829	0.023	-26.824
24 dB	0.712	1.473	-5.410	0.027	-26.125
22 dB	0.688	1.626	-5.053	0.031	-25.204
20 dB	0.641	1.932	-4.448	0.030	-26.039

Table 4-5 GRASP results for element 1x1 of the mixer array.

In this case, the best antenna directivity is 22 dB in terms of less S/N and maximum MaxE. Note the different behaviour between element 1x1 and 1x8 since they correspond to different sides of the ellipse drawn by the beam when the reflectors are moving.
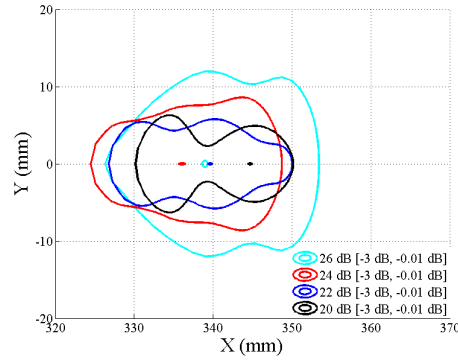
Fig. 4-23 Beam cut at -3 dB of element 1x1 for different antenna directivities at the imaging plane.

Fig. 4-23 depicts the beam cut at -3 dB obtained for element 1x1 at the imaging plane, i.e. at 4 m distance. The beam has an oval shape due to its position on the array. Again, the most circular shape is obtained for an antenna of 24 dB.

After analysing the complete array, see Appendix D, a compromise about the best antenna directivity used at the imaging system has to be reached. First of all, if the central elements are taking into account, the antenna directivity that fits better with the system in terms of S/N could be 26 or 24 dB, however, element 1x1 requires lower directivity to work in its best way. To get to an agreement, the parameter MaxE has to be analysed. This parameter corresponds to the level of the electrical field at the imaging cut plane, at distance of 4 metres to the system. If a directivity of 22 dBs is chosen the E field available for all elements is more equalized understood as less variation between elements (MaxE values range between 0.029 and 0.032, difference of 0.003), however the beam shape is distorted. On the other hand, if a directivity of 26 dB is selected the difference between these values (0.012) is larger enough not to have a balanced performance of the imaging array. An intermediate point would be in this case the use of a 24 dB antenna with a difference MaxE values of 0.008. On the other hand, if the S/N parameter is trying to be equalized the better antenna directivity would be 22 dB (variation between values 1.86) instead of 24 dB (variation

4.8) and 26 dB (variation 6.223). However, as commented, the beam cuts are less circular specially when analysing the elements situated at the left side of the array (elements 1x2 and 1x1, see Fig. 4-23).

For this reason, in order to get a compromise between the maximum MaxE value, the beam shape and the minimun S/N value a 24 dB antenna is finally chosen. This way, the array elements E field levels move between 0.027 and 0.035, values of S/N between -26.121 and -21.325 and a circular beam shape at -3 dB is obtained for all elements that forms the imaging array. Note that the imaging system has also been analysed for the 22 dB antenna obtaining similar results.

The quasi-optical system has been analysed taking into account all the elements of the array and the movement of the elliptical mirrors. This movement provides the possibility of scanning a complete vertical line of a length of approximately 2 metres. The beam cut at -3 dB at the imaging plane is depicted in Fig. 4-24 (a) for the complete array and the quasi-optical system in its initial position. Fig. 4-24 (b) depicts the beam cut of the array at different points: having the mirrors in its initial position and with the mirrors rotated to the position to scan the maximum distance.
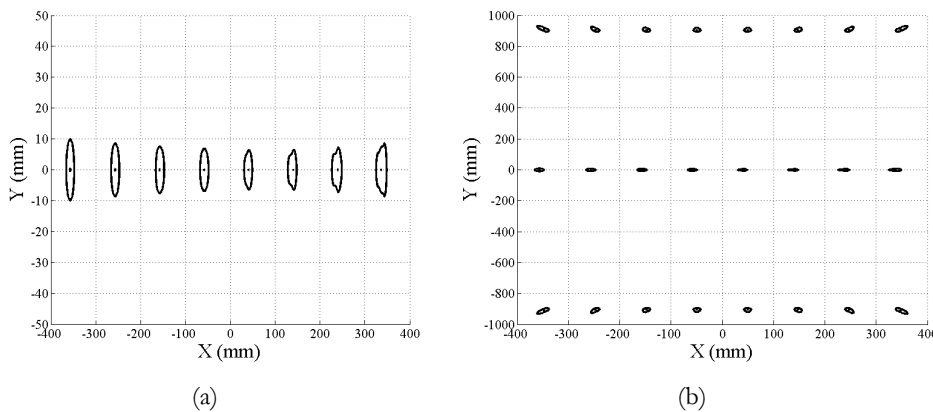

(a)   (b)

Fig. 4-24 Beam cuts at -3 dB at the imaging plane (a) for the central position. (b) Beam cuts -3 dB at the imaging plane simulating the maximum scanning area.

The rotation of the mirrors provides a vertical scanning of approximately two metres; see Fig. 4-24 (b). Thanks to the location of the array elements is also possible to obtain a horizontal scanning area of around 800 mm. Both factors give a scanning area of 2x0.8 m at a distance of 4 m, which is a sufficient area to scan a person.

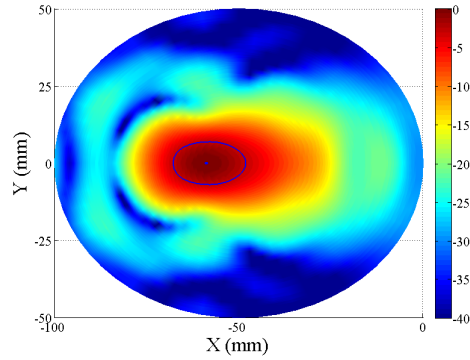Below the beam cuts of two of the analysed elements, using an antenna of 24 dB directivity, are presented.

Fig. 4-25 Bean cot of element 1x5.

Fig. 4-25 presents the beam cut at 4 m distance emitted by a receiver located in position 1x5 of the array. Here the most circular shape is appreciated since it is emitted by one of the central elements of the array.

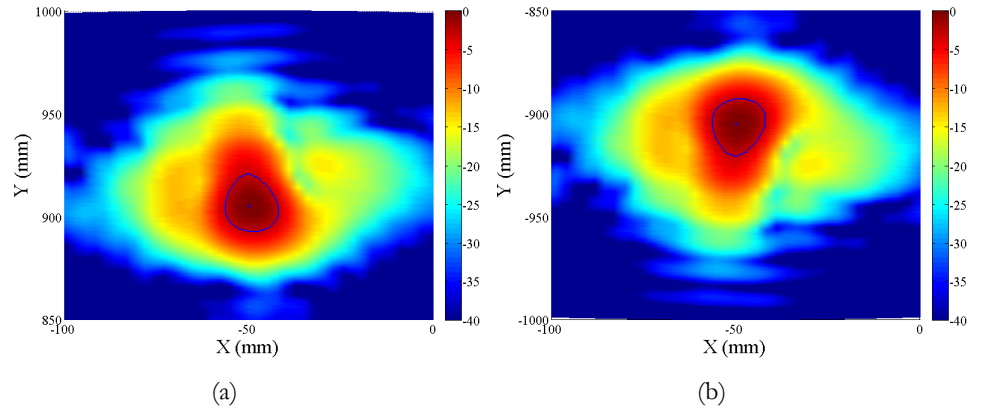(a)   (b)

Fig. 4-26 Beam cut of element 1x5 at the (a) upper and (b) lower position.

If the mirror rotation is done, the beam cut at the upper and lower positions is obtained, Fig. 4-26. A distortion of the beam shape is produced at these positions. It is due to the fact that the beam hits the mirror at the external zone so that, the aberration provoked by it is higher.
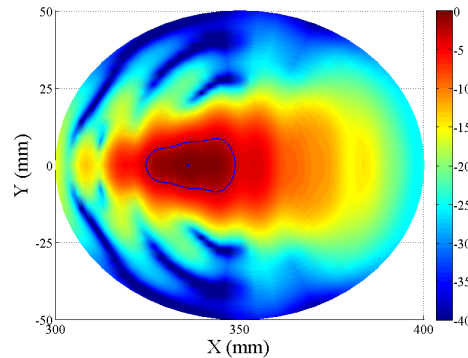

Fig. 4-27 Bean cot of element 1x1.

The results obtained from the simulation of element 1x1 of the array are presented in Fig. 4-27 and Fig. 4-28 for the central position and the lower and upper positions respectively. The beam cut at 4 metres distance for element 1x1 is less circular compared to previous elements. This can be explained due to the configuration of the system. Note that the main reflector and the sub-reflector had a slight tilt which produces a worse performance of one side of the array receiver (left side) since the distance to the mirror is larger. Moreover, the elements located at the far left and far right are further to the focal point than the central ones which also generated and aberration of the beam.
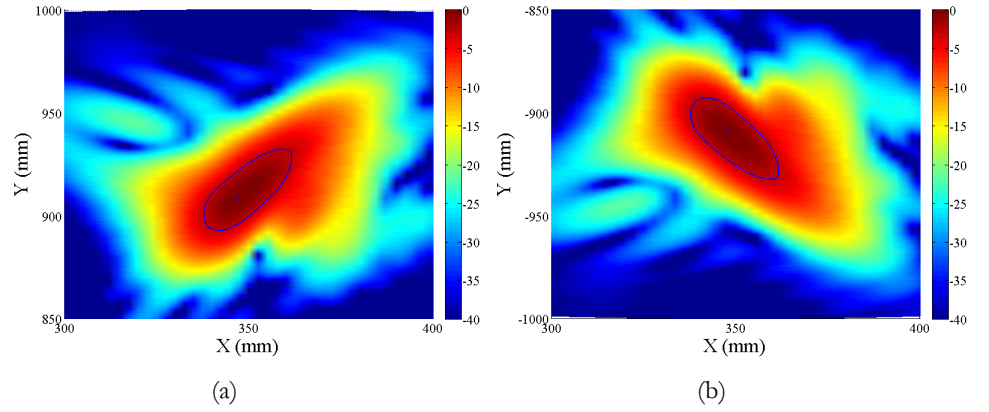
(a) (b)

Fig. 4-28 Beam cut of element 1x1 at the (a) upper and (b) lower position.

4.6   Conclusions

The design of the multi-pixel receiver has been carried out. The mechanical requirements has been analysed and finally, an array of 1x8 elements has been developed and measured obtaining a similar performance for all of them in terms of noise temperature and conversion loss.

Moreover, the simulated results of this array operating over a Cassegrain system for imaging applications have been reported. A study of the required antenna for the system to work in its best way has been done. A 24 dB antenna has been chosen for the receiver array as a compromise between the S/N, MaxE and the shape of the beam cuts at -3 dB.

CHAPTER 5

DEVELOPMENT OF SUB-MILLIMETRE WAVE COMPONENTS

5.1   Introduction

The current technology available at the sub-millimetre wave range does not provide, in most cases, enough power to feed the available components due to the high operational frequencies. This can result in an important problem when arrays of sub-harmonic mixers need to be pumped at these frequencies, such as the array presented in Chapter 4. For this reason, new approaches have to be done in order to fix this problem. This is why; a 4th-harmonic mixer is presented in this Chapter. The use of this kind of devices make possible to reach high RF frequencies having a compromise between the operational LO frequency and the power available at that frequency which results in an advantageous solution. This is possible thanks to the decrease in LO frequency which leads to have enough power to work at that frequency which is of great importance when high amounts of power are required to feed the array of mixers.

When designing imaging systems some parameters such as the operational frequency are taking into account. It is important to operate at frequencies in which an attenuation window is presented, but this is not the only reason. The operational frequency also sets the resolution and the penetration depth, which increase with frequency. For this reason, it is meaningful to have the possibility of increasing the RF frequency in order to improve the resolution and the performance of the system.

In this chapter a sub-harmonic mixer working at an RF frequency of 440 GHz built in COC substrate is presented. Moreover, the use of a 4th-harmonic mixer instead of the sub-harmonic mixer is studied. Both components are design, fabricated and measured and a comparison between them is done. In order to measure the sub-harmonic mixer with the equipment available at the Antenna Group facilities a doubler at 220 GHz has been design and is also presented in this Chapter.

5.2   Sub-harmonic mixer working at 440 GHz

As it was presented in Chapter 3 a sub-harmonic mixer is also presented in this section. The main difference between both designs is the choice of the RF frequency. In this case, an RF frequency of 440 GHz has been selected. The election of this frequency is due to several things. First of all, it is double the operational frequency of Chapter 3´s mixer. Moreover, the 4th-harmonic mixer that is going to be presented in this chapter will work at an LO frequency of 110 GHz (RF frequency of 440 GHz) due to the fact that the Antenna Group counts with a source with enough power at this frequency. For all of this, the operational RF frequency is set to 440 GHz and therefore, an LO frequency of 220 GHz is used with an IF band between 1 to 6 GHz in order to have the possibility to compare both mixers performance.

The design procedure employed for the sub-harmonic mixer at 440 GHz is the same as the one presented in Chapter 3. First of all an ideal approach of the performance of the sub-harmonic mixer has been calculated in ADS. The ideal model of the sub-harmonic mixer is presented in Fig. 5-1. This model counts with ideal filters to select the corresponding frequency in each band. The ideal conversion loss and noise temperature are calculated taking into account the RF and LO frequency impedances.
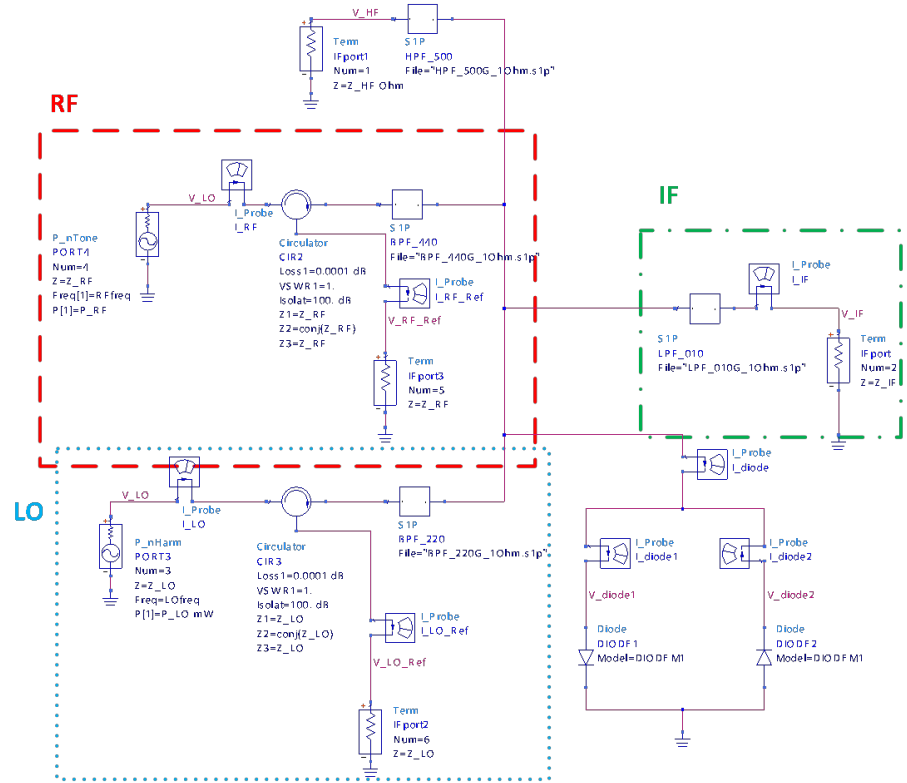
Fig. 5-1 Ideal mixer design of the sub-harmonic mixer working at 440 GHz.

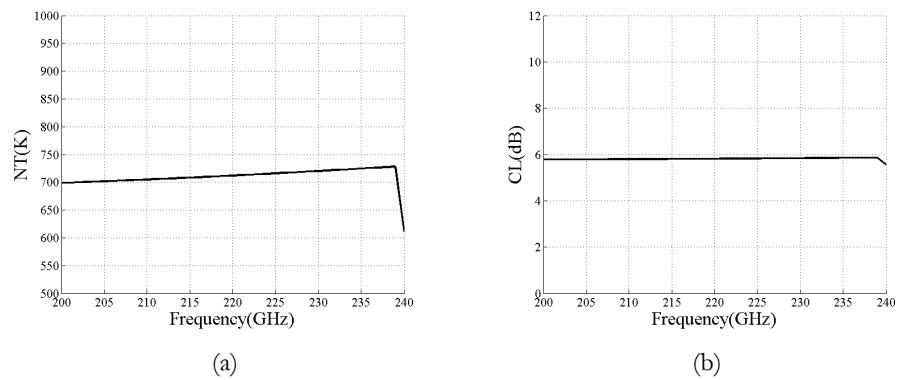Best value obtained varying these impedances is shown in Fig. 5-2.

(a)

(b)

Fig. 5-2 (a) Noise temperature and (b) conversion loss of the ideal sub-harmonic mixer.

Best conversion loss values reached are in the order of 6 dB using the VDI diodes and noise temperature values are around 700 K.

The diode impedances have been calculated form the currents and voltages at the LO and RF frequencies for the ideal mixer design presented in Fig. 5-1. The obtained impedances correspond to a minimal noise temperature of the mixer, see Chapter 3. Taking this into account, the impedance at the RF and LO ports can be expressed as $Z_{RF}=(Z_{diode1RF}/2)^*$ and $Z_{LO}=(Z_{diode1LO}/2)^*$. The obtained values related to the analysed LO frequency band are presented in Table 3-2.

Freq. (GHz)	ZdiodeLO (Ω)	ZdiodeRF (Ω)	ZLO (Ω)	ZRF (Ω)
200	261.21 - 298.05i	128.86 - 90.461i	130.61 + 149.03i	64.43 + 45.23i
201	259.72 - 298.05i	128.86 - 90.461i	129.86 + 149.03i	64.43 + 45.23i
202	258.22 - 298.09i	128.45 - 90.648i	129.11 + 149.05i	64.23 + 45.32i
203	256.73 - 298.13i	128.04 - 90.833i	128.37 + 149.06i	64.02 + 45.42i
204	255.25 - 298.16i	127.63 - 91.017i	127.62 + 149.08i	63.82 + 45.51i
205	253.77 - 298.19i	127.23 - 91.198i	126.89 + 149.09i	63.61 + 45.60i
206	252.30 - 298.20i	126.82 - 91.378i	126.15 + 149.1i	63.41 + 45.69i
207	250.84 - 298.22i	126.41 - 91.557i	125.42 + 149.11i	63.21 + 45.78i
208	249.38 - 298.23i	126 - 91.733i	124.69 + 149.11i	63.00 + 45.87i
209	247.93 - 298.23i	125.6 - 91.908i	123.96 + 149.12i	62.80 + 45.95i
210	246.48 - 298.23i	125.19 - 92.081i	123.24 + 149.11i	62.60 + 46.04i
211	245.05 - 298.22i	124.79 - 92.252i	122.52 + 149.11i	62.40 + 46.13i
212	243.61 - 298.21i	124.39 - 92.421i	121.81 + 149.1i	62.19 + 46.21i
213	242.19 - 298.19i	123.98 - 92.589i	121.09 + 149.1i	61.99 + 46.30i
214	240.77 - 298.17i	123.58 - 92.755i	120.38 + 149.08i	61.79 + 46.38i
215	239.35 - 298.14i	123.18 - 92.92i	119.68 + 149.07i	61.59 + 46.46i
216	237.95 - 298.11i	122.77 - 93.082i	118.97 + 149.05i	61.39 + 46.54i
217	236.54 - 298.07i	122.37 - 93.243i	118.27 + 149.04i	61.19 + 46.62i
218	235.15 - 298.03i	121.97 - 93.403i	117.57 + 149.01i	60.99 + 46.70i

219	233.76 - 297.98i	121.57 - 93.561i	116.88 + 148.99i	60.79 + 46.78i
220	232.38 - 297.93i	121.17 - 93.717i	116.19 + 148.97i	60.59 + 46.86i
221	231.00 - 297.88i	120.77 - 93.871i	115.5 + 148.94i	60.39 + 46.94i
222	229.63 - 297.81i	120.37 - 94.024i	114.81 + 148.91i	60.19 + 47.01i
223	228.26 - 297.75i	119.98 - 94.176i	114.13 + 148.87i	59.99 + 47.09i
224	226.91 - 297.68i	119.58 - 94.325i	113.45 + 148.84i	59.79 + 47.16i
225	225.55 - 297.61i	119.18 - 94.474i	112.78 + 148.8i	59.59 + 47.24i
226	224.21 - 297.53i	118.79 - 94.62i	112.1 + 148.76i	59.39 + 47.31i
227	222.87 - 297.45i	118.39 - 94.765i	111.43 + 148.72i	59.20 + 47.38i
228	221.53 - 297.36i	117.99 - 94.909i	110.77 + 148.68i	59.00 + 47.45i
229	220.2 - 297.27i	117.6 - 95.051i	110.1 + 148.63i	58.8 + 47.53i
230	218.88 - 297.18i	117.21 - 95.191i	109.44 + 148.59i	58.60 + 47.60i
231	217.56 - 297.08i	116.81 - 95.33i	108.78 + 148.54i	58.41 + 47.67i
232	216.25 - 296.97i	116.42 - 95.467i	108.12 + 148.49i	58.21 + 47.73i
233	214.94 - 296.87i	116.03 - 95.603i	107.47 + 148.43i	58.01 + 47.80i
234	213.64 - 296.76i	115.64 - 95.737i	106.82 + 148.38i	57.82 + 47.87i
235	212.35 - 296.64i	115.25 - 95.87i	106.17 + 148.32i	57.62 + 47.94i
236	211.06 - 296.52i	114.86 - 96.002i	105.53 + 148.26i	57.43 + 48.00i
237	209.78 - 296.40i	114.47 - 96.132i	104.89 + 148.2i	57.23 + 48.07i
238	208.50 - 296.28i	114.08 - 96.261i	104.25 + 148.14i	57.04 + 48.13i
239	207.23 - 296.15i	113.69 - 96.388i	103.61 + 148.07i	56.84 + 48.19i
240	205.96 - 296.02i	113.78 - 96.487i	102.98 + 148.01i	56.89 + 48.24i

Table 5-1 Ideal optimal diode impedance.

The diode impedance at the LO frequency has values around 220 Ω for the real part and 298 Ω for the imaginary part. On the other hand, the diode impedance at the RF frequency has values around 120 Ω for the real part and 149 Ω for the imaginary part.

Fig. 3-10 shows their corresponding LO and RF reflection coefficients. As it was already studied in Chapter 2, a good sub-harmonic mixer design should have diode impedances as close as possible to the

calculated ideally, in order to have the lowest conversion loss, related to Z_{RF}, with a low input power, related to Z_{LO}.

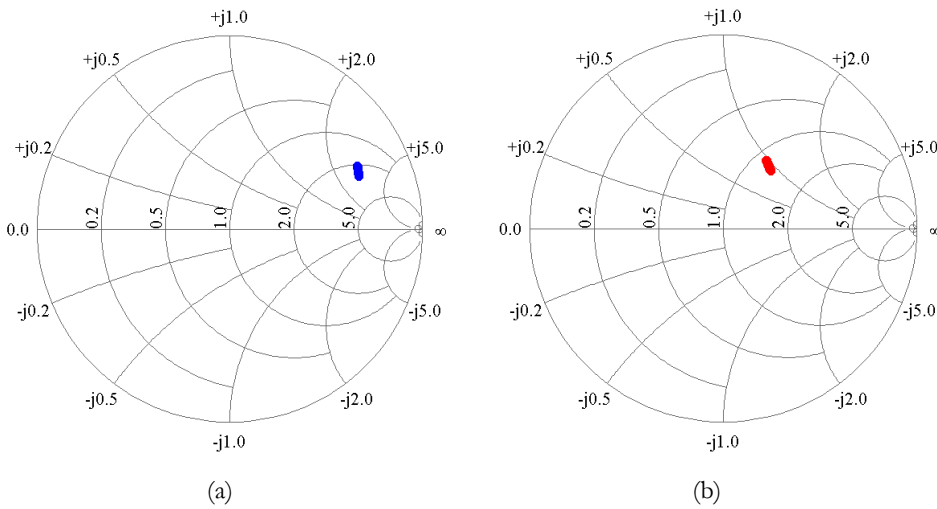(a)   (b)

Fig. 5-3 Optimum (a) LO, (b) RF reflection coefficient.

Once the ideal analysis of the sub-harmonic mixer working at 440 GHz has been carried out, the next step is the design of the mixer in HFSS. The longitudinal section of the complete mixer is presented in Fig. 3-15. Again, commercial diodes have been used for this mixer, namely the VDI SC1T2-D20 [VDI], with the characteristics described in Chapter 3. Moreover, the mixer has also been built in COC substrate [TOP] due to the better performances of this substrate (see Chapter 3, Section 3.7).
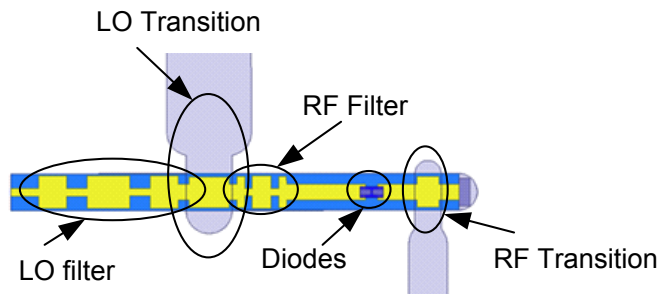
Fig. 5-4 Longitudinal section of the sub-harmonic mixer showing its different parts and components.

The coupling of the RF and LO signal is done by means of standard rectangular waveguides. The RF frequency has been set to 440 GHz so the rectangular waveguide chosen has the following dimensions: 508x254 μm, WR-2. For the LO waveguide the dimensions are: 1092x546 μm, WR-4.

The LO and RF filters are stepped-impedance Low Pass Filter, LPF, with a cut-off frequency below 220 GHz for the LO filter and between 440 and 220 GHz for the RF filter (see Fig. 3-16 (a) and Fig. 3-17 (a)) [Maa98]. Their S-parameters are presented in Fig. 3-16 (b) and Fig. 3-17 (b). The dimensions of both filters as well as the rest of sections that forms the mixer are presented in Appendix B.

(a)
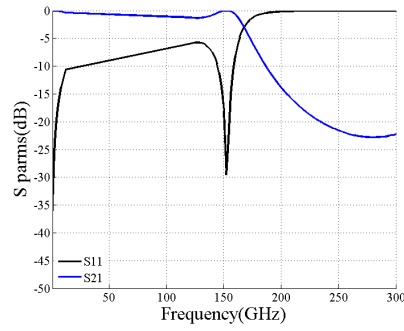
(b)

Fig. 5-5 (a) LO filter model and (b) S11 and S21.

(a)   (b)
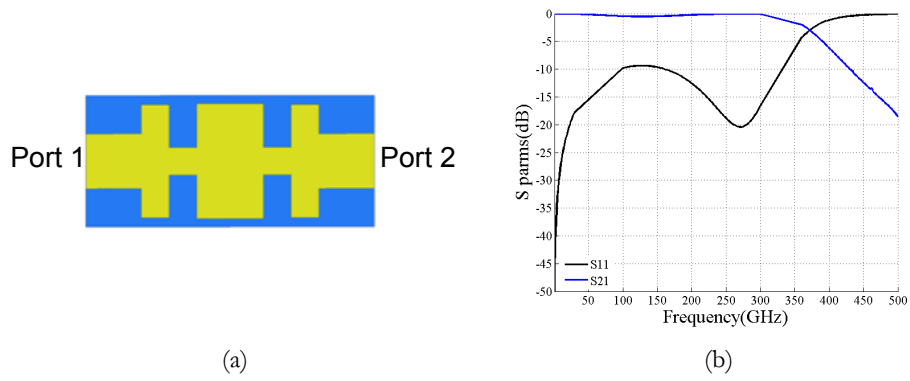
Fig. 5-6 (a) RF filter model and (b) S11 and S21.

The same way it was done in Chapter 3, the LO and RF transitions are designed to gather the maximum power for the mixer and they have also been reduced in height (300 x 1092 μm and 170 x 508 μm respectively) [Hes97; Shi97].

(a)   (b)

Port 2

Port 1

S parms(dB)

Frequency(GHz)
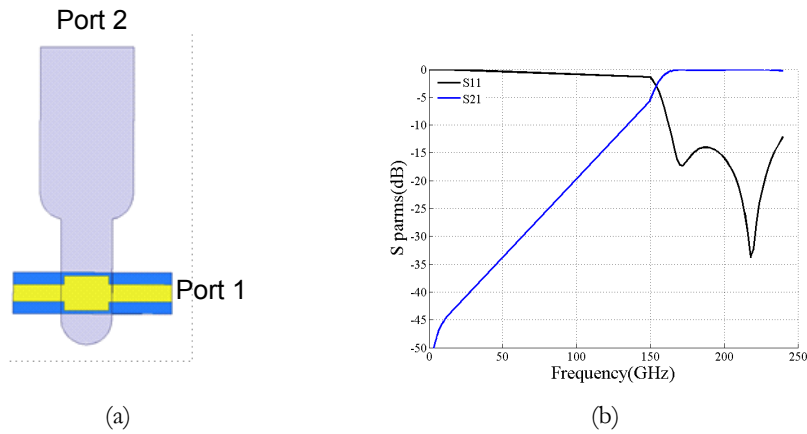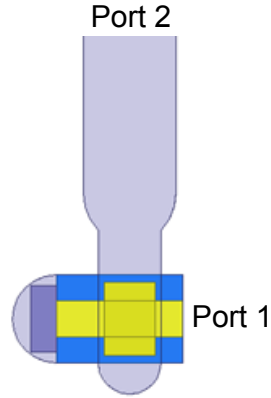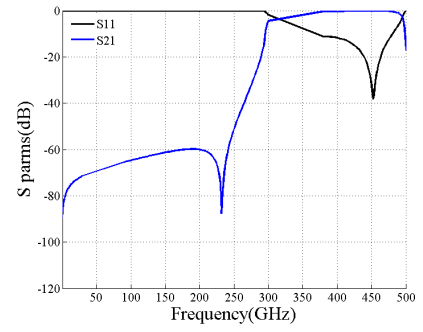
(c)   (d)

Fig. 5-7 (a) LO Transition, LOT, model and (b) LOT S11 and S21, (c) RF Transition , RFT, model, (d) RFT S11 and S21.

The microstrip channel dimensions are 240 x 200 μm (monomode operation). The TOPAS substrate employed in the design of this mixer is the same as in Chapter 3, i.e. it has a thickness of 101.6 μm, that´s why a 200 μm height waveguide has been chosen.

The ADS design procedure employed for this mixer is the same as the one presented in Chapter 3. This is the reason to show only the last simulation results. The ADS schematic is shown in Fig. 5-8.
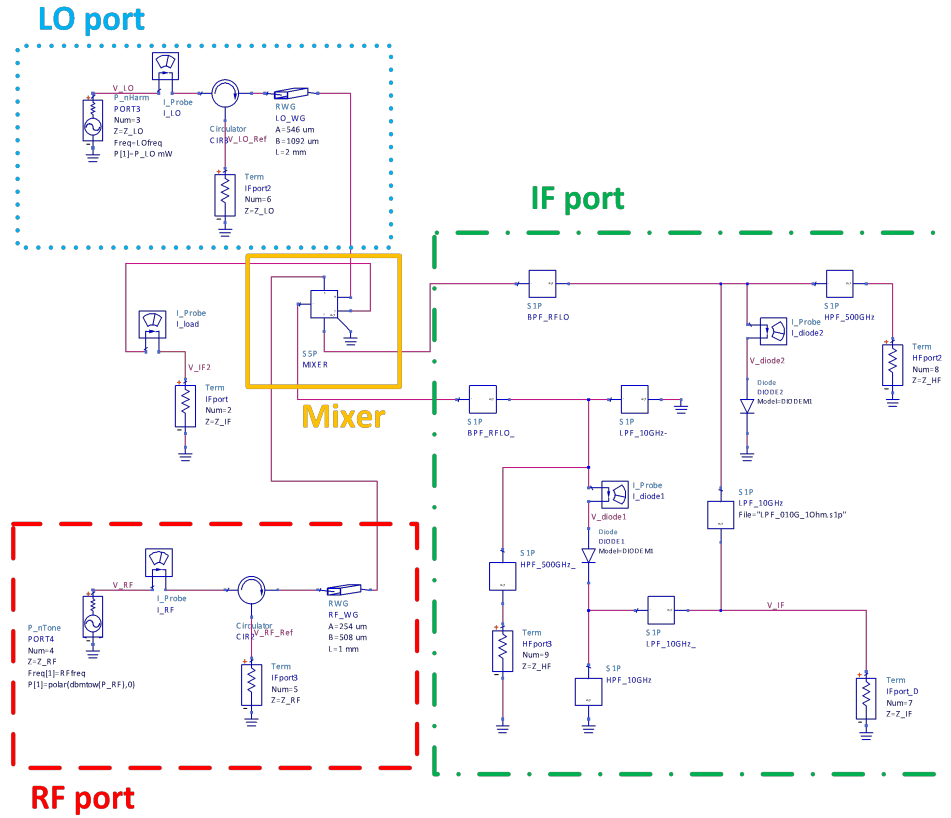
Fig. 5-8 ADS sub-harmonic mixer schematic.

The simulated noise temperature and conversion loss are presented in Fig. 5-9 (a) and (b) respectively. NT values around 1000 K are obtained for frequencies close to 214 GHz and 235 GHz, having a minimum value of 833 K at 233 GHz. On the other hand, the conversion loss stays below 8 dB from 208 to 236 GHz, having its minimum result, 6.3 dB, at 215 GHz.
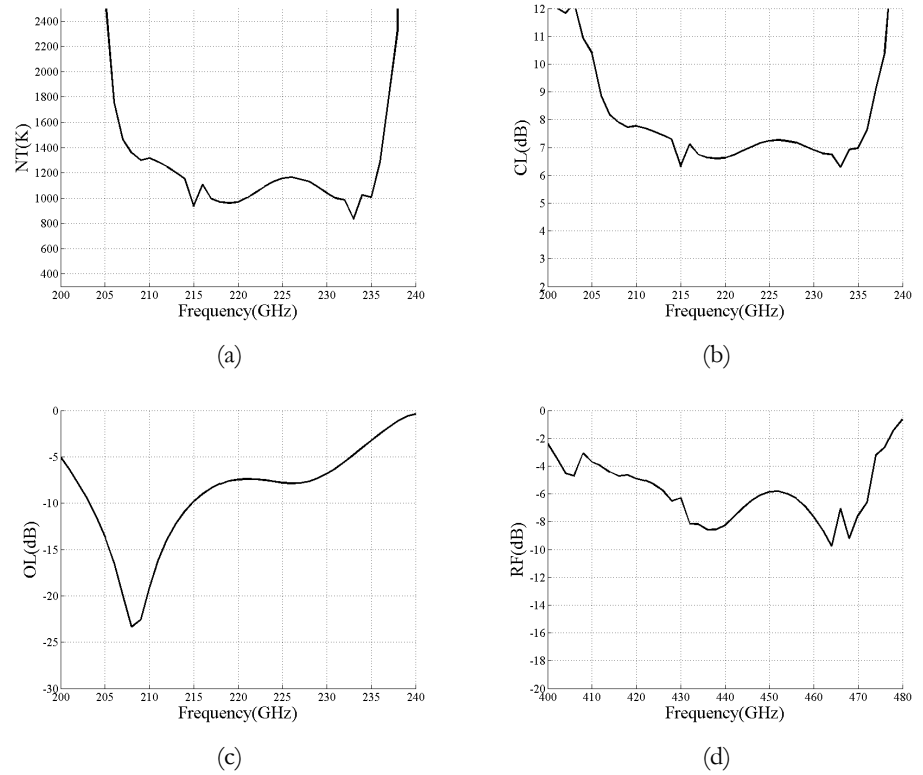
Fig. 5-9 Simulated (a) NT, (b) CL, (c) OL S_{11} and (d) RF S_{11}.

The LO and RF matching have also been calculated in ADS and the results are shown in Fig. 5-9 (c) and (d) respectively. The LO S_{11} is below -5 dB almost for the complete bandwidth which can assure a correctly performance of the device in terms of required input power. On the other hand, the RF S_{11} is below -5 dB from 425 GHz to 470 GHz. The small peaks presented in the figures are related to the ADS simulation tool and are not expected to appear in the measurements.

The impedance values of the diode and the ports at the LO and RF frequencies are gathered at Table 5-2.

Freq. (GHz)	ZdiodeLO (Ω)	ZdiodeRF (Ω)	ZLO (Ω)	ZRF (Ω)
200	242.66 - 382.34i	135.98 - 122.24i	121.33 + 191.17i	67.99 + 61.12i
201	254.67 - 354.99i	134.42 - 113.88i	127.34 + 177.5i	67.208 + 56.941i

202	261.16 - 334.5i	132.83 - 108.15i	130.58 + 167.25i	66.414 + 54.076i
203	263.92 - 319.59i	130.91 - 103.8i	131.96 + 159.8i	65.454 + 51.899i
204	266.03 - 307.46i	130.9 - 97.786i	133.02 + 153.73i	65.45 + 48.893i
205	266.86 - 298.71i	130.64 - 96.916i	133.43 + 149.35i	65.322 + 48.458i
206	267.08 - 292.62i	130.91 - 95.945i	133.54 + 146.31i	65.454 + 47.972i
207	266.79 - 288.8i	130.8 - 95.568i	133.4 + 144.4i	65.398 + 47.784i
208	266.09 - 286.88i	130.52 - 95.587i	133.04 + 143.44i	65.26 + 47.794i
209	264.96 - 286.52i	130.32 - 95.697i	132.48 + 143.26i	65.16 + 47.848i
210	263.55 - 287.53i	129.48 - 95.996i	131.78 + 143.77i	64.739 + 47.998i
211	261.81 - 289.76i	129.95 - 97.245i	130.91 + 144.88i	64.975 + 48.622i
212	259.75 - 292.99i	129.76 - 98.703i	129.88 + 146.5i	64.879 + 49.352i
213	257.38 - 297.02i	129.53 - 100.24i	128.69 + 148.51i	64.766 + 50.121i
214	254.7 - 301.61i	129.28 - 101.89i	127.35 + 150.81i	64.639 + 50.945i
215	251.73 - 306.4i	129.28 - 103.96i	125.87 + 153.2i	64.64 + 51.982i
216	248.74 - 310.91i	128.71 - 105.13i	124.37 + 155.46i	64.353 + 52.565i
217	245.8 - 315.05i	128.52 - 106.71i	122.9 + 157.53i	64.26 + 53.357i
218	242.95 - 318.48i	128.2 - 108.16i	121.48 + 159.24i	64.098 + 54.079i
219	240.47 - 321.09i	127.86 - 109.2i	120.24 + 160.55i	63.931 + 54.599i
220	238.34 - 322.7i	127.44 - 110.05i	119.17 + 161.35i	63.721 + 55.024i
221	236.62 - 323.34i	126.98 - 110.56i	118.31 + 161.67i	63.491 + 55.281i
222	235.27 - 323.14i	126.49 - 110.81i	117.63 + 161.57i	63.243 + 55.405i
223	234.2 - 322.37i	125.98 - 110.85i	117.1 + 161.19i	62.988 + 55.426i
224	233.25 - 321.35i	125.45 - 110.84i	116.62 + 160.67i	62.723 + 55.418i
225	232.24 - 320.46i	124.91 - 110.85i	116.12 + 160.23i	62.454 + 55.426i
226	230.99 - 320.06i	124.36 - 111.02i	115.5 + 160.03i	62.181 + 55.511i
227	229.31 - 320.48i	123.87 - 111.42i	114.65 + 160.24i	61.934 + 55.712i
228	223.9 - 325.05i	123.3 - 112.33i	113.51 + 161.03i	61.648 + 56.165i
229	219.71 - 329.69i	122.77 - 113.66i	111.95 + 162.53i	61.384 + 56.829i
230	214.12 - 336.15i	122.23 - 115.58i	109.85 + 164.84i	61.114 + 57.791i

231	206.68 - 344.61i	121.65 - 118.22i	107.06 + 168.07i	60.824 + 59.109i
232	196.78 - 355.15i	121.02 - 121.7i	103.34 + 172.31i	60.512 + 60.848i
233	183.55 - 367.9i	120.33 - 126.67i	98.389 + 177.58i	60.167 + 63.334i
234	165.55 - 382.75i	118.92 - 132.83i	91.774 + 183.95i	59.458 + 66.413i
235	141.25 - 398.88i	117.47 - 141.16i	82.777 + 191.37i	58.735 + 70.582i
236	109.89 - 414.41i	114.89 - 150.99i	70.624 + 199.44i	57.447 + 75.497i
237	72.346 - 426.89i	107.95 - 166.01i	54.946 + 207.2i	53.974 + 83.007i
238	38.137 - 434.4i	93.534 - 184.26i	36.173 + 213.44i	46.767 + 92.128i
239	21.124 - 440.18i	63.439 - 199.24i	19.068 + 217.2i	31.72 + 99.62i
240	242.66 - 382.34i	32.236 - 203.06i	10.562 + 220.09i	16.118 + 101.53i

Table 5-2 "Real" approx. diode impedances.

Again the reflection coefficients are calculated for the final mixer design. Note that there is a good agreement with the calculated for the ideal analysis, Fig. 3-10. However, the noise temperature values obtained for the ideal case, 700 K, are lower than the "real" approx. ones, 833 K, meanwhile the conversion loss has reached a good agreement, 6.3 dB.
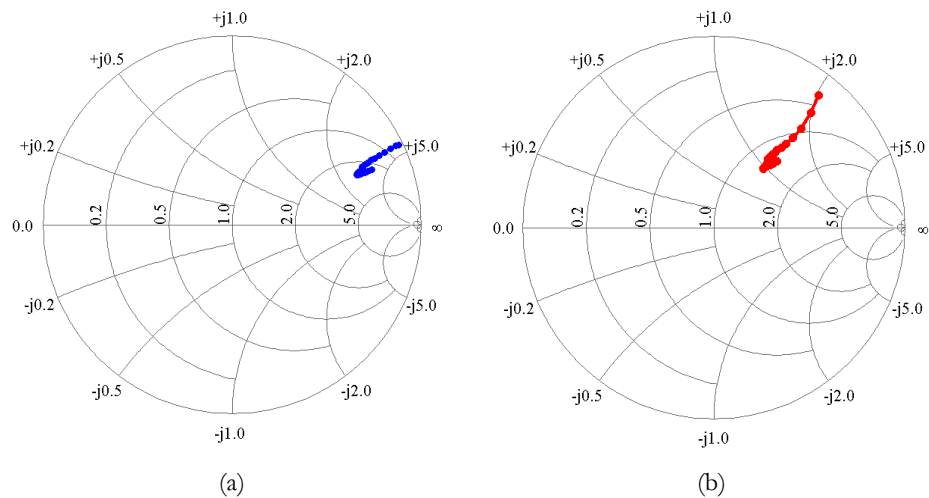
Fig. 5-10 Real (a) LO, (b) RF reflection coefficients.

If the real and imaginary part of the LO and RF impedance port are compared, a good agreement between the ideal and the "real" results are

obtained, especially for the RF impedance. That means that similar conversion loss values are obtained.
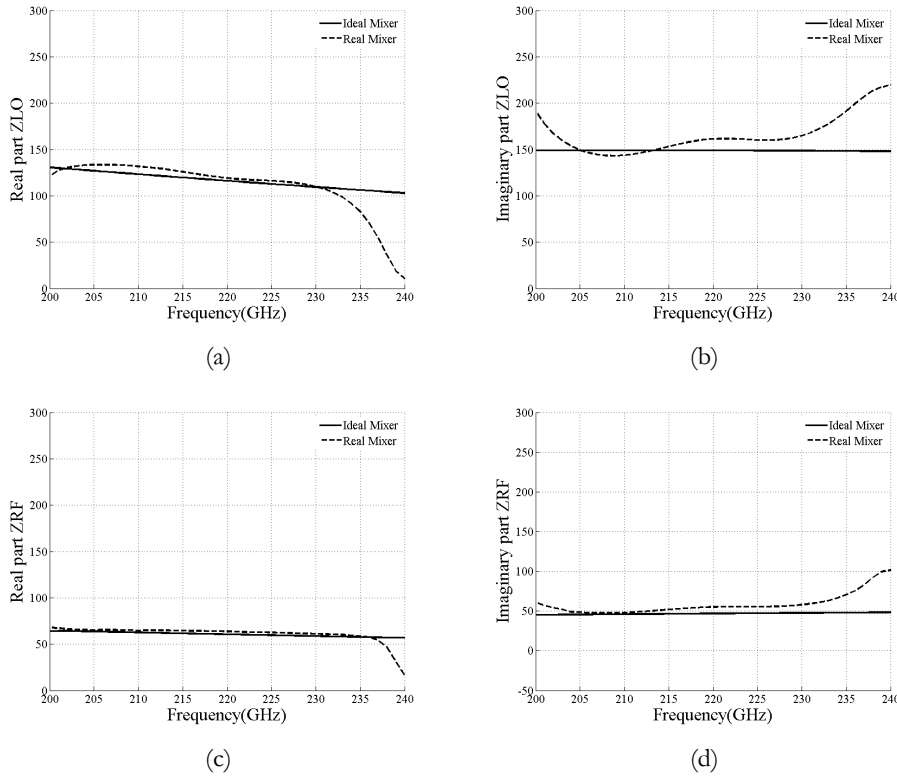

Fig. 5-11 LO and RF port impedances comparison between ideal and "real" mixer design (a) Z_{LO} real part, (b) Z_{LO} imaginary part, (c) Z_{RF} real part and (d) Z_{RF} imaginary part.

5.3   Doubler at 220 GHz

The design of this multiplier comes from the necessity of measuring the sub-harmonic mixer presented in previous section. Microwave multipliers usually employed varactor diodes which make use of the diode´s nonlinear capacitance characteristic, in order to get a multiplication of the input signal, [Ald10, Mae08b]. However, varactor diodes, [Mar01], are used to multiply microwave signal to low harmonics, rarely over four times the source frequency. This kind of components are inherently narrow band and

are able to obtained good efficiency and low noise when properly designed, some examples of doublers [Che13; Ald11; Sil11] and triplers [Li12; Mae08a;Lu12] can be found in bibliography. The dominant noise source in a varactor multiplier is the thermal noise of its series resistance and of its circuit losses and it is important to maintain them small [Maa03].

Varistor diode multipliers have not been employed widely in microwave systems due to they are significantly less efficient than varactor multipliers and are also limited in output power. Moreover, their efficiency decreases rapidly when harmonic number increases and they are rarely practical for generating harmonics above the second one. However, they offer great stability and are capable of wide bandwidths. Reactive multipliers, that is varactor multipliers, are capable in practice of achieving efficiencies varying as $1/n$ where n is the multiplication factor. On the other hand, resistive multipliers, that is varistor multipliers, are theoretically capable of efficiency no better that $1/n^2$ which is obviously much worse, [Maa03].

A doubler with varistor diodes, UMS DBES105a [UMS], is presented in this section. The selection of this kind of diodes is due to their low cost and the stock available at the Antenna Group facilities. It has been demonstrated the possibility of developing doublers [Wu12; Yao08; Che12; Hro13] and triplers [Zha10, Zha12, Zha13] using these diodes, however, the performance obtained by them presents a simulated doubler efficiency no better than 13 % and 16% for the tripler for an input power of 20 dBm, achieving a 3.5 % tripler measured efficiency and between 0.316% to 3.16% measured doubler efficiency.

A doubler with and input frequency of 110 GHz, so that the output frequency will set to 220 GHz, is presented next. The longitudinal section of the design doubler is shown in Fig. 5-12.
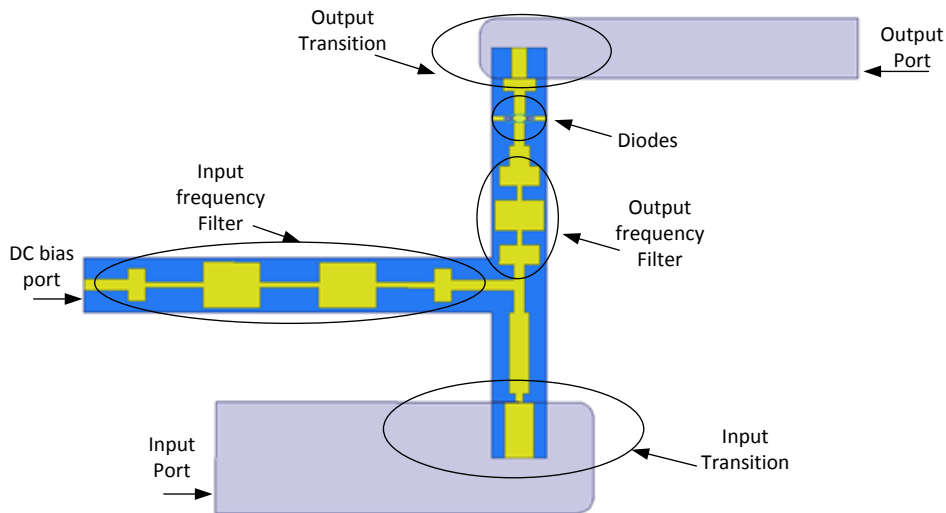
Fig. 5-12 Longitudinal section of the doubler showing its different parts and components.

The doubler design consists of two waveguide-to-microstrip transitions, two filters and a pair of diodes. Moreover, a DC bias port is also presented in order to feed the diodes.
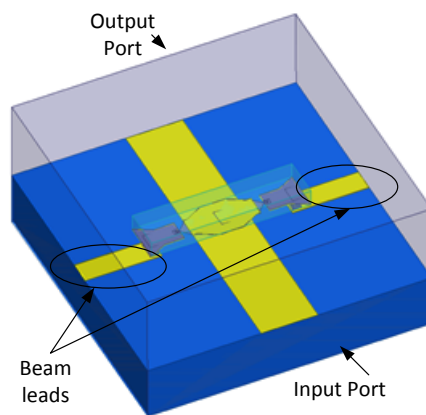

Fig. 5-13 Doubler HFSS 3D model.

The main characteristics of the UMS GaAs schottky barrier diodes employed for this design are: high cut-off frequency of 3 THz, high breakdown voltage, -5V, low parasitic inductances and a good ideally factor,

1.2. Every UMS DBES105a is a planar flip-chip type with two anodes arrange in series. For this design, the two anodes are split and connected in anti-series configuration. The 3 D model of the pair of diodes is presented in Fig. 5-13. Note that two beam leads are employed in order to connect the diodes to ground. In addition, note that the diodes are place in anti-series configuration in order to obtain the second harmonic of the input frequency signal, Equation 5-4.
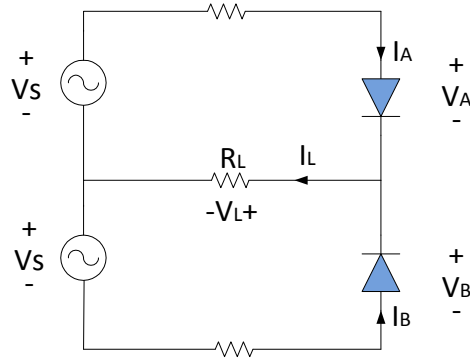
Fig. 5-14 Two diodes in anti-series configuration [Maa03].

Due to the circuit´s symmetry $V_A = V_B = V$ and therefore:

$$I_L = I_A + I_B \qquad\qquad 5\text{-}1$$

Where I_A and I_B can be calculated from Equation 3.5 and 3.6:

$$I_A = f(V) = aV + bV^2 + cV^3 + dV^4 + eV^5 + \cdots \qquad\qquad 5\text{-}2$$

$$I_B = f(-V) = -aV + bV^2 - cV^3 + dV^4 - eV^5 + \cdots \qquad\qquad 5\text{-}3$$

So that,

$$I_L = I_A + I_B = 2bV^2 + 2dV^4 + \cdots \qquad\qquad 5\text{-}4$$

The output current presented in the load, R_L, is an even-degree function of the voltage across the non-linear elements. It is also possible to calculate the loop current, i.e. the current trapped inside the diodes for this configuration, by recognizing that $I_A = -I_B$ for the current components presented in I_{loop}:

$$I_{loop} = I_A = -I_B = aV + cV^3 + \cdots \qquad\qquad 5\text{-}5$$

From Equation 5-5 is possible to see that I_{loop} is an odd-degree function of V. As it happened with the anti-parallel configuration, the anti-series configuration is able to separate the even- and odd-frequency components.

The input frequency filter will have a cut off frequency below 110 GHz and will avoid the input signal to go through the DC bias port. It has been chosen a stepped impedance filter.
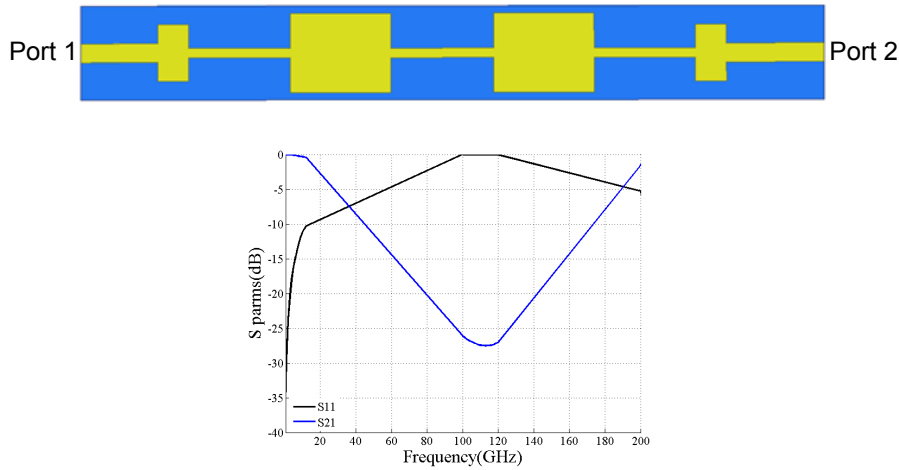

Fig. 5-15 S_{11} and S_{21} doubler input frequency filter.

The output frequency filter is also a stepped impedance filter. In this case, its purpose is to reject the output signal, second harmonic of the input signal, to go towards the input port and the DC bias port. Its cut-off frequency will be below 220 GHz.

(a)   (b)
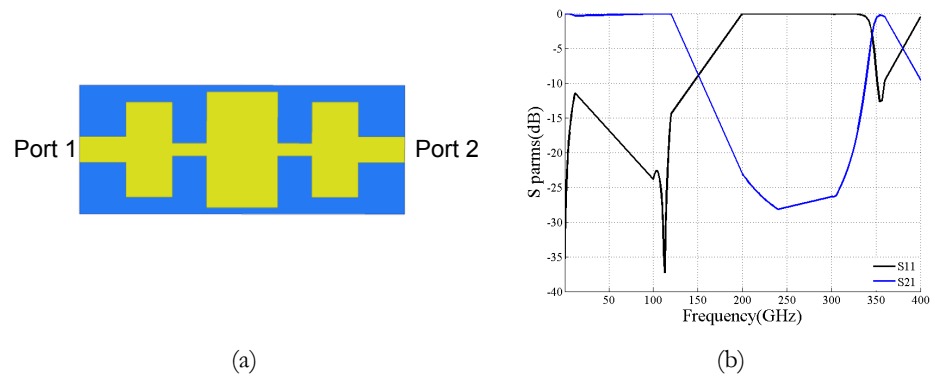
Fig. 5-16 Doubler output frequency filter (a) model and (b)S_{11} and S_{21}.

Two probe transitions have been designed in order to couple the signal from the waveguide to the microstrip channel. There are two common ways to develop a probe type transition. In both ways the microstrip enters the waveguide through a window on the broadwall of the waveguide. In the longitudinal case, which is the one presented here; the surface of the substrate aligns along the direction of propagation of the waveguide. A matching network consisting of a high impedance microstrip line and a quarter-wave impedance transformer is used to achieve broadband matching, [Leo99].

(a)   (b)

(c)   (d)
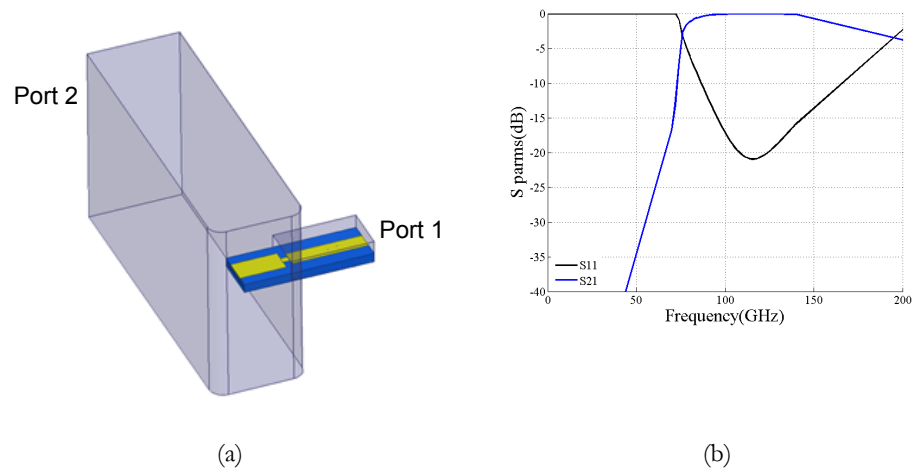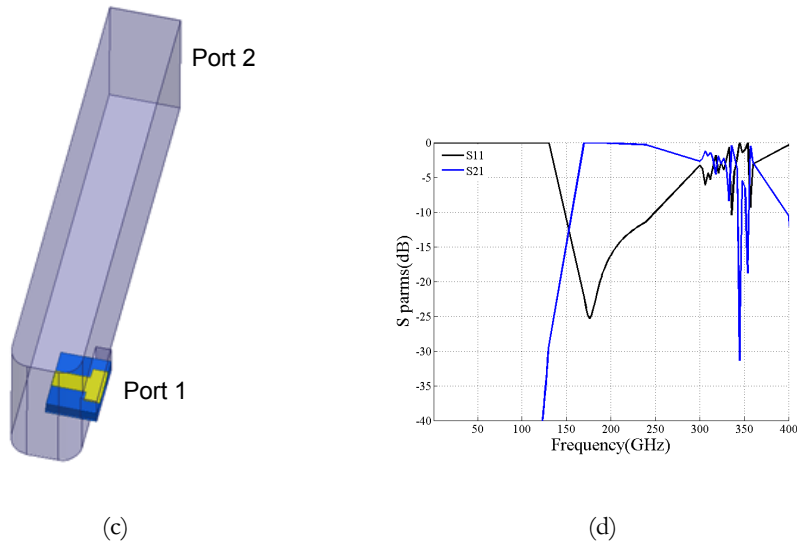
Fig. 5-17 (a) Input Transition model and (b) S_{11} and S_{21}, (c)Output Transition model and (d) S_{11} and S_{21}.

In order to have the possibility to fabricate the microstrip circuits using the laser machine and the sputtering equipment, the high impedance section of the RF transition was eliminated and afterwards the transition was optimized, see Fig. 5-17 (a). The reason to eliminate this section was due to the fact that laser equipment only has a resolution of 50 μm nevertheless the photolithography fabrication process is able to achieve widths below 20 μm.

The complete microstrip and block dimensions of the doubler are presented in Appendix B.

The doubler final ADS schematic is presented in Fig. 5-18. Note that the doubler is completely simulated in HFSS and imported to ADS. Also, the diodes are presented in an anti-series configuration and they are reversed biased, i.e. the input voltage is negative.
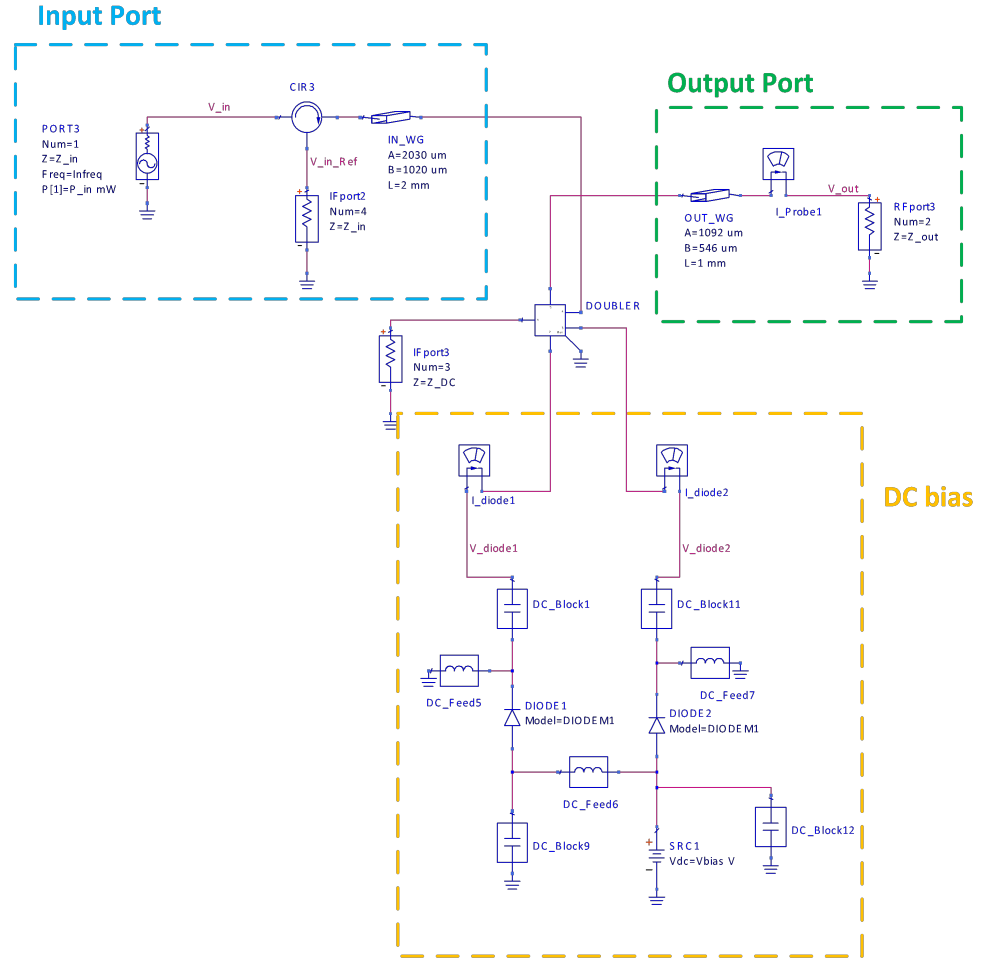
Fig. 5-18 ADS doubler schematic.

The efficiency simulation results as well as the simulated output power are presented in Fig. 5-19 and Fig. 5-20. Two input power cases have been analysed. First of all, an input power of 20 mW was chosen, Fig. 5-19, since the output power values obtained for this case would be the required ones to feed a single mixer. The second analysed case was taking into account an input power of 100 mW, which will be the required one to feed a possible array placed after the doubler.
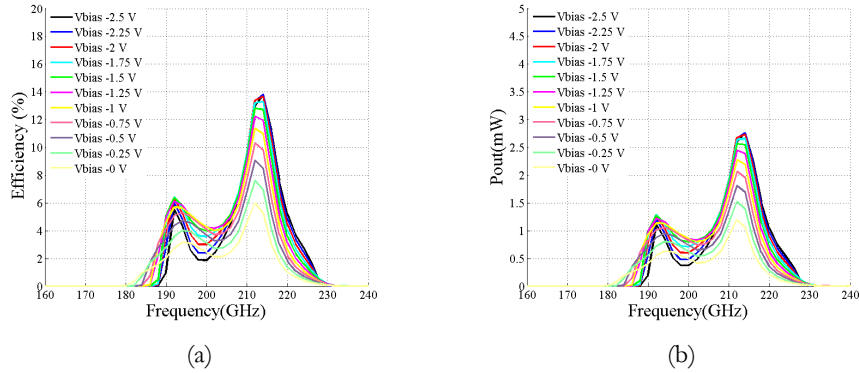
Fig. 5-19 Doubler simulated (a) efficiency and (b) output power for an input power of 20 mW.

A maximum efficiency value of 14 % is obtained at 215 GHz giving an output power of 2.75 mW, which is an optimal value to feed a typical sub-harmonic at these frequencies.

On the other hand, when the input power is increased to 100 mW, the efficiency is a bit lower, 12.8%, giving an output power of 12.8 mW which could be enough to feed an array of 4 sub-harmonic mixers.
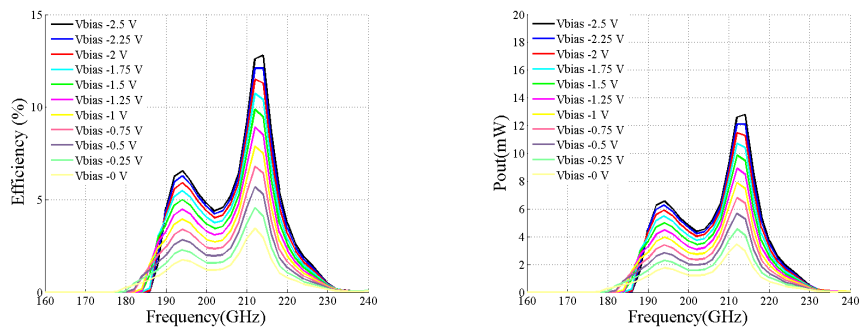
Fig. 5-20 Doubler simulated (a) efficiency and (b) output power for an input power of 100 mW.

5.4   Fourth-harmonic mixer working at 440 GHz

Usually, millimetre-wave mixer designs are focused on sub-harmonic mixers, in which the RF frequency is doubled the LO frequency, see Chapter 2 and section 2 of Chapter 5. The actual technology available at the sub-millimetre wave range does not provide in most cases enough power to feed the available components due to the high operational frequencies. This can result in an important problem when arrays of sub-harmonic mixers need to be pumped at these frequencies. However, a new approach for this issue is presented here; this is the use of a fourth-harmonic mixer in which the RF frequency is four times the LO frequency. This configuration is a good solution since the LO frequency can be a much lower frequency than in sub-harmonic mixer designs and as a consequence, a wide range of components can be found at those frequencies, i.e. 110 GHz [Qua03; Sch08; Gun08; Mao12; Mic13].

A fourth harmonic configuration mixer is developed here and measured for the first time at this frequency range. A fourth-harmonic mixer configuration consists on a harmonic mixer that by appropriate filtering selects the fourth mixing product of the local oscillator, LO, frequency and the radio frequency, RF. This solution is simpler than other configurations based on cancellation of the sub-harmonic mixing product by combining the response of 4 diodes with 90º phase difference [Sch08]. In this case, an LO frequency of 110 GHz has been chosen, so that, the RF frequency will be 440 GHz and the IF signal will be calculated by $f_{IF} = 4f_{LO} - f_{RF}$. It is well-know that the fourth harmonic mixing product has a lower level of power compared to the second harmonic mixing product ($f_{IF} = 2f_{LO} - f_{RF}$), for this reason a higher pumped of power will be required. This can be seen as a disadvantage but, if a sub-harmonic mixer is used instead an LO frequency of 220 GHz should be used and therefore, a more complicated and expensive LO power should be required. On the other hand, if a LO power working at 110 GHz is used, a doubler would be necessary to reach the LO frequency of the sub-harmonic mixer and hence

the same power problem as in the fourth harmonic mixer might be presented concerning the doubler efficiency. This topology has been studied in sections 5.2 and 5.3.

When analysing the diode configuration in a sub-harmonic mixer design, an anti-parallel interconnection is commonly used. The reason why this configuration is the most renowned is due to the fact that a suppression of half of the harmonics is well-done. When talking about fourth-harmonic mixers the same configuration is employed but in this case, the first mixing product, $2f_{LO}$, has to be filtered out and the second one, $4f_{LO}$, is selected.
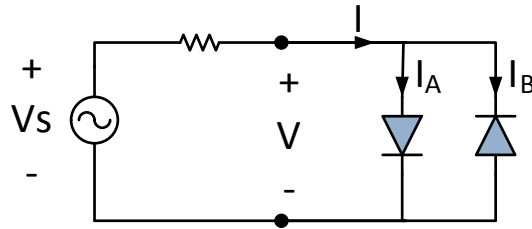
$$I_A = f(V) = aV + bV^2 + cV^3 + dV^4 + eV^5 + \cdots$$

$$I_B = -f(-V) = aV - bV^2 + cV^3 - dV^4 + eV^5 + \cdots$$

$$I = I_A + I_B = f(V) - f(-V) = 2aV + 2cV^3 + 2eV^5 + \cdots$$

The harmonics presented in a two diodes anti-parallel configuration with f_{LO}=110GHz and f_{RF}=440 are indicated in Table 5-3.

Frequency	Harmonic
0 GHz	4f_{LO}-f_{RF}
110 GHz	f_{LO}
220 GHz	2f_{LO}-f_{RF}
330 GHz	5f_{LO}-2f_{RF}
330 GHz	3f_{LO}
440 GHz	f_{RF}
550 GHz	3f_{LO}-2f_{RF}
550 GHz	5f_{LO}
660 GHz	2f_{LO}+f_{RF}

Frequency	Harmonic
1.210 THz	5f_{LO}-4f_{RF}
1.210 THz	3f_{LO}+2f_{RF}
1.320 THz	3f_{RF}
1.430 THz	3f_{LO}-4f_{RF}
1.430 THz	5f_{LO}+2f_{RF}
1.540 THz	2f_{LO}+3f_{RF}
1.650 THz	f_{LO}-4f_{RF}
1.760 THz	4f_{LO}-5f_{RF}
1.760 THz	4f_{LO}+3f_{RF}

769.8 GHz	$f_{LO}-2f_{RF}$		1.871 THz	$f_{LO}+4f_{RF}$
878.7 GHz	$4f_{LO}-3f_{RF}$		1.980 THz	$2f_{LO}-5f_{RF}$
881.7 GHz	$4f_{LO}+f_{RF}$		2.092 THz	$3f_{LO}+4f_{RF}$
990.6 GHz	$f_{LO}+f2_{RF}$		2.200 THz	$5f_{RF}$
1.099 THz	$2f_{LO}-3f_{RF}$			

Table 5-3 Mixing harmonics presented in two diodes anti-parallel configuration.

The schematic of the ideal ADS design of the 4th-harmonic mixer is presented in Fig. 5-21. In this case the LO frequency is set to 110 GHz and the RF to 440 GHz, see Fig. 5-22. Note also that the noise controllers are now selecting the noise of the fourth harmonic, i.e. $4f_{LO} - f_{RF}$, Fig. 5-23.

Fig. 5-21 ADS 4th-harmonic schematic.

HARMONIC BALANCE

HarmonicBalance
HB2
MaxOrder=11
Freq[1]=LOfreq
Freq[2]=RFfreq
Order[1]=10
Order[2]=10
BandwidthForNoise=1.0 Hz
Noisecon[1]="NC_USB"
NoiseConMode=yes

Fig. 5-22 Harmonic balance parameters.

HB NOISE CONTROLLER

NC_USB
InputFreq=RFfreq
FreqForNoise=4*LOfreq-RFfreq
NoiseInputPort=4
NoiseOutputPort=7
NoiseNode[1]=V_IF
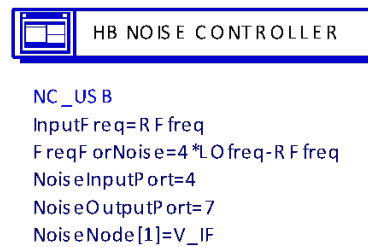
Fig. 5-23 Noise source parameters definition.

Fig. 5-21 model counts with ideal filters to select the corresponding frequency in each band. The ideal conversion loss and noise temperature are calculated taking into account the RF and LO frequency impedances. The best value obtained varying these impedances is shown in Fig. 5-24. Best conversion loss values obtained are in the order of 8.5 dB using the diodes VDI SC1T2-D20 [VDI], and noise temperature values are around 1550 K.

(a)   (b)
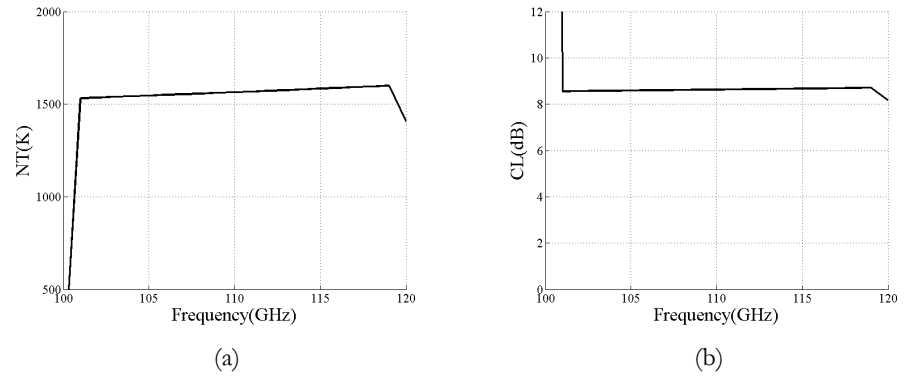
Fig. 5-24 (a) Noise temperature and (b) conversion loss of the ideal 4th -harmonic mixer.

The diode impedances have been extracted from the 4th-harmonic ideal mixer design and $Z_{RF}=(Z_{diode1RF}/2)^*$ and $Z_{LO}=(Z_{diode1LO}/2)^*$ where * means conjugate, have been calculated. The obtained values related to the analysed LO frequency band are presented in Table 5-4.

Freq. (GHz)	ZdiodeLO (Ω)	ZdiodeRF (Ω)	ZLO (Ω)	ZRF (Ω)
100	244.7 - 88.565i	81.428 - 32.343i	122.35 + 44.282i	40.714 + 16.172i
101	243.91 - 89.031i	81.428 - 32.343i	121.95 + 44.516i	40.714 + 16.172i
102	243.11 - 89.493i	81.164 - 32.511i	121.56 + 44.747i	40.582 + 16.255i
103	242.32 - 89.949i	80.899 - 32.675i	121.16 + 44.975i	40.45 + 16.338i
104	241.54 - 90.399i	80.635 - 32.838i	120.77 + 45.199i	40.317 + 16.419i
105	240.75 - 90.842i	80.371 - 32.998i	120.37 + 45.421i	40.185 + 16.499i
106	239.96 - 91.28i	80.107 - 33.156i	119.98 + 45.64i	40.053 + 16.578i
107	239.18 - 91.711i	79.844 - 33.311i	119.59 + 45.856i	39.922 + 16.656i
108	238.4 - 92.137i	79.58 - 33.464i	119.2 + 46.068i	39.79 + 16.732i
109	237.62 - 92.556i	79.318 - 33.615i	118.81 + 46.278i	39.659 + 16.808i
110	236.85 - 92.97i	79.055 - 33.763i	118.42 + 46.485i	39.528 + 16.882i
111	236.07 - 93.378i	78.793 - 33.909i	118.04 + 46.689i	39.397 + 16.955i
112	235.3 - 93.781i	78.531 - 34.052i	117.65 + 46.89i	39.266 + 17.026i
113	234.53 - 94.178i	78.27 - 34.194i	117.27 + 47.089i	39.135 + 17.097i
114	233.76 - 94.569i	78.009 - 34.332i	116.88 + 47.285i	39.004 + 17.166i

115	233 - 94.955i	77.748 - 34.469i	116.5 + 47.477i	38.874 + 17.234i
116	232.24 - 95.335i	77.488 - 34.603i	116.12 + 47.668i	38.744 + 17.301i
117	231.48 - 95.71i	77.228 - 34.735i	115.74 + 47.855i	38.614 + 17.367i
118	230.72 - 96.08i	76.968 - 34.864i	115.36 + 48.04i	38.484 + 17.432i
119	229.96 - 96.444i	76.709 - 34.992i	114.98 + 48.222i	38.355 + 17.496i
120	229.21 - 96.803i	78.473 - 35.019i	114.6 + 48.402i	39.237 + 17.51i

Table 5-4 Ideal diode impedances.

The diode impedance at the LO frequency has values around 230 Ω for the real part and 92 Ω for the imaginary part. On the other hand, the diode impedance at the RF frequency has values around 80 Ω for the real part and 33 Ω for the imaginary part. A straightforward relation between the impedance values obtained for the 4th-harmonic mixer and the sub-harmonic mixers (the one with an RF frequency of 220 GHz and the other one with an RF frequency of 440 GHz) cannot be observed. Although it is true that the real parts of the RF and LO impedances for the sub-harmonic mixer at 440 GHz and the 4th-harmonic mixer are not quite different ($Z_{diodeRF\_subharm}$=120 Ω and $Z_{diodeRF\_4th}$=80 Ω; $Z_{diodeLO\_subharm}$=230 Ω and $Z_{diodeLO\_4th}$=220 Ω).

In Fig. 5-25 the calculated LO and RF reflection coefficients are shown. It will be important to approximate as much as possible the values of the reflection coefficients of the real mixer design to the calculated ideally in order to obtain good results.
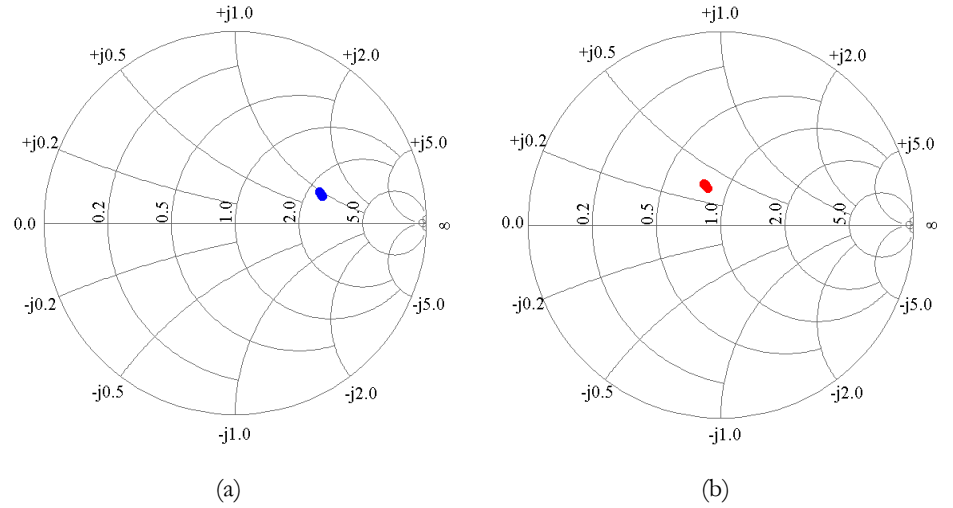
Fig. 5-25 Optimum (a) LO, (b) RF reflection coefficient.

Having a brief idea of the ideal performance of a 4th-harmonic mixer with the characteristics described previously, a complete design is developed. The same procedure presented previously in this dissertation has been followed in order to get the final mixer design. The longitudinal section of the mixer is depicted in Fig. 5-26.
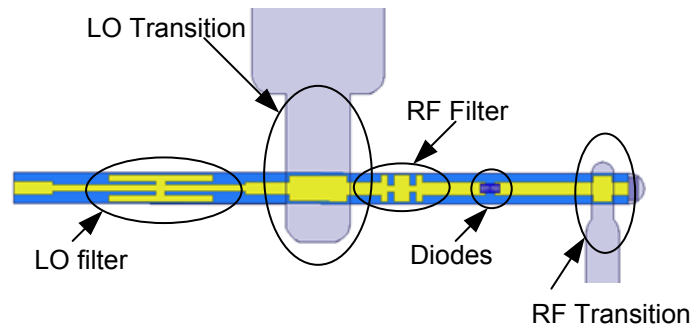
Fig. 5-26 Longitudinal section of the 4th -harmonic mixer showing its different parts and components.

The 4th-harmonic mixer consists of two microstrip filters, two waveguide to microstrip transitions and a pair of diodes. This mixer makes use of the same flip-chip schottky diodes employed for the rest of the mixers developed along in this thesis, i.e. VDI SC1T2-D20 [VDI].

The LO Filter is a Hammerhead filter. This filter will not let the LO signal pass through the IF port and will completely direct it towards the diodes. Its response is presented in Fig. 5-27 (b). The selection of this kind of filter, instead of the typically used stepped impedance LPF, is due to the dimensions determined by the channel, since it made really difficult to design a stepped filter at 110 GHz with such a limited width dimension.

(a)
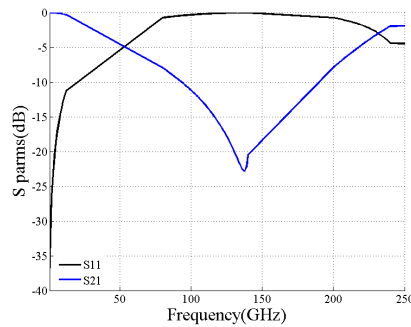
(b)

Fig. 5-27 (a) LO filter model and (b) S_{11} and S_{21} parameters.

The RF Filter is a stepped-impedance LPF with a cut-off frequency between 110 GHz and 440 GHz letting the LO frequency pass towards the diodes but avoiding the RF frequency to go through the LO and IF, Fig. 5-28.
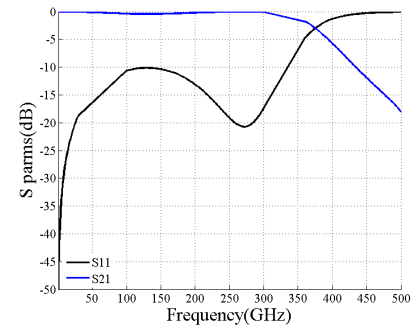
(a)   (b)

Fig. 5-28 (a) RF filter model and (b) S_{11} and S_{21} parameters.

The LO and RF transitions are designed to gather the maximum power for the mixer. Their performance is shown in Fig. 5-29 (b) and (d) respectively. Their dimensions are 0.5 x 2.030 mm and 0.170 x 0.254 mm respectively for the section reduced in height [Hes97; Shi97]. The complete bunch of dimensions is gathered in Appendix B.

(a)   (b)

Port 2

Port 1

(c)   (d)
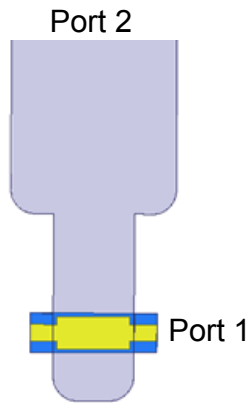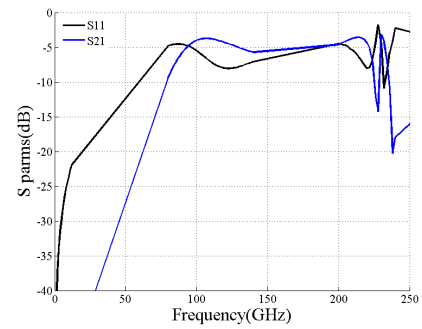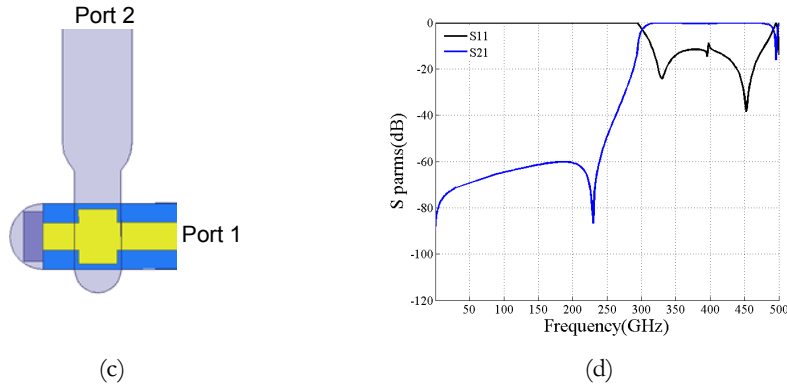
Fig. 5-29 (a) LO Transition, LOT, model and (b) LOT S_{11} and S_{21}, (c) RF Transition , RFT, model, (d) RFT S_{11} and S_{21}.

The RF transition is good enough (around -20 dB S_{11}) to couple the RF signal to microstrip line although the LO transition is not quite good. This will lead to an increase in the input power required to pump the diodes.

Once the different mixer parts are defined the optimization procedure can begin until the final design is obtained. Fig. 5-21 depicts the final ADS schematic of the 4th-harmonic mixer.
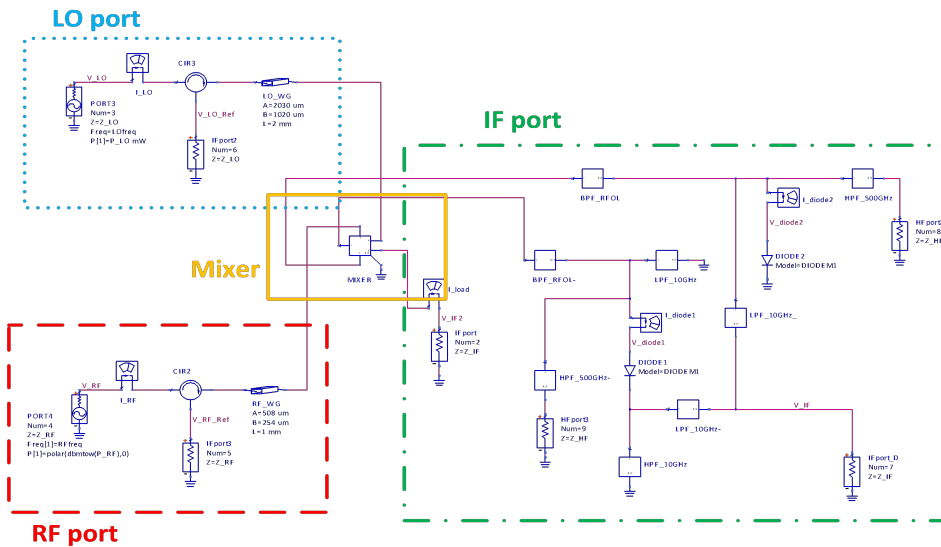
Fig. 5-30 ADS final schematic of the 4th-harmonic mixer.

Simulated noise temperature, Fig. 5-31 (a), has values below 2000 K over a 5 GHz bandwidth (centred on 111.5 GHz) with a minimum value of 1500 K at 110 GHz. On the other hand, conversion loss, Fig. 5-31 (b), has minimum values of 8.5 dB and they are below 10 dB in a bandwidth wider than 8 GHz (centred on 112 GHz).

(a)

(b)

(c)

(d)
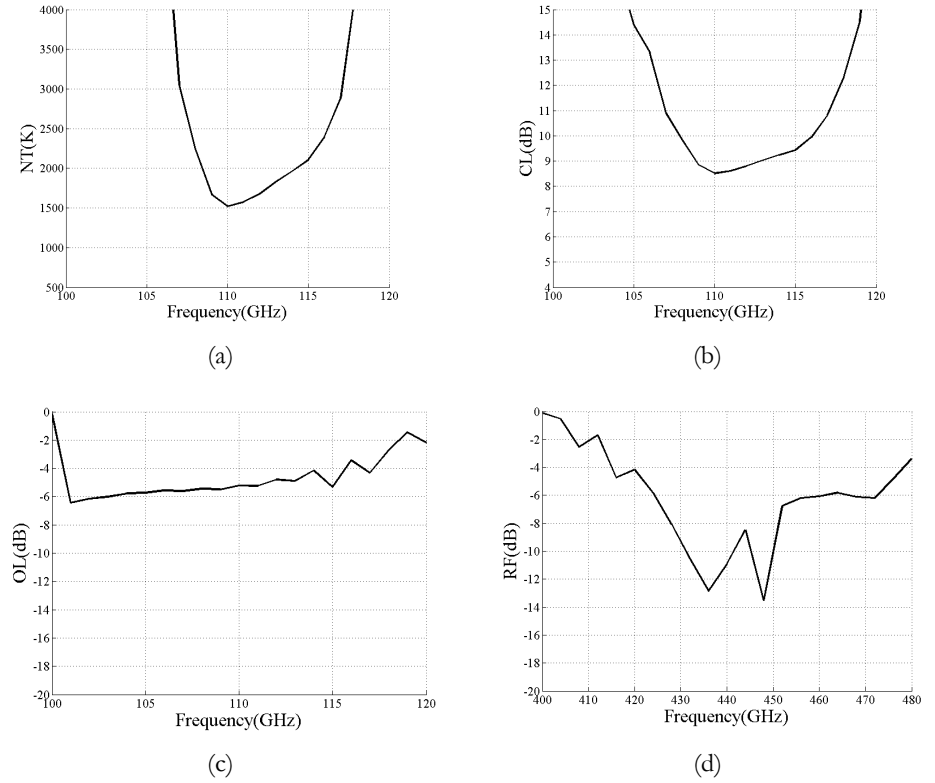
Fig. 5-31 Simulated (a) NT, (b) CL, (c) OL S11 and (d) RF S11.

The obtained LO matching is quite poor which will mean that a higher input power will be required. Nevertheless, the RF matching is good, having values below -8 dB from 428 GHz to 452 GHz.

The diode impedance and port impedance have also been calculated for this mixer. They are presented in Table 5.5.

Freq. (GHz)	ZdiodeLO (Ω)	ZdiodeRF (Ω)	ZLO (Ω)	ZRF (Ω)
100	NaN + NaNi	NaN + NaNi	NaN + NaNi	NaN + NaNi
101	250.66 - 45.738i	84.36 - 5.2828i	125.33 + 22.869i	42.18 + 2.6414i
102	253.83 - 48.075i	87.612 + 6.0062i	126.91 + 24.037i	43.806 - 3.0031i
103	257.24 - 49.381i	101.82 + 11.554i	128.62 + 24.69i	50.912 - 5.777i
104	259.81 - 51.898i	114.04 + 7.481i	129.91 + 25.949i	57.02 - 3.741i
105	259.59 - 53.044i	125.36 - 0.84558i	129.79 + 26.522i	62.68 + 0.423i
106	261.18 - 54.578i	133.08 - 11.8i	130.59 + 27.289i	66.54 + 5.9i
107	260.34 - 54.826i	136.49 - 23.162i	130.17 + 27.413i	68.25 + 11.58i
108	262.02 - 56.312i	135.47 - 39.354i	131.01 + 28.156i	67.74 + 19.68i
109	261.59 - 56.63i	133.85 - 50.771i	130.79 + 28.315i	66.93 + 25.39i
110	264.63 - 58.51i	126.41 - 61.097i	132.31 + 29.255i	63.20 + 30.55i
111	266.79 - 59.655i	116.95 - 66.253i	133.39 + 29.828i	58.47 + 33.126i
112	272.21 - 62.426i	107.97 - 69.959i	136.11 + 31.213i	53.99 + 34.98i
113	280.27 - 66.936i	100.96 - 69.562i	140.14 + 33.468i	50.48 + 34.78i
114	287.2 - 71.231i	94.867 - 68.123i	143.6 + 35.615i	47.43 + 34.06i
115	281.31 - 68.487i	89.832 - 63.022i	140.65 + 34.243i	44.92 + 31.51i
116	310.44 - 89.486i	86.3 - 64.499i	155.22 + 44.743i	43.15 + 32.25i
117	180.91 - 23.661i	79.337 - 33.983i	90.457 + 11.831i	39.67 + 16.99i
118	338.57 - 122.37i	83.594 - 56.639i	169.28 + 61.184i	41.80 + 28.32i
119	435.2 - 273.66i	97.831 - 72.145i	217.6 + 136.83i	48.92 + 36.07i
120	361.43 - 166.72i	93.833 - 64.72i	180.71 + 83.359i	46.92 + 32.36i

*NaN=Not available. It is employed for really high values.

Table 5-5 "Real" approx.. diode impedances.

Fig. 5-32 shows the calculated reflection coefficients of the mixer.
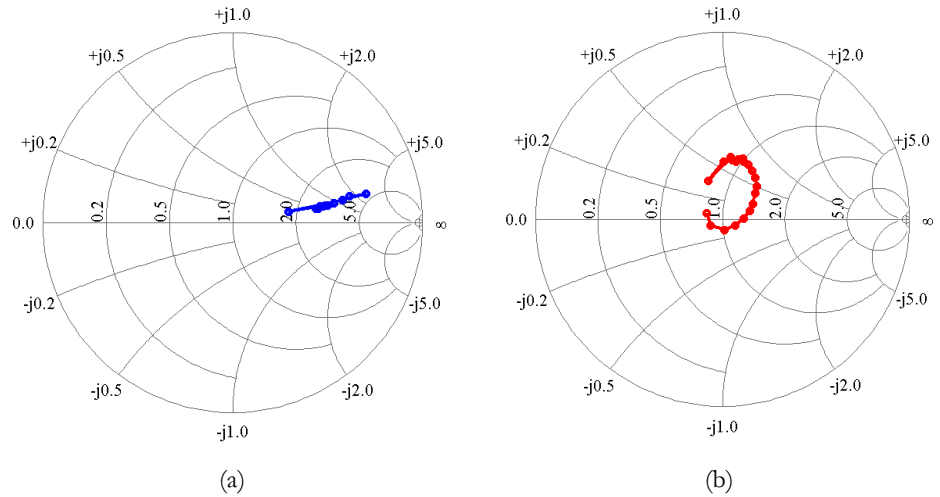
Fig. 5-32 "Real" approx.. (a) LO, (b) RF reflection coefficients

The real and imaginary parts of the mixer Z_{LO} and Z_{RF} impedances are compared to the ideal ones. It can be appreciated that a slight difference between them is presented but the variation is not extremely high, see Fig. 5-33. Note that the peaks that appear at high frequencies of Z_{LO} Real and Imaginary part are supposed to be simulation incoherencies produced by the software and not real results.
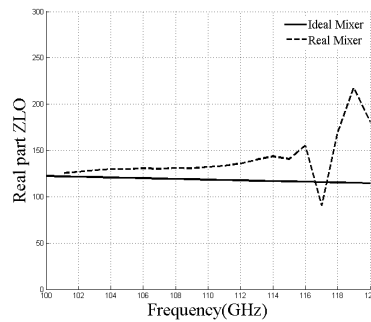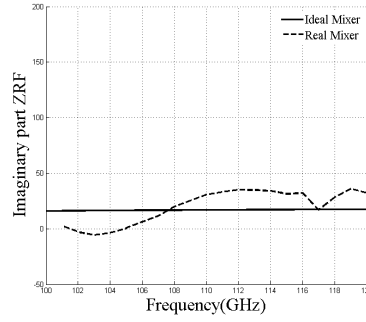

(a)
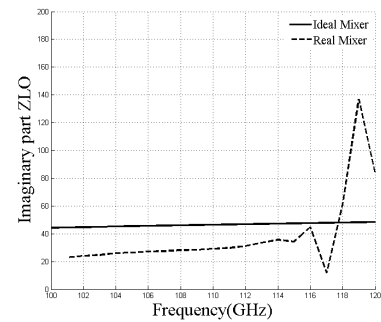
(b)
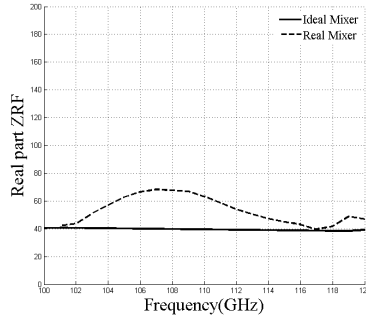
(c)   (d)

Fig. 5-33 LO and RF port impedances comparison between ideal and final mixer design
(a) Z_{LO} real part, (b) Z_{LO} imaginary part, (c) Z_{RF} real part and (d) Z_{RF} imaginary part.

The 4th-harmonic mixer design is considered quite good in terms of noise temperature and conversion loss taking into account that it is the first time such a device is developed at this frequency range. It will be important to compare the simulated results with the measured one in order to validate the simulation process.

However, if the hot electron noise source analyzed in Chapter 3 is included in the simulation of a 4th-harmonic mixer, a considerable increment on the noise temperature is appreciated since this noise is higher when the LO power increases. For this reason, it is really important to take it into account, since the LO power values handle at the 4th-harmonic mixer design are of 9 mW, considerably higher than for a sub-harmonic mixer (2.5 mW).

The spectral power density can be calculated from the current values of the different LO harmonics calculated in ADS. The series resistance, R_S is 13 Ω and the K value is $2.44*10^7$ K/A^2, see Chapter 3. Therefore the spectral power density is:

$$\langle v^2 \rangle = 4 * 1.38 * 10^{-23} 13 * 2.447 * 10^7 * 5.578 * 10^{-5} = 9.79 * 10^{-19} \frac{V^2}{Hz} = 9.8967 * 10^{-10} \frac{V}{\sqrt{Hz}} \qquad 5\text{-}6$$

The same way it was done in Chapter 3, the spectral power density is added to the mixer performance including two Noise voltage sources in series with the diodes.

The noise temperature of the 4th-harmonic including the hot electron noise source is depicted in Fig. 5-34.
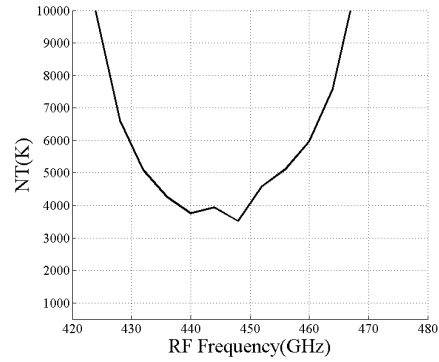
Fig. 5-34 Simulated 4th-harmonic noise temperature taking into account the hot electron noise source.

Note that the minimum NT is now around 3600 K, which is more than 2000 K degrees higher. For this reason it is of real importance to consider this noise when designing mixers that require high amounts of LO power.

If the mixer characteristics are simulated taking into account the hot electron noise and varying the input power Fig. 5-35 is achieved.

(a)   (b)
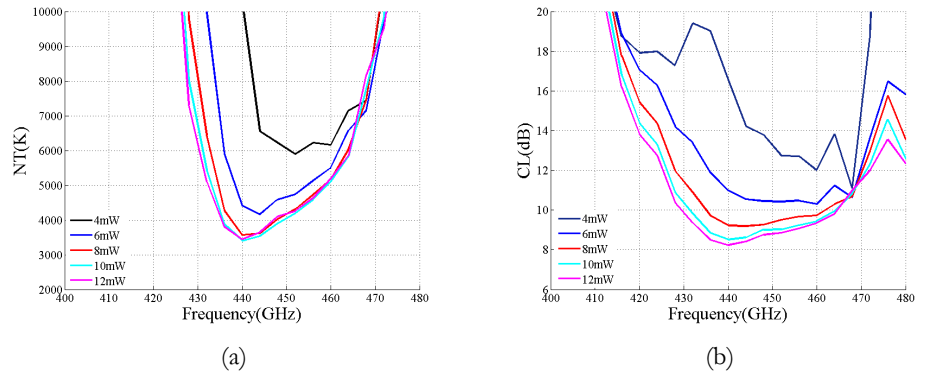
Fig. 5-35 Simulated noise temperature and conversion loss varying the input power.

Note that a slight difference is appreciated when the input power has values between 8 to 12 mW but it drastically increases when the input

power is below that. For this reason the differences between the simulation and measurements can be also a consequence of a bad couple of the power, mainly due to a bad LO transition. Remember that the designed LO transition was not really good. So that, a better performance could be obtained when improving it.

5.5   Mixers comparison performance

In this chapter a sub-harmonic mixer and a 4th-harmonic mixer both with RF frequency settled to 440 GHz have been developed. The simulated noise temperature and conversion loss of both mixers are presented in Fig. 5-36. The sub-harmonic mixer has a minimum noise temperature around 850 K and a minimum conversion loss of 6.3 dB. On the other hand, the fourth-harmonic mixer presents minimum noise temperature values close to 3800 K and 8.5 dB for the conversion loss when the hot electron noise source is taken into account. It is also remarkable that the sub-harmonic mixer presents a larger operational bandwidth. However, it is important to take into account the application in order to choose between one design and the other.

(a)   (b)
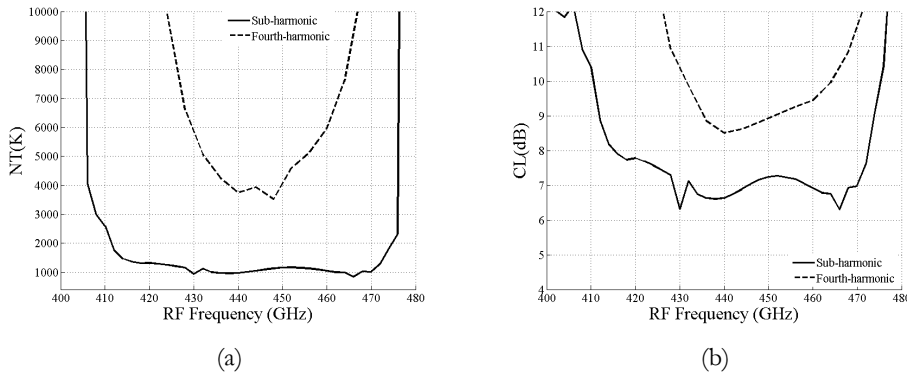
Fig. 5-36 Comparison of simulated (a) NT and (b) CL of the Sub-harmonic and 4th-harmonic mixers

5.6   Mixers measurements

The components presented in this Chapter have been fabricated following the same process as the one presented in Chapter 4. In the case of the sub-harmonic mixer and the 4th-harmonic mixer developed here, the dicing process becomes more difficult considering that the dimensions of the microstrip circuits are smaller.

Due to some fabrication issues related to the doubler, the measurements of both, the doubler and the sub-harmonic mixer, have not been included in the manuscript. Although both blocks have been fabricated and the sub-harmonic mixer is completely assembled, the manufacturing of the doubler, i.e. the microstrip and diodes welding process, has not been implemented. For this reason, the sub-harmonic mixer characterization has not been accomplished since the Antenna Group equipment does not contain up to now a 220 GHz power source. These measurements are expected to be included during the presentation of this dissertation.

5.6.1   4th-harmonic Mixer

The 4th-harmonic mixer has been fabricated and measured. The set-up employed to carry out with the measurement is the one previously used both in the measurements of the sub-harmonic mixer, described in Charter 3, and in the array, presented in Chapter 4. This set-up counts with an Elva Signal Generator, an isolator and the same IF chain with a bandwidth form 1 to 6 GHz, see Fig. 5-37. Note that in both cases (4th-harmonic mixer and sub-harmonic at 220 GHz) the LO frequency band employed is the same, the only difference is the power required to pump the diodes (around 9 mW and 2.5 mW respectively). The main difference between both measurements set-ups is the RF feed-horn antenna, which in this case is a WR-2.2 standard wave horn antenna.

IF CHAIN

POWER SENSOR
Hewlett Packard

EPM SERIES POWER
METER
Agilent

AMPLIFIERS +5V

IF Port

HOT/COLD
LOAD

LO Port   RF Port

SIGNAL
GENERATOR
ELVA 110 GHz   ISOLATOR   MIXER   RF ANTENNA
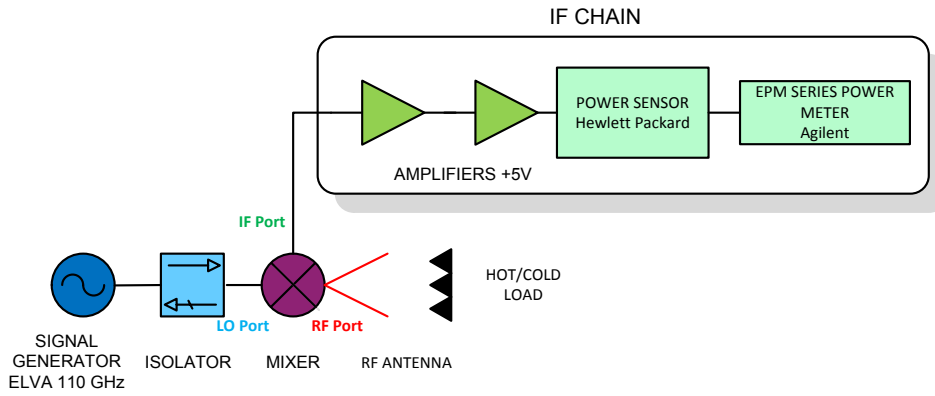
Fig. 5-37 Measurement set-up.

A first measurement gave unexpected results due to the high noise temperature and conversion loss obtained, see Measurement 1 Fig. 5-38. This increase in the mixer characteristics was mainly due to fabrication issues. The mixer channel had been reduced to 240 μm and the microstrip circuits were more difficult to be cut by means of the dicing machine. This process was improved and another 4th-harmonic mixer was fabricated and a great advancement was obtained, Measurement 2 Fig. 5-38. Note that all the results presented in the following graphs are obtained for the best input LO power which varies between 7 mW and 10 mW depending on the frequency.
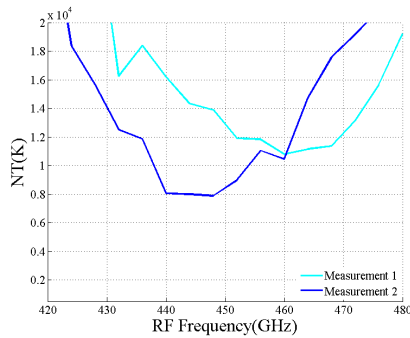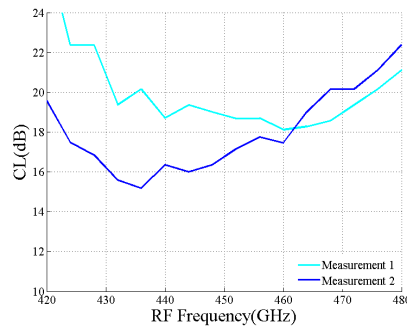
(a)   (b)

Fig. 5-38 4th.harmonic measurements 1 and 2.

The first measurement showed minimum noise temperature values of 10811 K at 460 GHz meanwhile the second one had 7887 K at 448 GHz. On the other hand, minimum conversion loss values were 18.1 dB at 460 GHz for the first one and 16 dB at 444 GHz for the second one. An improvement of 3000 K and 2 dB have been observed. Moreover, a shift between the first measurement and the second one is also obtained. All of this suggests that the fabrication of the first mixer was not the optimal one, and that the process has been improved considerable in the second one, i.e., the sputtering process has been perfected as well as the dicing of the microstrip circuits.

A third mixer was fabricated in order to confirm that the NT and CL results of the 4th-harmonic mixer were consistent since a considerable difference between measurements and simulation were presented, see Fig. 5-39.
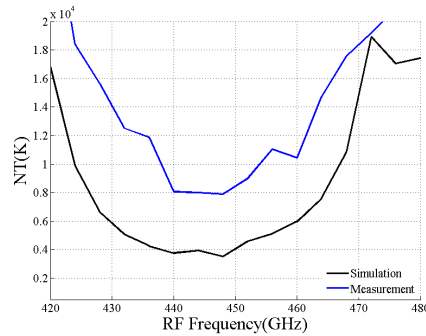
Fig. 5-39 Noise temperature comparison between simulation and measurement of the 4th-harmonic mixer.

Note that the noise temperature curve of both, the simulation and measurement, has the same tendency, the difference comes in the values (around 4000 K difference).

Four different measurements have been done of mixer 3 in order to check the stability of the device.

(a)   (b)
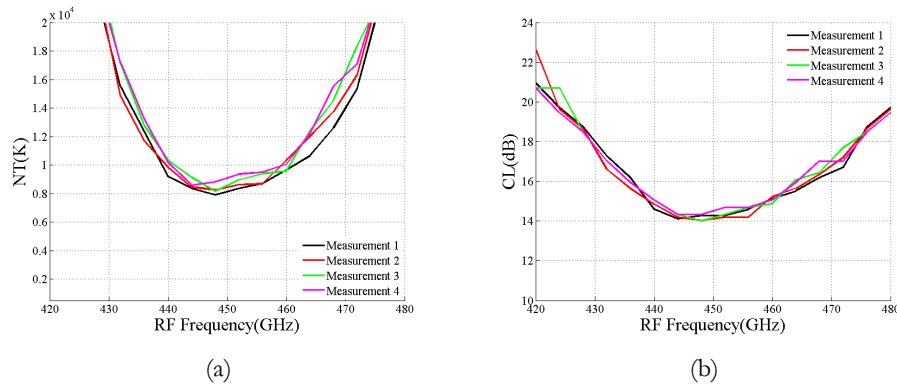
Fig. 5-40 Noise temperature and conversion loss of mixer 3.

All measurements were taken under the same conditions and employing the same set-up and IF chain but were taken in different days. It can be concluded that the 4th-harmonic mixer measurements are stable and repeatable. The NT and CL minimum values obtained for these measurements are presented in Table 5-6.

Measurement	Noise Temperature (K)	Conversion loss (dB)
1	7914 @ 448 GHz	14.11 @ 444 GHz
2	8260 @ 448 GHz	14 @ 448 GHz
3	8154 @ 448 GHz	14 @ 448 GHz
4	8587@ 444 GHz	14.3 @ 444 GHz

Table 5-6 Minimum measured NT and CL of mixer 3.

Note that almost all minimum values are taken at 448 GHz. Moreover, the differences appreciated in the conversion loss are negligible and a variation of 600 K (less than 8%) is obtained for the noise temperature.

Taking into account the differences between the measurements and simulation, see Fig. 5-41, it is believed that the ADS software is not taking into account correctly the influence of the second harmonic frequency (220 GHz) also generated by the diodes in the 4th-harmonic mixer topology.

(a)   (b)
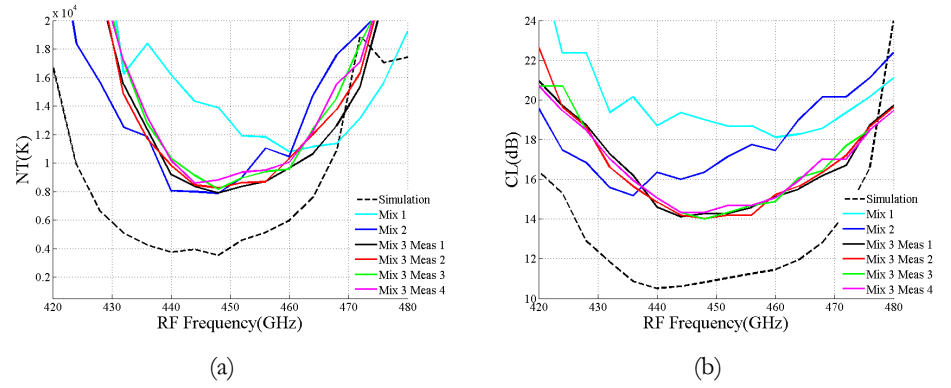
Fig. 5-41 NT and CL comparison between all the fabricated 4th-harmonic mixers and simulation.

Nevertheless, although more research needs to be done in the software definition, good measurements have been obtained and a state-of-the-art has been stablished with this design, since there is no bibliography in which 4th-harmonic mixers at 220 GHz are developed and measured.

Once the stability of the 4th-harmonic mixer design was validated, a measurement of Mixer 3 for different frequencies and LO powers was done, see Fig. 5-42.

(a)   (b)
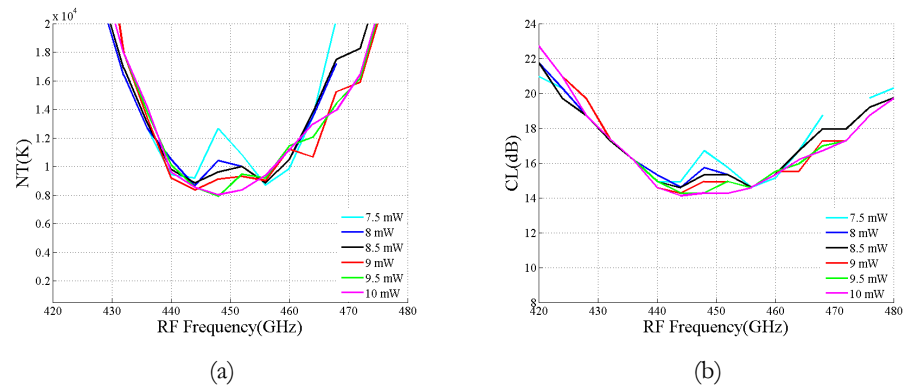
Fig. 5-42 NT and CL of the mixer for different LO powers.

Note that the mixer performance presents slight differences when the input LO power varies, giving acceptable performances from 7.5 mW to 10 mW.

5.7   Conclusions

This chapter has performed the design, fabrication and characterisation of a sub-harmonic mixer working at an RF frequency of 440 GHz as well as a 4th-harmonic mixer working at the same RF frequency. Moreover, the development of a doubler at 220 GHz has been done in order to obtain the required input frequency and power for the sub-harmonic mixer.

<div align="right">

CHAPTER 6

</div>

IMAGING RESULTS AT 220 GHz

6.1 Introduction

Along this dissertation the interest related to the design of imaging cameras at the millimetre and sub-millimetre wave range has been shown. Chapter 3 presented the development of a sub-harmonic mixer at 220 GHz and Chapter 4 a complete array of eight elements. For this reason, the main goal of this chapter is to present the performance of both devices working as a mm-wave imaging receiver. First of all, the performance of the sub-harmonic mixer has been characterized at the Antenna Group laboratory working as a single pixel. Afterwards, the array receiver has been tested using the Alfa Imaging cuasi-optical system in a not-controlled environment.

6.2 Imaging Sub-harmonic Mixer 220 GHz

The objective that is pursuing with these measurements is to check the correctly performance of the sub-harmonic mixer presented in Chapter 3 working as an imaging receiver for security and defense applications. In order to check this statement different images have been obtained. When taking about security and defense applications the main goal is to detect guns or hazardous objects. For this reason, having the ability to detect metals or ceramic materials is decisive in these kinds of applications.

The set-up employed to carry out the measurements is presented in Fig. 6-1. This set-up consists on a feedhorn attached to the sub-harmonic

mixer RF port and two lenses placed in front of them to improve the imaging resolution. At the output of the IF port two amplifiers (GAMP0100.0600SM10) with 35dB gain are placed before the IF detector (ACSP-2656NZC3).
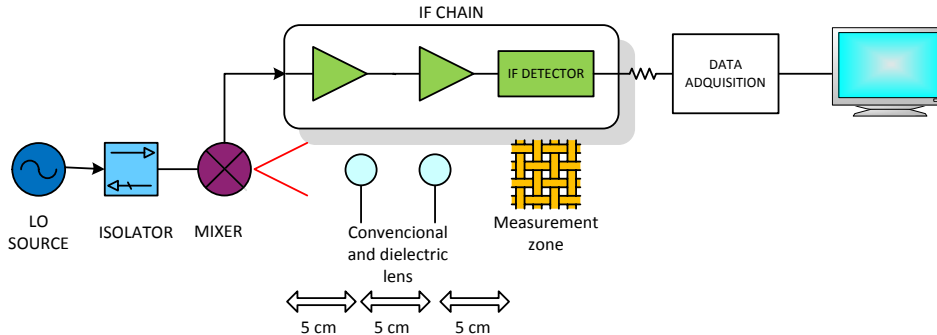
Fig. 6-1 Imaging set-up at 220 GHz.

The measurement zone is located in a XY-positioning system which is able to move in both axes. A zone of 150x150 mm is swept taking 100 points in each direction. The integration time is set to 100 milliseconds so that, T=0.16 K has been achieved. An image of 100x100 pixels is obtained.

The results are recorded by a computer using Labview homemade software and presented without any post-processing in Fig. 6-2 for the case of a LO frequency of 118 GHz and compared with its corresponding image at the visible range. In this image it is possible to identify clearly a hand and a silver ring in one of her fingers. Note that when taking the image, the hand was introduced inside a plastic glove, Fig. 6-2 a). A really good resolution has been obtained since the edge of both, the hand and the ring, are perfectly distinguished. Moreover, the passive sub-mm wave receiver is able to see through the plastic glove.

(a)   (b)

(c)
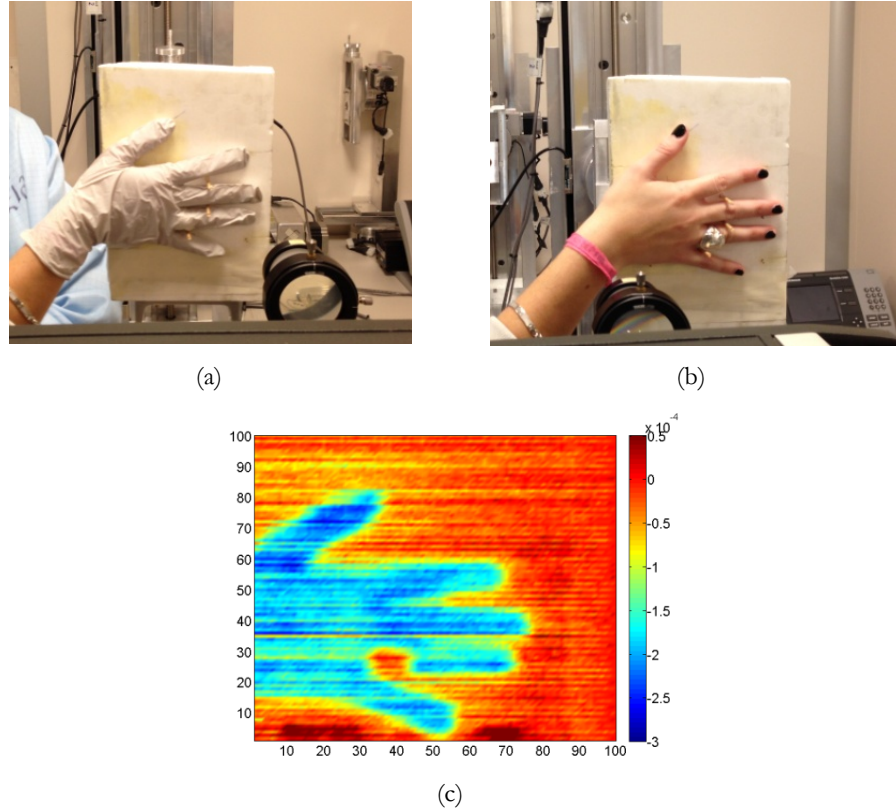
Fig. 6-2 a) Image measured at the visible range, b) Image without the plastic glove at the visible range, c) millimetre image at 220 GHz.

Some other examples of the possibilities of the imaging system are presented below. All these images have been taken under the same conditions of the mixer performance, i.e. LO power 2.5 mW and LO frequency 118 GHz. Fig. 6-3 clearly shows a hand and a metallic sheet situated on it. It is possible to identify the metallic sheet and its contour. This is of real importance since it can be conclude that the sub-harmonic mixer working as a single pixel is able to perfectly detect metals.

(a) (b)
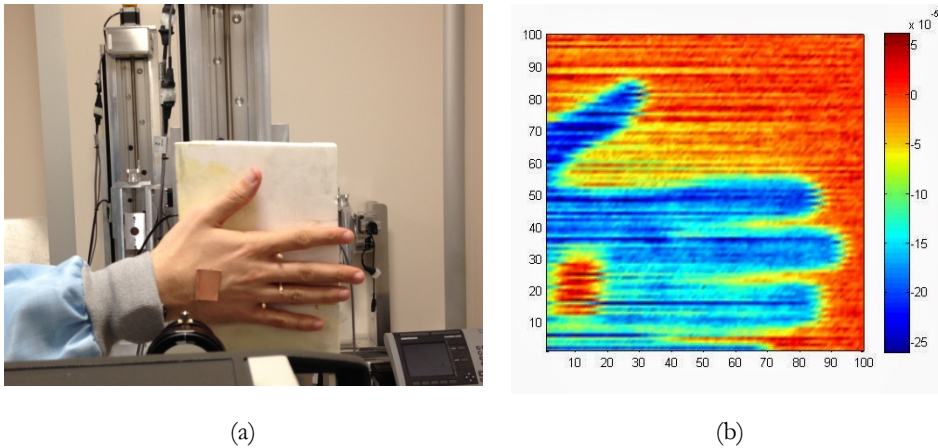
Fig. 6-3 a) Image measured at the visible range, b) millimetre image at 220 GHz.

In the case of Fig. 6-4 a ceramic knife was measured. Here it is possible to distinguish the knife shape and although the power differences between the reflected power of the scene and the knife are low, it is feasible to detect it.

(a) (b)
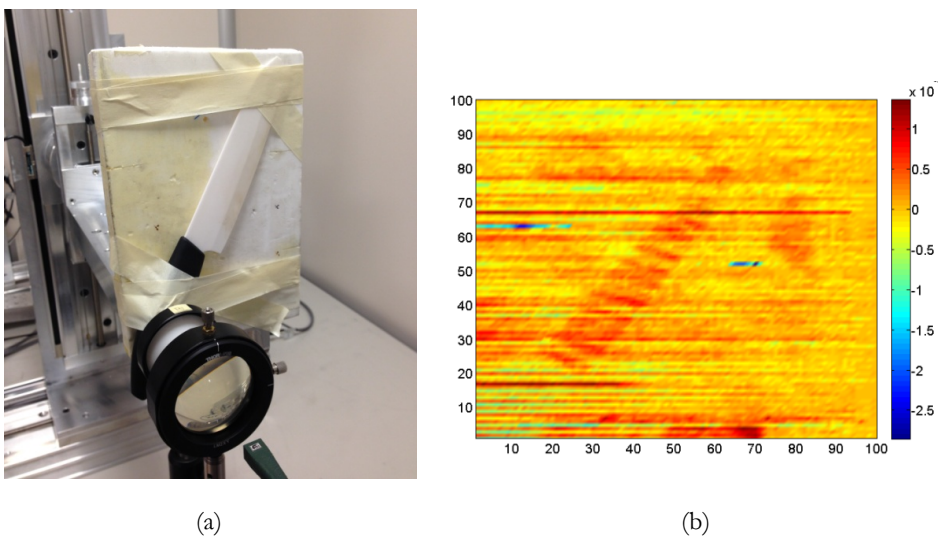
Fig. 6-4 a) Image measured at the visible range, b) millimetre image at 220 GHz.

Two other images have been obtained using a metallic adhesive tape to draw the shape of a gun, Fig. 6-5, and a fish, Fig. 6-6. Both images perfectly show the contour and are clearly identified.

(a)   (b)
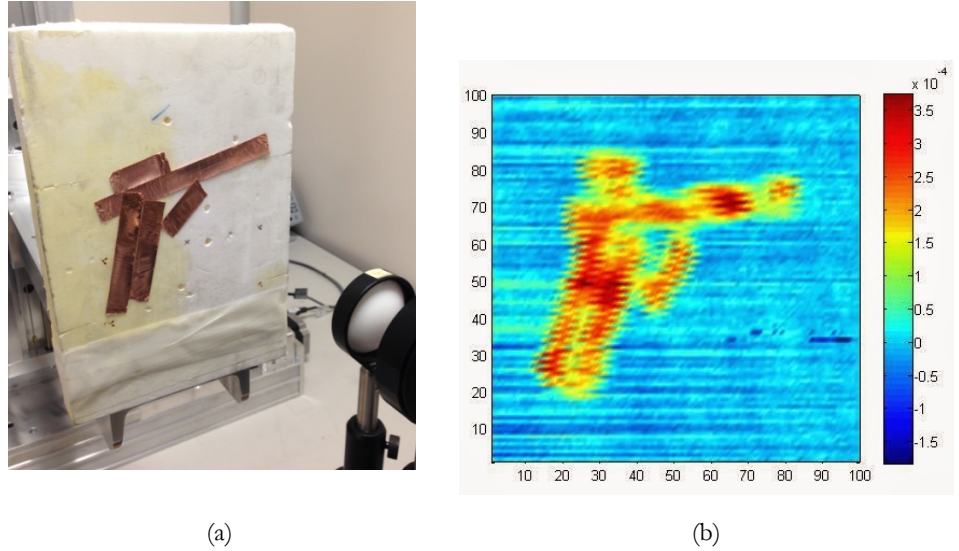
Fig. 6-5 a) Image measured at the visible range, b) millimetre image at 220 GHz.

(a)   (b)
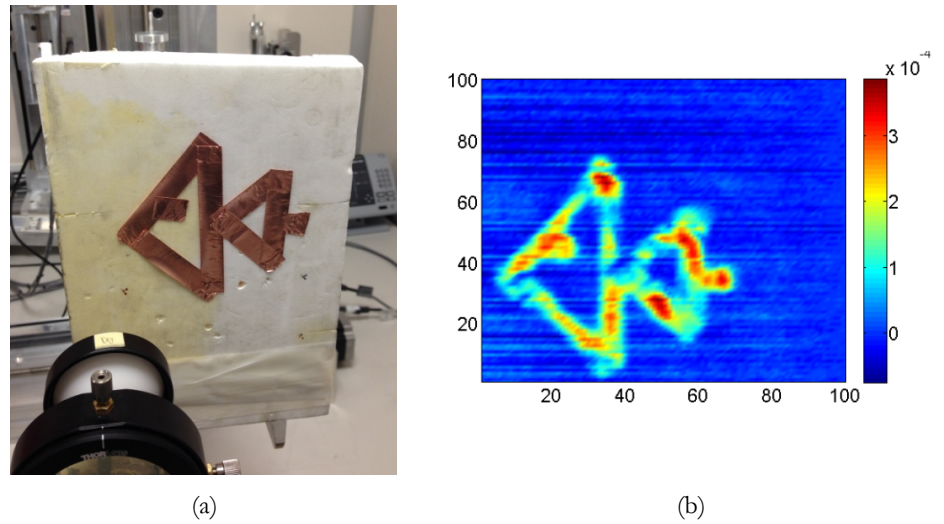
Fig. 6-6 a) Image measured at the visible range, b) millimetre image at 220 GHz.

After analyzing the whole bunch of images taken at 220 GHz it has been proven that the sub-harmonic mixer developed in Chapter 3 is able to work as an imaging camera. It is able to perfectly detect metals and ceramic materials opening the possibility to use it in security and defense applications such as detection guns and hazardous objects.

6.3   Imaging Mixer Array 220 GHz

Chapter 4 presented a mixer array composed of 8 sub-harmonic mixers working at an RF frequency of 220 GHz. Here the imaging results will be shown.

The quasi-optical system also presented in Chapter 4 will be employed in order to take some images at 220 GHz. Note that, as commented before, this system is optimized for an RF frequency of 94 GHz, which makes the system not to work in its best when the frequency changes. The images were taken at the Alfa Imaging facilities in Madrid.

Alfa Imaging counts with an imaging camera made up by two mirrors located in a Cassegrain configuration, see Fig. 6-7. Note that the complete system was analysed carefully in Chapter 4.
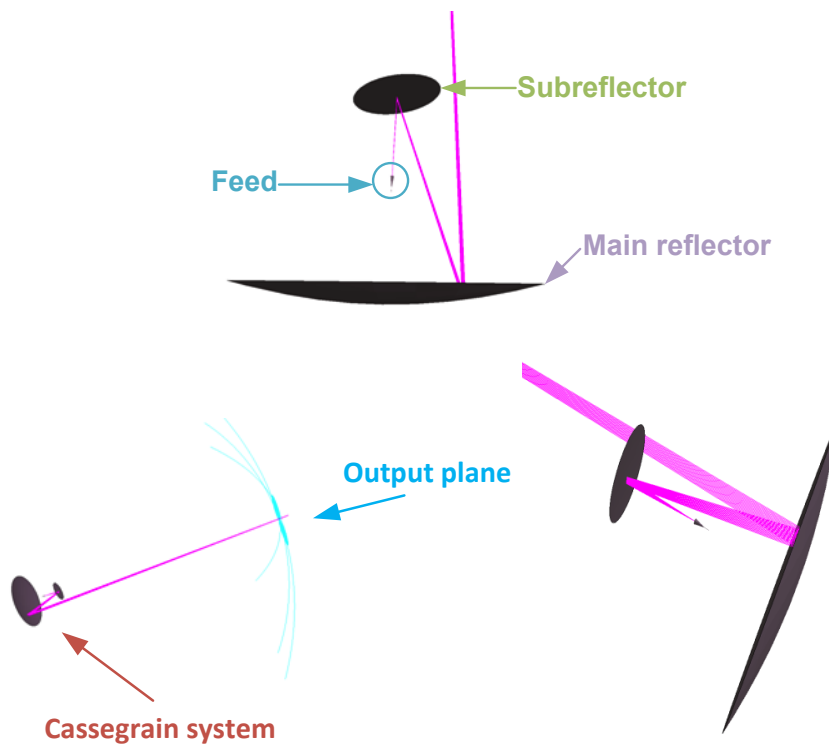
Fig. 6-7 Alfa Imaging quasi-optical system

The data employed for the images acquisition is presented in Table 6-1.

Frame Rate	10 fps
Resolution at 4 m	2.5 cm
Field of view	1.2 x 0.5 m
Number of pixels	16 x 16

Table 6-1 Alfa Imaging system acquisition data.

First of all the complete system array was assembled as well as the acquisition data card. The acquisition data card was developed by Alfa Imaging and no information is available. Moreover the imaging data was taken by a single detector instead of the completed array (8 detectors). The reason why only a single device was employed was due to some imbalance with the acquisition data and the mirrors programing.

In order to feed the complete array an Elva Q-A.M source at a single frequency, 110 GHz, has been used, Fig. 6-8 . The output power required to feed the diodes has been adjust and a power splitter has been used to divide the input power into eight output channels in order to feed the eight mixers that form the array. The input power to each mixer was set to 2.2 mW. Note that the main limitations of these measurements are the LO frequency and the LO input power. The LO frequency is set to 110 GHz and it does not correspond to the best frequency point in terms of less noise temperature and conversion loss, see Chapter 4. In addition, the input power is the same value in all mixers and although the array elements have similar behaviour, see Chapter 4, some discrepancies in the performance can be seen.
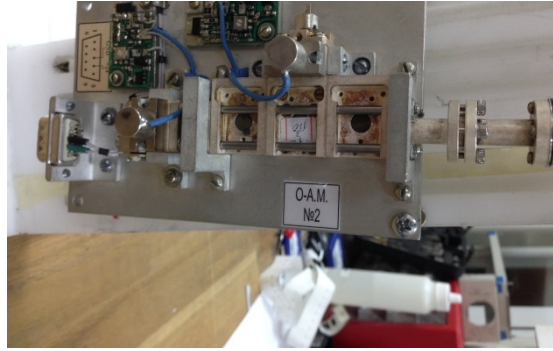
Fig. 6-8 Local oscillator source.

Fig. 6-9 shows some images of the final block assembled with four RF antennas and the power splitter analysed in Chapter 4.
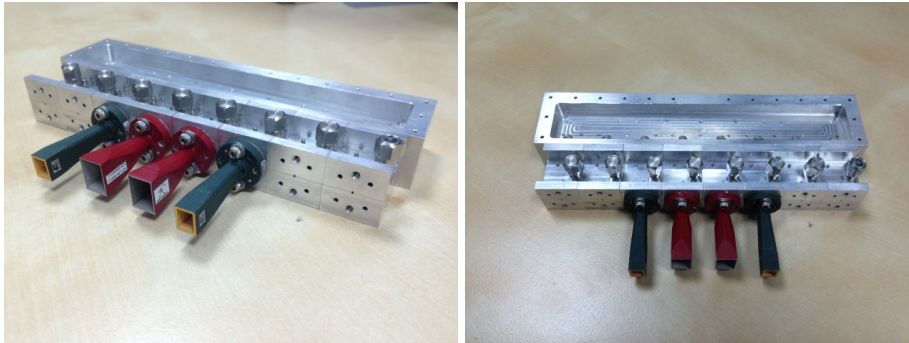

Fig. 6-9 Mixer array and splitter assembly.

Note that the complete array is perfectly aligned with the splitter. It is important since a misalignment can lead to a loss of LO power and deteriorate the array performance. Fig. 6-9 also shows two different pairs of antennas. Both of them are standard gain horns but the red ones are WR-4 (170-220 GHz) with 26 dB gain, and the green ones have less gain, 24 dB, and are WR-3 (220-325 GHz). These antennas were used since they were part of the Antenna Group material. Although the cuasi-optical system was analyzed in Chapter 4 and the best behavior was obtained for antennas of 24 dB, they were fabricated after these measurements were performed.
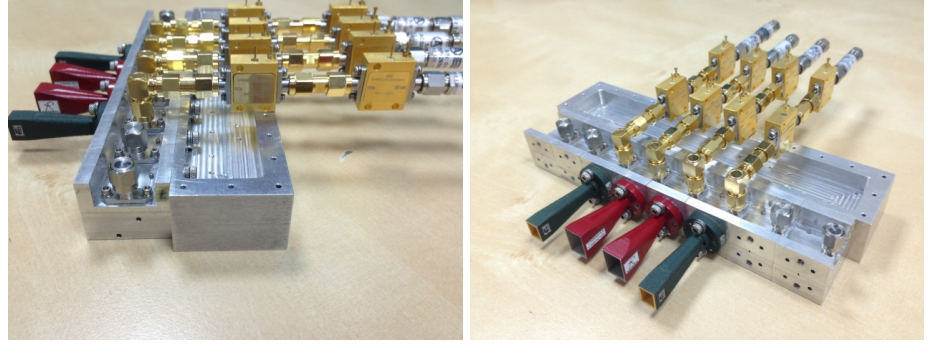
Fig. 6-10 Mixer array with the IF chain assembled.

Moreover, four of the IF chain are also assembled in Fig. 6-10. They consist on 2 amplifiers, GAMP0100.0600SM10, with 35 dB gain, and an IF detector, ACSP-2656NZC3, same IF chain used in Section 6.2. Following the detector a 3 dB attenuator has been used in order to adequate the output signal to an optimal working zone of the detector, see the detector Voltage-Power curve Fig. 6-11.
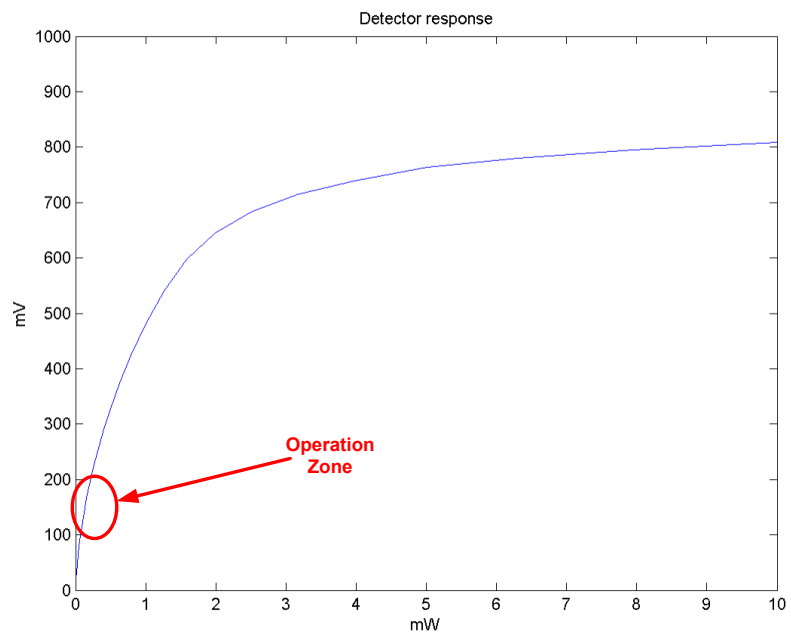
Fig. 6-11 Detector response.

The output voltage measured for the four mixer elements were between 105 mV and 135 mV which corresponds to the zone in which the angle of slope of the detector response is steeper, see Fig. 6-11.

The quasi-optical system requires the mixer array to be located at the optical axis therefore, a support has been used to elevate and adjust the position of receiver. This support was made of Teflon and it was also secured to the camera. Some images of the array and the support are shown in Fig. 6-12.

Fig. 6-12 Array and base used for the imaging set-up.

Whenever the receiver is situated on the support and perfectly adjusted, the complete device is located within the quasi-optical system. Some photos of the final configuration are presented in Fig. 6-13. Note that

the Teflon support is fixed to an XY-positioning system which will move in the horizontal axis in order to take an image.

Fig. 6-13 Complete receiver inside the quasi-optical system.

The acquisition card developed by Alfa Imaging is also assembled in the system.

Some previous tests have been done with Mixer 2. Note that this mixer is neither at the optical axis nor at a central position which will be lead to a loss of information and the image will be unfocused. However, the system is not taking images as an array but as a single element configuration. Moreover, the support and therefore the mixer will be sweeping a horizontal zone in order to take an image. For this reason, Mixer 2 has been the selected one in order to take the image, since it will be able to sweep a larger zone due to its location inside the camera.

Some of the first captured images are presented in Fig. 6-14, Fig. 6-15 and Fig. 6-16.
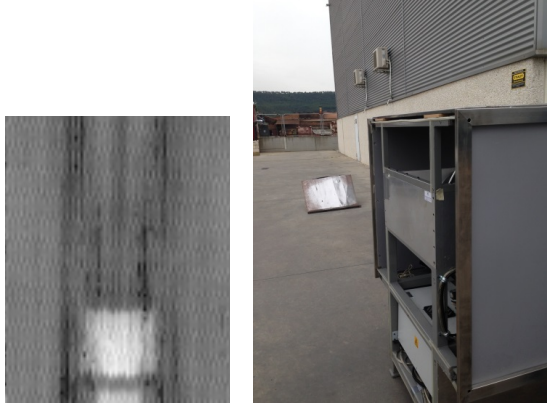
Fig. 6-14 Image of a metallic sheet at 5 metres distance.

Floor reflection
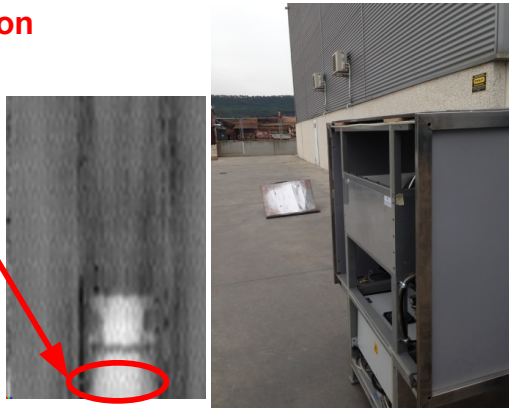
Fig. 6-15 Image of a metallic sheet at 6 metres distance.

Fig. 6-14 and Fig. 6-15 show a metallic sheet located at 5 and 6 metres distance respectively. In both cases it is perfectly identified. Note also that a great part of the image corresponds to the reflection of the floor.
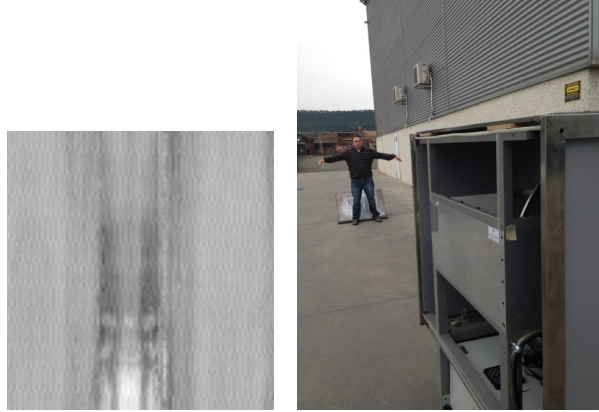
Fig. 6-16 Image of a person with a metallic sheet behind at 6 metres distance.

However, Fig. 6-16 does not have a clear image of the person who is in front of the metallic sheet. It can be known intuitively that there has been a change regarding images of Fig. 6-14 and Fig. 6-15 but nothing else.

A second group of tests have been done. In this case, four mixers have been capturing images at the same time. The assembly of the complete system has been improved trying to have everything assembled more carefully and fastened stronger in order to avoid any uncertainty. In addition, the location of the receiver inside the camera has also been adjusted and the antennas of the array are located at the focal line. Some photos of the set-up process are depicted in Fig. 6-17.
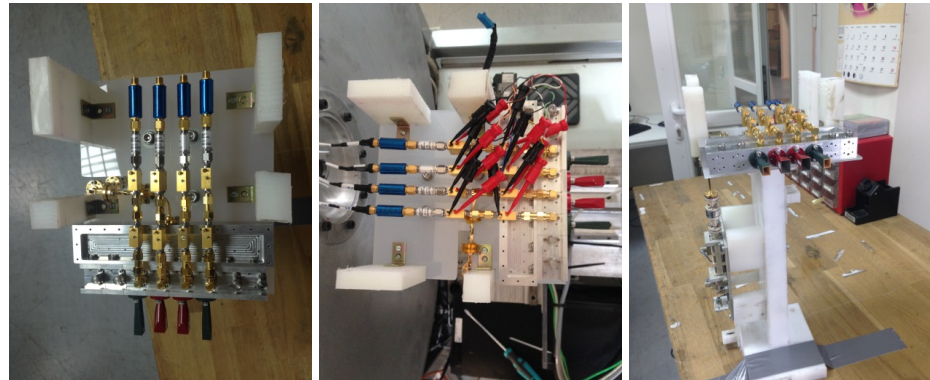
Fig. 6-17 Photos of the mixer array set-up.

The left image of Fig. 6-17 shows a top view of the splitter, mixer array, RF antennas and the complete IF chain (amplifiers, detector and 3 dB attenuator) place on the Teflon stand employed to fix the receiver inside the imaging camera. In the central image the amplifier´s feeding cables have been added. A complete view of the Teflon stand and the array are depicted in the right image. Note that the LO source also appears at the photo.
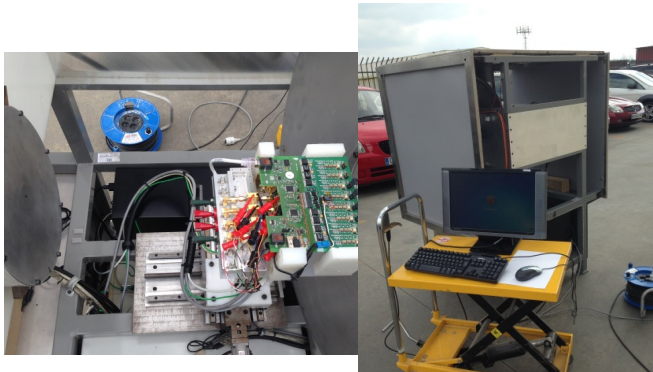

Fig. 6-18 Photos of the complete imaging camera.

Fig. 6-18 presents the inside part of the imaging camera (left side) and the complete camera and the computer employed to run the imaging acquisition software.

During this second group of tests four of the eight mixers are operating. Note that these mixers are working as single receivers and not as an array. The operational mixes, situated from the right to the left, are: Mixer 2, Mixer 6, Mixer 8 and Mixer 1. See Chapter 4 to have a view of their performance in terms of noise temperature and conversion loss.

The output signal of these mixers after the IF chain was measured and the obtained values are presented in Table 6-2.

Mixer Element	IF Output (mV)
Mixer 2	-110
Mixer 6	-130
Mixer 8	-123

Mixer 1	-124

Table 6-2 Output voltage of the mixers.

The output voltage of the mixers is similar in the four cases as well as the mixer performance, see Chapter 4. For this reason a similar behavior is expected. However, it is important to take into account that the mixers are located at different positions regarding the imaging system, and therefore, the field of view of each mixer will be slightly different. Moreover, the array is moving horizontally thanks to the XY-positioning system, and the same image will be taken 4 times (one time for each horizontal sweeping).

Some of the obtained results are presented below. Note that the measurements have been done outside in order to take advantage of the sun light illumination.
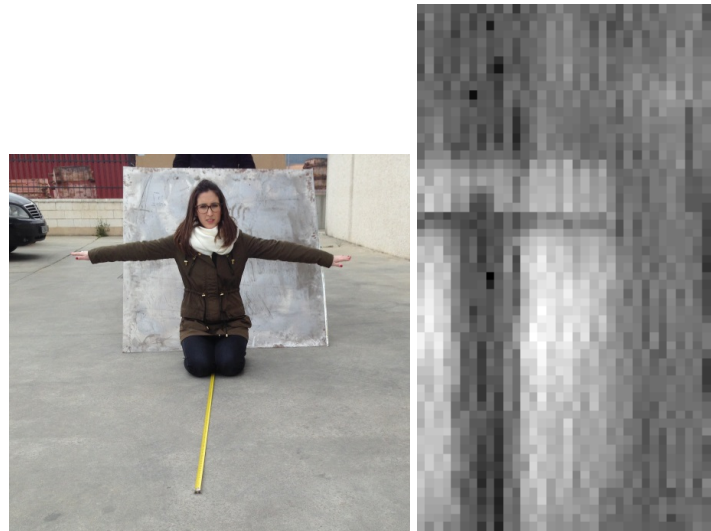
Fig. 6-19 A person on her knees at a distance of 4 metres.

The silhouette of the person is shown perfectly in Fig. 6-19. The arms, head and trunk are perfectly distinguished. However, a lengthening of the image is observed. It is due to the reflection provoked by the floor since the measurements are taken outside. This reflection will be appreciated in all the images.
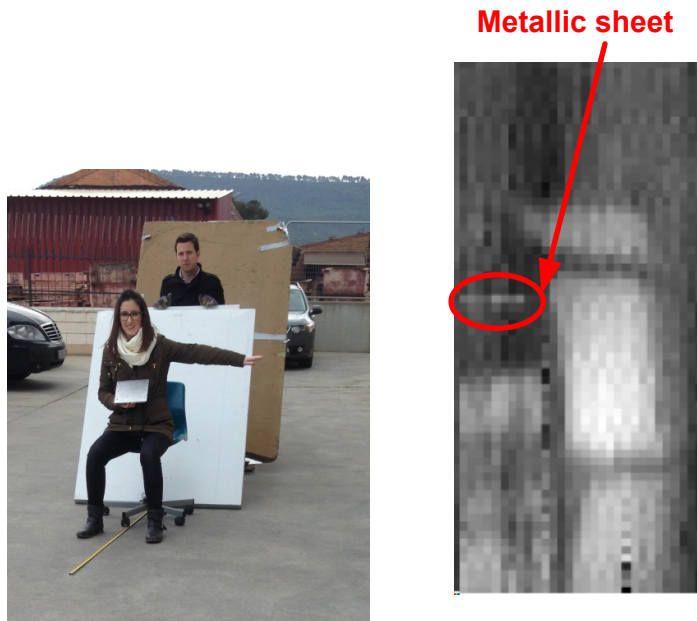
Metallic sheet

Fig. 6-20 A person holding a metallic sheet at a distance of 4 metres.

Fig. 6-20 depicts a person holding a metallic sheet. Note that this sheet is identified in the image taken at 220 GHz. This is an important achievement since it demonstrates that the system is able to distinguish between different materials such as clothes and metals which can be of relevant interest for defence applications.
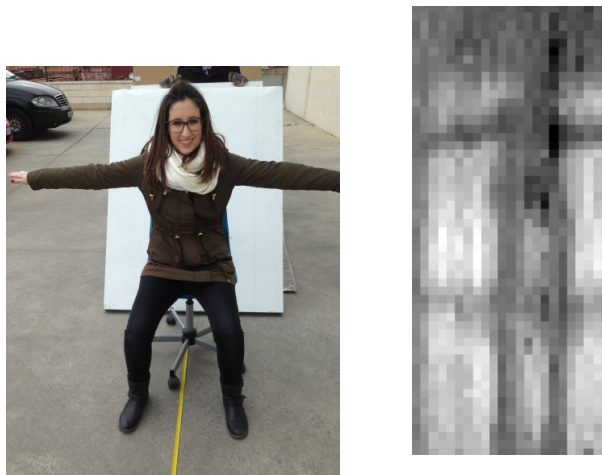

Fig. 6-21 A person seated on a chair at a distance of 4 metres.

Again, a person seated on a chair is captured in Fig. 6-21. The metallic sheet behind the person is detected as well as the silhouette of the person. This metallic sheet is used in order to increase the contrast between the person and the scene in view of the fact that a passive system has been designed.
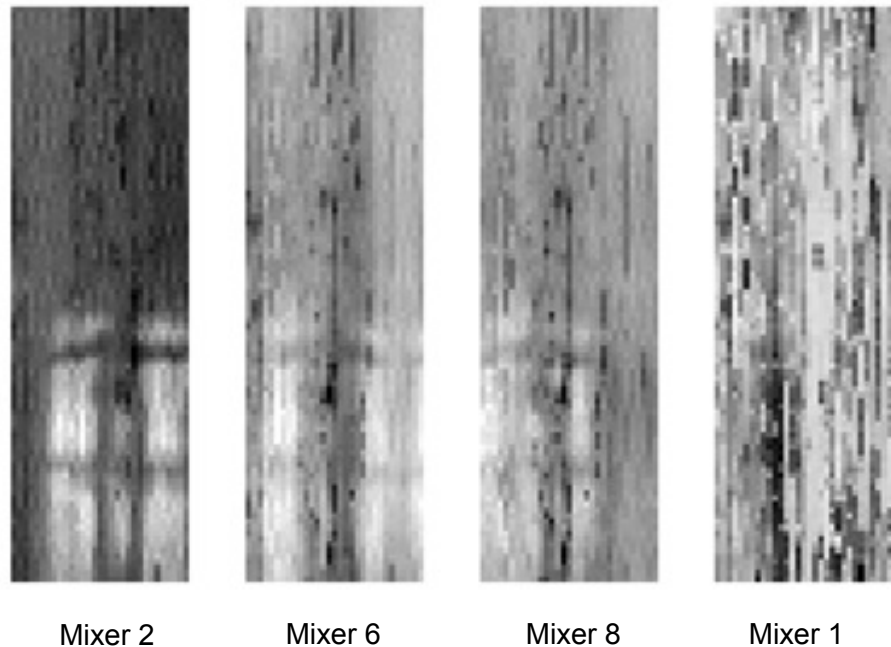

| Mixer 2 | Mixer 6 | Mixer 8 | Mixer 1 |

Fig. 6-22 A person seated on a chair at a distance of 4 metres taken by the four operational mixers.

An image of a person seated on a chair at 4 m distance has been taken with the four operational mixers (mixer 2, mixer 6, mixer 8 and mixer 1 of Chapter 4), Fig. 6-22. Note that the mixers are working as single receivers which are sweeping the horizontal axis therefore, the images taken by them are different from each other depending on the position with respect to the centre of the mirror configuration. For example it is possible to appreciate how Mixer 2 is able to scan entirely the person while the rest of the mixers only see part of her.

6.4   Conclusions

The performance of the mixer built in COC as a receiver of a passive imaging camera has been measured for two different scenarios. The first one employing a single detector and two lenses, the second one as an imaging array located inside a quasi-optical system. Both cases offer the possibility of taking images at the millimetre wave range and are capable of detecting metallic objects.

In the case of the mixer laboratory measurements working as a single pixel, images of 15x15 cm have been taken and metallic objects smaller than 2 cm have been detected. Moreover, the images have great quality and different contours and shapes are perfectly distinguished. In addition, the option of distinguishing ceramic materials has been tried giving good results.

On the other hand, the images captured outdoor by Alfa´s imaging system shows its ability to scan a person completely. Images of 1.2 x 0.5 m have been obtained with a resolution of 2.5 cm. Moreover, the feasibility of detecting hidden metallic objects has been proved. Post-processing techniques can be applied in order to improve their quality, i.e. avoid the floor reflection, improve the contrast, etc. However, it stays out of the scope of this dissertation and is expected to be done by Alfa Imaging.

Finally, it is important to highlight the fact that the system was operating a single receiver and not as an array. Nevertheless, it is expected to work properly in an array configuration regarding the behaviour presented in Chapter 4 and this one.

CHAPTER 7

CONCLUSIONS AND GUIDELINES FOR FUTURE RESEARCH

In this chapter the main results obtained in this thesis will be summarized. Then, some guidelines for future research will be provided.

7.1 Conclusions

The promising THz applications developed on the last few years have made of this field an attractive and with future potential sector. For this reason, the Spanish Government, as well as many others, has launched meaningful research programmes focused on the development of technology at these frequencies. Consequently, this thesis is framed within 4 research projects given to the Antenna Group focused on the development of millimetre and sub-millimetre wave components. Moreover, the Antenna Group has also been able to set a THz lab with the required equipment to fabricate and measure these components becoming a reference research Group in Spain.

In this thesis the design, fabrication and measurement of several mm and sub-mm wave components, and particularly Schottky diode mixers, have been done. Schottky diode mixers are still used as the first element of receiver front-ends to down-convert the signal collected by the antenna to microwave frequencies where it can be amplified, demodulated and analysed in an easy way. Schottky diode mixers have the advantage over other sensor technologies to work at room temperature as well as cryogenic temperatures

for improved noise performance, which make them the technology of choice for many different applications; such as THz imaging cameras, biochemical material identification, medical imaging, wideband wireless communication systems, etc. Planar Schottky technology made great progress in late 1990s, and nowadays it is a well-known technology. Nevertheless, some improvements and new developments have been proposed within this thesis.

In Chapter 2, two important analyses were reported, a comparison between three different measurement procedures as well as three detection methods, and the study of the impact of use of an isolator between the mixer and the IF chain in the mixer performance. Talking about the calculation method, the Gain method resulted to be the most reliable one. Independently of the detection method used, the gain method always had more constant values and comparing them to other methods employed, they were closer to the average between all of them. Moreover, there can´t be said that a performance detection method is the best but when using the Spectrum Analyser more information is obtained. This detection method provides the highest resolution at the IF frequency range, so gives a better idea of the performance of the mixer along different frequencies. According to the isolator study, Chapter 2 proved that the increased on the noise temperature of the mixer due to the inclusion of an isolator can be explained by the mismatch existing between devices presented in the receiver. Otherwise, although the inclusion of an isolator has been proven that increments the NT of the mixer, it has been also checked that results obtained using it had similar values independently the calculation procedure used, the gain, attenuator or noise injection method. This suggested that the pre-amplifier possess a better matching with the mixer but less stable with frequency, which produced a larger variation of the NT along the frequency. Another important issue is the fact that depending on the IF chain used to measure the performance of a mixer, this performance can be altered by the mismatching existed between the mixer and the IF chain, which can lead to an increase or a decrease of the mixer NT and CL. It is of

real importance to characterize this mismatching since the performance of several mixers are not comparable if they haven´t been measured under the same conditions since, as it has been proven in Chapter 2, the performance of the mixer is related to the matching between components.

Chapter 3 presented the development of a sub-harmonic mixer implemented on COC substrate which thanks to its electrical characteristics, leads to less losses and therefore, to a better performance of the mixer. This mixer had best noise temperature values below 1000 K and conversion loss of 7.2 dB. Moreover, a comparison between this mixer and the same one implemented on Rogers 5880 was done. The COC mixer performance showed in Chapter 3 represents 300K noise temperature and 0.5 dB conversion loss reduction with respect to those obtained by the same mixer built on a Rogers substrate. Therefore, the use for the first time of COC substrate at these frequencies has led to obtain better performances when designing mm and sub-mm wave devices due to its lower losses. Although the mixer presented in Chapter 3 does not improve the state-of-the-art mainly due to the use of flip-chip diodes; the use of COC material opens the possibility of improving the state-of-the-art performances of mm-wave mixers by integrating the discrete diodes on this substrate.

In Chapter 4, a complete Schottky diode mixer array was presented and its performance was measured. In addition, the mechanical design of the array was analysed and a configuration of 1x8 mixer elements array was done. The repeatability of the mixer design that makes up the array was confirmed. The mixer elements of the array have minimum noise temperature values around 1000 K most of them located at 116 GHz. Conversion loss results were between 6.8 and 7.8 dB for the eight elements. Moreover, the simulated results of this array operating over a Cassegrain system for imaging applications have been reported. The best performance obtained as a compromise between the S/N value, maximum value of the E field and shape of the beam cut at -3 dB was reached with an antenna of 24 dB gain. This is the first time an imaging operational array formed by eight Schottky diode mixers is presented.

Chapter 5 included new approaches in the development of heterodyne receivers. This chapter presented the design and for the first time fabrication and measurements of a 4th-harmonic Schottky diode mixer operating at an RF frequency of 440 GHz. Best noise temperature measurements of 7914 K and conversion loss of 14 dB were obtained. This kind of device offers an attractive solution in imaging applications when arrays of harmonic mixers need to be implemented and not enough local oscillator power is available to feed them appropriately. Moreover, a sub-harmonic mixer working at the same RF frequency was also developed and the performances of both devices were compared. Furthermore, a frequency doubler from 110 GHz to 220 GHz was designed in order to feed the subharmonic mixer operating at 440GHz.

In Chapter 6, diverse images taken by a single mixer or the complete array together with the cuasi-optical system, provided by Alfa Imaging, are shown. In this chapter, the possibility of taken images with the designed components in this thesis is proven in both cases. Firstly, a single pixel is used, i.e. the sub-harmonic mixer presented in Chapter 3, which is helped by two lenses to improve the definition over the image. Results show a high resolution of the objects and a variation of the level of the obtained power depending on its nature. Images of 15x15 cm were obtained, with an integration time of 100 milliseconds and 100x100 pixels, observing a good resolution. The user was able to distinguish between elements such as the human body, a metallic sheet or a ceramic material, giving the possibility to identify, via the shape, and detect them. Finally, some images of a whole person are taken using the array presented in Chapter 4 and Alfa Imaging mirror´s system. The images are taken outdoors and at a distance of 4 metres from the imaging system. Alfa´s system provides a field of view of 1.2x0.5 m, a resolution of 2.5 cm and a frame rate of 10 fps. The person is completely distinguished and moreover, a metallic sheet placed on the chest of the person is also detected, offering an alternative to the actual airport scanners.

7.2 Guidelines for future research

In this thesis different millimetre and sub-millimetre wave components have been designed, fabricated and measured for the first time in Spain.

Concerning Schottky diode mixers it is the first time these devices are developed by the Antenna Group. For that reason some guidelines for future research are the improvement of the design and simulation processes trying to develop more accurate results which can predict in a better way the measurements. Although the hot electron noise source added to the mixer simulation gave a better idea of the real noise temperature and a good agreement was obtained for the sub-harmonic mixer, it didn´t happen the same with the 4th-harmonic mixer. Moreover, a complete optimization of the filters impedance and structure could be done in ADS at the same time the mixer performance characterization is done maybe obtaining more competitive results.

A complete integration of a THz camera can also be entirely developed, taking into account the applications, scatter configuration (i.e. Casegrain, Gregorian, Offset, etc.) and operational frequency, obtaining better imaging results.

Related to the 4th-harmonic mixer design more research can be done in this field. It is believed that the ADS software is not taking into account the second harmonic frequency, 220 GHz, in the calculation of the mixer characteristics due to the differences appreciated between the simulation and measurements. For this reason, a new simulation model should be employed in order to estimate the noise temperature and conversion loss. Moreover, the study of a new configuration which can derive the second harmonic could be implemented in order to the decrease the mixer noise or even a 5th-harmonic configuration could be implemented.

Finally, a new doubler design could be implemented using the most commonly employed diodes, varactor diodes, which can offer a better performance in terms of efficiency and operational bandwidth.

Analysing the complete thesis, future research could be done looking for other applications rather than security. For example, an imaging camera for skin cancer detection or plants water control could be promising applications.

APPENDIX A

MISMATCHING ANALYSIS

The S parameters of the IF mixer port, and the IF chain with and without the isolator have been measured for the eight mixers that form the array presented in Chapter 4. Moreover, the noise temperature and conversion loss of each mixer has been calculated taking into account the mismatching analysis presented in Chapter 2.

A.1   Mixer 1
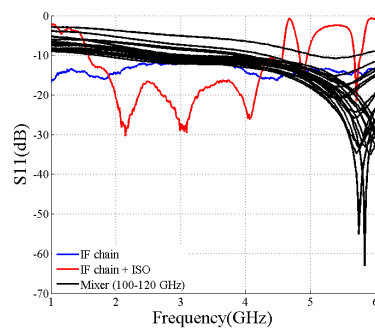
(a)
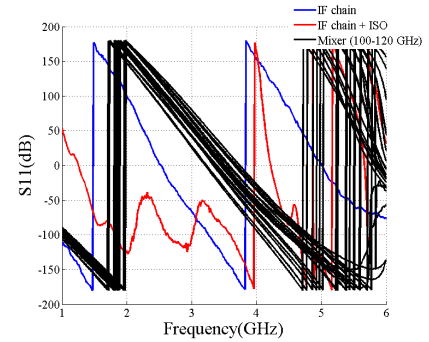
(b)
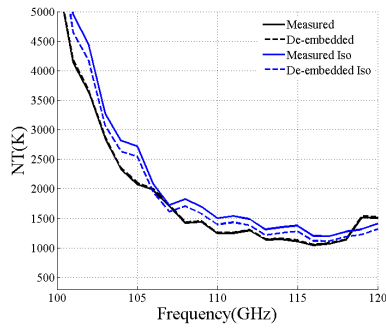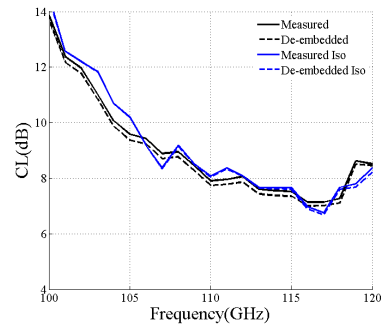
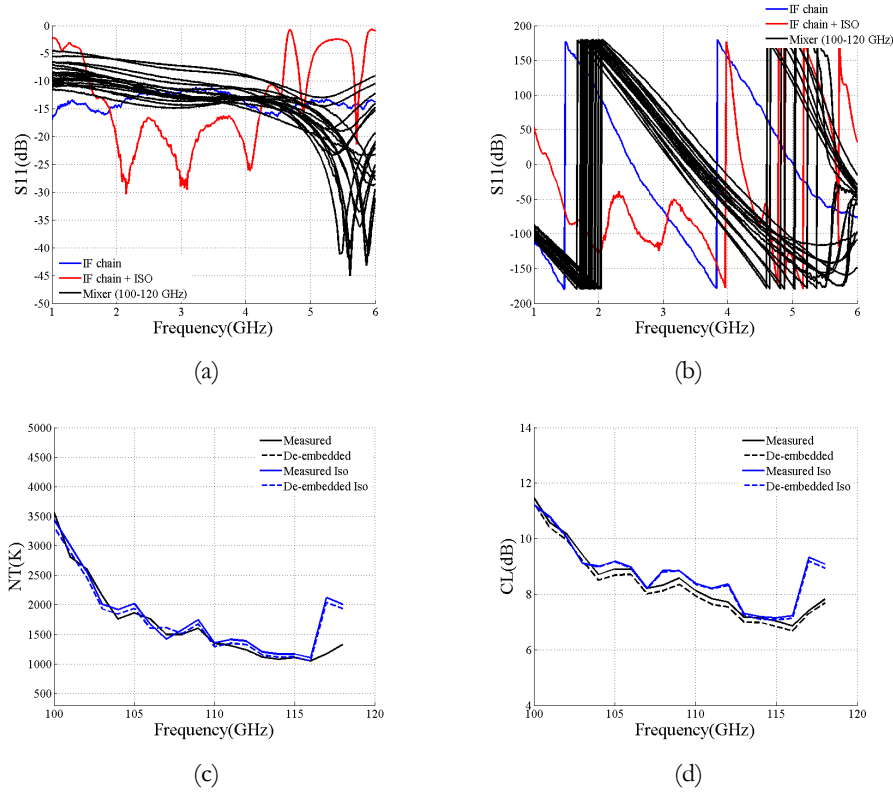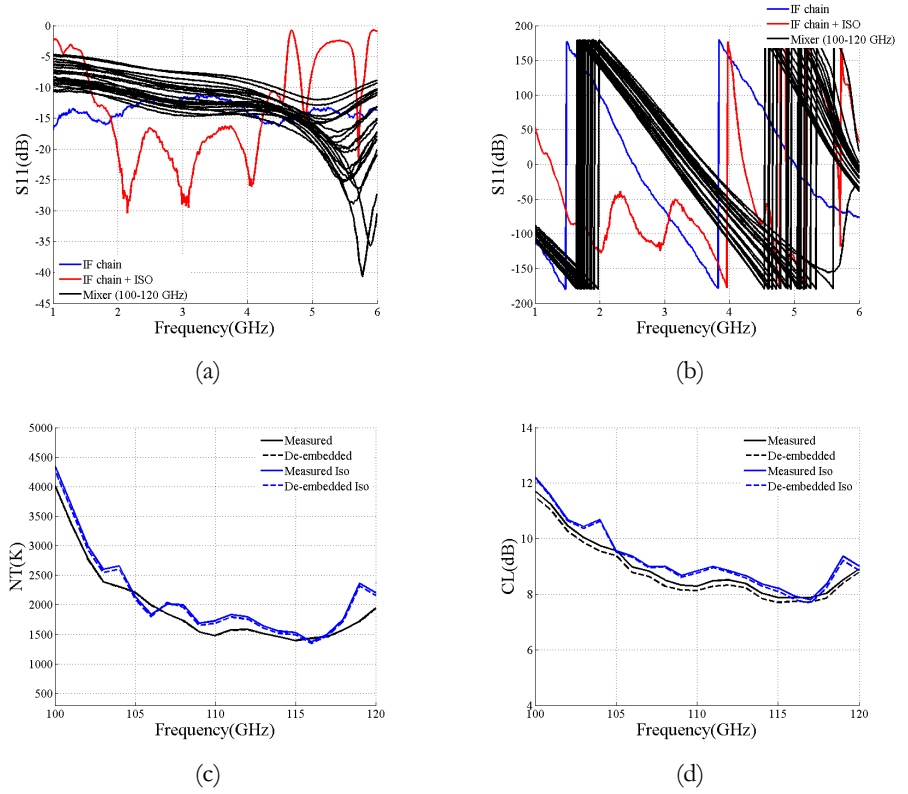(c)   (d)

Fig. A-1 (a) and (b) Measured S11 receiver components, NT (c) and CL (d) comparison between measured and de-embedded values.

A.2   Mixer 2
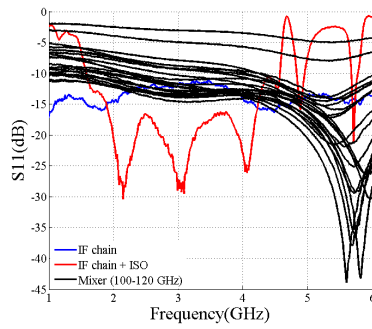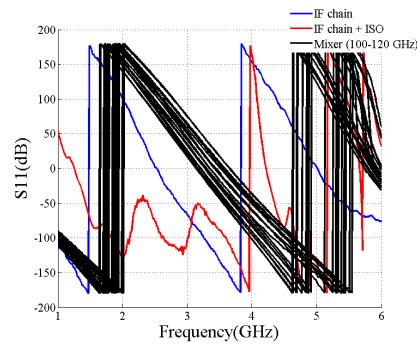
(a)   (b)
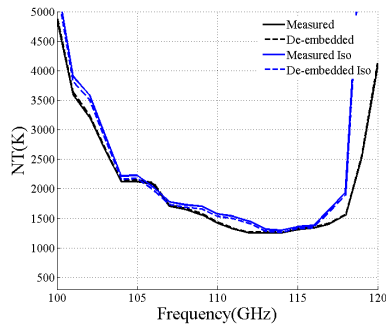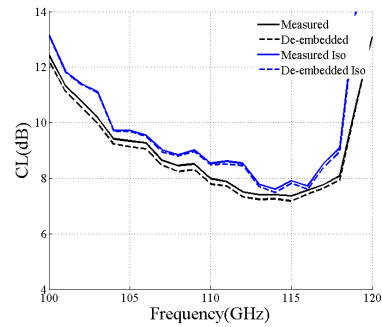
(c)   (d)

Fig. A-2 (a) and (b) Measured S11 receiver components, NT (c) and CL (d) comparison between measured and de-embedded values.

A.3 Mixer 3

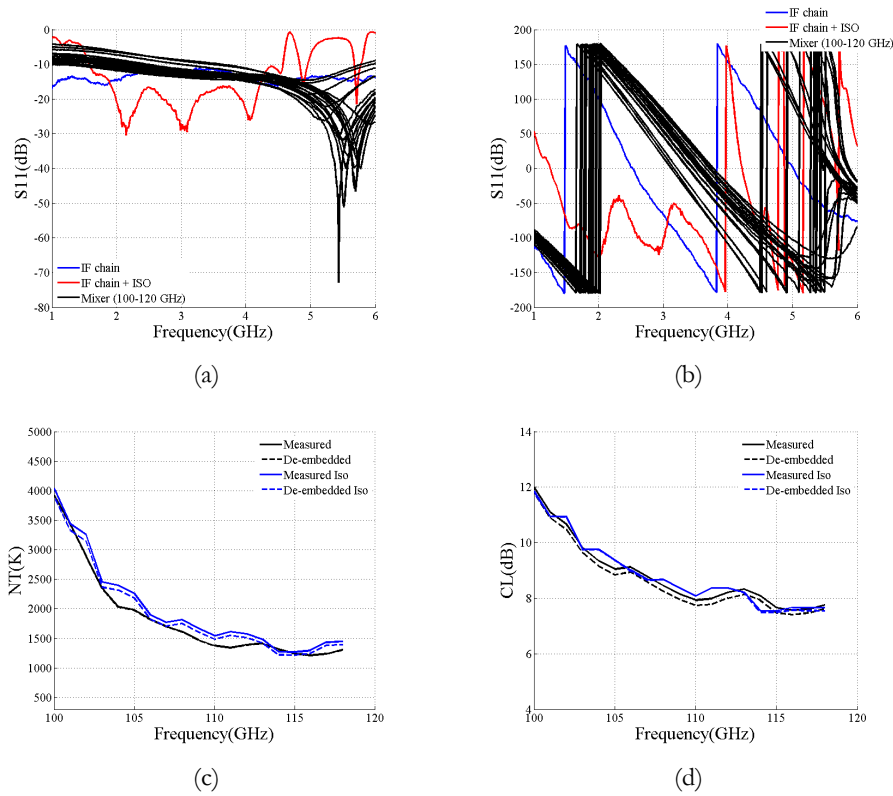(a)   (b)

(c)   (d)
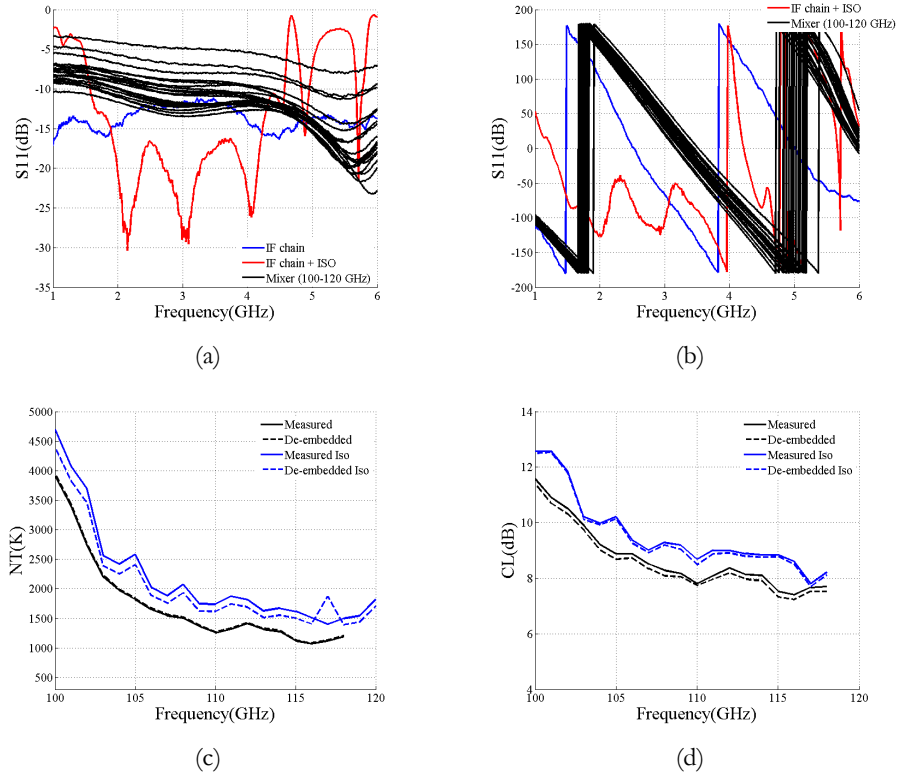
Fig. A-3 (a) and (b) Measured S11 receiver components, NT (c) and CL (d) comparison between measured and de-embedded values.

A.4   Mixer 4

(a)

(b)

(c)

(d)
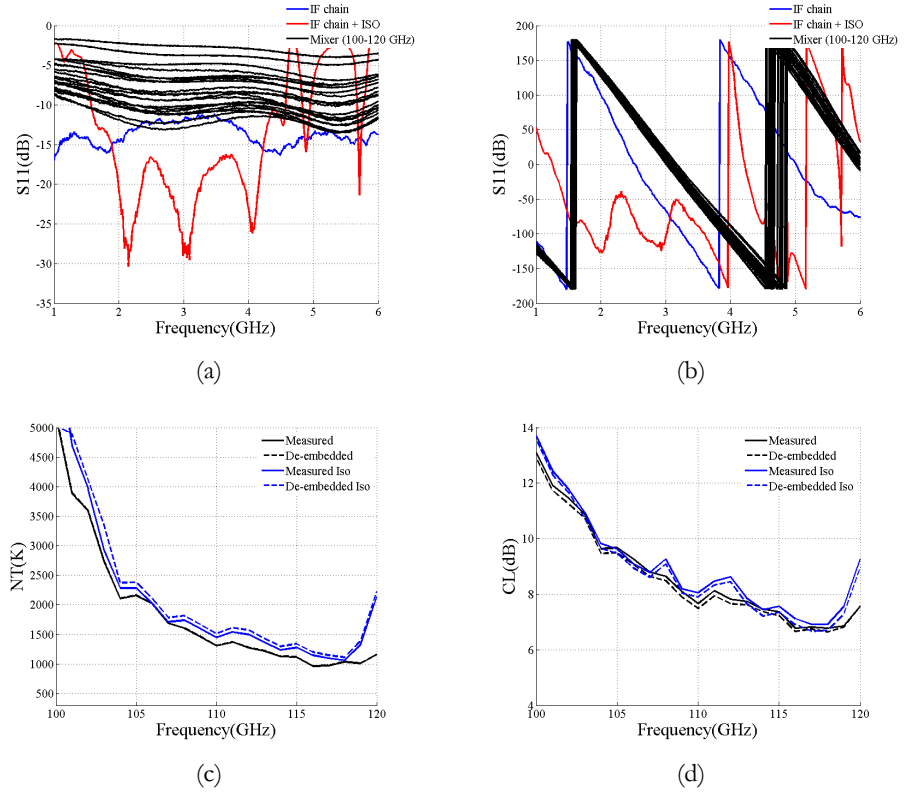
Fig. A-4 (a) and (b) Measured S11 receiver components, NT (c) and CL (d) comparison between measured and de-embedded values.

A.5   Mixer 5

(a)

(b)

(c)

(d)

Fig. A-5 (a) and (b) Measured S11 receiver components, NT (c) and CL (d) comparison between measured and de-embedded values.

A.6   Mixer 6

(a)

(b)

(c)

(d)

Fig. A-6 (a) and (b) Measured S11 receiver components, NT (c) and CL (d) comparison between measured and de-embedded values.

A.7   Mixer 7

(a)

(b)

(c)

(d)

Fig. A-7 (a) and (b) Measured S11 receiver components, NT (c) and CL (d) comparison between measured and de-embedded values.

A.8   Mixer 8

(a)
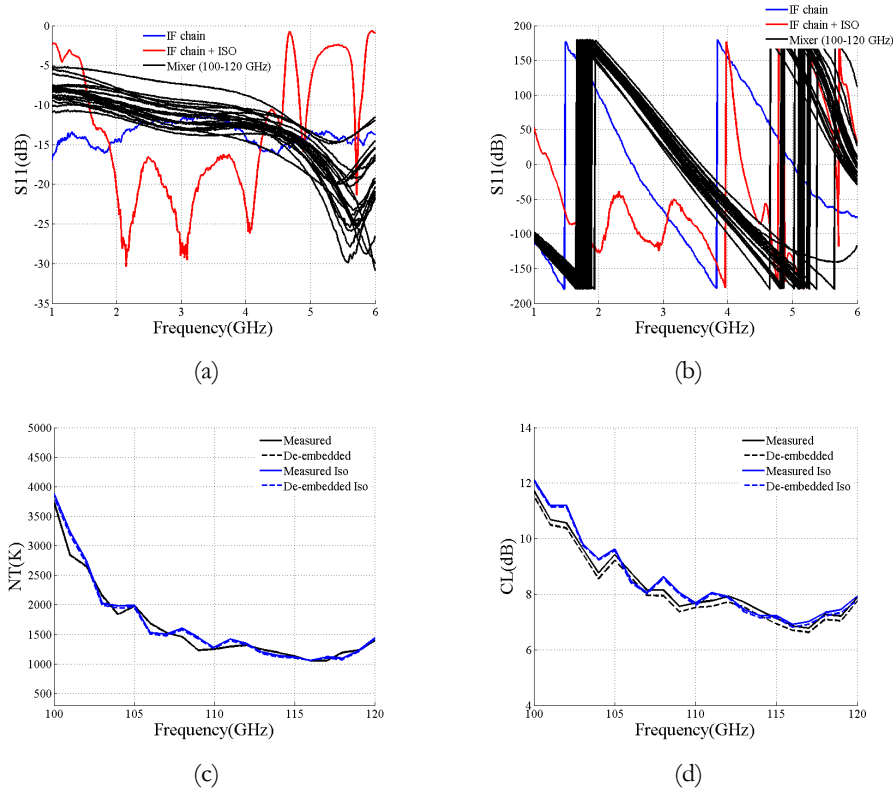

(b)

(c)

(d)

Fig. A-8 (a) and (b) Measured S11 receiver components, NT (c) and CL (d) comparison between measured and de-embedded values.

APPENDIX B

# DESIGNED DEVICES DIMENSIONS AND ADS SOFTWARE COMPONENTS

The aim of this appendix is to present the dimensions of the sub-harmonic mixer developed in Chapter 3, as well as the sub-millimetre wave devices developed in Chapter 5. Moreover, the ADS simulation blocks used for the simulation process are also depicted and explained here.

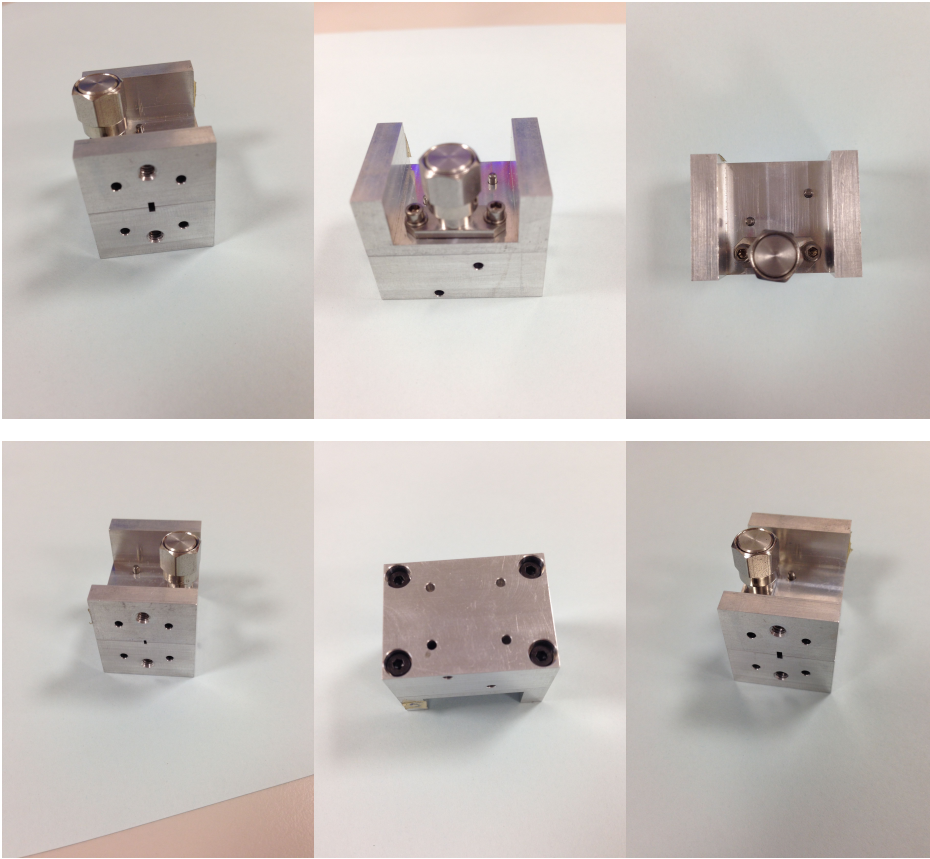## B.1 Sub-harmonic Mixer with RF frequency equal to 220 GHz

The dimensions of the sub-harmonic mixer circuit developed in Chapter 3 are depicted here:
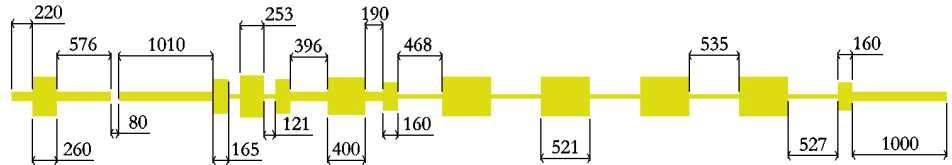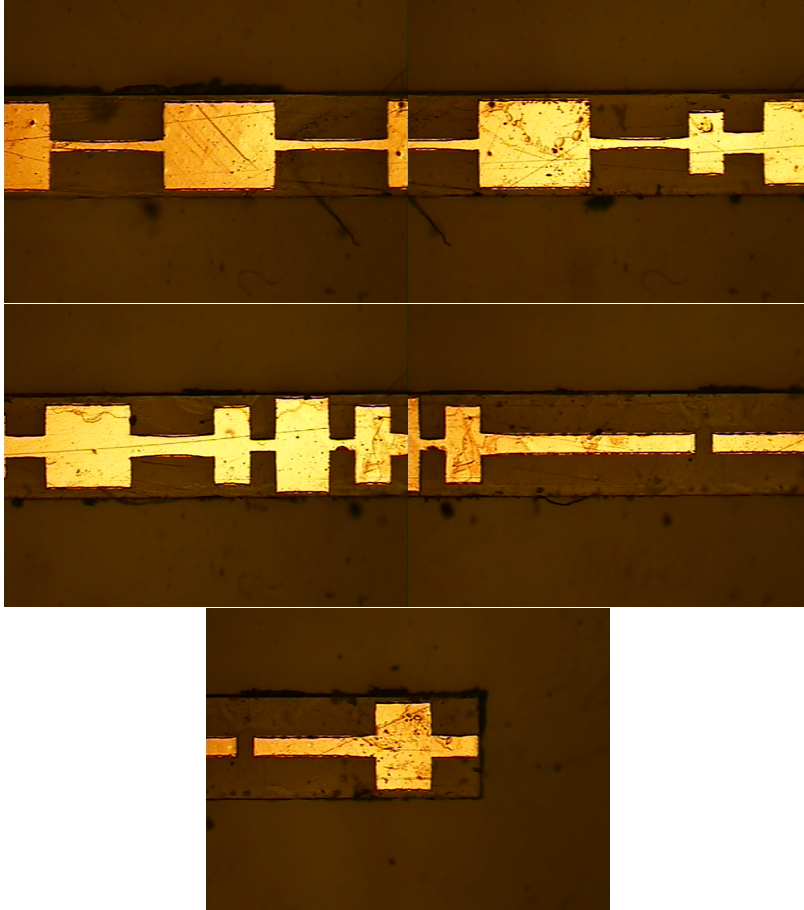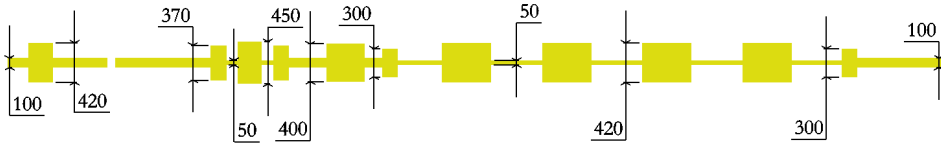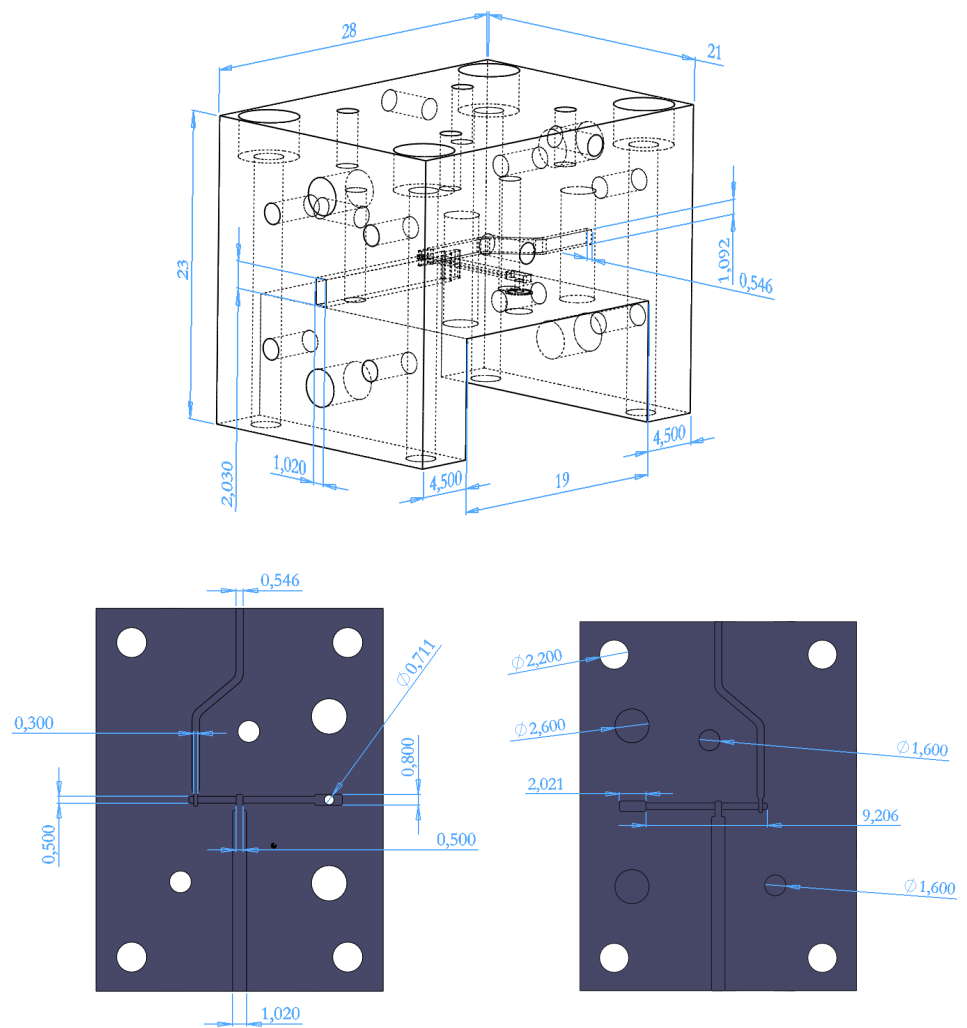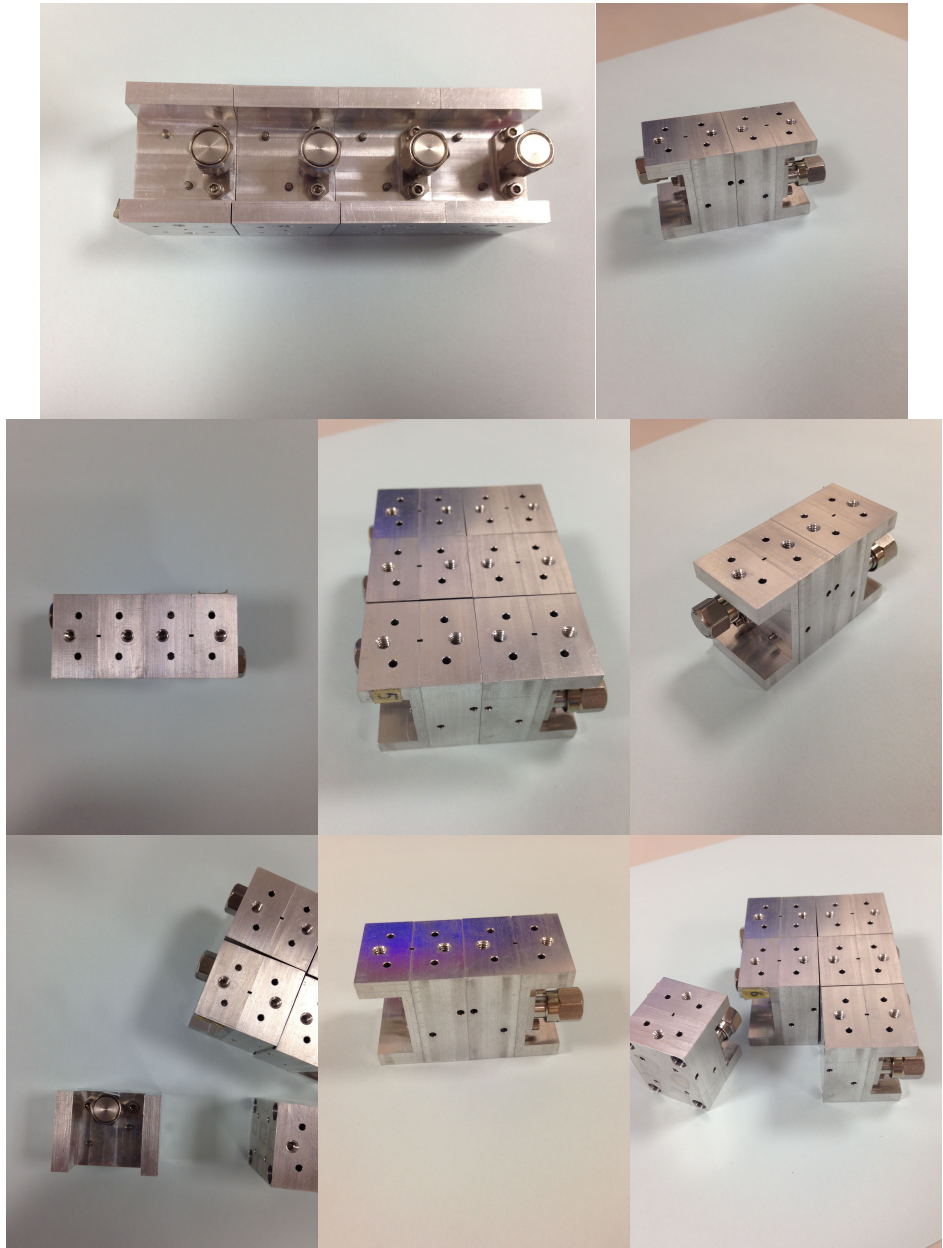
Some images of the final fabricated block are shown here:

Some images of the elements of the array are shown below:

Some images of the complete array attached to the splitter and the antennas with the optimum gain are presented here:

B.2 Sub-harmonic Mixer with RF frequency equal to 440 GHz

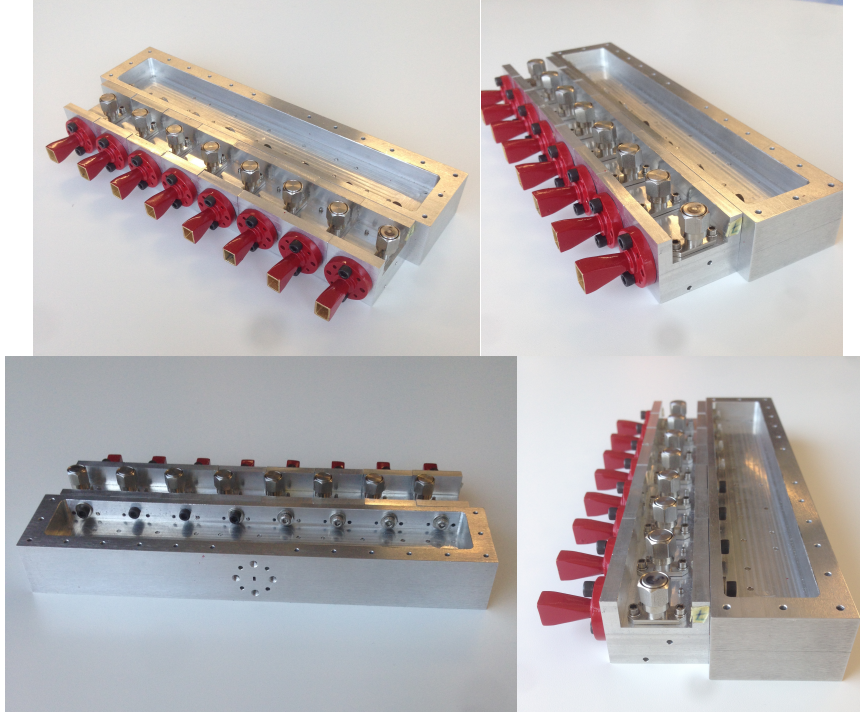The dimensions of the sub-harmonic mixer circuit developed in Chapter 5 are depicted here:
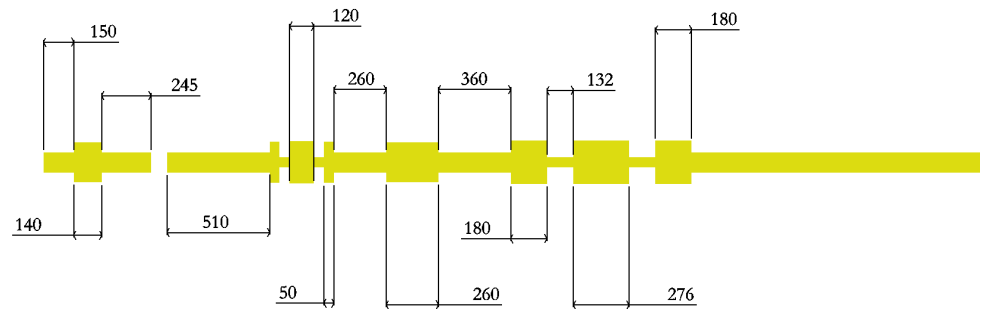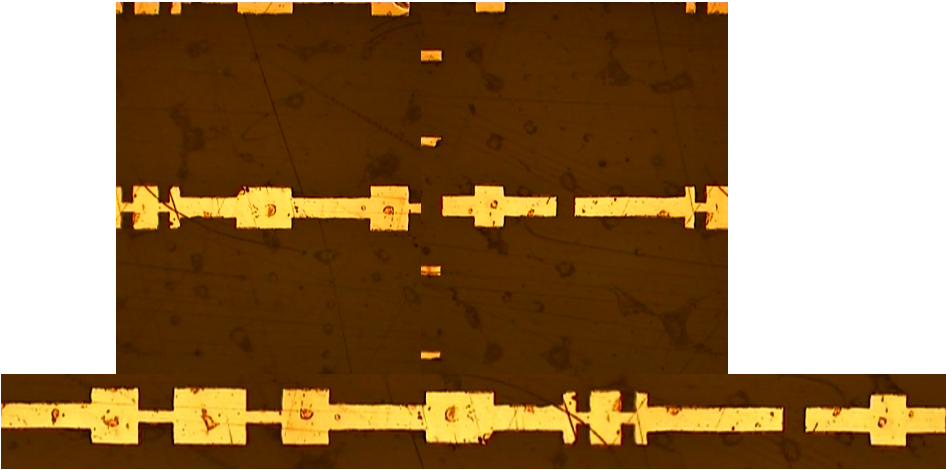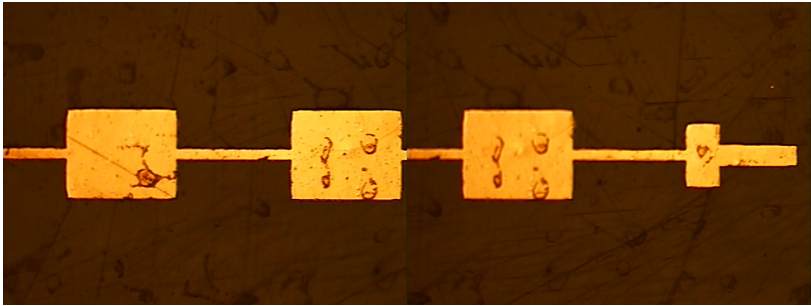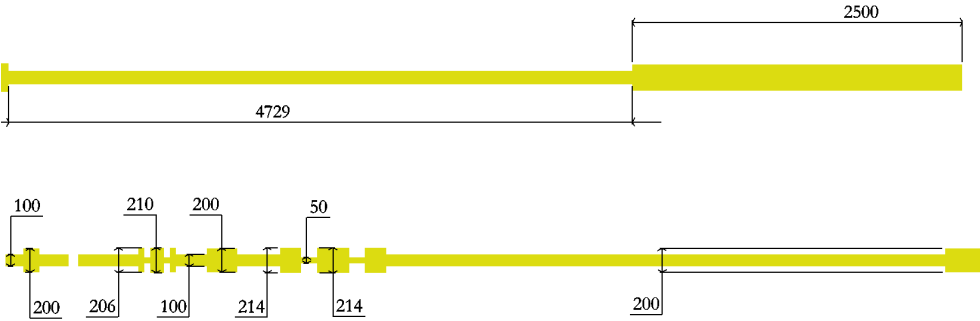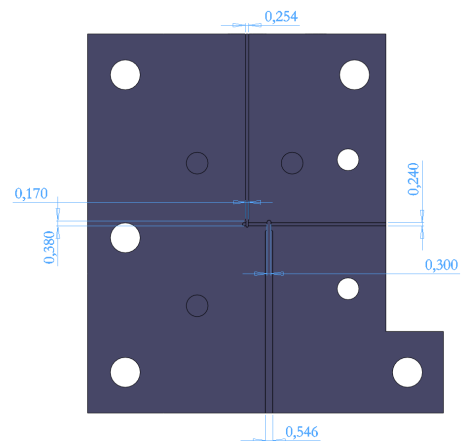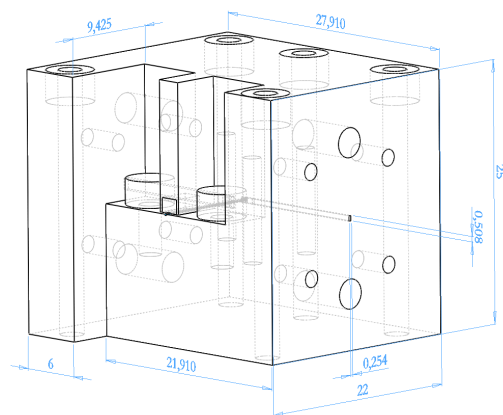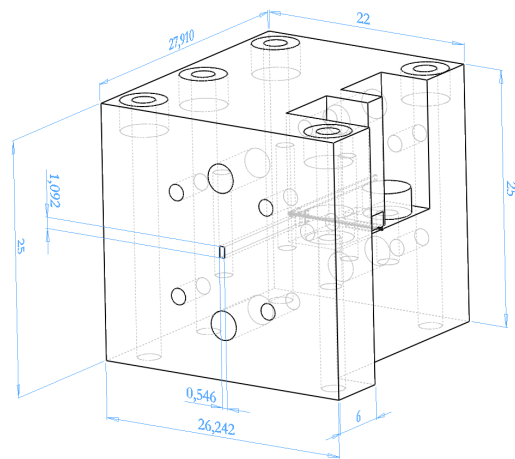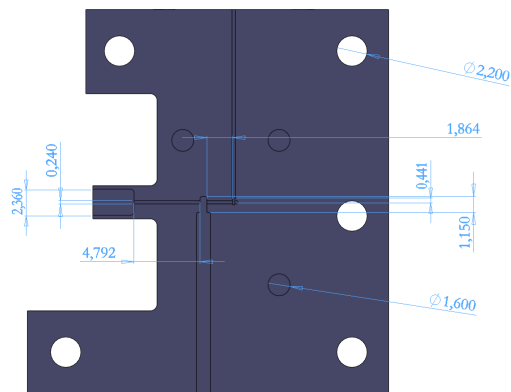
Some photos of the real block are gathered below:
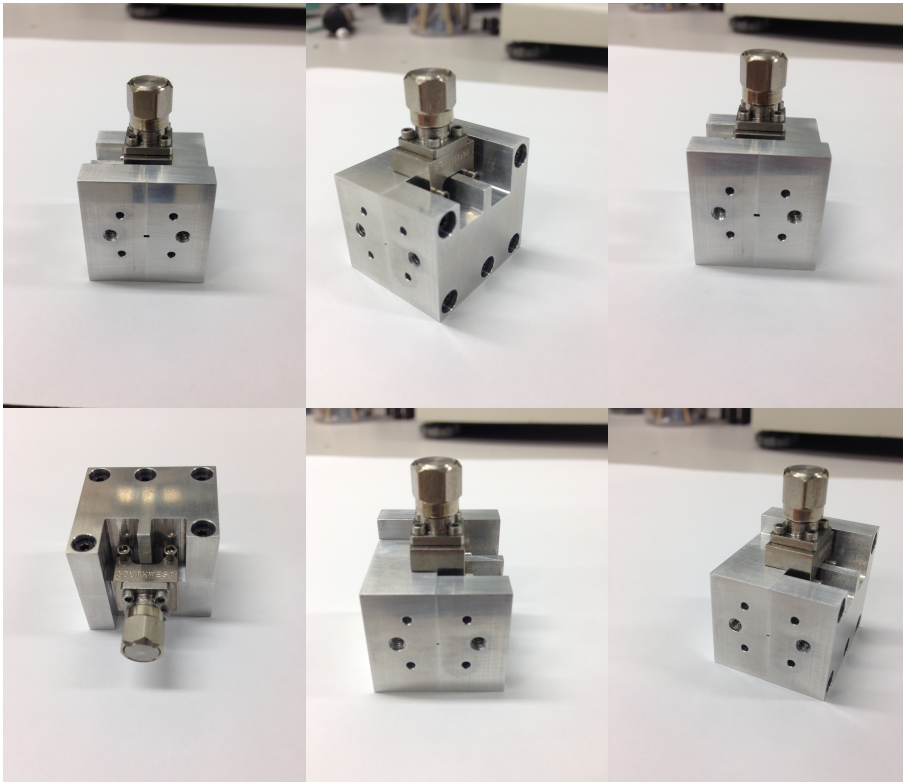
B.3   Frequency Doubler 110 to 220 GHz

The dimensions of the doubler circuit developed in Chapter 5 are depicted here:
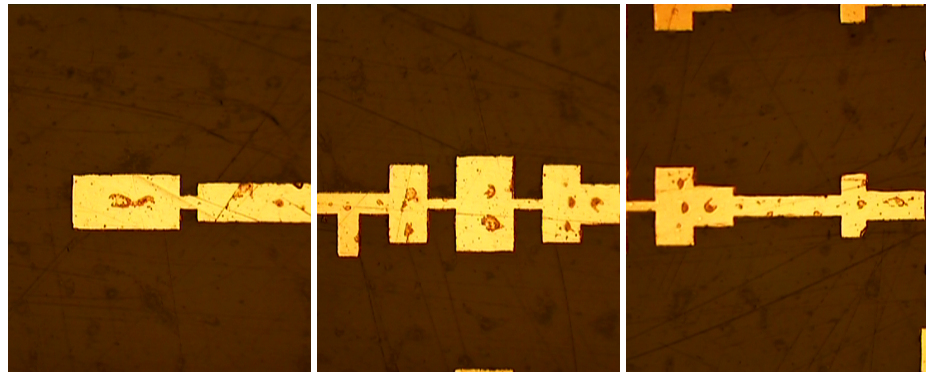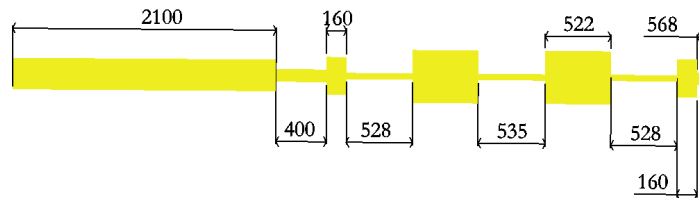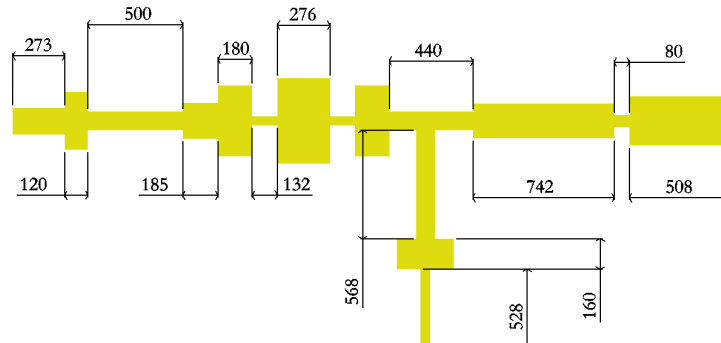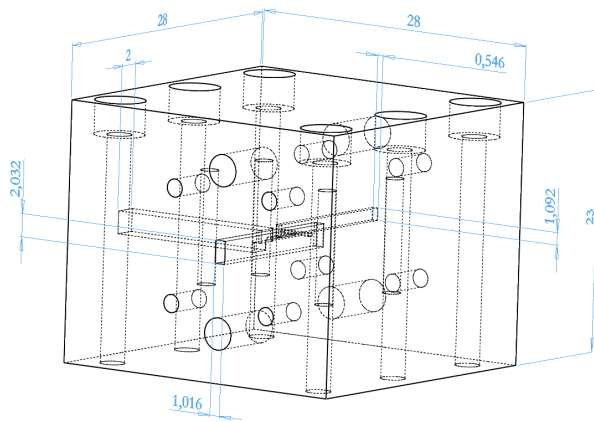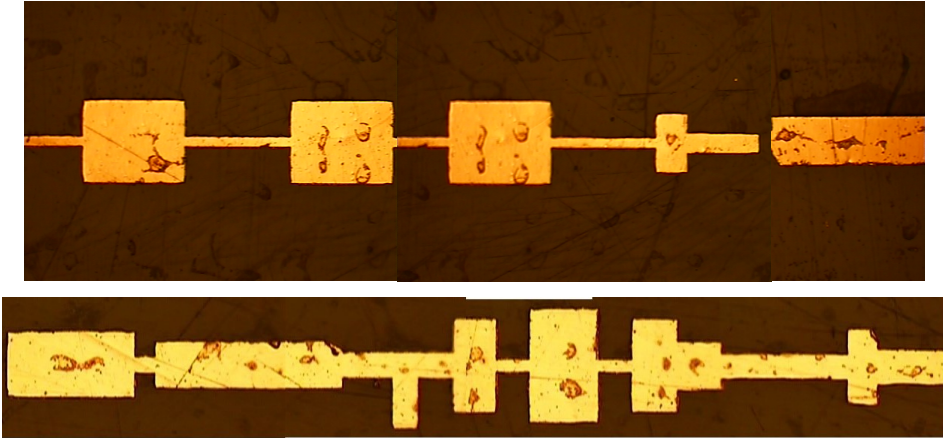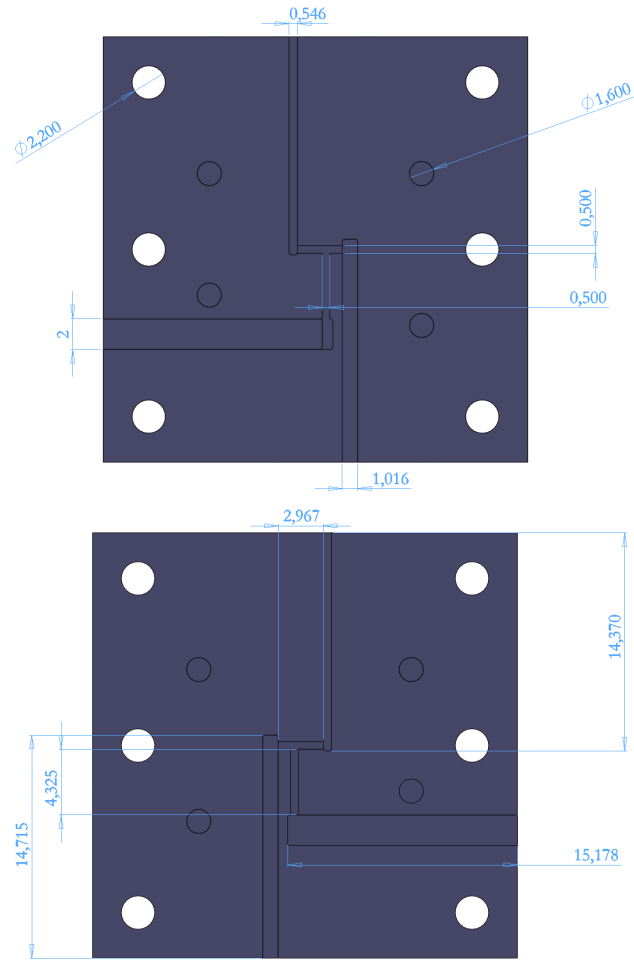
Some images of the doubler metallic block:
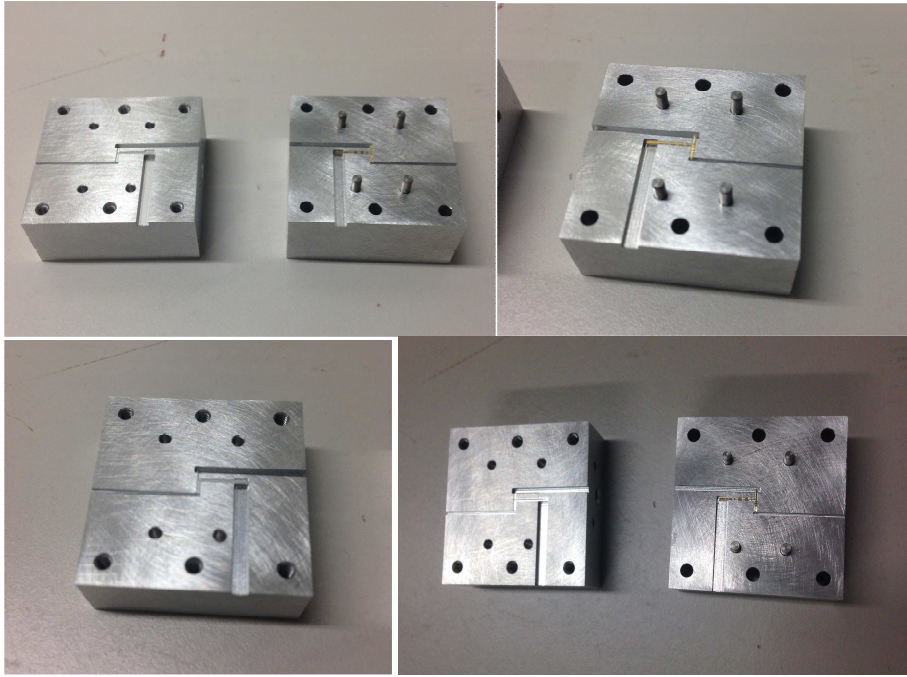
B.4   4ᵗʰ-harmonic Mixer with RF frequency equal to 440 GHz

The dimensions of the 4ᵗʰ-harmonic mixer circuit developed in Chapter 5 are depicted here:
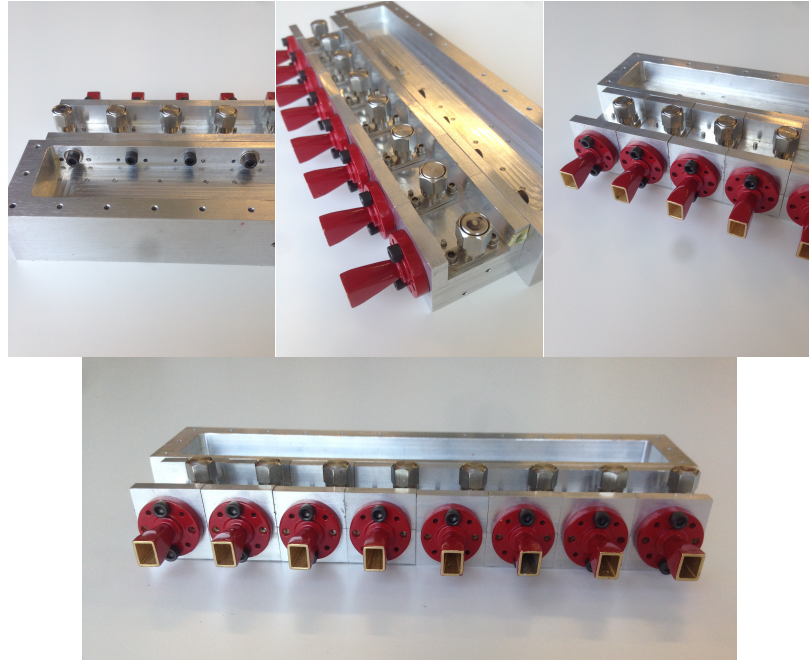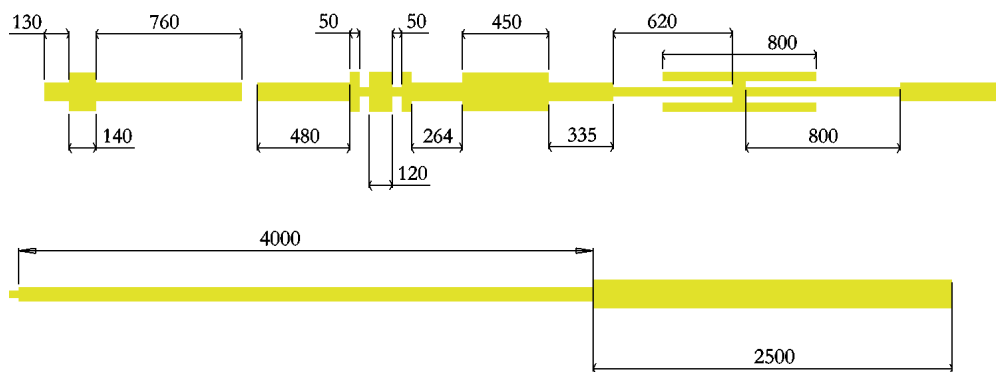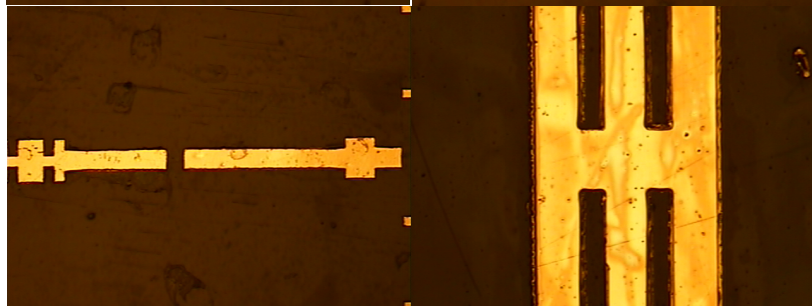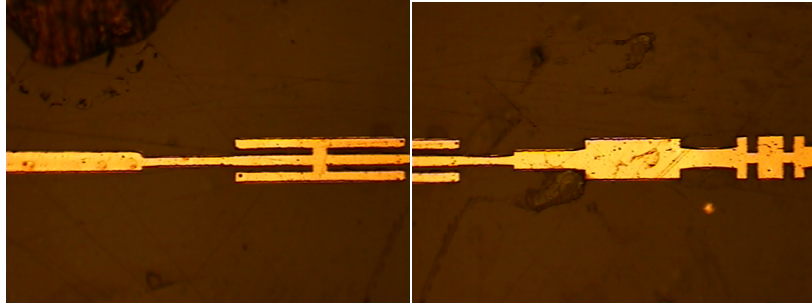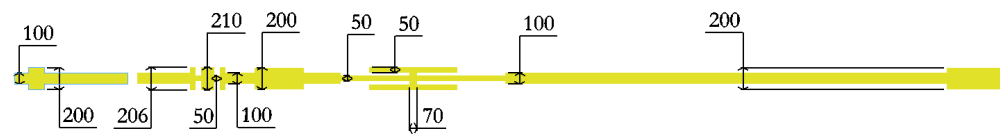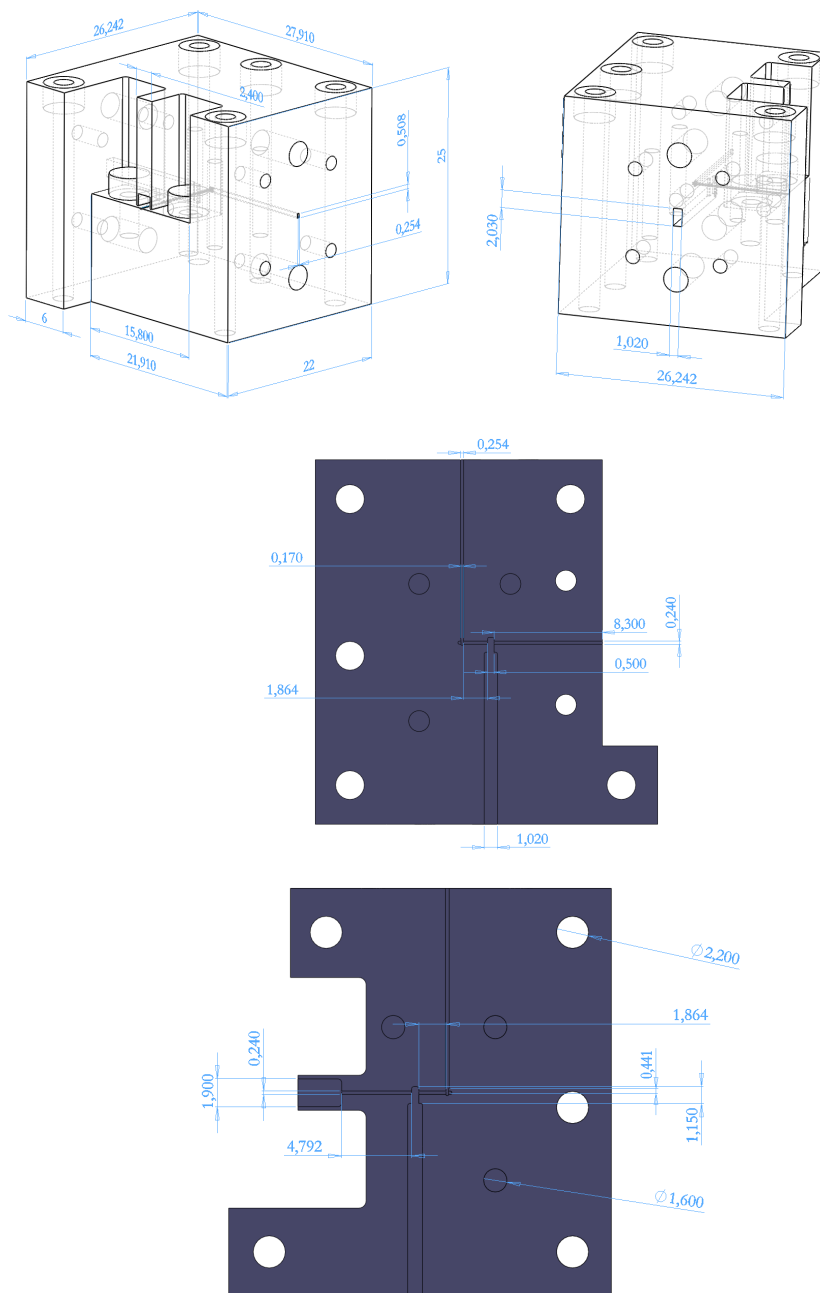
Some real images of the final fabricated and assembled block are shown below:
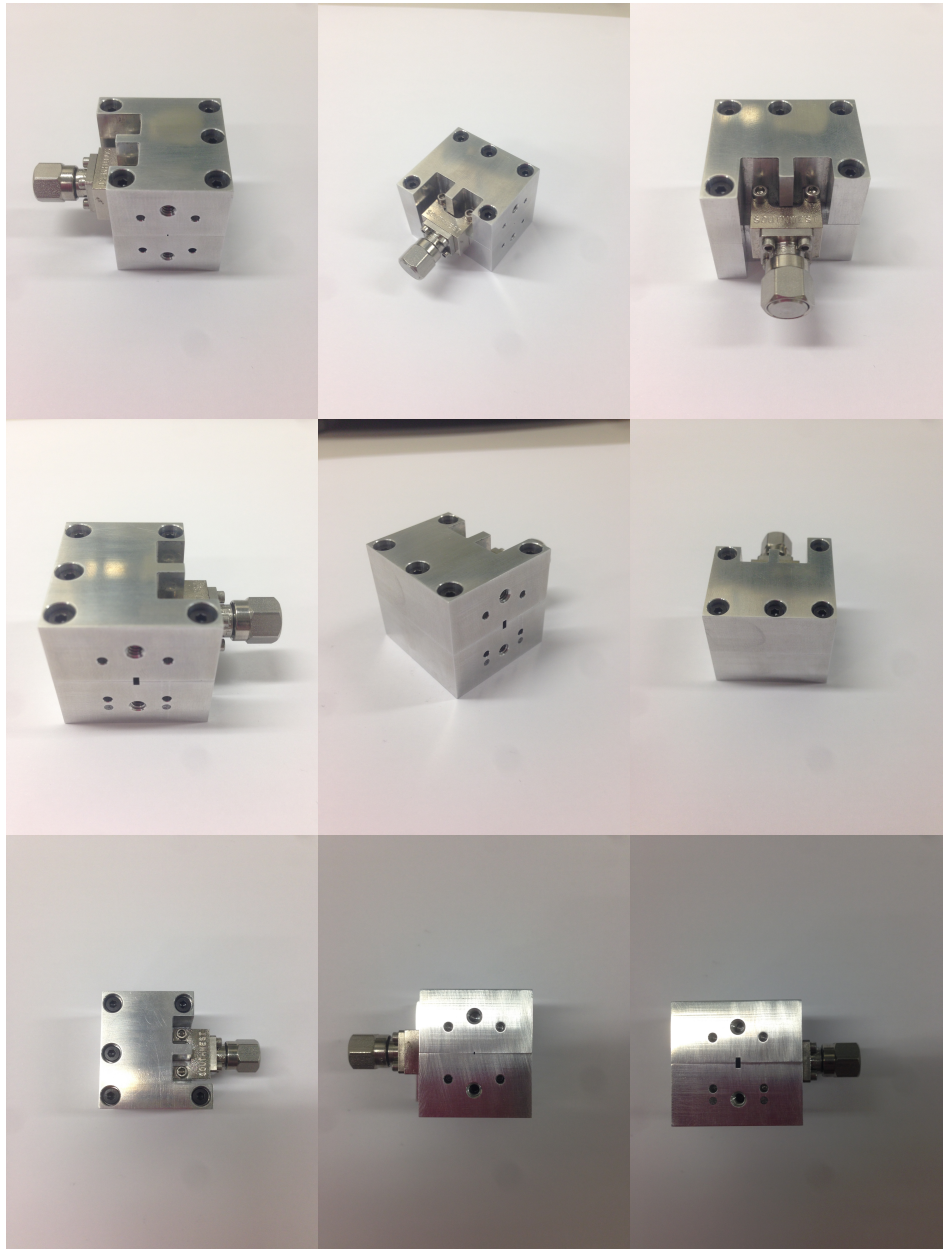
Images of the open block and the microstrip line welded to the Block and connector are shown below:
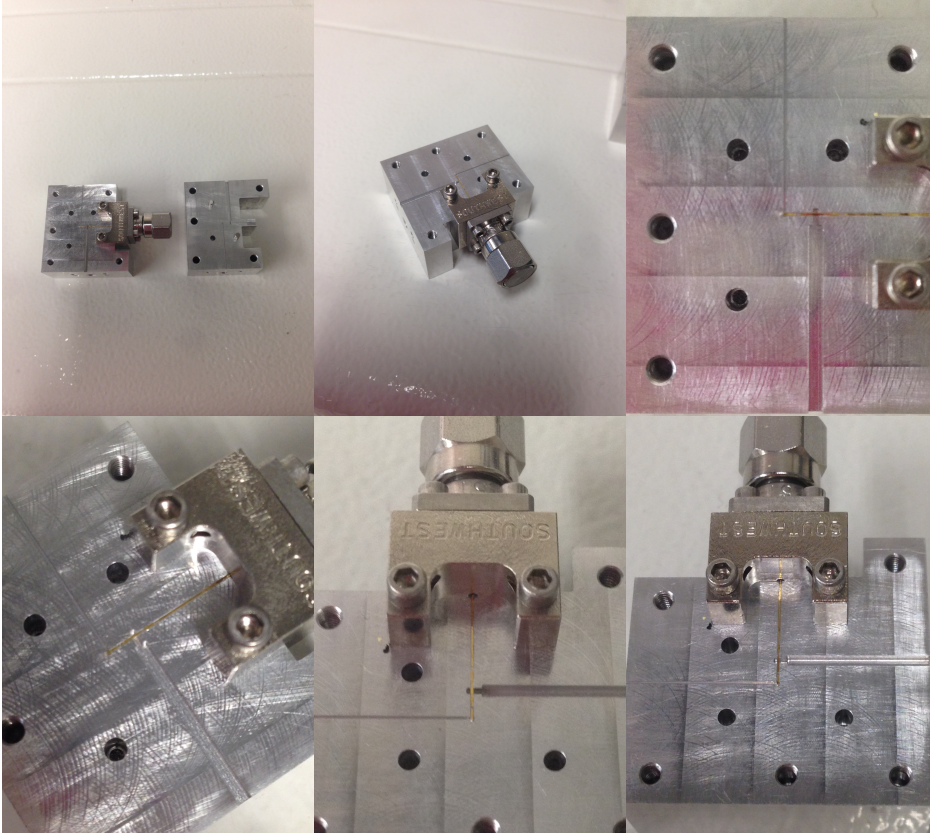
B.5   ADS Symbols
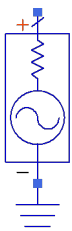
P_nHarm
PORT3
Num=3
Z=Z_LO
Freq=LOfreq
P[1]=P_LO mW

P_nTone
PORT4
Num=4
Z=Z_RF
Freq[1]=RFfreq
P[1]=polar(dbmtow(P_RF),0)

Term
IF port2
Num=6
Z=Z_LO
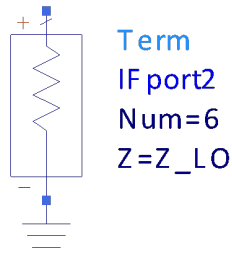
Num: Port number

Z: Source impedance (Ohm)

Freq: fundamental frequency (GHz)

P: N-th harmonic power level. Use polar(dbmtow(0),0) for phase

RWG
LO_WG
A=2032 um
B=1016 um
L=2 mm

RWG
RF_WG
A=1092 um
B=546 um
L=1 mm
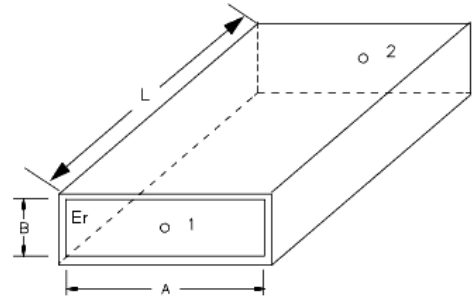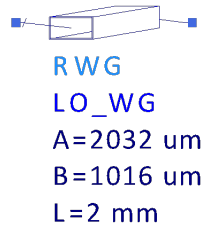
A: Inside width of enclosure

B: Inside height of enclosure

L: Waveguide length
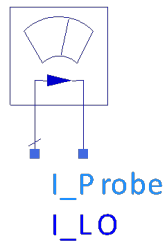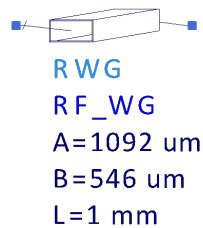
I_Probe
I_LO

Current probe used to measure the current at a reference point.

V_LO

Represents a variable that measures the voltage at a reference point.

Diode
DIODE1
Model=DIODEM1
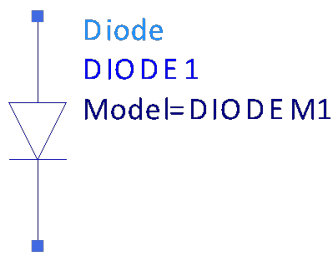
Model: Model instance name which is refer to the diode model defined.

Diode_Model
DIODEM1
Is=0.2 fA
Rs=13 Ohm
N=1.3
Cjo=1.3 fF
Vj=0.73 V
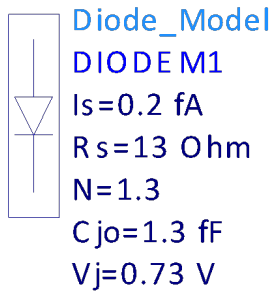
Is: Saturation current

Rs: Ohmic resistance

N: Emission Coefficient (with Is, determines diode DC characteristics)

Cjo: Zero-bias Junction capacitance

Vj: Junction Potential
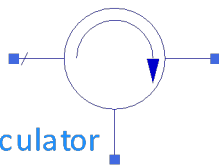
Circulator
CIR3
Isolat=100. dB
Z1=Z_LO
Z2=conj(Z_LO)
Z3=Z_LO

Isolat: Isolation (dB)

Z1: Reference Impedance port 1

Z2: Reference Impedance port 2

Z3: Reference Impedance port 3
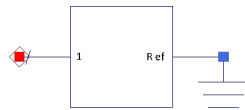
S 1P
S NP 1
F ile=
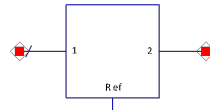
S 2P
S NP 2
F ile=
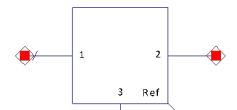
S 3P
S NP 3
F ile=
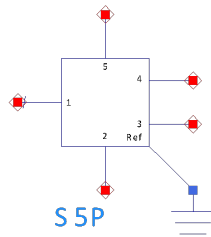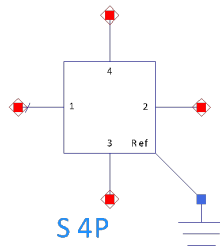
S 5P
S NP 5
F ile=

SNPn: Name of S-parameter data block, in which n represents the number of ports.

File: Name of data file containing 1-port S-, Y-, or Z-parameters for this component. The file extension and directory path are optional. Default extension is *.s1p* and the default directory is *<prj>/data* where <prj> is your current project directory.

S 4P
S NP 4
F ile=

240

APPENDIX C

CHARACTERIZATION OF THE MIXER ARRAY ELEMENTS

This appendix gathers the series resistance measurements of every mixer element of the array presented in Chapter 4 for two cases: first for the diodes employed in every mixer, and after for the complete block (once the diodes and the IF connectors are welded to the microstrip circuit placed in the metallic block). Moreover, the noise temperature and the conversion loss of every mixer are presented here.

C.1   Mixer 1

Series Resistance (Ω)	Single Diode		Complete block	
	Positive side	Negative Side	Positive Side	Negative Side
	13.5	12.4	20.7	21.5
Best Performance	Noise Temperature (K)		Conversion Loss (dB)	
	1044		7.1	
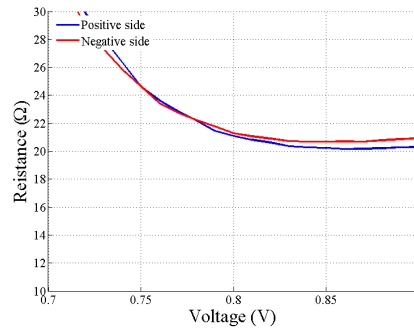
Fig. C-1 Series resistance Mixer 1.

| (a) | (b) |
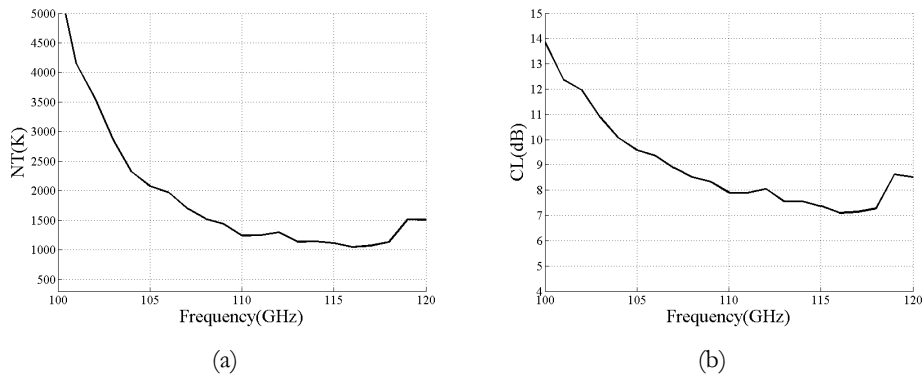
Fig. C-2 Measured (a) noise temperature and (b) conversion loss Mixer 1.

C.2 Mixer 2

Series Resistance (Ω)	Single Diode		Complete block	
	Positive side	Negative Side	Positive Side	Negative Side
	14.5	14.7	17.27	17.32
Best Performance	Noise Temperature (K)		Conversion Loss (dB)	
	1082		6.8	
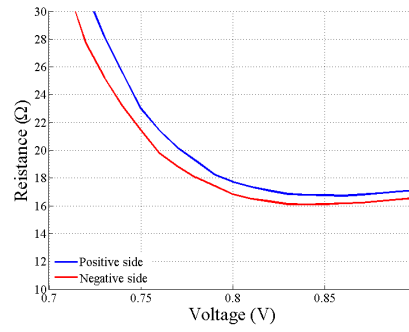
Fig. C-3 Series resistance Mixer 2.

| | (a) | | (b) |
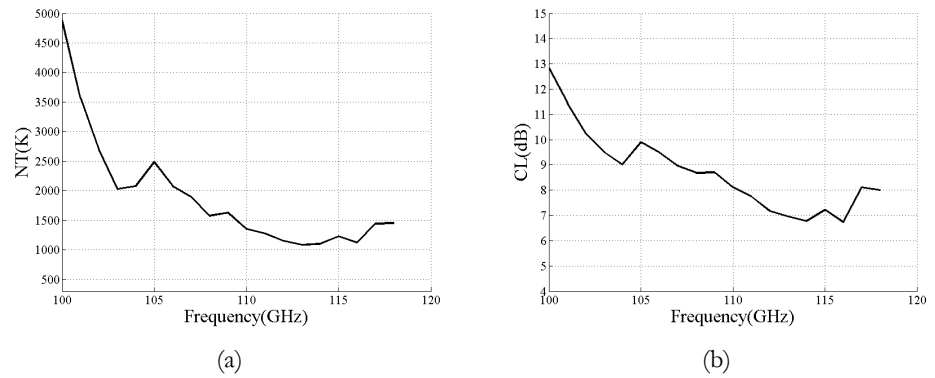
Fig. C-4 Measured (a) noise temperature and (b) conversion loss Mixer 2.

C.3 Mixer 3

Series Resistance (Ω)	Single Diode		Complete block	
	Positive side	Negative Side	Positive Side	Negative Side
	12.5	12.4	17.57	17.24
Best Performance	Noise Temperature (K)		Conversion Loss (dB)	
	1066		7.4	
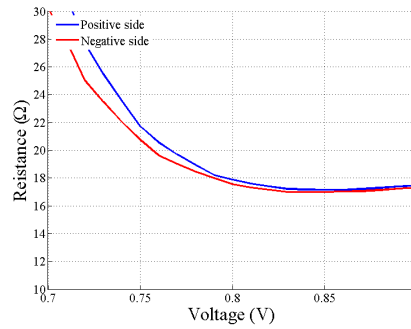
Fig. C-5 Series resistance Mixer 3.

(a)	(b)
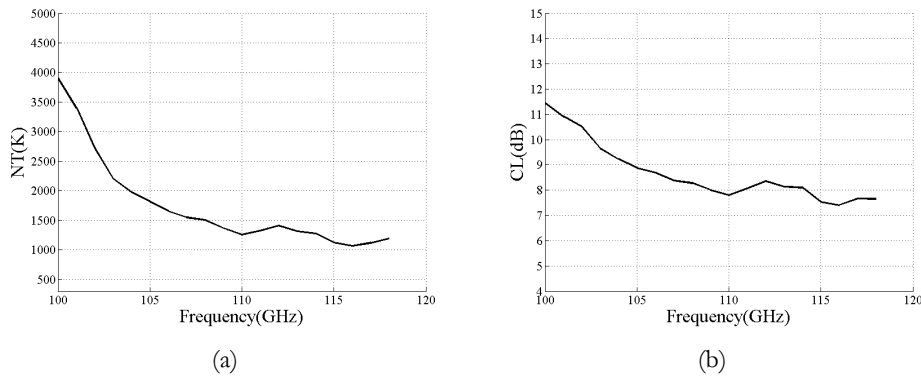
Fig. C-6 Measured (a) noise temperature and (b) conversion loss Mixer 3.

C.4   Mixer 4

Series Resistance (Ω)	Single Diode		Complete block	
	Positive side	Negative Side	Positive Side	Negative Side
	11.7	12	23.62	24.09
Best Performance	Noise Temperature (K)		Conversion Loss (dB)	
	1052		6.8	
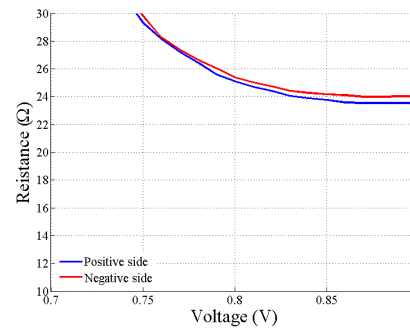
Fig. C-7 Series resistance Mixer 4.

| (a) | (b) |
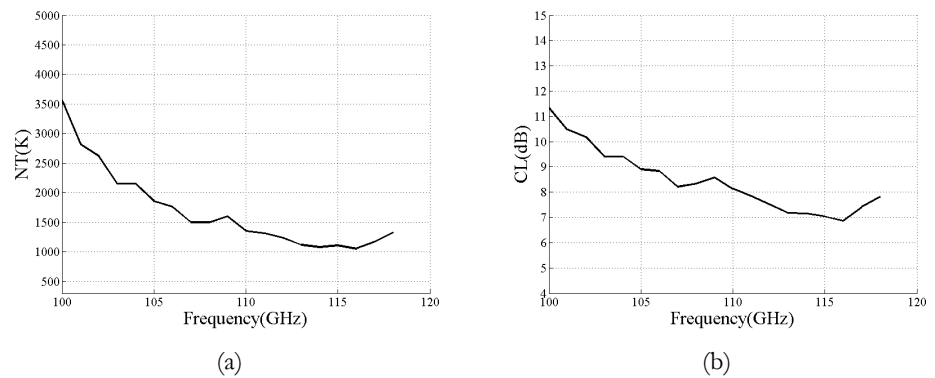
Fig. C-8 Measured (a) noise temperature and (b) conversion loss Mixer 4.

C.5 Mixer 5

Series Resistance (Ω)	Single Diode		Complete block	
	Positive side	Negative Side	Positive Side	Negative Side
	12.7	14.1	23.41	24.54
Best Performance	Noise Temperature (K)		Conversion Loss (dB)	
	1394		7.8	
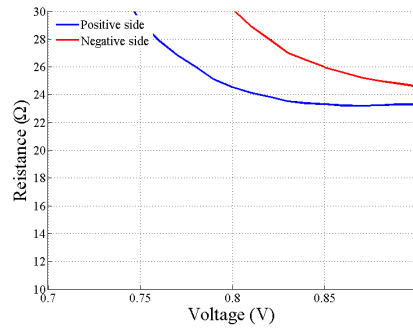
Fig. C-9 Series resistance Mixer 5.

(a)	(b)
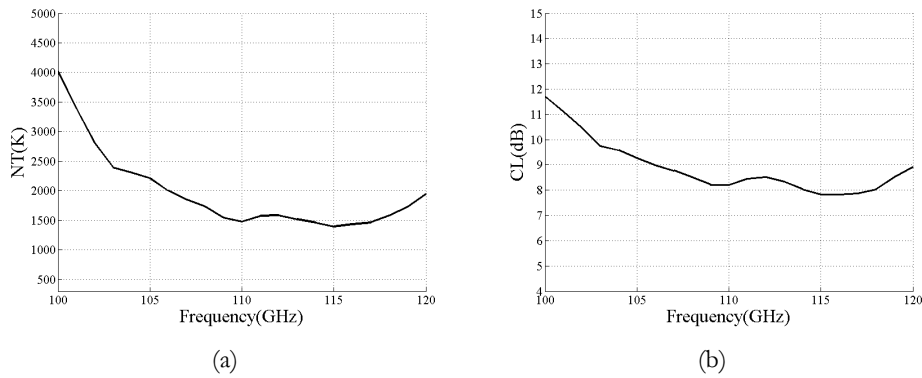
Fig. C-10 Measured (a) noise temperature and (b) conversion loss Mixer 5.

C.6   Mixer 6

Series Resistance (Ω)	Single Diode		Complete block	
	Positive side	Negative Side	Positive Side	Negative Side
	13.7	15.3	18.97	20.31
Best Performance	Noise Temperature (K)		Conversion Loss (dB)	
	1211		7.5	
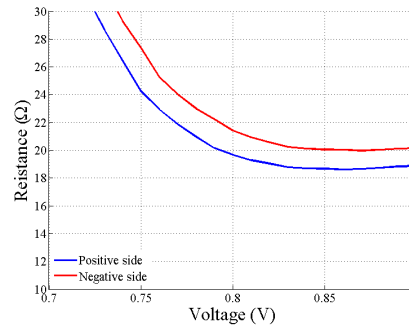
Fig. C-11 Series resistance Mixer 6.
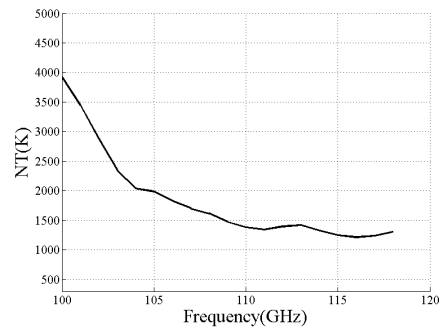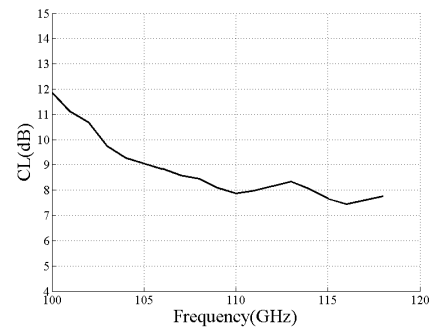
(a)	(b)

Fig. C-12 Measured (a) noise temperature and (b) conversion loss Mixer 6.

C.7   Mixer 7

Series Resistance (Ω)	Single Diode		Complete block	
	Positive side	Negative Side	Positive Side	Negative Side
	14.3	14.6	20.97	21.53
Best Performance	Noise Temperature (K)		Conversion Loss (dB)	
	962		6.7	
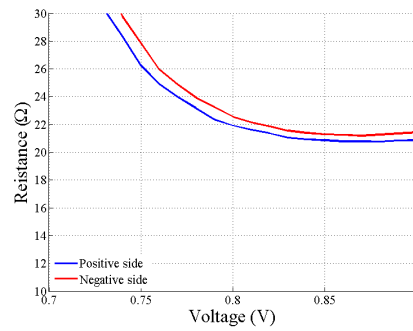
Fig. C-13 Series resistance Mixer 7.

(a)   (b)
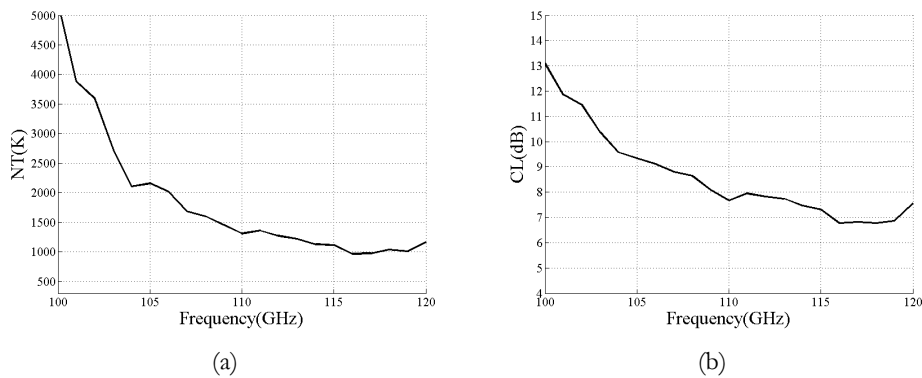
Fig. C-14 Measured (a) noise temperature and (b) conversion loss Mixer 7.

C.8   Mixer 8

Series Resistance (Ω)	Single Diode		Complete block	
	Positive side	Negative Side	Positive Side	Negative Side
	13.2	12.6	15.58	14.5
Best Performance	Noise Temperature (K)		Conversion Loss (dB)	
	1052		6.8	
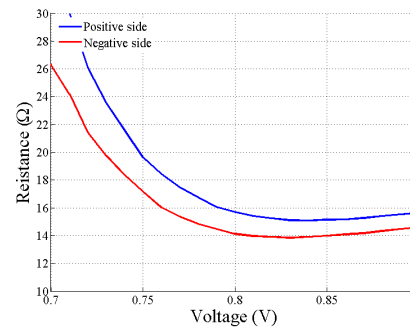
Fig. C-15 Series resistance Mixer 8.

(a)   (b)
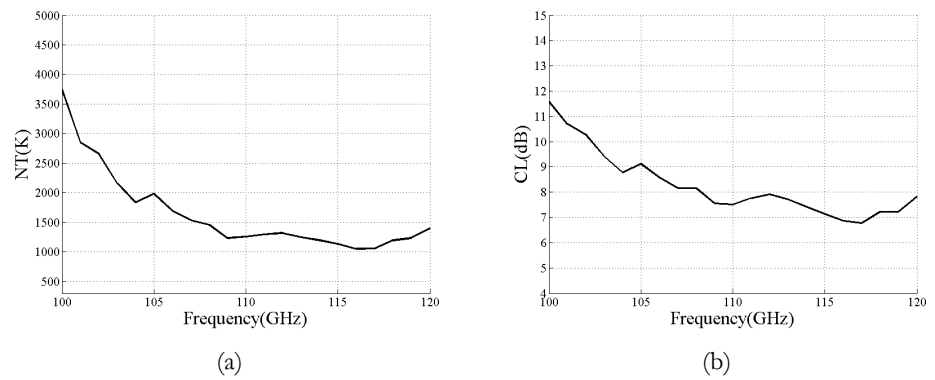
Fig. C-16 Measured (a) noise temperature and (b) conversion loss Mixer 8.

APPENDIX D

IMAGING ARRAY GRASP ANALYSIS

This appendix gathers the analysis of the imaging array presented in Chapter 4 using GRASP. First of all the results of spill-over efficiency and SNR for every element of the array and 26, 24, 22 and 20 dB directivities are presented. Finally, the beam cuts at -3 dB of the complete array for 24 dB antenna directivity are shown.

D.1   Antenna Directivity 26 dB

Array Element	TASK 1		TASK 2		TASK 4	
	η_{spill}	η_{spill} (dB)	η_{spill}	η_{spill} (dB)	η_{spill}	η_{spill} (dB)
1x1	0.944	0.252	0.931	0.310	0.192	7.161
1x2	0.961	0.172	0.935	0.291	0.172	7.646
1x3	0.967	0.145	0.943	0.255	0.153	8.152
1x4	0.973	0.120	0.948	0.230	0.136	8.650
1x5	0.971	0.128	0.951	0.220	0.121	9.171
1x6	0.972	0.125	0.952	0.212	0.106	9.736
1x7	0.965	0.156	0.946	0.243	0.086	10.675
1x8	0.957	0.192	0.938	0.277	0.068	11.687

Array Elelement	Imaging plane				
	η_{spill}	η_{spill} (dB)	Spill over	Max E	SNR
1x1	0.739	1.315	-5.829	0.023	-26.824

251

1x2	0.763	1.174	-6.255	0.026	-25.479
1x3	0.790	1.024	-6.778	0.029	-23.974
1x4	0.812	0.905	-7.258	0.032	-22.748
1x5	0.829	0.812	-7.683	0.033	-21.921
1x6	0.846	0.725	-8.130	0.035	-21.088
1x7	0.860	0.655	-8.537	0.035	-20.606
1x8	0.870	0.603	-8.873	0.034	-20.601

Table D-1 GRASP results mixer array with an antenna directivity of 26 dB.

D.2 Antenna Directivity 24 dB

Array Element	TASK 1		TASK 2		TASK 4	
	η_{spill}	η_{spill} (dB)	η_{spill}	η_{spill} (dB)	η_{spill}	η_{spill} (dB)
1x1	0.925	0.337	0.920	0.363	0.208	6.827
1x2	0.950	0.224	0.921	0.357	0.188	7.264
1x3	0.959	0.181	0.924	0.344	0.169	7.728
1x4	0.961	0.171	0.928	0.323	0.152	8.193
1x5	0.963	0.162	0.930	0.314	0.134	8.734
1x6	0.961	0.174	0.930	0.317	0.113	9.459
1x7	0.958	0.187	0.931	0.310	0.095	10.219
1x8	0.938	0.277	0.915	0.385	0.062	12.074

Array Elelement	Imaging plane				
	η_{spill}	η_{spill} (dB)	Spill over	Max E	SNR
1x1	0.712	1.473	-5.410	0.027	-26.125
1x2	0.733	1.347	-5.740	0.030	-24.717
1x3	0.755	1.220	-6.110	0.033	-23.546
1x4	0.777	1.098	-6.510	0.035	-22.634
1x5	0.796	0.988	-6.914	0.035	-22.180
1x6	0.816	0.881	-7.361	0.035	-21.757

1x7	0.836	0.777	-7.854	0.035	-21.389
1x8	0.853	0.690	-8.332	0.033	-21.325

Table D-2 GRASP results mixer array with an antenna directivity of 24 dB.

- Phi 1 cut (lower position)

The system has the following characteristics:

Rotation Main reflector	-90
Rotacion Sub-reflector	90

Array Element	TASK 1		TASK 2		TASK 4	
	η_{spill}	η_{spill} (dB)	η_{spill}	η_{spill} (dB)	η_{spill}	η_{spill} (dB)
1x1	0.934	0.297	0.914	0.393	0.001	28.466
1x2	0.956	0.197	0.935	0.292	0.002	27.741
1x3	0.960	0.177	0.938	0.276	0.002	27.447
1x4	0.963	0.162	0.940	0.267	0.002	27.325
1x5	0.963	0.162	0.940	0.267	0.002	27.325
1x6	0.960	0.177	0.938	0.276	0.002	27.359
1x7	0.956	0.197	0.935	0.292	0.002	27.724
1x8	0.934	0.297	0.914	0.393	0.001	28.447

Array Elelement	Imaging plane				
	η_{spill}	η_{spill} (dB)	Spill over	Max E	SNR
1x1	0.912	-0.399	-10.562	0.026	-21.307
1x2	0.933	-0.300	-11.757	0.029	-18.995
1x3	0.937	-0.284	-11.979	0.031	-18.083
1x4	0.939	-0.275	-12.120	0.033	-17.589
1x5	0.939	-0.275	-12.120	0.033	-17.589
1x6	0.937	-0.285	-11.976	0.031	-18.085
1x7	0.933	-0.300	-11.757	0.029	-18.995

| 1x8 | 0.912 | -0.399 | -10.563 | 0.026 | -21.307 |

Table D-3 GRASP results mixer array with an antenna directivity of 24 dB for Phi 1 cut.

- Phi 2 cut (upper position)

The system has the following characteristics:

Rotation Main reflector	90
Rotacion Sub-reflector	-90

Array Element	TASK 1		TASK 2		TASK 4	
	η_{spill}	η_{spill} (dB)	η_{spill}	η_{spill} (dB)	η_{spill}	η_{spill} (dB)
1x1	0.934	0.297	0.914	0.393	0.001	28.466
1x2	0.956	0.197	0.935	0.292	0.002	27.741
1x3	0.960	0.177	0.938	0.276	0.002	27.447
1x4	0.963	0.162	0.940	0.267	0.002	27.325
1x5	0.963	0.162	0.940	0.267	0.002	27.325
1x6	0.960	0.177	0.938	0.276	0.002	27.359
1x7	0.956	0.197	0.935	0.292	0.002	27.724
1x8	0.934	0.297	0.914	0.393	0.001	28.447

Array Elelement	Imaging plane				
	η_{spill}	η_{spill} (dB)	Spill over	Max E	SNR
1x1	0.912	-0.399	-10.562	0.026	-21.307
1x2	0.933	-0.300	-11.757	0.029	-18.995
1x3	0.937	-0.284	-11.979	0.031	-18.083
1x4	0.939	-0.275	-12.120	0.033	-17.589
1x5	0.939	-0.275	-12.120	0.033	-17.589
1x6	0.937	-0.285	-11.976	0.031	-18.085
1x7	0.933	-0.300	-11.757	0.029	-18.995

| 1x8 | 0.912 | -0.399 | -10.563 | 0.026 | -21.307 |

Table D-4 GRASP results mixer array with an antenna directivity of 24 dB for Phi 2 cut.

D.3   Antenna Directivity 22 dB

Array Element	TASK 1		TASK 2		TASK 4	
	η_{spill}	η_{spill} (dB)	η_{spill}	η_{spill} (dB)	η_{spill}	η_{spill} (dB)
1x1	0.931	0.313	0.923	0.347	0.236	6.279
1x2	0.940	0.267	0.926	0.333	0.217	6.629
1x3	0.952	0.214	0.927	0.327	0.199	7.001
1x4	0.962	0.170	0.928	0.325	0.181	7.412
1x5	0.965	0.154	0.929	0.321	0.165	7.819
1x6	0.961	0.172	0.926	0.335	0.144	8.424
1x7	0.947	0.236	0.912	0.401	0.112	9.507
1x8	0.934	0.299	0.898	0.467	0.081	10.924

Array Elelement	Imaging plane				
	η_{spill}	η_{spill} (dB)	Spill over	Max E	SNR
1x1	0.688	1.626	-5.053	0.031	-25.204
1x2	0.709	1.495	-5.358	0.032	-24.594
1x3	0.728	1.379	-5.654	0.032	-24.298
1x4	0.746	1.270	-5.958	0.031	-24.159
1x5	0.764	1.171	-6.264	0.031	-23.994
1x6	0.782	1.068	-6.616	0.030	-23.727
1x7	0.800	0.970	-6.986	0.030	-23.530
1x8	0.817	0.877	-7.378	0.029	-23.344

Table D-5 GRASP results mixer array with an antenna directivity of 22 dB.

D.4 Antenna Directivity 20 dB

Array Element	TASK 1		TASK 2		TASK 4	
	η_{spill}	η_{spill} (dB)	η_{spill}	η_{spill} (dB)	η_{spill}	η_{spill} (dB)
1x1	0.902	0.446	0.879	0.560	0.238	6.230
1x2	0.932	0.304	0.888	0.514	0.224	6.500
1x3	0.937	0.282	0.899	0.465	0.210	6.770
1x4	0.935	0.290	0.903	0.443	0.196	7.067
1x5	0.933	0.300	0.903	0.445	0.183	7.382
1x6	0.933	0.302	0.901	0.453	0.163	7.874
1x7	0.934	0.297	0.901	0.453	0.145	8.400
1x8	0.923	0.346	0.890	0.506	0.119	9.260

Array Elelement	Imaging plane				
	η_{spill}	η_{spill} (dB)	Spill over	Max E	SNR
1x1	0.641	1.932	-4.448	0.030	-26.039
1x2	0.665	1.774	-4.745	0.031	-25.541
1x3	0.688	1.623	-5.061	0.028	-25.934
1x4	0.707	1.508	-5.326	0.026	-26.543
1x5	0.720	1.427	-5.528	0.023	-27.238
1x6	0.738	1.320	-5.815	0.022	-27.336
1x7	0.756	1.212	-6.133	0.022	-26.862
1x8	0.771	1.127	-6.411	0.023	-26.279

Table D-6 GRASP results mixer array with an antenna directivity of 20 dB.

D.5 Comparison
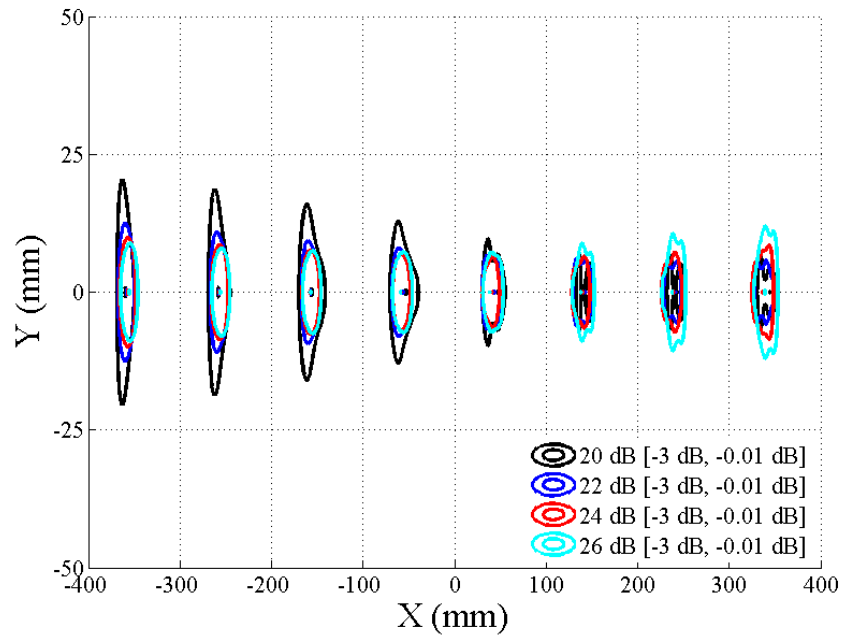
Fig. D-1 Bean cut of the mixer array for different antenna directivities.

D.6 Element 1x1 24 dB antenna
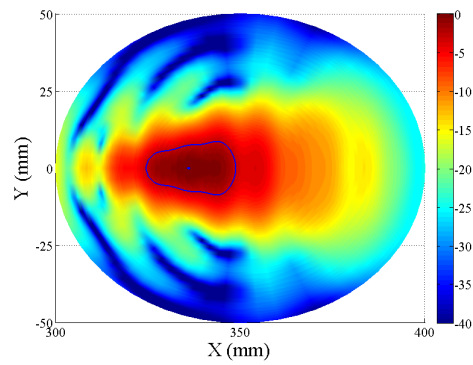
Fig. D-2 Bean cut of element 1x1.
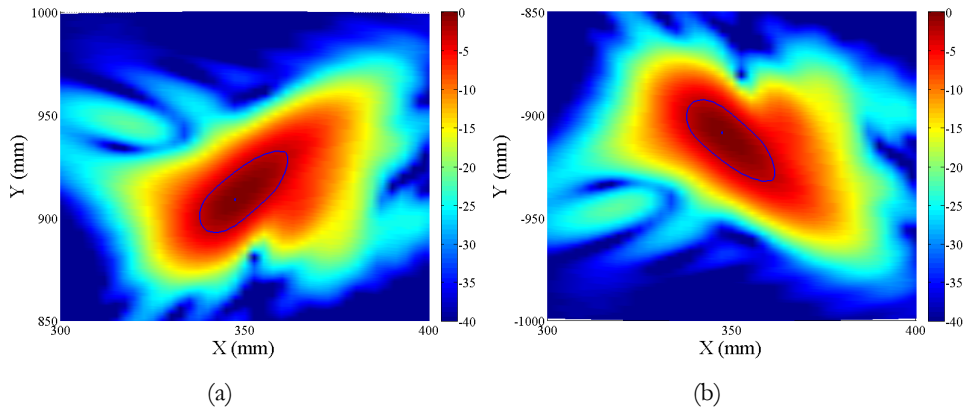
Fig. D-3 Beam cut of element 1x1 at the (a) upper and (b) lower position..

D.7   Element 1x2 24 dB antenna

Fig. D-4 Bean cut of element 1x2.
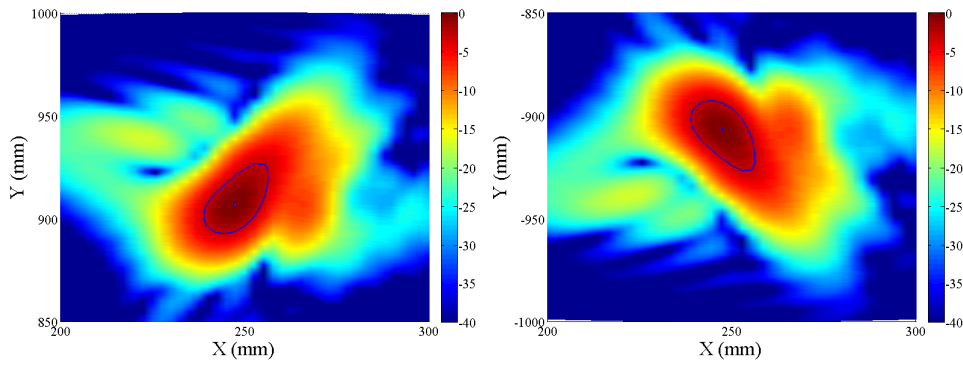
(a)   (b)

Fig. D-5 Beam cut of element 1x2 at the (a) upper and (b) lower position.

D.8 Element 1x3 24 dB antenna

Fig. D-6 Bean cut of element 1x3.

(a)   (b)
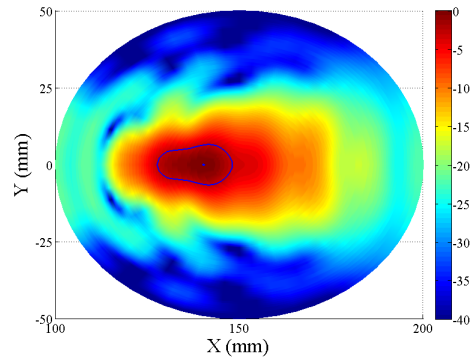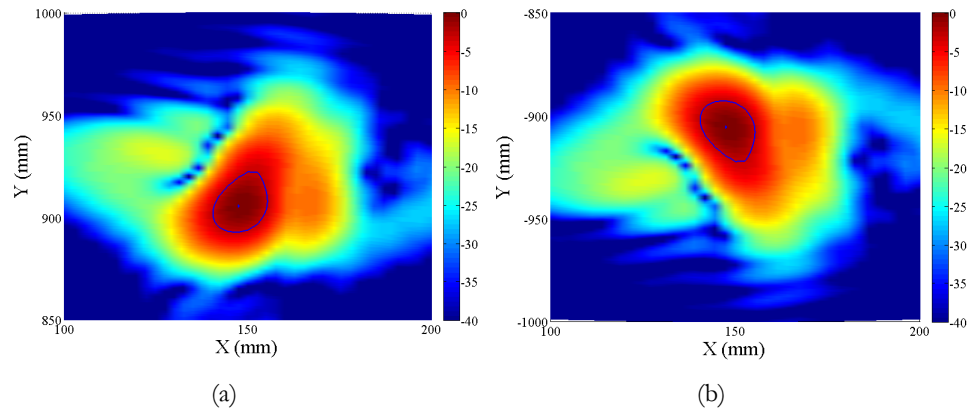
Fig. D-7 Beam cut of element 1x3 at the (a) upper and (b) lower position.

D.9 Element 1x4 24 dB antenna

Fig. D-8 Bean cut of element 1x4.

(a)   (b)
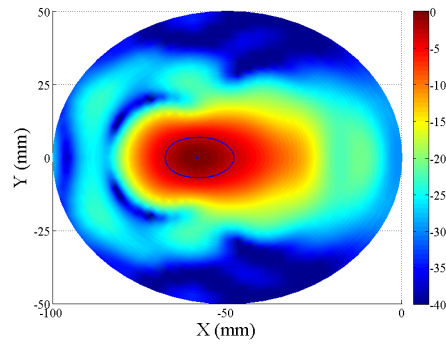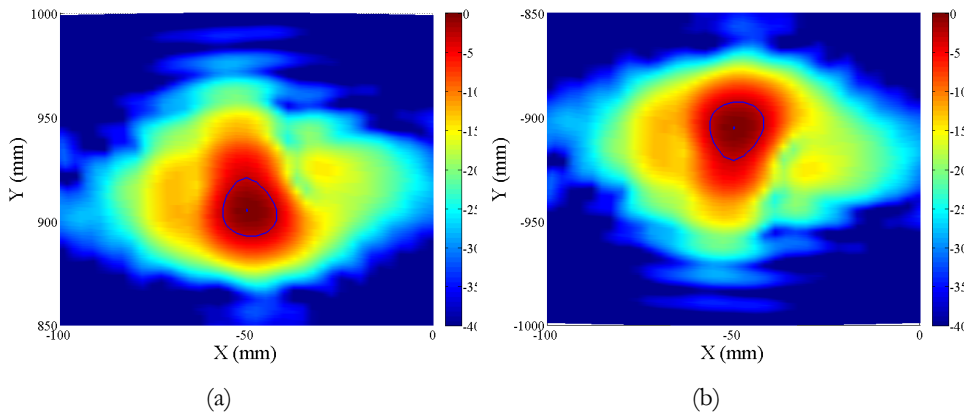
Fig. D-9 Beam cut of element 1x4 at the (a) upper and (b) lower position.

D.10 Element 1x5 24 dB antenna

Fig. D-10 Bean cut of element 1x5.

(a)

(b)
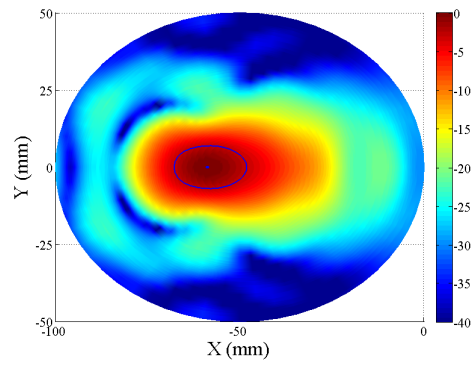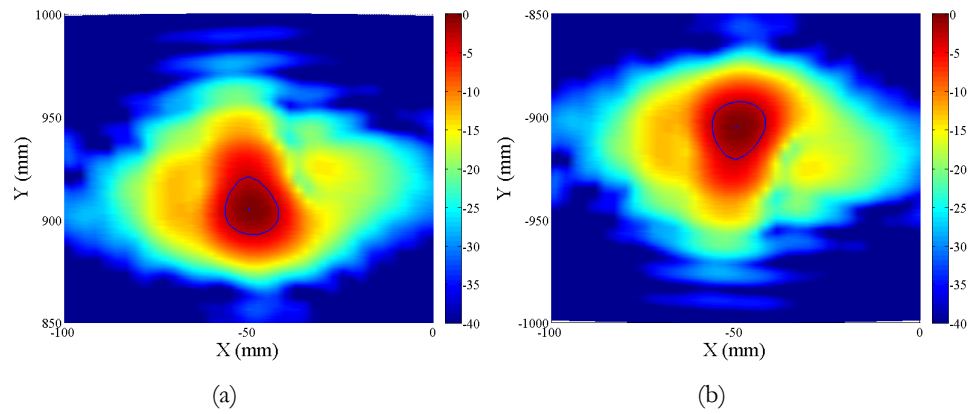
Fig. D-11 Beam cut of element 1x5 at the (a) upper and (b) lower position.

D.11 Element 1x6 24 dB antenna

Fig. D-12 Bean cut of element 1x6.

(a)

(b)
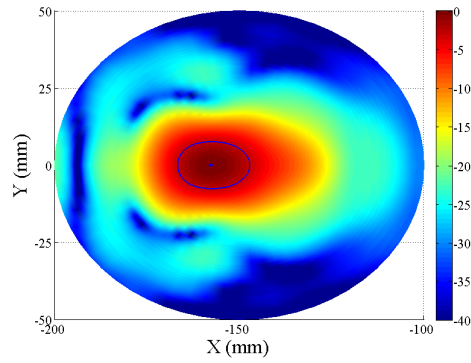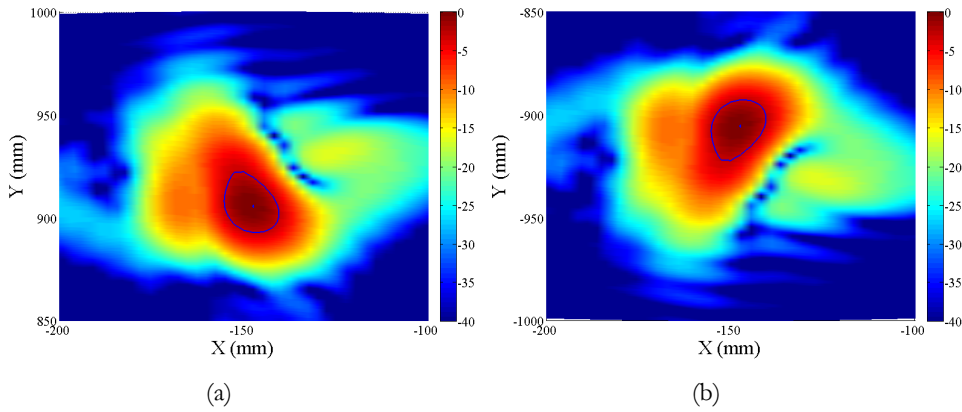
Fig. D-13 Beam cut of element 1x6 at the (a) upper and (b) lower position.

D.12 Element 1x7 24 dB antenna

Fig. D-14 Bean cut of element 1x7.

(a)   (b)
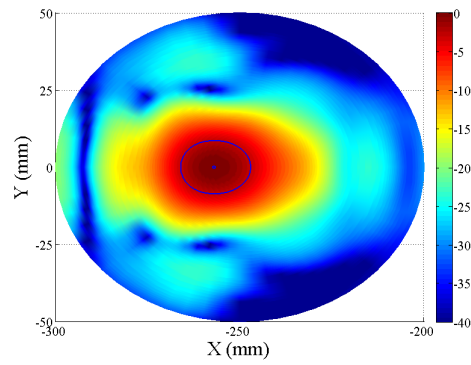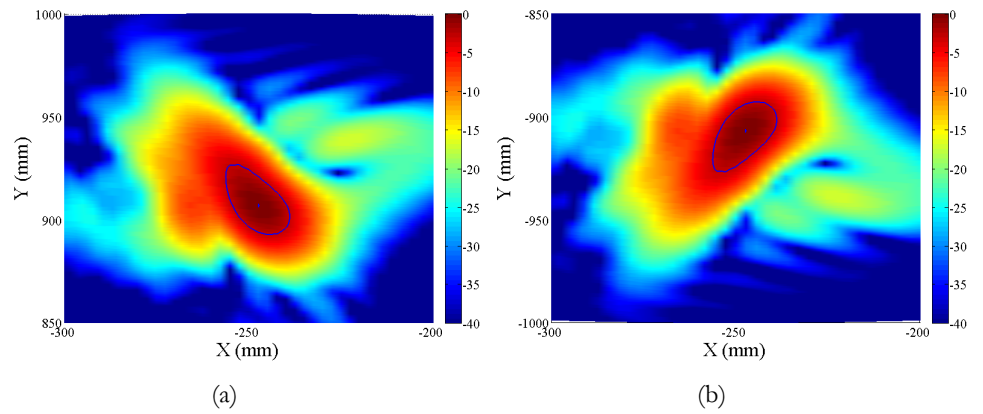
Fig. D-15 Beam cut of element 1x7 at the (a) upper and (b) lower position.

D.13 Element 1x8 24 dB antenna

Fig. D-16 Bean cut of element 1x8.

(a)   (b)
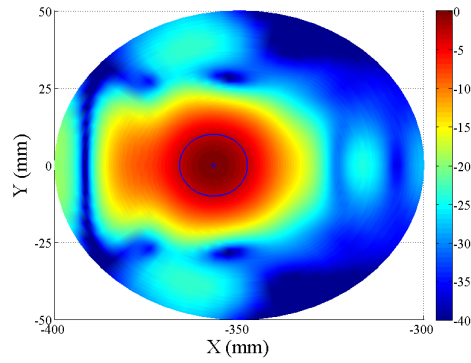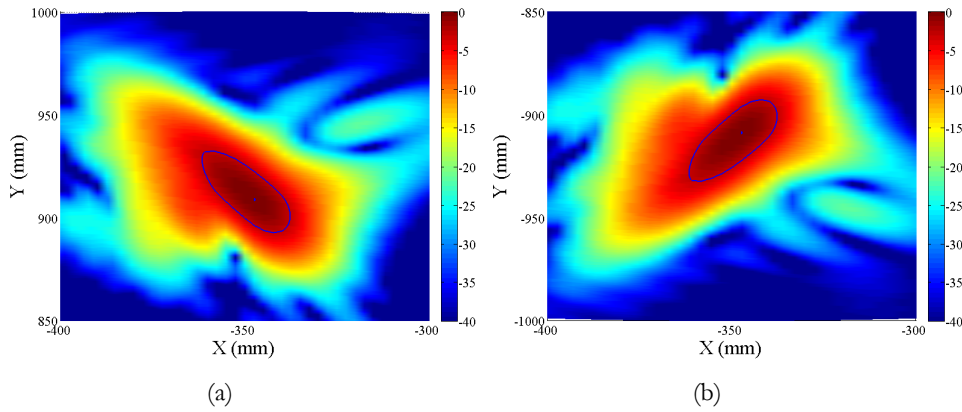
Fig. D-17 Beam cut of element 1x8 at the (a) upper and (b) lower position.

BIBLIOGRAPHY

[ACST]   http://www.acst.de/

[Agi10]   Agilent Technologies, "Fundamentals of RF and Microwave Noise Figure Measurements," Applicat. Note 57-1, August 2010.

[Agi14]   Agilent Technologies, "Noise Figure Measurement Accuracy-The Y Factor Method," Applicat. Note 57-2, February 2014.

[AGI]   http://www.home.agilent.com/en/pc-1297113/advanced-design-system-ads?&cc=ES&lc=eng.

[Aji11]   Ajito, K.; Ueno, Yuko, "THz Chemical Imaging for Biological Applications," Terahertz Science and Technology, IEEE Transactions on , vol.1, no.1, pp.293,300, Sept. 2011 doi: 10.1109/TTHZ.2011.2159562

[Ald08]   Alderman, B.; Sanghera, H.; Thomas, B.; Matheson, D.; Maestrini, A.; Hui Wang; Treuttel, J.; Siles, J.V.; Davies, S.; Narhi, T., "Integrated schottky structures for applications above 100 GHz," in Microw. Integrated Circuit Conf. vol., no., pp. 202, 205, 27-28 Oct. 2008. doi: 10.1109/EMICC.2008.4772264.

[Ald10]   Alderman, B.; Henry, M.; Maestrini, A.; Grajal, J.; Zimmermann, R.; Sanghera, H.; Hui Wang; Wilkinson, P.; Matheson, D., "High power frequency multipliers to 330

GHz," Microwave Integrated Circuits Conference (EuMIC), 2010 European , vol., no., pp.232,233, 27-28 Sept. 2010

[Ald11]   Alderman, B.; Henry, M.; Sanghera, H.; Hui Wang; Rea, S.; Ellison, B.; de Maagt, P., "Schottky diode technology at Rutherford Appleton Laboratory," Microwave Technology & Computational Electromagnetics (ICMTCE), 2011 IEEE International Conference on , vol., no., pp.4,6, 22-25 May 2011 doi: 10.1109/ICMTCE.2011.5915577

[ALFA]   http://www.alfaimaging.com/

[ANS]

            http://www.ansys.com/Products/Simulation+Technology/Electromagnetics/Signal+Integrity/ANSYS+HFSS

[Ali93]   W.Y. Ali-Ahmad and W. L. Bishop, "An 86-106 GHz quasi-integrated low noise schottky receiver," in IEEE Trans. Microw. Theory and Tech., vol. 41, no. 4, pp. 558-564, Apr. 1993. doi: 10.1109/22.231646.

[App07]   Appleby, R.; Anderton, R.N., "Millimeter-Wave and Submillimeter-Wave Imaging for Security and Surveillance," Proceedings of the IEEE , vol.95, no.8, pp.1683,1690, Aug. 2007 doi: 10.1109/JPROC.2007.898832

[Bae11]   Tae-Jon Baek; Dong-Sik Ko; Sang-Jin Lee; Yong-Hyun Baek; Min Han; Seok-Gyu Choi; Jae-Hyun Choi; Wan-Joo Kim; Jin-Koo Rhee, "A Transceiver Module for FMCW Radar Sensors Using 94-GHz Dot-Type Schottky Diode Mixer," Sensors Journal, IEEE , vol.11, no.2, pp.370,376, Feb. 2011 doi: 10.1109/JSEN.2010.2057419

[Bal97]   C.A. Balanis, "Antena Theory," 2nd ed. John Wiley & Sons, 1997.

[Bar06]   Baryshev, A.M.; Mena, F. P.; Hesper, R.; Zijlstra, T.; Lodewijk, C. F J; Wild, W.; Klapwijk, T.M., "A Waveguide NbTiN SIS Mixer for THz Array Applications," Infrared Millimeter Waves and 14th International Conference on Teraherz Electronics, 2006. IRMMW-THz 2006. Joint 31st International Conference on , vol., no., pp.392,392, 18-22 Sept. 2006 doi: 10.1109/ICIMW.2006.368600

[Bass12] Bassi, M.; Bevilacqua, A.; Gerosa, A.; Neviani, A., "Integrated SFCW Transceivers for UWB Breast Cancer Imaging: Architectures and Circuit Constraints," Circuits and Systems I: Regular Papers, IEEE Transactions on , vol.59, no.6, pp.1228,1241, June 2012 doi: 10.1109/TCSI.2011.2173400

[Bed04]   Bedorf, S.; Munoz, P.; Brandt, M.; Pütz, P.; Honingh, N.; Jacobs, K., "Development of phonon-cooled NbTiN HEB heterodyne mixers for THz applications," Infrared and Millimeter Waves, 2004 and 12th International Conference on Terahertz Electronics, 2004. Conference Digest of the 2004 Joint 29th International Conference on , vol., no., pp.455,456, 27 Sept.-1 Oct. 2004 doi: 10.1109/ICIMW.2004.1422160

[Bee29]   Beers, G. L.; Carlson, W. L., "Recent Developments in Superheterodyne Receivers," Radio Engineers, Proceedings of the Institute of , vol.17, no.3, pp.501,515, March 1929 doi: 10.1109/JRPROC.1929.221699

[Ber10]   Berenguer, R.; Gui Liu; Akhiyat, A.; Kamtikar, K.; Yang Xu, "A 43.5mW 77GHz receiver front-end in 65nm CMOS suitable for FM-CW Automotive Radar," Custom Integrated Circuits Conference (CICC), 2010 IEEE , vol., no., pp.1,4, 19-22 Sept. 2010 doi: 10.1109/CICC.2010.5617449

[Bil12]   Billade, B.; Nystrom, O.; Meledin, D.; Sundin, E.; Lapkin, I.; Fredrixon, M.; Desmaris, V.; Rashid, H.; Strandberg, M.; Ferm, S.-E.; Pavolotsky, A.; Belitsky, V., "Performance of the First

ALMA Band 5 Production Cartridge," Terahertz Science and Technology, IEEE Transactions on , vol.2, no.2, pp.208,214, March 2012 doi: 10.1109/TTHZ.2011.2182220

[Bo12]   Xiang Bo; Dou Wenbin; He Minmin, "A subharmonic mixer at W band," Microwave and Millimeter Wave Technology (ICMMT), 2012 International Conference on , vol.3, no., pp.1,3, 5-8 May 2012 doi: 10.1109/ICMMT.2012.6230211

[Bog09]   Bogue, R., 2009. Terahertz imaging: A report on progress. Sensor Review, 29(1), 6-12.

[Car02]   A. Cardama, L. Jofre, J.M. Rius, J. Romeu, S. Blanch and M. Ferrando, "Antenas," Ed. UPC, 2nd ed., 2002.

[Cha07]   Chan, W.L., Deibel, J. and Mittleman, D.M., 2007. Imaging with terahertz radiation. Reports on Progress in Physics, 70(8), 1325-1379.

[Che10a]   Zhe Chen; Bo Zhang; Yong Fan; Shixi Zhang; Xiaofan Yang, "Design of a 118-GHz sub-harmonic mixer using foundry diodes," in Int. Symp. on Signals Systems and Electronics (ISSSE), vol.1, no., pp.1-3, 17-20 Sept. 2010. doi: 10.1109/ISSSE.2010.5607108.

[Che10b]   Chen, A.Y.-K.; Baeyens, Y.; Chen, Y.-K.; Lin, J., "21 dB gain 87 GHz low-noise amplifier using 0.18 m SiGe BiCMOS," Electronics Letters , vol.46, no.5, pp.332,333, March 4 2010 doi: 10.1049/el.2010.0155

[Che10c]   Chun-Cheng Wang; Zhiming Chen; Jain, V.; Heydari, P., "A 80-92-GHz Receiver Front-End Using Slow-Wave Transmission Lines in 65nm CMOS," Compound Semiconductor Integrated Circuit Symposium (CSICS), 2010 IEEE , vol., no., pp.1,4, 3-6 Oct. 2010 doi: 10.1109/CSICS.2010.5619664

[Che12]   Zhenhua Chen; Jinping Xu, "Design of a V-band single-substrate single-waveguide power-combined frequency doubler covering 50–75 GHz band," Microwave Workshop Series on Millimeter Wave Wireless Technology and Applications (IMWS), 2012 IEEE MTT-S International , vol., no., pp.1,4, 18-20 Sept. 2012 doi: 10.1109/IMWS2.2012.6338234.

[Che13]   Peng Chen; Xian-Jin Deng; Bin-Bin Cheng; Cheng Wang, "A 220GHz frequency doubler based on plannar Schottky diodes," Infrared, Millimeter, and Terahertz Waves (IRMMW-THz), 2013 38th International Conference on , vol., no., pp.1,2, 1-6 Sept. 2013 doi: 10.1109/IRMMW-THz.2013.6665892

[Chr02]   Christopher, S.; Rewankar, G. R.; Abid Hussain, V.A; Rama Prasad, N., "Rugged receiver for airborne application," Microwaves, Radar and Wireless Communications, 2002. MIKON-2002. 14th International Conference on , vol.2, no., pp.663,668 vol.2, 2002 doi: 10.1109/MIKON.2002.1017932

[Cie00]   Ciesla, C.M., Arnone, D.D., Corchia, A., Crawley, D., Longbottom, C., Linfield, E.H. and Pepper, M., 2000. Biomedical applications of Terahertz Pulse Imaging, Commercial and Biomedical Applications of Ultrafast Lasers II, 24 January 2000 through 25 January 2000, Society of Photo-Optical Instrumentation Engineers pp73-81.

[Coo11]   Cooper, K.B.; Dengler, R.J.; Llombart, N.; Thomas, B.; Chattopadhyay, G.; Siegel, P.H., "THz Imaging Radar for Standoff Personnel Screening," Terahertz Science and Technology, IEEE Transactions on, vol.1, no.1, pp.169,182, Sept. 2011 doi: 10.1109/TTHZ.2011.2159556

[Cro87]   Crowe, T.W.; Mattauch, R.J., "Analysis and Optimization of Millimeter-And Submillimeter-Wavelength Mixer Diodes," Microwave Theory and Techniques, IEEE

Transactions on , vol.35, no.2, pp.159,168, Feb 1987 doi: 10.1109/TMTT.1987.1133618

[Cun11]   Cunningham, Paul D.; Valdes, Nestor N.; Vallejo, Felipe A.; Hayden, L. Michael; Polishak, Brent; Zhou, Xing-Hua; Luo, Jingdong; Jen, Alex K.-Y.; Williams, Jarrod C.; Twieg, Robert J., "Broadband terahertz characterization of the refractive index and absorption of some important polymeric and organic electro-optic materials," in J. Appl. Phys., vol. 109, 043505, pp. 043505-043505-5, 2011. doi: 10.1063/1.3549120.

[Day03]   Peter K. Day, Henry G. LeDuc, Benjamin A. Mazin, Anastasios Vayonakis & Jonas Zmuidzinas "A broadband superconducting detector suitable for use in large arrays". Nature Vol 425, 23 October 2003.

[Dav08]   Davies, A.G., Burnett, A.D., Fan, W., Linfield, E.H. and Cunningham, J.E., 2008. Terahertz spectroscopy of explosives and drugs. Materials Today, 11(3), 18-26.

[Dea07]   Deal, W.R.; Mei, X.B.; Radisic, V.; Yoshida, W.; Liu, P. -H; Uyeda, J.; Barsky, M.; Gaier, T.; Fung, A.; Lai, R., "Demonstration of a S-MMIC LNA with 16-dB Gain at 340-GHz,"Compound Semiconductor Integrated Circuit Symposium, 2007. CSIC 2007. IEEE , vol., no., pp.1,4, 14-17 Oct. 2007 doi: 10.1109/CSICS07.2007.19

[Dem11]   Demirel, N.; Severino, R.R.; Ameziane, C.; Taris, T.; Begueret, J-B; Kerherve, E.; Mariano, A.; Pache, D.; Belot, D., "Millimeter-wave chip set for 77–81 GHz automotive radar application," New Circuits and Systems Conference (NEWCAS), 2011 IEEE 9th International , vol., no., pp.253,256, 26-29 June 2011 doi: 10.1109/NEWCAS.2011.5981303

[Den98]   R.J. Dengler, A. Hampachern, P. H. Siegel, "A Fully Automated High-Accuracy RF/IF Test System for Millimeter- and Submillimeter-wave Mixers", IEEE MTT-S International Microwave Symposium Digest, vol.3, no., pp.1719-1722 vol.3, 7-12 Jun 1998.

[DIG]   http://www.digitalbarriers.com/

[Dra13]   Drakinskiy, V.; Sobis, P.; Zhao, H.; Bryllert, T.; Stake, J., "Terahertz GaAs Schottky diode mixer and multiplier MIC's based on e-beam technology," Indium Phosphide and Related Materials (IPRM), 2013 International Conference on , vol., no., pp.1,2,   19-23   May   2013 doi: 10.1109/ICIPRM.2013.6562606

[End09]   Endo, A.; Noguchi, Takashi; Kroug, M.; Shitov, S.V.; Shan, W.; Tamura, T.; Kojima, T.; Uzawa, Y.; Sakai, T.; Inoue, H.; Kohno, K., "A THz SIS Mixer With a NbTiN-Ground Plane and SIS Microtrilayers Directly Grown on a Quartz Substrate," Applied Superconductivity, IEEE Transactions on , vol.19,   no.3,   pp.400,404,   June   2009   doi: 10.1109/TASC.2009.2019053

[ESA11]   European Space Agency, "Reliability Assesment of Mixers and Multipliers for Microwave Imaging Radiomenters", Statement of Work, Appendix 1 to AO 1-6900/11/NL/CT, IPD-SOW-189, 25-07-2011

[Eta11]   Etayo, D.; Iriarte, J.-C.; Palacios, I.; Maestrojuan, I.; Teniente, J.; Ederra, I.; Gonzalo, R., "THz imaging system for industrial quality control," Microwave Workshop Series on Millimeter Wave Integration Technologies (IMWS), 2011 IEEE MTT-S International , vol., no., pp.172,175, 15-16 Sept. 2011 doi: 10.1109/IMWS3.2011.6061867

[Fab85]   M. T. Faber, J. W. Archer, "Computed Aided Testing of Mixers Between 90 and 350 GHz", IEEE Transactions on Microwave Theory and Techniques, vol.33, no.11, pp. 1138- 1145, Nov 1985.

[FAR]   http://www.farran.com/shop/sub-harmonic-mixers/

[Fis53]   Fisher, D.H.; Segrave, P.A; Watts, AJ., "The design of a superheterodyne receiver for television," Electrical Engineers, Journal of the Institution of , vol.1953, no.4, pp.179,180, April 1953 doi: 10.1049/jiee-2.1953.0120

[Fis13]   Fischer, B.M.; Wietzke, S.; Reuter, M.; Peters, O.; Gente, R.; Jansen, C.; Vieweg, N.; Koch, M., "Investigating Material Characteristics and Morphology of Polymers Using Terahertz Technologies, "Investigating material characteristics and morphology of polymers using terahertz technologies," in IEEE Trans. on Terahertz Science and Technology, vol. 3, no. 3, pp. 259-267, May 2013. doi: 10.1109/TTHZ.2013.2255916.

[Foc04]   Focardi, P.; McGrath, William R., "Analysis and design of Terahertz HEB mixers and detectors [hot electron bolometer mixers]," Antennas and Propagation Society International Symposium, 2004. IEEE , vol.1, no., pp.986,989 Vol.1, 20-25 June 2004 doi: 10.1109/APS.2004.1329838

[Fri11]   Friederich, F.; Von Spiegel, W.; Bauer, M.; Fanzhen Meng; Thomson, M.D.; Boppel, S.; Lisauskas, A.; Hils, B.; Krozer, V.; Keil, A.; Loffler, T.; Henneberger, R.; Huhn, A.K.; Spickermann, G.; Bolivar, P.H.; Roskos, H.G., "THz Active Imaging Systems With Real-Time Capabilities," Terahertz Science and Technology, IEEE Transactions on , vol.1, no.1, pp.183,200, Sept. 2011 doi: 10.1109/TTHZ.2011.2159559

[Fut12]   Futatsumori, S.; Kohmura, A.; Yonemoto, N.; Kobayashi, K.; Okuno, Y., "Small transmitting power and high sensitivity

76GHz millimeter-wave radar for obstacle detection and collision avoidance of civil helicopters," Radar Conference (EuRAD), 2012 9th European , vol., no., pp.178,181, Oct. 31 2012-Nov. 2 2012

[Gai98] Gaidis, M.C.; Pickett, H.M.; Siegel, P.H.; Smith, C. D.; Smith, R.P.; Martin, S.C., "A 2.5 THz receiver front-end for spaceborne applications," Terahertz Electronics Proceedings, 1998. THz Ninety Eight. 1998 IEEE Sixth International Conference on , vol., no., pp.13,17, 3-4 Sep 1998 doi: 10.1109/THZ.1998.731652

[Gal95] Galin, I., "Millimeter-wave mixers with Schottky diodes, for superheterodyne spaceborne radiometers-review and predictions," Signals, Systems, and Electronics, 1995. ISSSE '95, Proceedings., 1995 URSI International Symposium on , vol., no., pp.153,156, 25-27 Oct 1995 doi: 10.1109/ISSSE.1995.497956

[Ger05] Gerecht, E.; Gu, D.; Yngvesson, S.; Rodriguez-Morales, F.; Zannoni, R.; Nicholson, J., "HEB FPA imaging technology for security and biomedical applications," Infrared and Millimeter Waves and 13th International Conference on Terahertz Electronics, 2005. IRMMW-THz 2005. The Joint 30th International Conference on , vol.1, no., pp.9,10 vol. 1, 19-23 Sept. 2005 doi: 10.1109/ICIMW.2005.1572380

[Ger07] Gerecht, E.; Gu, D.; You, L.; Yngvesson, S., "Advanced imaging and spectroscopy of biological and chemical agents at terahertz frequencies," Infrared and Millimeter Waves, 2007 and the 2007 15th International Conference on Terahertz Electronics. IRMMW-THz. Joint 32nd International Conference on , vol., no., pp.750,751, 2-9 Sept. 2007

[Gib10] Gibson, H.J.E.; Walber, A.; Zimmermann, R.; Alderman, B.; Cojocari, O., "Improvements in schottky harmonic and sub-

harmonic mixers for use up to 900 GHz," in Proc. of the European Integrated Circuits Conf., Paris, France, vol., no., pp. 230,231, 27-28 Sept. 2010.

[Gue13]   Guerra, J.M.; Siligaris, A.; Lampin, J.-F.; Danneville, F.; Vincent, P., "A 283 GHz low power heterodyne receiver with on-chip local oscillator in 65 nm CMOS process,"Radio Frequency Integrated Circuits Symposium (RFIC), 2013 IEEE , vol., no., pp.301,304, 2-4 June 2013 doi: 10.1109/RFIC.2013.6569588

[Gui05]   Le Guillou, Y.; Gaborieau, O.; Gamand, P.; Isberg, M.; Jakobsson, P.; Jonsson, L.; Le Deaut, D.; Marie, H.; Mattisson, S.; Monge, L.; Olsson, T.; Prouet, S.; Tired, T., "Highly integrated direct conversion receiver for GSM/GPRS/EDGE with on-chip 84-dB dynamic range continuous-time ADC," Solid-State Circuits, IEEE Journal of , vol.40, no.2, pp.403,411, Feb. 2005 doi: 10.1109/JSSC.2004.841036

[Gun08]   S.E. Gunnarsson,"Analysis and Design of a Novel x 4 Subharmonically Pumped Resistive HEMT Mixer," Microwave Theory and Techniques, IEEE Transactions on , vol.56, no.4, pp.809,816, April 2008

[Guo08]   Fan Guoli; Jiang Yuesong; Qu Xiaosheng, "Optimization of a Schottky Mixer Diode for THz Heterodyne Detection," Education Technology and Training, 2008. and 2008 International Workshop on Geoscience and Remote Sensing. ETT and GRS 2008. International Workshop on , vol.1, no., pp.468,471, 21-22 Dec. 2008 doi: 10.1109/ETTandGRS.2008.142

[Hai07]   Hai-Bo Liu; Zhong, Hua; Karpowicz, Nicholas; Chen, Yunqing; Xi-Cheng Zhang, "Terahertz Spectroscopy and Imaging for Defense and Security Applications," Proceedings of the IEEE ,

vol.95, no.8, pp.1514,1527, Aug. 2007 doi: 10.1109/JPROC.2007.898903

[Han11] Hantscher, S.; Hagelen, M.; Lang, S.; Essen, H.; Wieneke, M.; Koch, W.; Tessmann, A., "Security assistant system combining millimetre wave radar sensors and chemical sensors," Antennas and Propagation (APSURSI), 2011 IEEE International Symposium on , vol., no., pp.216,219, 3-8 July 2011 doi: 10.1109/APS.2011.5996681

[Heg85] Hegazi, G.; Jelenski, A., "Limitations of Microwave and Millimeter-Wave Mixers Due to Excess Noise," Microwave Symposium Digest, 1985 IEEE MTT-S International , vol., no., pp.431,435, 4-6 June 1985 doi: 10.1109/MWSYM.1985.1132003

[Her11] Herschell Space Observatory, "HIFI Observers´ Manual, Update for Start of GT2 Observations," HERSCHEL-HSC-DOC-0784, version 2.3, 31-March-2011.

[Hes96] J.L. Hesler, "Planar Schottky Diodes in Submillimeter-wavelength Waveguides Receivers," Ph.D. Dissertation, University of Virginia, VA, January 1996.

[Hes97] J. L. Hesler, K Hui, R M Weikle, T W Crowe, "Design, analysis and scale model testing of fixed-tuned broadband waveguide to microstrip transitions," in 8th Int. Symp. on Space Terahertz Technology, Harvard University, Mar. 1997.

[Hes99] J. L. Hesler, K. Hui, S. He, T. W. Crowe, "A Fixed-Tuned 400 GHz Subharmonic Mixer Using Planar Schottky Diodes" 10th International Symposium on Space Terahertz Technology, Charlottesville, March 1999.

[Hes00] J.L. Hesler, "Broadband fixed-tuned subharmonic receivers to 640 GHz," Proceeding to 11th Int. Symposium on Space and Terahertz Tech., pp. 172-178, Michigan May 2000.

[Hoe14]   Hoefle, M.; Penirschke, A.; Cojocari, O.; Decoopman, T.; Trier, M.; Piironen, P.; Périchaud, M.G.; Jakoby, R., "89 GHz zero-bias Schottky detector for direct detection radiometry in European satellite programme MetOp-SG," Electronics Letters , vol.50, no.8, pp.606,608, April 10 2014 doi: 10.1049/el.2014.0222

[Hro13]   Hrobak, M.; Sterns, M.; Schramm, M.; Stein, W.; Poprawa, F.; Ziroff, A; Schur, J.; Schmidt, L.-P., "Planar D-band frequency doubler and Y-band tripler on PTFE laminates," Infrared, Millimeter, and Terahertz Waves (IRMMW-THz), 2013 38th International Conference on , vol., no., pp.1,2, 1-6 Sept. 2013 doi: 10.1109/IRMMW-THz.2013.6665856

[Hu95]   HU, B.B. and NUSS, M.C., 1995. Imaging with terahertz waves. Opt.Lett., 20(16), 1716-1718.

[Hu11]   Sanming Hu; Yong-Zhong Xiong; Lei Wang; Jinglin Shi; Teck-Guan Lim, "A 77–135GHz down-conversion IQ mixer for 10Gbps multiband applications," Integrated Circuits (ISIC), 2011 13th International Symposium on , vol., no., pp.29,34, 12-14 Dec. 2011 doi: 10.1109/ISICir.2011.6131872

[Hui00]   Hui, K.; Hesler, J.L.; Kurtz, D.S.; Bishop, W.L.; Crowe, T.W., "A micromachined 585 GHz Schottky mixer," Microwave and Guided Wave Letters, IEEE , vol.10, no.9, pp.374,376, Sept. 2000 doi: 10.1109/75.867855

[Hwa05]   J. S. Hwang and K. I. Lin, "Characteristics of terahertz radiation and its applications in imaging and material science," Appl. Phys. Lett. 86, 054105, 2005.

[Iac09]   Iacono, A; Neto, A; Gerini, G.; Baselmans, J.; Yates, S.; Baryshev, A; Hoevers, H., "Kinetic inductance detectors based receiver array architectures for imaging at THz

frequency,"Microwave Conference, 2009. EuMC 2009. European , vol., no., pp.830,833, Sept. 29 2009-Oct. 1 2009.

[Iha95] Ihara, T.; Manabe, T.; Fujita, M.; Matsui, T.; Sugimoto, Y., "Research activities on millimeter-wave indoor wireless communication systems at CRL," Universal Personal Communications. 1995. Record., 1995 Fourth IEEE International Conference on , vol., no., pp.197,200, 6-10 Nov 1995 doi: 10.1109/ICUPC.1995.496887

[Iri11] Iriarte, J.-C.; Etayo, D.; Palacios, I.; Maestrojuan, I.; Liberal, I.; Rebollo, A.; Teniente, J.; Ederra, I.; Gonzalo, R., "Water content evolution in leaves based on active THz imaging system," Antennas and Propagation (EUCAP), Proceedings of the 5th European Conference on , vol., no., pp.1049,1050, 11-15 April 2011

[Kan10] Kangaslahti, P., "Recent developments in 180 GHZ MMIC LNA and receiver technology," Microwave Radiometry and Remote Sensing of the Environment (MicroRad), 2010 11th Specialist Meeting on , vol., no., pp.272,275, 1-4 March 2010 doi: 10.1109/MICRORAD.2010.5559547

[Kan11] T. W. Kang, J. H. Kim, J. G. Lee, J. I. Park, D. C. Kim, "Determing Noise Temperature of a Noise Source Using Calibrated Noise Sources and RF Attenuator", IEEE Transactions on Instrumentation and Measurement, vol.60, no.7, pp.2558-2563, July 2011.

[Ker14] Kerr, A.R.; Shing-Kuo Pan; Claude, S.M.X.; Dindo, P.; Lichtenberger, A.W.; Effland, J.E.; Lauria, E.F., "Development of the ALMA Band-3 and Band-6 Sideband-Separating SIS Mixers," Terahertz Science and Technology, IEEE Transactions on , vol.4, no.2, pp.201,212, March 2014 doi: 10.1109/TTHZ.2014.2302537

[Kim05]   Young Jin Kim; Young-Suk Son; Parkhomenko, V.N.; In-Chul
           Hwang; Je-Kwang Cho; Kyung-Suc Nah; Byeong-Ha Park, "A
           GSM/EGSM/DCS/PCS direct conversion receiver with
           integrated synthesizer," Microwave Theory and Techniques,
           IEEE Transactions on , vol.53, no.2, pp.606,613, Feb. 2005
           doi: 10.1109/TMTT.2004.840737

[Kim12]   Kim, G.; Lee, S. D.; Moon, J. H.; Kim, K. B.; Lee, D. K.,
           "Terahertz technology for the detection of food
           contaminants," Infrared, Millimeter, and Terahertz Waves
           (IRMMW-THz), 2012 37th International Conference on , vol.,
           no., pp.1,2, 23-28 Sept. 2012 doi: 10.1109/IRMMW-
           THz.2012.6380163

[Lau01]   E. F. Lauria, A. R. Kerr, M. W. Popieszalski, S. K. Pan, J. E.
           Effland, A.W. Lichtenberger, "Alma MEMO 378: A 200-300
           GHz SIS Mixer-preamplifier with 8GHz IF Bandwidth", 2001
           IEEE International Microwave Symposium, Phoenix, AZ, May
           2001.

[Leo99]   Yoke-Choy Leong; Weinreb, S., "Full band waveguide-to-
           microstrip probe transitions," Microwave Symposium Digest,
           1999 IEEE MTT-S International , vol.4, no., pp.1435,1438
           vol.4, 13-19 June 1999 doi: 10.1109/MWSYM.1999.780219

[Li12]   Hao Li; Bo Zhang; Yong Fan, "A terahertz frequency tripler
           with single serial varactor diode," Microwave and Millimeter
           Wave Circuits and System Technology (MMWCST), 2012
           International Workshop on , vol., no., pp.1,4, 19-20 April 2012
           doi: 10.1109/MMWCST.2012.6238137.

[Liu07]   Liu, H.-., Zhong, H., Karpowicz, N., Chen, Y. and Zhang, X.-.,
           2007. Terahertz spectroscopy and imaging for defence and
           security applications. Proceedings of the IEEE, 95(8), 1514-
           1527.

[Liu12]   Wei Liu; Yong Zhang; Qiuquan Lu, "Design of a compact 150 GHz subharmonic mixer with high isolation," Microwave and Millimeter Wave Technology (ICMMT), 2012 International Conference on , vol.2, no., pp.1,3, 5-8 May 2012 doi: 10.1109/ICMMT.2012.6230096

[Llo08]   Llombart, N.; Bryllert, T.; Chattopadhyay, G.; Cooper, K.; Dengler, R.; Gill, J.; McNary, A.J.; Mehdi, I.; Schlecht, E.; Skalare, A.; Siegel, P.H., "THZ Heterodyne Imaging Applicatiions, Instruments and Directions," Microwave Conference, 2008. EuMC 2008. 38th European , vol., no., pp.947,950, 27-31 Oct. 2008 doi: 10.1109/EUMC.2008.4751611

[Llo10]   Llombart, N.; Cooper, K.B.; Dengler, R.J.; Bryllert, T.; Siegel, P.H., "Confocal Ellipsoidal Reflector System for a Mechanically Scanned Active Terahertz Imager," Antennas and Propagation, IEEE Transactions on , vol.58, no.6, pp.1834,1841, June 2010 doi: 10.1109/TAP.2010.2046860

[Löf01]   Löffler, T., Bauer, T., Siebert, K.J., Roskos, H.G., Fitzgerald, A. and Czasch, S., 2001. Terahertz dark-field imaging of biomedical tissue. Optics Express, 9(12), 616-621.

[Lu12]   Qiuquan Lu; Yong Zhang; Wei Liu; Peihan Zhou; Yonglun Wu, "Design of a 225 GHz frequency tripler using planar Schottky diode," Microwave and Millimeter Wave Technology (ICMMT), 2012 International Conference on , vol.4, no., pp.1,4, 5-8 May 2012 doi: 10.1109/ICMMT.2012.6230243

[Maa93]   S.A. Maas, "Microwave Mixers", 2nd ed., Artech House microwave library, Dec. 1, 1993.

[Maa98]   S.A. Maas "The RF and Microwave Circuit Design Cookbook," Artech House microwave library, 1998.

[Maa03]   S.A. Maas, "Nonlinear Microwave and RF Circuits", 2nd ed. Artech House microwave library, 2003.

[Maa05]   Stephen A. Maas, "Noise in Linear and Nonlinear Circuits", The Artech House Microwave Library, August 31, 2005.

[Mae08a]   Maestrini, A.; Ward, J.S.; Tripon-Canseliet, C.; Gill, J.J.; Choonsup Lee; Javadi, H.; Chattopadhyay, G.; Mehdi, I., "In-Phase Power-Combined Frequency Triplers at 300 GHz,"Microwave and Wireless Components Letters, IEEE , vol.18, no.3, pp.218,220, March 2008 doi: 10.1109/LMWC.2008.916820

[Mae08b]   Maestrini, A.; Ward, J.; Chattopadhyay, G.; Schlecht, E.; Gill, J.; Choonsup Lee; Javadi, H.; Mehdi, I., "In-phase power combining of submillimeter-wave multipliers," Infrared, Millimeter and Terahertz Waves, 2008. IRMMW-THz 2008. 33rd International Conference on , vol., no., pp.1,2, 15-19 Sept. 2008 doi: 10.1109/ICIMW.2008.4665533

[Man98]   C. M. Mann, "Mixers for the Millimetre, Submillimetre and Terahertz Regions", 28th European Microwave Conference Amsterdam 1998

[Mao12]   Yanfei Mao, K. Schmalz, J. Borngraber, J.C. Scheytt, "245-GHz LNA, Mixer, and Subharmonic Receiver in SiGe Technology," Microwave Theory and Techniques, IEEE Transactions on , vol.60, no.12, pp.3823,3833, Dec. 2012

[Mar01]   Martin, S.; Nakamura, B.; Fung, A.; Smith, P.; Bruston, J.; Maestrini, A.; Maiwald, F.; Siegel, P.; Schlecht, E.; Mehdi, I., "Fabrication of 200 to 2700 GHz multiplier devices using GaAs and metal membranes," Microwave Symposium Digest, 2001 IEEE MTT-S International , vol.3, no., pp.1641,1644 vol.3, 20-24 May 2001 doi: 10.1109/MWSYM.2001.967219

[Mar12]   Richard Martin, Christopher Schuetz, Thomas Dillon, Daniel Mackrides, Peng Yao, Kevin Shreve, Charles Harrity, Alicia Zablocki, Brock Overmiller, Petersen Curt, James Bonnett, Andrew Wright, John Wilson, Shouyaun Shi and Dennis Prather"Optical up-conversion enables capture of millimeter-wave video with an IR camera," 13 August 2012, SPIE Newsroom. DOI: 10.1117/2.1201208.004406

[Meh68]   Mehal, E.W.; Wacker, R.W., "GaAs integrated microwave circuits," Electron Devices, IEEE Transactions on , vol.15, no.7, pp.513,516, Jul 1968 doi: 10.1109/T-ED.1968.16390

[Meh98]   Mehdi, I.; Marazita, S.M.; Humphrey, D.A.; Trong-Huang Lee; Dengler, R.J.; Oswald, J.E.; Pease, A.J.; Martin, S.C.; Bishop, W.L.; Crowe, T.W.; Siegel, P.H., "Improved 240-GHz subharmonically pumped planar Schottky diode mixers for space-borne applications," Microwave Theory and Techniques, IEEE Transactions on , vol.46, no.12, pp.2036,2042, Dec 1998 doi: 10.1109/22.739280

[Meh04]   Mehdi, I.; Mazed, M.; Dengler, R.; Pease, A.; Natzic, M.; Siegel, P.H., "Planar GaAs Schottky diodes integrated with quartz substrate circuitry for waveguide subharmonic mixers at 215 GHz," Microwave Symposium Digest, 1994., IEEE MTT-S International , vol., no., pp.779,782 vol.2, 23-27 May 1994 doi: 10.1109/MWSYM.1994.335240

[MIC]   http://www.microsemi.com/products/screening-solutions

[Mic13]   R.S. Michaelsen, T.K. Johansen, V. Krozer, "Design of a ×4 subharmonic sub-millimeter wave diode mixer, based on an analytic expression for small-signal conversion admittance parameters,"Microwave & Optoelectronics Conference (IMOC), 2013 SBMO/IEEE MTT-S International , vol., no., pp.1,4, 4-7 Aug. 2013

[MIL]   http://www.millivision.com/

[Mit05]   MITTLEMAN, D.M., 2005. Imaging and sensing with terahertz radiation, Review of Progress in Quantitative Nondestructive Evaluation, 25 July 2004 through 30 July 2004 2005, pp25-32.

[Mit99]   MITTLEMAN, D.M., GUPTA, M., NEELAMANI, R., BARANIUK, R.G., RUDD, J.V. and KOCH, M., 1999. Recent advances in terahertz imaging. Applied Physics B: Lasers and Optics, 68(6), 1085-1094.

[Miy05]   Miyamaru, F.; Otani, C.; Kawase, K., "Terahertz imaging and sensing," Lasers and Electro-Optics Society, 2005. LEOS 2005. The 18th Annual Meeting of the IEEE , vol., no., pp.118,119, 22-28 Oct. 2005 doi: 10.1109/LEOS.2005.1547898

[Mor05]   Morschbach, M.; Muller, A.; Schollhorn, C.; Oehme, M.; Buck, T.; Kasper, E., "Integrated silicon Schottky mixer diodes with cutoff frequencies above 1 THz," Microwave Theory and Techniques, IEEE Transactions on , vol.53, no.6, pp.2013,2018, June 2005 doi: 10.1109/TMTT.2005.848831

[Nal13]   Nallappan, K.; Dash, J.; Ray, S.; Pesala, B., "Identification of adulterants in turmeric powder using terahertz spectroscopy," Infrared, Millimeter, and Terahertz Waves (IRMMW-THz), 2013 38th International Conference on , vol., no., pp.1,2, 1-6 Sept. 2013 doi: 10.1109/IRMMW-THz.2013.6665688

[Nar13]   Naruse, M.; Sekimoto, Y.; Noguchi, T.; Miyachi, A; Karatsu, K.; Nitta, T.; Sekine, M.; Uzawa, Y.; Taino, T.; Myoren, H., "Optical Efficiencies of Lens-Antenna Coupled Kinetic Inductance Detectors at 220 GHz," Terahertz Science and Technology, IEEE Transactions on , vol.3, no.2, pp.180,186, March 2013 doi: 10.1109/TTHZ.2012.2237029

[Nas13]   Nasr, I.; Weigel, R.; Kissinger, D., "Broadband millimeter-wave receiver front-ends in silicon-germanium technology for multi-band communication systems," Microwave Symposium Digest (IMS), 2013 IEEE MTT-S International , vol., no., pp.1,3, 2-7 June   2013
           doi: 10.1109/MWSYM.2013.6697542

[Nie09]   K. Nielsen H. K. Rasmussen, A. J. L. Adam, P.C. M. Planken, O.Bang, P.Uhd Jepsen, "Bendable, low-loss topas fibers for the terahertz frequency range," in Opt. Express 17, pp.8592-9601, 2009.

[OMN]   http://www.omnisys.se/index.php

[Pav13]   Pavanello, Fabio; Garet, Frederic; Kuppam, Mohan-Babu; Peytavit, Emilien; Vanwolleghem, Mathias; Vaurette, Francois; Coutaz, Jean-Louis; Lampin, Jean-Francois, "Broadband ultra-low-loss mesh filters on flexible cyclic olefin copolymer films for terahertz applications," in Appl. Physics Lett., vol. 102, 111114, 2013. doi:10.1063/1.4798522.

[Pey11]   Peytavit, E.; Donche, C.; Lepilliet, S.; Ducournau, G.; Lampin, J.-F., "Thin film transmission lines using cyclic olefin copolymer for millimeter-wave and terahertz integrated circuits," Elec. Lett., vol. 47, no. 7,pp. 453, 454, March 31 2011. doi: 10.1049/el.2011.0369.

[Pic06]   Pickwell, E. and Wallace, V.P., 2006. Biomedical applications of terahertz technology. Journal of Physics D: Applied Physics, 39(17).

[Por03]   Porterfield, David; Hesler, J.; Crowe, Thomas; Bishop, William; Woolard, D., "Integrated Terahertz Transmit/Receive Modules," Microwave Conference, 2003. 33rd European , vol., no., pp.1319,1322, Oct. 2003 doi: 10.1109/EUMA.2003.340862

[Pos86]   M. W. Pospeszalski, "On the Noise Parameters of Isolator and Receiver with Isolator at the Input",IEEE Transactions on Microwave Theory and Techniques, vol.34, no.4, pp. 451- 453, Apr 1986.

[Poz01]   D.M. Pozar, "Microwave and RF Design of Wireless Systems," John Wiley & Sons, 2001.

[Poz05]   D. M. Pozar, "Microwave Engineering," 3rd ed., John Wiley & Sons, Inc. 2005.

[Puk08]   Pukala, D.; Samoska, L.; Gaier, T.; Fung, A.; Mei, X.B.; Yoshida, W.; Lee, J.; Uyeda, J.; Liu, P. -H; Deal, W.R.; Radisic, V.; Lai, R., "Submillimeter-Wave InP MMIC Amplifiers From 300–345 GHz," Microwave and Wireless Components Letters, IEEE , vol.18, no.1, pp.61,63, Jan. 2008 doi: 10.1109/LMWC.2007.912047

[Qua03]   Quan Xue; Karn Man Shum; Chi-Hou Chan, "Low conversion-loss fourth subharmonic mixers incorporating CMRC for millimeter-wave applications," Microwave Theory and Techniques, IEEE Transactions on , vol.51, no.5, pp.1449,1454, May 2003

[QIN]   http://www.qinetiq.com/Pages/default.aspx

[Räi80]   A. Räisänen, "Experimental studies on cooled millimeter wave mixers," Acta Polytechnica Scandinavica 46, 1980.

[RAP]   http://www.rapiscansystems.com/

[Roh12]   Rohde&Schwarz, "The Y Factor Technique for Noise Figure Measurements," Applicat. Note 1MA178-1E, July 2012.

[Rod10]   Rodriguez-Morales, F.; Yngvesson, K.S.; Dazhen Gu, "Wideband IF-Integrated Terahertz HEB Mixers: Modeling and Characterization," Microwave Theory and Techniques, IEEE

Transactions on , vol.58, no.5, pp.1140,1150, May 2010 doi: 10.1109/TMTT.2010.2045566

[Sem08]   Semenov, A., Richter, H., Böttger, U. and Hübers, H.-., 2008. Imaging terahertz radar for security applications, Terahertz for Military and Security Applications VI, 18 March 2008 through 19 March 2008 2008.

[Sen06]   Sengupta, A.; Bandyopadhyay, A.; Bowden, B.F.; Harrington, J.A.; Federici, J.F., "Characterisation of olefin copolymers using terahertz spectroscopy," in Electronics Lett., vol. 42, no. 25, 7th Dec. 7 2006. doi: 10.1049/el:20063148.

[Sch99]   Schwaab, G.W.; Sirmain, G.; Schubert, J.; Hubers, H.-W.; Gol'tsman, G.; Cherednichenko, S.; Verevkin, A.; Voronov, B.; Gershenzon, E., "Investigation of NbN phonon-cooled HEB mixers at 2.5 THz,"Applied Superconductivity, IEEE Transactions on , vol.9, no.2, pp.4233,4236, June 1999 doi: 10.1109/77.783959

[Sch02]   Schmidt, L.-P.; Biber, S.; Rehm, G.; Huber, K., "THz measurement technologies and applications," Microwaves, Radar and Wireless Communications, 2002. MIKON-2002. 14th International Conference on , vol.2, no., pp.581,587 vol.2, 2002 doi: 10.1109/MIKON.2002.1017914

[Sch06]   B. Schiek, I. Rolfes, H. J. Siweris, "Noise in high-frequency circuits and oscillators," Wiley-Interscience; 1 edition, June 30, 2006.

[Sch08]   Schur, J.; Ruf, M.; Schmidt, L.-P., "A 4th harmonic schottky diode mixer - facilitated access to THz frequencies," Infrared, Millimeter and Terahertz Waves, 2008. IRMMW-THz 2008. 33rd International Conference on , vol., no., pp.1,2, 15-19 Sept. 2008 doi: 10.1109/ICIMW.2008.4665574

[Sch10] Schlecht, E.T.; Gill, J.J.; Lin, R.H.; Dengler, R.J.; Mehdi, I., "A 520–590 GHz Crossbar Balanced Fundamental Schottky Mixer," Microwave and Wireless Components Letters, IEEE , vol.20, no.7, pp.387,389, July 2010 doi: 10.1109/LMWC.2010.2049432

[She04] Shen, Y., Taday, P.F. and Kemp, M.C., 2004. Terahertz spectroscopy of explosive materials, APPLEBY R., CHAMBERLAIN J.M. and KRAPELS K.A., eds. In: Passive Millimetre-Wave and Terahertz Imaging and Technology, 27 October 2004 through 28 October 2004 2004, pp82-89.

[Shi97] S.C. Shi and J. Inatani, "A waveguide-to-microstrip transition with a DC/IF return path and an offset probe," in IEEE Tran. Microw. Theory and Tech., vol. 45, no.3, pp. 442, 446, Mar. 1997. doi: 10.1109/22.563346.

[Sie03a] Siegel, P.H., 2003. THz Technology: An Overview. International Journal of High Speed Electronics and Systems, 13(2), 351-394.

[Sie03b] M. Sierra Pérez, B. Galocha Iragüen, J.L. Fernández Jambrina and M. Sierra Castañer, "Electrónica de Comunicaciones," Pearson Educación, S. A., Madrid, 2003.

[Sie04] Siegel, P.H., "Terahertz technology in biology and medicine," Microwave Symposium Digest, 2004 IEEE MTT-S International , vol.3, no., pp.1575,1578 Vol.3, 6-11 June 2004 doi: 10.1109/MWSYM.2004.1338880

[Sim09] SIM, Y.C., MAENG, I. and SON, J.-., 2009. Frequency-dependent characteristics of terahertz radiation on the enamel and dentin of human tooth. Current Applied Physics, 9(5), 946-949.

[Sil05] Siles, J.V.; Grajal, J.; Krozer, V.; Leone, B., "Schottky diode-based mixers design and optimization at millimetre and

submillimetre-wave bands," Microwave Conference, 2005 European , vol.2, no., pp.4 pp.,, 4-6 Oct. 2005 doi: 10.1109/EUMC.2005.1610086

[Sil11]   Siles, J.V.; Maestrini, A.; Alderman, B.; Davies, S.; Hui Wang; Treuttel, J.; Leclerc, E.; Narhi, T.; Goldstein, C., "A Single-Waveguide In-Phase Power-Combined Frequency Doubler at 190 GHz," Microwave and Wireless Components Letters, IEEE , vol.21, no.6, pp.332, 334, June 2011 doi: 10.1109/LMWC.2011.2134080

[SMI]   http://www.smithsdetection.com/

[Sta10]   Stake, J.; Bryllert, T.; Sobis, P.; Aik-Yean Tang; Huan Zhao; Vukusic, J.; Malko, A.; Drakinskiy, V.; Olsen, A.Ø.; Emrich, A., "Development of integrated submillimeter wave diodes for sources and detectors,"Microwave Integrated Circuits Conference (EuMIC), 2010 European , vol., no., pp.226,229, 27-28 Sept. 2010

[Sti94]   Stimson, P.A.; Dengler, R.J.; LeDuc, H.G.; Siegel, P.H., "A prototype quasi-optical SIS array receiver," Microwave Symposium Digest, 1994., IEEE MTT-S International , vol., no., pp.1337,1339 vol.3, 23-27 May 1994 doi: 10.1109/MWSYM.1994.335320

[Tan09]   C. W. Tan, J. Miao, "Optimization of sputtered Cr/Au thin film for diaphragm-based MEMS applications", Thin Solid Films 517, 4921-4925, 2009.

[TERAa]   http://www.teraview.com/

[TERAb]   http://www.teratechcomponents.com/

[Tes07]   A. Tessman, A. Leuther, H. Massler, M. Riessle, M. Kuri, M. Zink, W. Reinert., "220 GHz low-noise amplifier MMICs and modules based on a high performance 50 nm metamorphic

HEMT technology," in phys. stat. sol. (c) 4, no. 5, pp. 1667–1670 (2007). doi: 10.1002/pssc.200674264.

[Tes08]   Tessmann, A.; Leuther, A.; Massler, H.; Kuri, M.; Loesch, R., "A Metamorphic 220 320 GHz HEMT amplifier MMIC," in IEEE Compound Semicond. Int. Circuit Symp. vol., no., pp. 1,4, 12-15 Oct. 2008, doi: 10.1109/CSICS.2008.12.

[Tho04a]   B. Thomas, A. Maestrini, G. Beaudin, "Design of a Broadband Sub-Harmonic Mixer Using Planar Schottky Diodes at 330 GHz," Joint 29th Int. Conf. on Infrared and Millimeter Waves and 12th Int. Conf. on Terahertz Electronics, vol., no., pp. 457, 548, 27 Sept.-1 Oct. 2004. doi: 10.1109/ICIMW.2004.1422161.

[Tho04b]   B. Thomas, "Etude et realization d´une tête de reception heterodyne en ondes submillimétriques pour l´étude des atmosphères et surfaces de planètes," These de Doctorat de l´Université Paris 6-Pierre et Marie Curie, Décembre 2004.

[Tho05]   B. Thomas, A. Maestrini, G. Beaudin, "A low-noise fixed-tuned 300-360-GHz sub-harmonic mixer using planar schottky diodes," in IEEE Trans. Microw. and Wireless Compon. Lett., vol. 15, no. 12, pp. 865, 867, Dec. 2005. doi: 10.1109/LMWC.2005.859992.

[Tho08a]   B. Thomas, B. Alderman, D. Matheson, P. De Maagt, "A combined 380 GHz mixer/doubler circuit based on planar schottky diodes," in IEEE Microw. and Wireless Compon. Lett., vol.18, no.5, pp.353-355, May 2008. doi: 10.1109/LMWC.2008.922130.

[Tho08b]   Thomas, B.; Maestrini, A.; Matheson, D.; Mehdi, I.; de Maagt, P., "Design of an 874 GHz biasable sub-harmonic mixer based on MMIC membrane planar schottky diodes," in Infrared, 33rd Int. Conf. on Millimeter and Terahertz Waves, vol., no., pp.1-2, 15-19 Sept. 2008. doi: 10.1109/ICIMW.2008.4665424.

[Tho09]   B. Thomas, A. Maestrini, J. Ward, E. Schlecht, G. Chattopadhyay, J. Gill, C. Lee, R. Lin, I. Mehdi, "Terahertz cooled sub-harmonic Schottky mixers for planetary atmospheres", 5th ESA Workshop on Millimetre Wave Technology and Applications & 31st ESA Antenna Workshop, 2009.

[Tho10]   B. Thomas, A. Maestrini, J. Gill, C. Lee, R. Lin, I. Mehdi, P. de Maag, "An 874 GHz Fundamental Balanced Mixer Based on MMIC Membrane Planar Schottky Diodes," 21st Intenational Symposium on Space Terahertz Technology, Oxford, 23-25 March, 2010.

[Tho11]   Bertrand Thomas, Hugh Gibson, Achim Walber, Michael Brandt, Martin Philipp, Jan Ceru, Oleg Cojocari, Byron Alderman, Harald Czekala and Thomas Rose, "Submillimetre Wave Transmitter/Receiver Devices and Test Equipment For the ICI Instrument Onboard MetOp-SG", The Advanced RF Sensors and Remote Sensing Instruments, ESA/ESTEC, Noordwijk, The Netherlands13-15 September, 2011.

[Tho12]   Bertrand Thomas, J. Siles, E. Schlect, A. Maestrini, G. Chattopadhyay, C. Lee, C. Jung, I. Mehdi, S. Gulkis, "First results of a 1.2 THz MMIC sub-harmonic mixer based GaAs Schottky diodes for planetary atmospheric remote sensing", ISSTT Proceedings, 2012.

[Tre09]   J. Treuttel, B. Thomas, A. Maestrini, H. Wang, B. Alderman, J.V. Siles, S. Davis, T. Narhi, "A 380 GHz sub-harmonic mixer using MMIC foundry based schottky diodes transferred onto quartz substrate," in 20th Int. Symp. on Space Terahertz Technology, Charlottestville, 20-22 Apr. 2009.

[TRE]   http://www.ecs.umass.edu/ece/labs/thzlab/trend/

[TREX]   http://www.trexenterprises.com/Pages/Subsidiaries/sago.html

[Toh14]   Tohidian, M.; Madadi, I; Staszewski, R.B., "3.8 A fully integrated highly reconfigurable discrete-time superheterodyne receiver," Solid-State Circuits Conference Digest of Technical Papers (ISSCC), 2014 IEEE International , vol., no., pp.1,3, 9-13 Feb. 2014 doi: 10.1109/ISSCC.2014.6757343

[TOP]   http://www.topas.com/

[Tra83]   R. Trambarulo, H.S. Berger, "Conversion Loss and Noise Temperature of Mixers From Noise Measurements", IEEE MTT-S International Microwave Symposium Digest, vol., no., pp.364-365, May 31 1983-June 3 1983.

[Ula73]   Ulaby, F., "Absorption in the 220 GHz atmospheric window," Antennas and Propagation, IEEE Transactions on, vol.21, no.2, pp.266, 269, Mar1973 doi: 10.1109/TAP.1973.1140456

[UMS]   http://www.ums-gaas.com/

[Ves97]   M. Vestel and K. Ngan, "TEM, XPS and EDX characterization of the Si wafer backside sputtered Cr/Au metallization films," in 42nd Int. SAMPE Symp., May 4-8, 1997.

[VDI]   http://vadiodes.com/index.php/products/diodes

[Vil02]   R. Vila, J. Mollá, R. Heidinger, A. Moroño, E.R. Hodgson, "Electrical and dielectric properties of irradiated KU1 quartz glass from DC to 145 GHz", Journal of Nuclear Materials 307-311 (2002) 1273-1276

[Wal11]   Waliwander, T. Crowley, M.; Fehilly, M.; Lederer, D., "Sub-millimeter Wave 183 GHz and 366 GHz MMIC membrane sub-harmonic mixers," Microwave Symposium Digest (MTT), 2011 IEEE MTT-S International.

[Wan06]   Wang, H., Rollin, J., Thomas, B., Davies, S. and Maestrini, A., "Design of a low noise integrated sub-harmonic mixer at 183

GHz using European schottky diode technology," in 4th ESA Workshop on Millimetre Wave Technology and Applications, Espoo, Finland, Feb. 15-17, 2006.

[Wan08] H. Wang, A. Maestrini, B. Thomas, B. Alderman, G. Beudin, "Development of a Two-Pixel Integrated Heterodyne Schottky Diode Receiver at 183 GHz", 19th International Sympisium on Space Terahertz Technology, Groningen, 28-30 April 2008.

[Wan09] Hui Wang, "Conception et modélisation de circuits monolithiques à diode Schottky sus substrat GaAs aux longueurs d´onde millimétriques et submillimétriques pour des récepteurs hétérodynes multi-pixels embarqués sur satellites et dédiés à l´aéronomie ou la planetology," These de Doctorat de L´universite Pierre et Marie Curie, Mai 2009.

[Wan12a] H. Wang, H. Sanghera, B. Alderman, S. P. Rea, B. N. Ellison, and P. de Maagt, "A Performance Comparison of Discrete and Integrated Sub-Harmonic Schottky Diode Mixers at 664 GHz," 23rd International Symposium on Space Terahertz Technology, Tokyo, 2-4 April 2012.

[Wan12b] Zhenyu Wang; Yong Zhang; Xiaoqiang Xie; Wei Zhao, "Design of 215–225 GHz subharmonic mixer using planar Schottky diodes," Microwave and Millimeter Wave Technology (ICMMT), 2012 International Conference on , vol.3, no., pp.1,4, 5-8 May 2012 doi: 10.1109/ICMMT.2012.6230220

[Wan13] Hui Wang, Simon Rea, Byron Alderman, Brian Moyna and Nick Brewster "Schottky diode mixers for MetOp SG satellites", Millimeter Waves and THz Technology Workshop (UCMMT), 2013 6th UK, Europe, China.

[War08] Ward, J.S.; Lee, K.A.; Kawamura, J.; Chattopadhyay, G.; Stek, P., "Sensitive broadband SIS receivers for microwave limb sounding," Infrared, Millimeter and Terahertz Waves, 2008.

IRMMW-THz 2008. 33rd International Conference on , vol., no., pp.1,2, 15-19 Sept. 2008 doi: 10.1109/ICIMW.2008.4665436

[Weg09]   Weg, C.A.; Spiegel, W. V.; Senzel, F.; Henneberger, R.; Zimmermann, R.; Loffler, T.; Roskos, H.G., "Fast active THz-camera with global illumination," Infrared, Millimeter, and Terahertz Waves, 2009. IRMMW-THz 2009. 34th International Conference on , vol., no., pp.1,2, 21-25 Sept. 2009 doi: 10.1109/ICIMW.2009.5325550

[WIKI]   http://en.wikipedia.org/wiki/Black-body_radiation

[Woo11]   Wood, K.; Doyle, S.; Pascale, E.; Rowe, S.; Hargrave, P.; Dunscombe, C.; Grainger, W.; Papageorgiou, A; Spencer, L.; Mauskopf, P., "KIDCAM — A passive THz imager," Infrared, Millimeter and Terahertz Waves (IRMMW-THz), 2011 36th International Conference on , vol., no., pp.1,2, 2-7 Oct. 2011 doi: 10.1109/irmmw-THz.2011.6105184

[Wu12]   Santong Wu; Bo Zhang; Yong Fan, "Design of a 136GHz–146GHz doubler," Microwave and Millimeter Wave Technology (ICMMT), 2012 International Conference on , vol.5, no., pp.1,3, 5-8 May 2012 doi: 10.1109/ICMMT.2012.6230387.

[Yan12]   Xiaofan Yang; Hui Wang; Alderman, B.; Yong Fan; Bo Zhang, "Design of a 380 GHz sub-harmonically pumped mixer based on planar Schottky diodes," Microwave and Millimeter Wave Technology (ICMMT), 2012 International Conference on , vol.2, no., pp.1,3, 5-8 May 2012 doi: 10.1109/ICMMT.2012.6230108

[Yam04]   Yamashita, M.; Ogawa, Y.; Shibuya, T.; Otani, C.; Kawase, K.; Inoue, H.; Kanamori, T., "Non-destructive detection of chemicals by scattering and fingerprinting in the THz

band," Infrared and Millimeter Waves, 2004 and 12th International Conference on Terahertz Electronics, 2004. Conference Digest of the 2004 Joint 29th International Conference on , vol., no., pp.411,412, 27 Sept.-1 Oct. 2004 doi: 10.1109/ICIMW.2004.1422136

[Yao08]   Changfei Yao; Jinping Xu; Kang Ying, "Design of a D-Band frequency doubler using GaAs Schottky barrier diodes," Microwave and Millimeter Wave Technology, 2008. ICMMT 2008. International Conference on , vol.3, no., pp.1193,1195, 21-24 April 2008 doi: 10.1109/ICMMT.2008.4540642.

[Yon07]   Yoneyama, H.; Yamashita, M.; Kasai, S.; Ito, H.; Ouchi, T., "Application of terahertz spectrum in the detection of harmful food additive," Infrared and Millimeter Waves, 2007 and the 2007 15th International Conference on Terahertz Electronics. IRMMW-THz. Joint 32nd International Conference on , vol., no., pp.281,282, 2-9 Sept. 2007

[Yu10]   Xinmin Yu; Sah, Suman Prasad; Belzer, B.; Heo, D., "Performance evaluation and receiver front-end design for on-chip millimeter-wave wireless interconnect," Green Computing Conference, 2010 International , vol., no., pp.555,560, 15-18 Aug. 2010 doi: 10.1109/GREENCOMP.2010.5598263

[Yuj03]   Yujiri, L.; Shoucri, M.; Moffa, P., "Passive millimeter-wave imaging," in IEEE Microwave Mag., vol. 4, no. 3, pp. 39, 50, Sep. 2003. doi: 10.1109/MMW.2003.1237476.

[Zha07]   Zhang, Z., Zhang, Y., Zhao, G. and Zhang, C., 2007. Terahertz time-domain spectroscopy for explosive imaging. Optik, 118(7), 325-329.

[Zha10a]   Bo Zhang; Yong Fan; Yang, X.F.; Zhong, F.Q.; Zhe Chen; Lin, X.Q.; Zhao, M.H., "Optimization and design of a suspended

215–235-GHz subharmonically pumped mixer for space-borne radiometers," Microwave and Millimeter Wave Technology (ICMMT), 2010 International Conference on , vol., no., pp.1279,1281, 8-11 May 2010 doi: 10.1109/ICMMT.2010.5524955

[Zha10b]   Shixi Zhang; Bo Zhang; Yong Fan, "Design of a 114GHz-135GHz passive tripler," Signals Systems and Electronics (ISSSE), 2010 International Symposium on , vol.2, no., pp.1,3, 17-20 Sept. 2010 doi: 10.1109/ISSSE.2010.5606975.

[Zha12]   Bo Zhang; Yong Fan; Zhang, S. X.; Yang, X.F.; Zhong, F. Q.; Zhe Chen, "110GHz high performance varistor tripler," Microwave and Millimeter Wave Circuits and System Technology (MMWCST), 2012 International Workshop on , vol., no., pp.1,2, 19-20 April 2012 doi: 10.1109/MMWCST.2012.6238180.

[Zha13]   Xiaoyang Zhang; Hongxi Yu; Hui Xu; You Lv, "Design of a high-performance balanced frequency tripler at 94GHz," Radar Conference 2013, IET International , vol., no., pp.1,3, 14-16 April 2013 doi: 10.1049/cp.2013.0237.

[Zho12]   Fuqun Zhong; Bo Zhang; Yong Fan; Minghua Zhao; Xiaofan Yang, "A broadband W-band subharmonic mixers circuit based on planar schottky diodes," in Int. Conf. on Industrial Control and Electronics Engineering (ICICEE), vol., no., pp.792-794, 23-25 Aug. 2012. doi: 10.1109/ICICEE.2012.211.

[Zhu14]   Fang Zhu; Wei Hong; Ji-Xin Chen; Xin Jiang; Ke Wu; Pin-Pin Yan; Chun-Lin Han, "A Broadband Low-Power Millimeter-Wave CMOS Downconversion Mixer With Improved Linearity," Circuits and Systems II: Express Briefs, IEEE Transactions on , vol.61, no.3, pp.138,142, March 2014 doi: 10.1109/TCSII.2013.2296196

LIST OF PUBLICATIONS AND RESEARCH STAYS

Books

1. Contributor author to Chapter Six of the Book "Semiconductor THz Technology: From Components to Systems", Wiley Editorial.

Journal Papers

1. **Itziar Maestrojuan**, Iñigo Ederra and Ramón Gonzalo, "4th-Harmonic Schottky Diode Mixer Development at Sub-millimeter Frequencies", Microwave and Wireless Components Letters (under review).

2. **Itziar Maestrojuan**, Iñigo Ederra and Ramón Gonzalo, "Use of COC Substrates for Millimetre-wave Devices", Microwave and Optical Technology Letters, AID MOP28848 (to be published).

3. **Itziar Maestrojuan**, Simon Rea, Iñigo Ederra and Ramón Gonzalo, "Experimental Analysis of Different Measurement Techniques for Characterization of Millimeter-wave Mixers", Microwave and Optical Technology Letters, Vol 56, Issue 6, start page 1441 AID MOP28364.

4. David Etayo Salinas, **I. Maestrojuan**, J. Teniente, I. Ederra, R. Gonzalo, "Experimental Explosive Characterization for Counterterrorist Investigation", Journal of Infrared Millimeter and Terahertz Waves, 34(7-8), pp. 468–479, (2013).

Convened International Conferences

1. **Itziar Maestrojuan**, Inés Palacios, Iñigo Ederra, Ramón Gonzalo, "Use of Low Loss Substrate for Developing Sub‑Millimeter‑Wave Mixers", Proceedings of the 8th European Conference on Antennas and Propagation, EuCAP 2014.

International Conferences

1. I. Maestrojuan, I. Ederra, R. Gonzalo, "Comparison of a Sub-Harmonic and a Fourth-Harmonic Mixer Working at 440 GHz", IRMMW-THz 2014, Tucson, Arizona.

2. **I. Maestrojuan**, S.Rea, I. Ederra, R. Gonzalo, "Millimeter-wave Mixer Measurement: Comparison of different Methods", IRMMW-THz 2013, Mainz, Germany.

3. **I. Maestrojuan**, I. Palacios, I. Ederra, R. Gonzalo, "Implementation of a multi-pixel sub-mm wave Imaging Receiver", Proceedings of the 7th European Conference on Antennas and Propagation, EuCAP 2013.

4. A. Rebollo**, I. Maestrojuan**, Belén Larumbe-Gonzalo, R. Gonzalo, I. Ederra, "Parametric Study of Pin Surface Used to Suppress Undesired Modes in a Packaged W-band Microstrip Receiver ", Proceedings of the 7th European Conference on Antennas and Propagation, EuCAP 2013.

5. S.P.Rea, M.Henry, H.Wang, B.Alderman, B.N.Ellison, J.Treuttel**, I. Maestrojuan**, P.de Maagt, "A Compact 340 GHz Receiver Array Front-End", ISSTT 2012.

6. A. Rebollo**, I. Maestrojuan**, Belén Larumbe-Gonzalo, R. Gonzalo, I. Ederra, "Design and Characterization of W-band Components in

Planar Technology", Proceedings of the 6th European Conference on Antennas and Propagation, EUCAP 2012.

7. J. Teniente, R.M. Gomez, **I. Maestrojuan**, A. Rebollo, R. Gonzalo, C. del Río, "Corrugated Horn Antenna Noise Temperature Characterisation for the NRL Water Vapor Millimeter-Wave Spectrometer Project", EuCAP 2011.

8. **I. Maestrojuan**, I. Palacios, A. Rebollo, David Etayo Salinas, J. Teniente, I. Ederra, R. Gonzalo, "Development of a Sub-Harmonic Mixer Working at 220GHz", Microwave Workshop Series on Millimeter Wave Integration Technologies (IMWS), 2011 IEEE MTT-S International.

9. A. Rebollo, **I. Maestrojuan**, R. Gonzalo, I. Ederra, "A broadband Radiometer Configuration at 94GHz in Planar Technology", Microwave Workshop Series on Millimeter Wave Integration Technologies (IMWS), 2011 IEEE MTT-S International.

10. David Etayo Salinas, J.C. Iriarte, I. Palacios, **I. Maestrojuan**, J. Teniente, I. Ederra, R. Gonzalo, "THz Imaging System for Industrial Quality Control", Microwave Workshop Series on Millimeter Wave Integration Technologies (IMWS), 2011 IEEE MTT-S International.

11. J.C. Iriarte, David Etayo Salinas, I. Palacios, **I. Maestrojuan**, I. Liberal, A. Rebollo, J. Teniente, I. Ederra, R. Gonzalo, "Water Content Evolution in Leaves Based on Active THZ Imaging System", Proceedings of the 5th European Conference on Antennas and Propagation, EUCAP 2011.

12. **I. Maestrojuan**, R. Gonzalo, I. Ederra, J. Teniente, "Study of a Confocal Configuration for Imaging Cameras Working at 220 GHz", EUCAP 2011.

13. **I. Maestrojuan**, I. Palacios, David Etayo Salinas, J.C. Iriarte, J. Teniente, I. Ederra, R. Gonzalo, "Explosives Characterization in Terahertz Range", SPIE 2011.

14. J.C. Iriarte, José Luis Martínez de Falcón, **I. Maestrojuan**, I. Liberal, A. Rebollo, I. Ederra, R. Gonzalo, "Broadband RCS Reduction Using AMC Technology", Proceedings of the 5th European Conference on Antennas and Propagation, EUCAP 2011.

National Conferences

1. **Itziar Maestrojuan**, Inés Palacios, Iñigo Ederra, Ramón Gonzalo, "Low Loss COC Substrates for Developing Millimeter-Wave Devices", URSI 2014.

2. **I. Maestrojuan**, S.Rea, I. Ederra, R. Gonzalo, "Caracterización de técnicas de medida de mezcladores a frecuencias milimétricas", URSI 2012.

3. **I. Maestrojuan**, David Etayo Salinas, I. Palacios, J. Teniente, I. Ederra, R. Gonzalo, "Caracterización de Explosivos en el Rango de los THz", URSI 2011.

4. **I. Maestrojuan**, I. Palacios, J. Teniente, I. Ederra, R. Gonzalo, "Desarrollo de un Mezclador Sub-armónico trabajando a 220 GHz", URSI 2011.

5. David Etayo Salinas, J.C. Iriarte, I. Palacios, **I. Maestrojuan**, I. Liberal, A. Rebollo, J. Teniente, I. Ederra, R. Gonzalo, "Evolución del contenido en agua de hojas basado en imágenes activas en Terahercios", URSI 2011.

6. A. Rebollo, **I. Maestrojuan**, R. Gonzalo, I. Ederra, "Configuración de Receptor de Banda Ancha a 94GHz en Tecnología Plana", URSI 2011.

7. J. Teniente, **I. Maestrojuan**, R. Gonzalo, C. del Río, "Antenas de bocina corrugadas con alta eficiencia de correlación a un modo gaussiano fundamental", URSI 2010.

8. David Etayo Salinas, J.C. Iriarte, I. Palacios, I. Liberal, José Luis Martínez de Falcón, **I. Maestrojuan**, I. Ederra, J. Teniente, R. Gonzalo, "Tecnología de THz para la Caracterización del Contenido en Agua en Plantas", URSI 2010.

Research Stays

1. **MMT Group RAL Space**, Rutherford Appleton Laboratory.

    September 2011-March 2012,

    Harwell Oxford, Didcot. (England).

This disertation presents the design, fabrication and measurement of different Terahertz systems for Imaging applications. A couple of sub-harmonic mixers, a 1x8 sub-harmonic mixer array, a 4th-harmonic mixer and a frequency doubler are implemented within this Thesis.

Itziar Maestrojuán Biurrun

Development of Terahertz Systems
for Imaging Applications

upna
Universidad
Pública de Navarra
Nafarroako
Unibertsitate Publikoa